EXPRESSION AND FUNCTION OF THE ASD-ASSOCIATED MET RECEPTOR TYROSINE KINASE DURING MAMMALIAN FOREBRAIN DEVELOPMENT

By

Matthew C. Judson

Dissertation

Submitted to the Faculty of the

Graduate School of Vanderbilt University

in partial fulfillment of the requirements

for the degree of

DOCTOR OF PHILOSOPHY

in

Neuroscience

May, 2010

Nashville, Tennessee

Approved:

Professor Pat Levitt

Professor David Miller

Professor Greg Mathews

Professor Matthew Tyska

To my amazing wife, Erin. I learned through this experience that patience is certainly not the least of your many virtues! I love you.

ACKNOWLEDGEMENTS

In terms of growing both as a scientist and a person, I could not have found myself in a more fortunate environment than what I experienced at Vanderbilt University over the past 6-plus years. It all began with the IGP, where countless individuals helped me to focus a quite broad interest in science into a true passion for neuroscience research. Most notable, however, were my laboratory rotation preceptors, who altruistically committed time, energy, and considerable financial resources to the development of my laboratory skills and interests. These generous individuals include Drs. Jeff Conn, David Miller, and Pat Levitt who, of course, served so well as my Ph.D. thesis advisor. Pat, thank you so much for setting such a great example for me to follow in your laboratory. It is a rare person, as you are, who can get so much out of, and give so much to, scientific research and still have plenty of "self" leftover for the other great things in life. It was truly my privilege to have worked with you and learned from you.

I had one other principle mentor during my Ph.D. experience at Vanderbilt: Dr. Kathie Eagleson. Kathie, without your help I would still be struggling to choreograph the management of a mouse colony and the planning of histological experiments with a developmental purpose. Succinctly, I would still be working on my thesis, and it would probably be of a quality less than half that presented in the document to follow. I would also be lacking a great friend. Other influential Levitt lab members to whom I would like to extend special thanks and appreciation include Dr. Phil Ebert, Dr. Dan Campbell, Dr. Barb Thompson, Dr. Elizabeth Hammock, Dr. Alexandre Bonnin, Mica Bergman, Phil Gorrindo, Dr. Liz Catania, Donte Smith, Lisa McFadyen-Ketchum, and Gail Ingle.

Finally, I would like to offer a special thanks to the faculty who served on my committee: Dr. David Miller (chair), Dr. Doug Vaughaun, Dr. Greg Mathews, and Dr. Matthew Tyska. Not only did you serve me well during my committee meetings, but in many cases provided me with additional experimental advice, support, and reagents in the confines of your own laboratories. This especially applies to Greg! Thanks also to other faculty who helped me in a similar capacity: Dr. Gregg Stanwood, Dr. Ariel Deutch, Dr. Roger Colbran (and Dr. AJ Baucum), Dr. Bethann McLaughlin, and Dr. Karoly Mirnics.

TABLE OF CONTENTS

LIST OF FIGURES

Chapter

I. INTRODUCTION

Figure Page

II. DYNAMIC GENE AND PROTEIN EXPRESSION PATTERNS OF THE AUTISM-ASSOCIATED MET RECEPTOR TYROSINE KINASE IN THE DEVELOPING MOUSE FOREBRAIN

Figure Page

Supplemental Figure Page

Supplemental Figure Page

V. FUTURE DIRECTIONS

Figure Page

CHAPTER I

INTRODUCTION

Cytoarchitectural foundations of forebrain circuit organization and function: focus on the neocortical minicolumn

Planning, calculation, and the assimilation of current sensory input and emotional states with prior experience are among the most sophisticated functions of the mammalian forebrain, and no forebrain structure has been more sculpted by evolution than the neocortex to facilitate these exquisitely complex forms of information processing. Remarkably, over the last 100 million years, the surface area of this laminated tissue has expanded by a factor of ~1,000 in the human as compared to the mouse, while the lamination architecture itself has remained relatively unchanged (Rakic, 2009). From this observation and advances in the understanding of neocortical ontogeny has emerged the concept of the minicolumn- a radially organized, minimal component of neocortical information processing whose numerical expansion is positively correlated with increasingly sophisticated forebrain function throughout mammalian evolution.

The neocortical minicolumn has been championed by Mountcastle as the basic information processing module within the neocortex (Mountcastle, 1997). These functional units are comprised of 100-150 neurons arranged in a vertical column that spans the six horizontal neocortical laminae (**Fig. 1A**), and they are innervated by specific input modalities (Mountcastle, 1997; Markram, 2008). In primary sensory cortex, excitatory, glutamatergic pyramidal neurons within layer 2/3 of the minicolumn

receive modality-specific, ascending thalamic information via feed-forward connections from the granule cells in layer 4. Within these neurons, this information is integrated with coincident cortical inputs and thalamic feedback, allowing for higher-order,

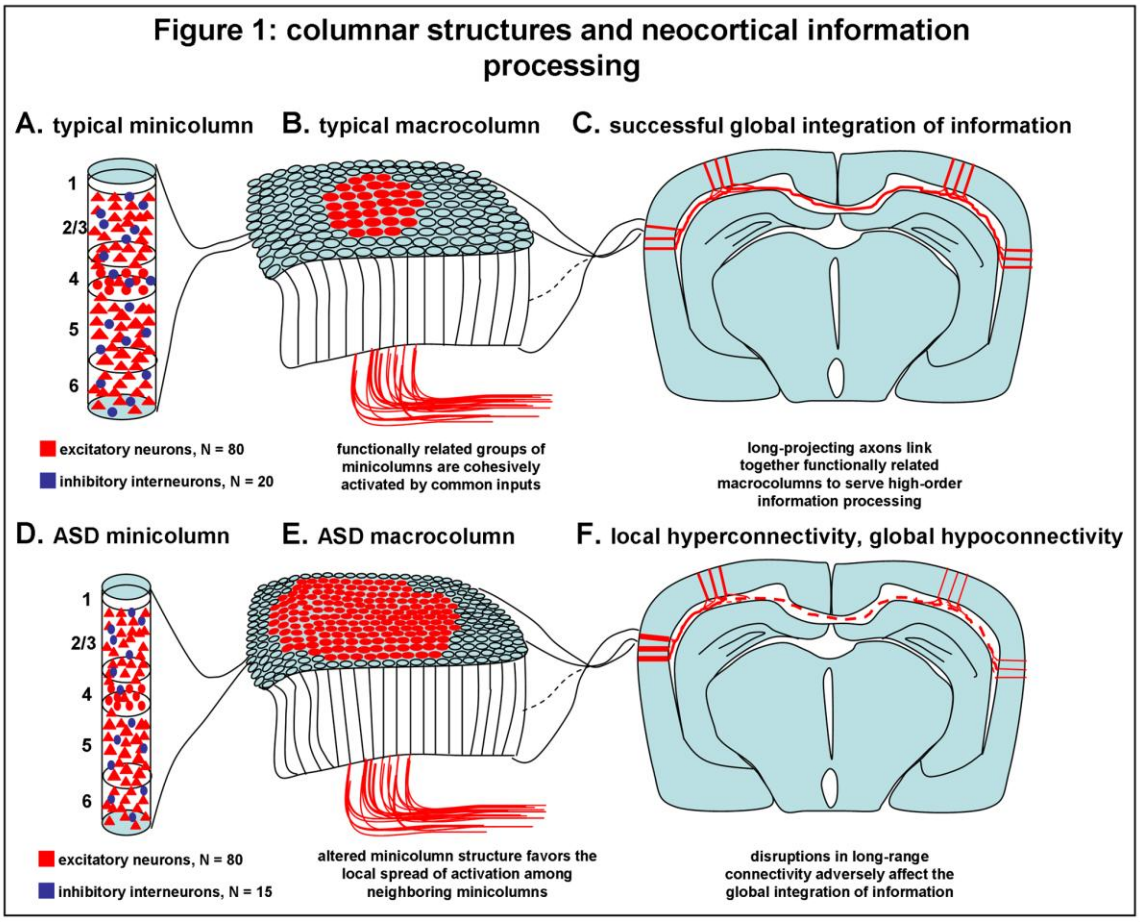

associative processes such as attention (Jones, 2002; Rubio-Garrido et al., 2009). Layer 2/3 pyramidal neurons predominantly project their intra-columnar axons to pyramidal neurons in layer 5 to propagate the descending flow of information through the minicolumn. Layer 5 pyramidal neurons, in turn, distribute resultant minicolumnar outputs to other cortical areas and important subcortical forebrain centers including the

striatum and thalamus. A schematic summarizing basic excitatory connectivity within the neocortical minicolumn can be viewed in **Figure 2**.

From a qualitative observation of pyramidal cell dendritic morphology alone (**Fig. 3**), one can infer that these neurons are able to integrate information entering the

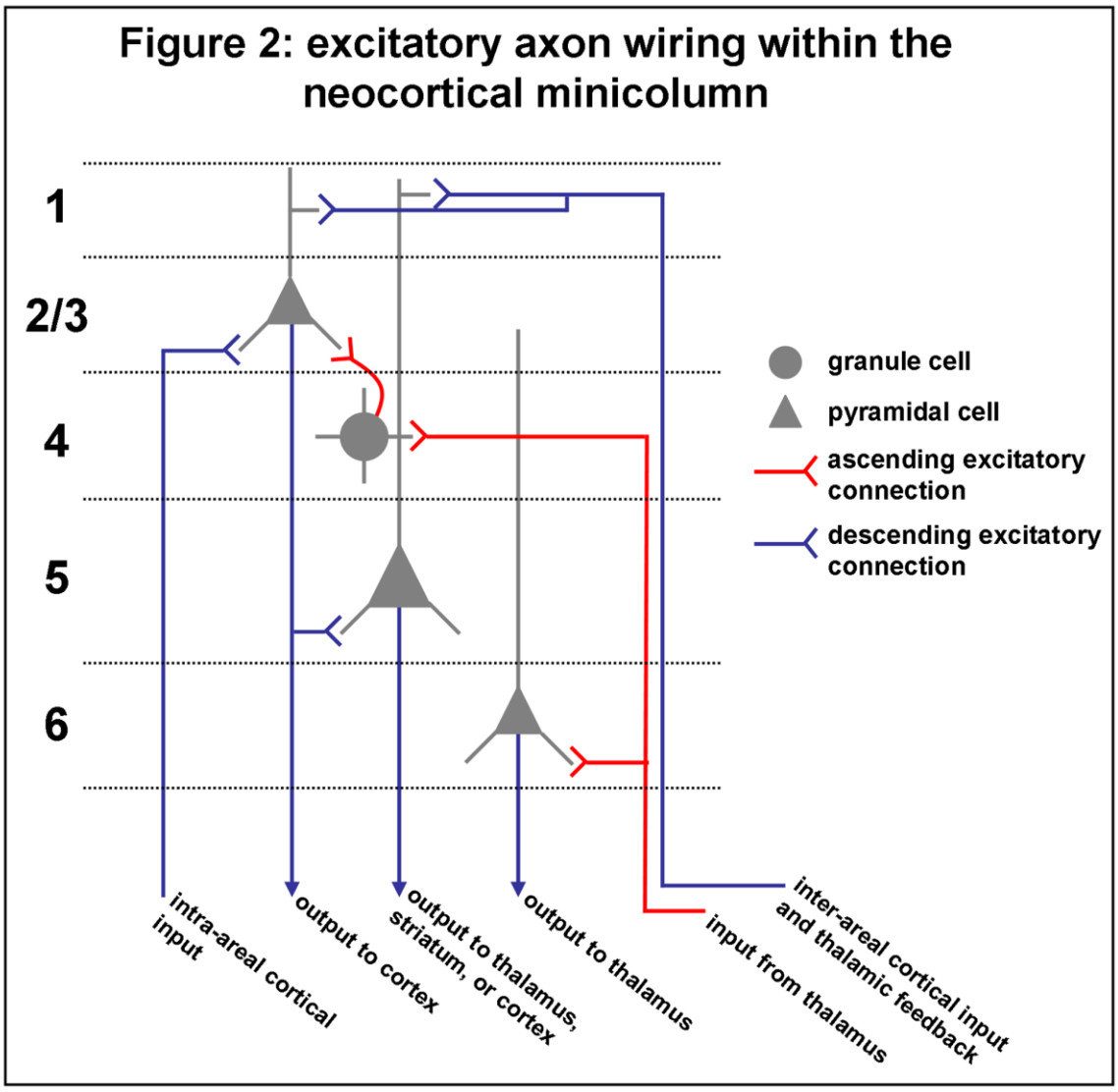

minicolumn at different vertical levels. Dendritic compartmentalization is an important morphological feature that supports this capacity. For example, using a high-resolution

approach, Petreanu and colleagues revealed that afferents from both ascending peripheral sources and descending central sources impinge upon discrete but overlapping domains of the pyramidal cell dendritic arbor, according to layer-specific patterns (Petreanu et al., 2009). At the molecular level, varied distributions of voltage-dependent ion channels can

Figure 3: pyramidal dendrite morphology and interneuron axon morphology: relationship to inhibitory connections across minicolumns

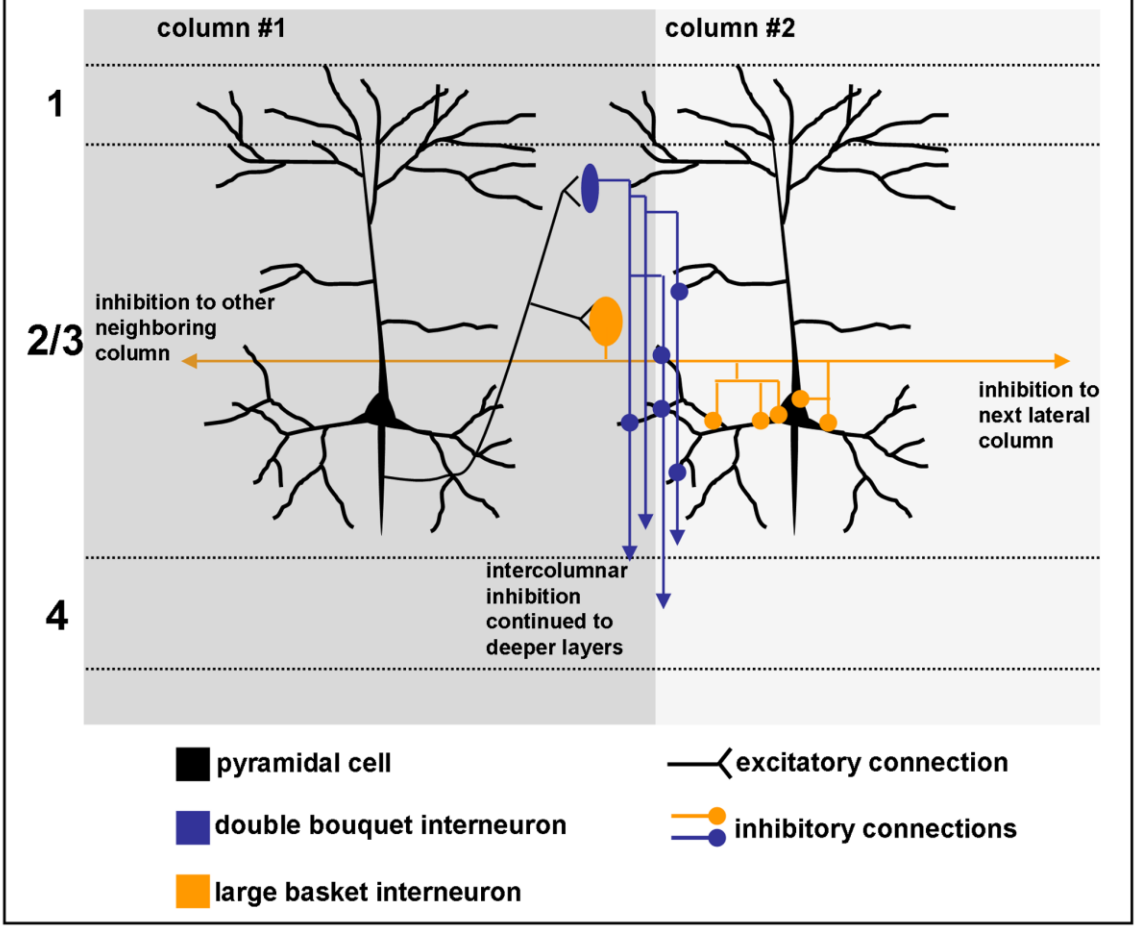

influence local dendritic excitability and affect input-output relationships in neurons (Hausser et al., 2000). For example, a recent study implicated a down-regulation of Kv4.2 K^+ channels in the potentiation of local dendritic branch strength (Losonczy et al., 2008), and modeling studies indicate that nonuniform ion channel distributions best explain the backpropagation of action potentials within the basal dendritic arbors of pyramidal neurons (Nevian et al., 2007; Acker and Antic, 2009). Collectively, these findings indicate that minicolumnar pyramidal neurons may be able to simultaneously process and store unique combinations of circuit-level information within specific dendritic domains.

How does cytoarchitecture contribute to the cohesive activation of excitatory neurons and the vertically constrained flow of information within the minicolumn? First, axo-dendritic overlap is maximal among excitatory neurons located directly above or below one another within a minicolumn. Second, columnar boundaries of axo-dendritic overlap predict functional connectivity (Shepherd et al., 2005). Third, the inputs to a mincolumn, whether ascending or descending, tend to be highly focused (Mountcastle, 1997; Mountcastle, 2003; Markram, 2008). However, neurons in neighboring minicolumns are certainly not completely disconnected from each other, either anatomically or functionally, allowing for the spread of activation among them. Inhibitory interneurons are integral in controlling excitation both across and within minicolumns.

Minicolumnar inhibitory interneurons mediate inhibitory neurotransmission by releasing gamma-amino butyric acid (GABA) onto their target neurons. They are fully intercalated within all layers of the neocortex (**Fig. 1A; Fig. 2**) and they exhibit diverse

axonal morphologies, which relate to their ability to mediate inhibition across (lateral inhibition) or within (intrinsic inhibition) minicolumns (Markram et al., 2004). For example, parvalbumin-expressing basket interneurons in the superficial cortical layers are particularly suited to mediate inhibition across mincolumns, considering their horizontally aligned axonal arbors and perisomal targeting of pyramidal neurons (**Fig. 2**). The lateral extent and the efficacy of this inhibition are dictated by the axonal arbor width and the ratio of pyramidal neurons to other interneurons contacted, respectively (Krimer and Goldman-Rakic, 2001). Layer II calbindin- and calretinin-expressing double-bouquet interneurons also facilitate lateral inhibition. However, they do so via vertically oriented axonal arbors, which effectively form an inhibitory curtain within the neuropil surrounding each minicolumn (DeFelipe et al., 1990; Buxhoeveden and Casanova, 2002; Yanez et al., 2005) (**Fig. 2)**. In addition to different patterns of synaptic connections, interneuron subtypes within a minicolumn also exhibit different thresholds for excitation. Therefore, the amplitude and frequency of an incoming excitatory stimulus will determine the subset of interneurons that become activated within the minicolumn and, thus, the quality of the information processed therein (Porter et al., 2001; Markram et al., 2004).

The minicolumn is the basic unit of neocortical information processing, and groups of minicolumns enable increasingly complex computations. Provided they share common inputs and are linked by short-range horizontal connections, as many as 70-80 neighboring minicolumns can be locally and cohesively activated. These so-called macrocolumns (**Fig. 1B**) provide an anatomical basis for information processing modules in sensory and association cortices that share similar functional properties (Mountcastle,

1997; Mountcastle, 2003). Long-range axonal projections connect functionally related macrocolumns in distant neocortical areas and also link them to lower centers (**Fig. 1C**). In this way, information processed in local circuits throughout the forebrain can be bound together to support the most sophisticated cognitive functions.

The developmental basis of neocortical circuit formation: from neurogenesis to synaptic pruning and in-between

Neurogenesis and migration of minicolumnar neurons

The cytoarchitectural framework of the neocortical minicolumn is determined developmentally by modes of neurogenesis and neuronal migration in the dorsal forebrain that are conserved across all mammals. Both symmetrical and asymmetrical divisions of radial glial progenitor cells within the proliferative zones of the dorsal pallium are essential to neocortical neurogenesis. During the earliest phases of neurogenesis, symmetrical divisions predominate and amplify the radial glial progenitor cell pool (Takahashi et al., 1996; Takahashi et al., 1997; Kornack and Rakic, 1998). Subsequently, each radial glial precursor undergoes iterative asymmetrical divisions to generate a lineage of daughter neurons that migrate along their radially oriented processes to populate the overlaying layers of the incipient neocortex in an inside-out fashion. That is, more recently born neurons populate increasingly superficial neocortical layers (Angevine and Sidman, 1961; Sidman and Rakic, 1973). Because each radial glial progenitor cell seeds only one or a few minicolumns, they are referred to as radial ontogenetic units (Rakic, 1988). It logically follows then that numbers of asymmetric radial glial divisions dictate the radial extent of the minicolumn, and thus, the thickness of the neocortex, while numbers of symmetric divisions dictate the available pool of

radial ontogenetic units, and thus, the surface area of the neocortex. Therefore, mechanisms enhancing symmetric radial glial progenitor cell divisions have likely evolved to support the massive expansion of neocortical surface area in higher mammals (Rakic, 1988; Kornack and Rakic, 1998; Rakic, 2009).

Approximately 85% of neurons in the neocortical minicolumn arise from the dorsal pallial mechanisms of neurogenesis and radial migration described above, and they are exclusively excitatory projection neurons. The remaining 15% are local inhibitory interneurons, which take a far more circuitous path to their minicolumnar residences. It was once thought that inhibitory and excitatory neurons migrate in tandem to the cortex from within a common region of the dorsal pallial proliferative zone, but this concept began to unravel during the past two decades. Initial dye labeling and time-lapse microscopy experiments in developing ferret brain slices showed some postmitotic neurons to migrate orthogonally to radial glia processes across very long distances within the cortical intermediate zone (O'Rourke et al., 1992). Further experiments in the rodent brain confirmed that these tangentially migrating cells originate in the ganglionic eminences (GE) of the ventral forebrain (de Carlos et al., 1996). Finally, Anderson and colleagues demonstrated the restricted expression of Dlx 1/2 transcription factors in the GE, the ablation of which prevented the tangential migration of nearly all GABA-ergic interneurons to the neocortex (Anderson et al., 1997). In rodents, these findings meshed well with previous data that cortical and subcortical proliferative zones contain immiscible progenitor cell populations (Fishell et al., 1993; Neyt et al., 1997); since they are not generated amongst the precursors of cortical pyramidal cells, inhibitory interneurons necessarily take a tangential migration from the GE to the dorsal pallium in

order to form local circuits within columns of cortical pyramidal cells (**Fig. 4**). More recent studies in the developing human forebrain have demonstrated a conserved mode of tangential migration for interneurons, albeit from expanded zones of origin, which include the dorsal pallium in addition to the GE (Letinic et al., 2002).

Figure 4: radial and tangential cell migration seed the incipient neocortical minicolumn with excitatory and inhibitory neurons

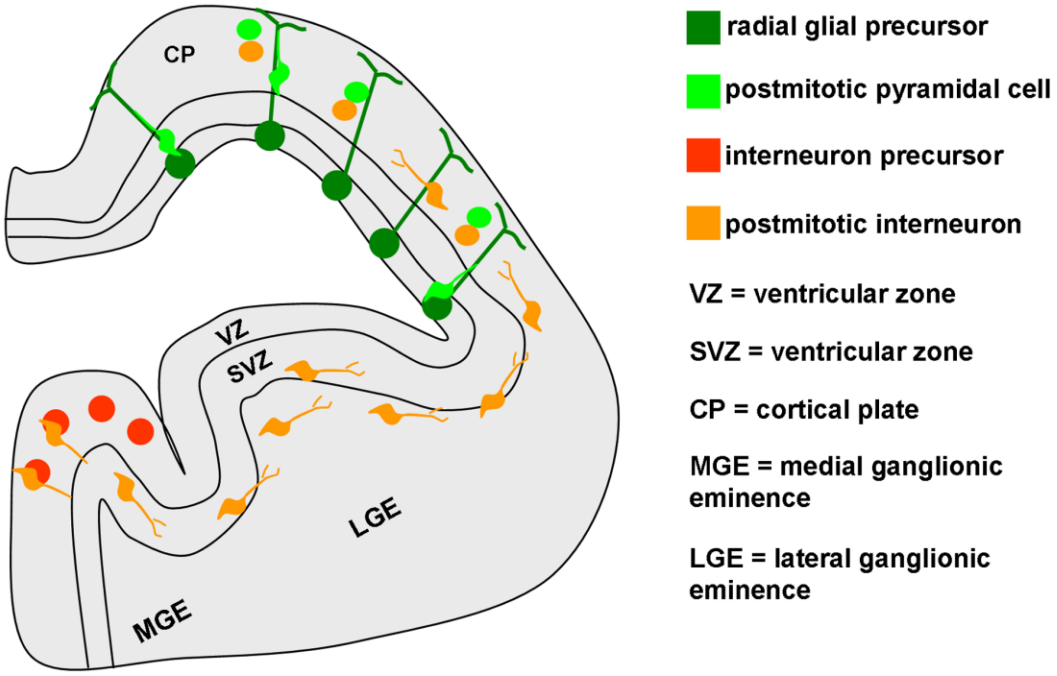

Axon and dendrite outgrowth and guidance: morphological scaffolding for intrinsic and extrinsic minicolumnar connections

Following neurogenesis, the initiation of neuronal migration coincides with relatively undifferentiated minicolumnar neurons establishing polarity, the precursor to

developing their characteristic dendritic and axonal morphologies, and consequently, the assembly of the initial framework for intrinsic and extrinsic minicolumnar connectivity. Connectivity between any two neurons, minicolumnar or otherwise, depends on the interaction between their presynaptic (i.e., axonal) and postsynaptic (i.e., dendritic) elements, which are developmentally specified. Growing, differentiating neurons initially extend a symmetrical array of short neurites from their cell bodies, each of which possesses a highly dynamic growth cone structure at its distal end. A single neurite is then specified to become the neuron's sole axon. This selective transformation requires changes in cytoskeletal actin and microtubule stability that result in a dramatic increase in both neurite growth rate and growth cone size (Bradke and Dotti, 1999; Gonzalez-Billault et al., 2001; Witte et al., 2008). An equally selective, though less dramatic, increase in neurite growth rate may also underlie the specification of an apical dendrite among basilar dendrites in the arbors of neocortical pyramidal neurons (Horton et al., 2006). Though still unclear, the inductive mechanisms of neuronal polarity are at least partly cell-autonomous in nature, as even dissociated neurons cultured at low-density develop axons and asymmetrical dendritic arbors (Dotti et al., 1988; Horton et al., 2006).

Newly specified axons and dendrites undergo further outgrowth and branching, which is carefully organized to yield characteristic pyramidal neuron and interneuron morphologies. Numerous soluble and extracellular matrix- or membrane-bound molecules serve as growth and/or guidance cues for developing axons and dendrites. While neurons could conceivably receive growth signals broadly across their axonal and dendritic membranes, attractive and repulsive guidance signals are sensed by their growth cones (O'Donnell et al., 2009). Guidance molecule receptors at the growth cone cell

membrane are poised to transduce directional cues into intracellular signaling cascades that, whether attractive or repulsive, culminate in the local recruitment or dispersion of actin and microtubles, respectively (Quinn and Wadsworth, 2008). Such asymmetrical rearrangements of the cytoskeleton effectively steer the growing axon or dendrite through the developing forebrain.

There is a great diversity of families of membrane-bound and secreted axon guidance molecules expressed by mammalian species (Chilton, 2006; O'Donnell et al., 2009), which reflects the complexity of establishing precise connections between neurons that are separated by great distances within the developing forebrain. Even in the smallest mammalian forebrain, long-projecting axons navigate tortuous paths that are thousands of microns long, and they make numerous intermediate guidance "decisions" en route to reaching their targets. For example, commissural corticocortically projecting pyramidal neurons in layer 2/3 likely depend upon attractive Netrin-1 signaling through DCC receptors for outgrowth and guidance toward the midline, as *Netrin-1* knockout mice exhibit agenesis of the corpus callosum and other forebrain commissures (Serafini et al., 1996). At the midline, glial populations both superior to (i.e., the indusium griseum) and inferior to (i.e., the glial wedge) the callosum secrete repulsive guidance cues, which callosal axons avoid by coursing through the body of this incipient tract toward their target areas in contralateral cortex (**Fig. 5**). These molecules include Slits, which are sensed by Robo receptors expressed on the callosal axon growth cones (Shu et al., 2003), and even Wnts signaling through noncanonical pathways (Yoshikawa et al., 2003).

Comparatively little, however, is known about the cues that guide callosal axons to their targets within homotopic neocortical areas once they cross the midline (Lindwall et al., 2007). Our current understanding of inter-areal and intra-areal targeting mechanisms is primarily based on studies of the thalamocortical and corticothalamic projection systems. Aspects of inter-areal targeting are likely to be set up by axon sorting

Figure 5: intermediate guidance decisions of callosally projecting cortical pyramidal axons

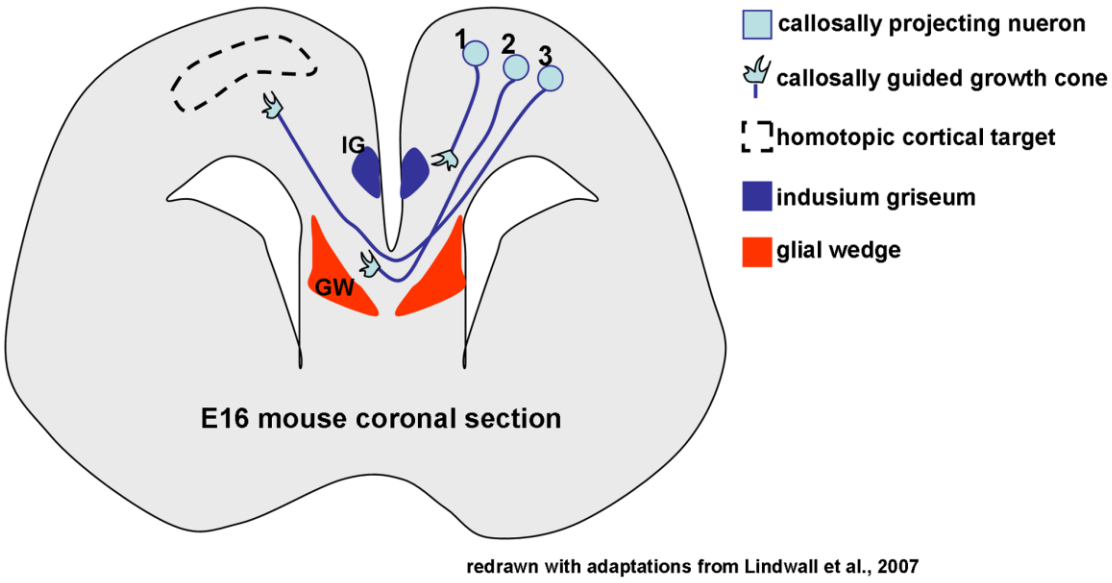

redrawn with adaptations from Lindwall et al., 2007

1. Callosal axons are attracted to the midline via Netrin/DCC signaling.

2. The boundaries of a permissive corridor through the incipient corpus callosum are marked by repulsive cues including Slit2 and Wnt, which are secreted by dorsal and ventral glial cells in the indusium griseum (IG) and glial wedge (GW), respectively.

3. Unknown attractive cues guide callosal axons to target regions in homotopic cortical areas.

events before potential target areas are even encountered. Dufour and colleagues demonstrated complementary gradients of Ephrin-A5 ligand and EphA4/EphA5 receptor expression within the thalamus and ventral forebreain, respectively, which proved to dictate both the path of thalamocortical axons to the neocortex and their inter-areal targeting therein. For example, because Ephrin-A5 is a repulsive guidance cue, anterior dorsal thalamic neurons that express high Eph receptor levels project their axons through the anterior ventral forebrain where Ephrin-A5 levels are low, and consequently, target anterior neocortical areas (Dufour et al., 2003). Recent studies showing that serotonin can modulate Netrin-1-mediated thalamocortical trajectories through the ventral forebrain indicate that the sorting of long-projecting forebrain axons is a highly complex and regulated process (Bonnin et al., 2007).

Ephrin/Eph systems also play a role in intra-areal targeting. Remarkably, in the study described above, Dufour and colleagues also showed that a neocortical Ephrin-A5 expression gradient emerges perinatally to complement the expression of EphA4/EphA5 receptors in the somatosensory thalamus and preserve the somatotopic organization of the thalamocortical afferents (Dufour et al., 2003). Deletion of ephrin-A5 results in the misguidance of specific thalamic axons to cortical areas which they normally do not target (Uziel et al., 2002). Reciprocal intra-areal targeting of corticothalamic projections within the thalamus was shown to depend on neocortical gradients of yet another Ephrin-A5 receptor, EphA7. However, unlike EphA4/EphA5 disruptions, manipulations of EphA7 were shown not to affect corticothalamic axon sorting or guidance en route to the target (Torii and Levitt, 2005).

The axon guidance events discussed thus far serve to organize connectivity in the tangential neocortical domain- that is, the specific neocortical areas, and therein, the specific minicolumns or groups of minicolumns to be innervated. How then is connectivity organized in the radial neocortical domain, across the vertical structure of the minicolumn? Studies of the ascending thalamocortical projection to layer 4 have yielded the majority of progress toward answering this question. The initial step in the process concerns the ability of the thalamocortical axons to breach the neocortical-subcortical boundary. Upon arriving at the neocortex, thalamocortical axons interact with a transient population of neurons called subplate neurons, which are located just inferior to the deepest neocortical layers (Lund and Mustari, 1977; Rakic, 1977; Shatz and Luskin, 1986). Subplate neurons themselves project axons to layers 4 and 1 of the neocortex (Friauf et al., 1990); it has been suggested that they pioneer a path used by thalamocortical axons to invade the neocortex in the radial dimension (Allendoerfer and Shatz, 1994). Consistent with this hypothesis is the observation that ascending axons from visual thalamus pass over their preferred target regions when the subplate neurons beneath visual neocortex are specifically ablated (Ghosh and Shatz, 1992).

Stop signals are thought to instruct the invading thalamocortical axons to cease their radial progress through the cortical laminae once they reach layer 4. The exact nature of these signals has yet to be elucidated, but it is known that thalamocortical axons are likely sensing a change in the levels of a guidance cue across layers (i.e., a gradient), rather than the absolute presence or absence of one. In culture, thalamocortical axons will only stop and connect with layer 4 neurons if their growth is oriented perpendicular to the cortical laminae; thalamocortical axons that encounter layer 4 parallel to the

cortical laminae will grow within it without stopping (Yamamoto, 2002). Importantly, lamina-specific targeting and lamina-specific growth and connectivity may not be interdependent processes. For example, Ephrin-A5 knockout mice exhibit normal laminar targeting, but severely reduced axonal branching, of thalamocortical afferents within layer 4 (Uziel et al., 2002).

Dendrite guidance is also essential to establishing forebrain connectivity, and this process is regulated by some of the same guidance molecules that regulate axon guidance. For example, Whitford and colleagues demonstrated that Slit signaling through Robo receptors can promote the outgrowth and branching of cortical neurons in culture (Whitford et al., 2002). Another study showed that Semaphorin-3A expression in superficial layers of neocortex may attract the apical dendrites of pyramidal neurons and orient them perpendicularly to the pial surface (Polleux et al., 2000). Axon and dendrite growth and guidance can be differentially mediated by conserved classes of signaling molecules, presumably because of distinct downstream signal transduction mechanisms that are specific to each cellular compartment (Jan and Jan, 2003). Similarly, distinct pyramidal neuron subtypes may signal divergently downstream of dendritic neurotrophin receptor activation, perhaps explaining the opposing effects BDNF and NT-3 on dendritic growth and branching in different neocortical layers (McAllister et al., 1997).

Through a developmental process known as “tiling”, neurons with similar functional properties communicate with each other through their dendritic arbors to ensure a complete but nonredundant occupation of receptive space in nervous system tissues. Specifically, contact-mediated and/or short-range guidance cues emitted from a dendrite are thought to repel the growth of any encroaching dendrites if they are from the

same functional class. This rule applies to dendrites that originate from either the same neuron (i.e., isoneural repulsion) or different neurons (i.e., heteroneural repulsion) (Jan and Jan, 2003). Though best studied in drosophila and the mammalian retina (Wassle et al., 1981; Grueber et al., 2002; Grueber et al., 2003; Huckfeldt et al., 2009), tiling could also underlie the function of neocortical circuits. For example, for a given visual stimulus feature such as orientation, layer 4 granule cells in primary visual cortex exhibit shifts in receptive field properties at a periodicity that conforms to the physical dimensions of the minicolumn (Mountcastle, 1997); dendritic tiling could support a morphological basis for this phenomenon by minimizing the overlap of dendritic arbors that originate from orientation-sensitive granule cells in neighboring minicolumns.

Synaptogenesis and activity-dependent refinement of minicolumnar connectivity

Carefully orchestrated outgrowth and guidance events succeed in bringing specific axonal and dendritic elements into close proximity so that the appropriate intrinsic and extrinsic connections of the neocortical minicolumn can be made. Synaptogenesis is the process by which focal junctions are made between these elements to facilitate the transmission of information between them. The axonal, or presynaptic, side of the junction consists of calcium-sensitive protein complexes, which trigger the fusion of neurotransmitter vesicles with the cell membrane upon receipt of anterogradely propagated information from the cell body, encoded as an electrical impulse (Kandel et al., 2000). Released neurotransmitter diffuses freely across a narrow synaptic cleft to be bound by ionotropic receptors at a postsynaptic dendritic site. Neurotransmitter binding allows the selective flow of ions through these receptors, thus transducing the chemical

signal into an electrical current and propagating the flow of information through the postsynaptic neuron (Kandel et al., 2000). Biochemical and ultra-structural studies have revealed complex networks of membrane and scaffolding proteins, which are integrated with the cytoskeleton through equally complex networks of linker proteins, both pre- and postsynaptically (McGee and Bredt, 2003; Okabe, 2007; Siksou et al., 2009). The observation of such an elaborate architecture evokes some basic questions about synapse development: 1) how is synaptic contact initially made? 2) is synaptogenesis induced from the pre- or postsynaptic side? 3) can any axonal or dendritic site form a synapse? and 4) how are synapses stabilized?

Synaptic contact between developing axons and dendrites is either initiated passively, through en passant contacts of their overlapping branches, or directly, through the extension of long, thin filapodial branches or their growth cones (McAllister, 2007). These initial contacts are extremely transient in nature, and very few become stabilized as synaptic sites (Niell et al., 2004). At least two reasons could explain why some contacts yield synapses and others do not: 1) highly specific mechanisms of axon and dendrite guidance are at play, which allow stereotyped circuit partners to seek each other out using soluble cues and/or cell adhesion molecules that stabilize contact and allow the recruitment of synaptic proteins, and/or 2) synaptogenesis occurs at those contacts where an *a priori* organization of either pre- or postsynaptic elements transcellularly induces the recruitment of their respective counterparts. Regarding the former postulate, there is abundant evidence that transynaptic, bidirectional signaling between cell adhesion molecules supports selective synaptogenic events (Barbe and Levitt, 1992; Fannon and Colman, 1996; Graf et al., 2004). Evidence supporting the latter postulate has recently

been obtained from experiments utilizing time-lapse imaging of fluorescently tagged pre- and postsynaptic proteins in culture models of synaptogenesis. For example, Sabo and colleagues demonstrated that vescicles containing machinery for neurotransmitter vesicle release pause and cycle repeatedly with the axonal cell membrane, and that stable contacts with dendritic filopodia were preferentially made at these pause sites (Sabo et al., 2006). A similar experimental design was also used to show that stationary clusters of postsynaptic proteins, including the scaffolding protein Neuroligin-1, transcellularly recruit actively recycling neurotransmitter vesicles to directly apposed foci in contacted axons (Gerrow et al., 2006). Collectively, these findings indicate that synaptogenesis can be induced both pre- and postsynaptically, and that specific axonal and dendritic sites become "predestined" to form synapses (**Fig. 6A,B**) (McAllister, 2007).

What factors contribute to the stabilization and maturation of a newly formed synapse? In purely descriptive, morphological terms, the maturation of a nascent excitatory synapse requires the transformation of axonal elements into presynaptic terminals and dendritic elements into dendritic spines. Marked increases in pre- and postsynaptic protein localization are necessary, but beyond the initial recruitment of the presynaptic release machinery and postsynaptic neurotransmitter receptors, the precise blueprint for constructing (or deconstructing) a mature synapse is unknown (McAllister, 2007). What is known is that synapse maturation correlates with increases in synaptic size and strength (i.e., the efficacy of neurotransmission), whereas opposing changes occur in a synapse that is being eliminated or "pruned". In all nervous systems, including the mammalian forebrain, the total synaptic population at any single time-point is comprised of strong/stabilizing and weak/destabilizing types of synapses, with the

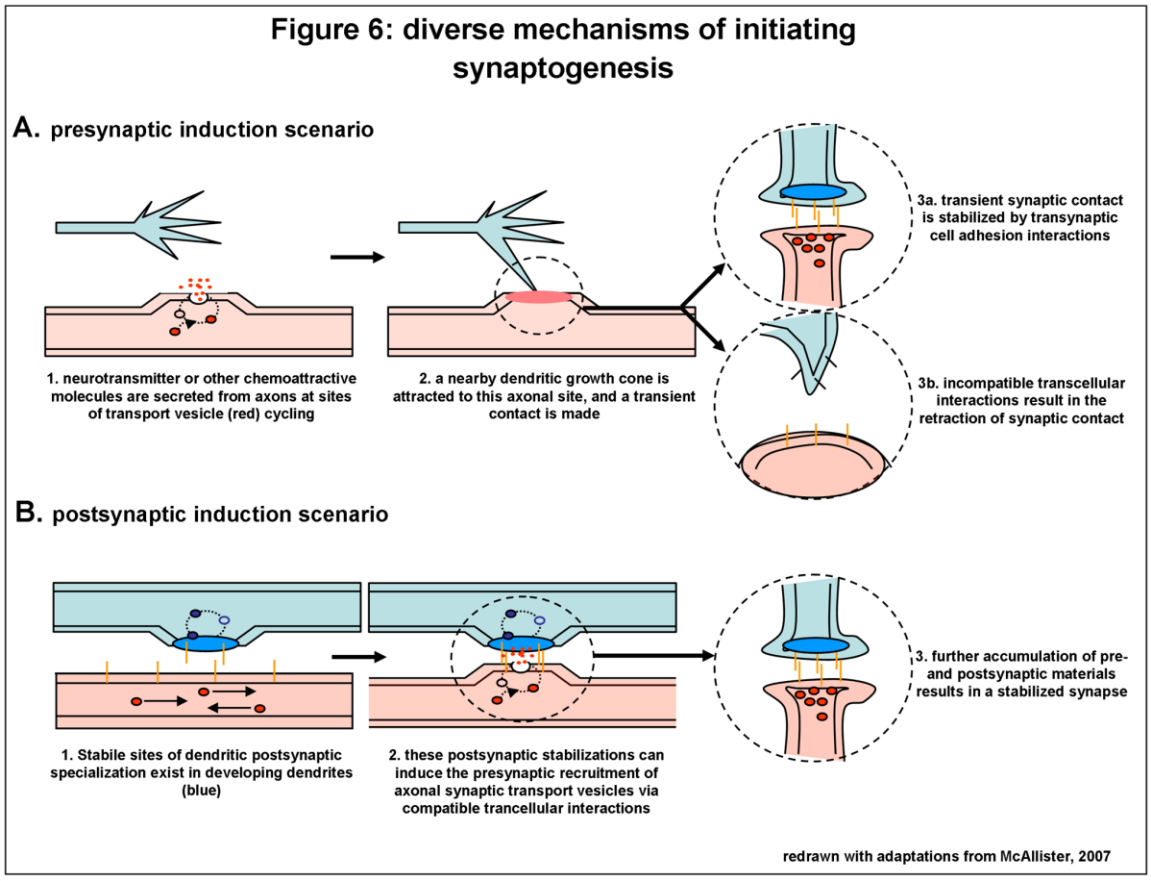

relative capacity for change toward either type described as "plasticity". Robust periods of plasticity in the developing mammalian forebrain are essential to translating experience-driven neuronal activity into changes in connectivity that will support adaptive behavioral responses in a maturing individual (Hensch, 2003; Knudsen, 2004).

Ocular dominance plasticity is by far the best characterized example of adaptive plasticity within columnar modules of the mammalian neocortex. In the primary visual cortex of carnivores and primates, thalamocortical axons transducing right-eye and left-eye visual information target segregated populations of layer 4 granule cells in arrays of adjacent macrocolumns (Katz and Crowley, 2002). The thalamocortical inputs representing each eye typically impinge upon neocortical territories of equivalent size,

but this can change dramatically should an eye become deprived of visual input during developmental periods of heightened neocortical plasticity. In their seminal work, Hubel and Wiesel demonstrated that monocular deprivation (MD) in cats, when applied within a critical 3-4 week period postnatally, results in a large increase in the proportion of visual cortical neurons responding to inputs from the intact (i.e., dominant) eye and a concomitant decrease in that responding to deprived eye inputs (Hubel and Wiesel, 1970; Sawtell et al., 2003). Moreover, they reported that the recovery of deprived eye vision subsequent to the removal of the (MD) was minimal if it occurred beyond the critical period. This does not mean that mature, adult animals lack a capacity for cortical plasticity. In fact, though mechanistically distinct from juvenile plasticity, adult ocular dominance plasticity has recently been demonstrated in mice (Sawtell et al., 2003; Hofer et al., 2006). Plasticity later in life, however, is most certainly constrained by the outcomes of preceding critical periods (Knudsen, 2004). For example using the feline MD paradigm, Shatz and Stryker showed expansions in the dominant eye thalamocortical projection and corresponding retractions in the deprived eye projection, indicating that the poor deprived eye recovery seen in mature animals after the cessation of MD is in large part due to there being too few remaining connections to strengthen (Shatz and Stryker, 1978). The rearrangement of thalamocortical projections subsequent to MD exemplifies a very common theme in the development of connectivity. That is, patterned activity strengthens strong connections and results in a further weakening or elimination of weak connections. However, decreased activity does sometimes result in paradoxical, homeostatic increases in growth and connectivity, and *vice versa*. Such responses may be most relevant to earlier developmental periods when pre- and postsynaptic elements

are still making initial contact (Lund et al., 1991; McAllister et al., 1996; Tripodi et al., 2008).

Forebrain circuit abnormalities in neurodevelopmental disorders: focus on autism spectrum disorders

Down's syndrome, Rett Syndrome, autism spectrum disorders (ASD) and virtually all neurodevelopmental disorders are defined by deficits in higher-order forebrain functions that unfold as an individual develops. Because appropriate forebrain function depends on the integrity of the underlying forebrain circuitry, it is accepted that neurodevelopmental disorders share in common an aberrant or insufficient establishment of forebrain connectivity. Presumably, the ontogeny of disrupted forebrain connectivity- that is, when, how, and which specific circuits are affected- dictates the presentation of clinical phenotypes that characterize each neurodevelopmental disorder.

Connectivity-based etiological hypotheses for ASD are rooted in the earliest clinical history of the disorder. In 1943, Kanner first published a clinical description of the related disorders we now know as ASD, which led to the identification of a defining triad of core features that includes impaired social interaction, communication deficits, and repetitive and restricted interests and behaviors (Kanner and Eisenberg, 1957; American Psychiatric Association. and American Psychiatric Association. Task Force on DSM-IV., 2000). Kanner's descriptions also evoked conceptualizations relating to the causes of the disorder. For instance, he noted in affected individuals, "the inability to experience wholes without full attention to the constituent parts", which seems to comport with Frith's weak central coherence theory that states that individuals with ASD tend to process detailed situational elements without recognizing relationships between

them (Happe and Frith, 1996). For example, as compared to typically developing or intellectually disabled children, individuals with ASD are expert at remembering random word strings, but poor at recalling meaningful sentences of a similar length (Tager-Flusberg, 1996). Recognition of this cognitive style prompted a testable hypothesis concerning the state of forebrain circuitry in ASD. Namely, that local connectivity (e.g., synapses within or between nearby minicolumns) is enhanced at the expense of long-range connectivity (e.g., synapses linking distant, functionally related minicolumns to each other or other forebrain structures) (**Fig. 1F**).

Recent functional data support predictions of global hypo-connectivity in forebrain circuits in ASD. Functional magnetic resonance imaging (fMRI) during either face processing or sentence comprehension tasks revealed reduced prefrontal activation relative to other cortical areas in the brains of individuals with autism (Just et al., 2004; Koshino et al., 2008). More recent magnetoencephalographic analyses of high-functioning children with ASD showed they have enhanced parietal lobe synchrony and decreased prefrontal lobe synchrony relative to typically developing children during the performance of executive function tasks (Perez Velazquez et al., 2009). Collectively, these and other studies indicate that long-range circuits between the frontal cortices and other brain regions are functionally disconnected in ASD (Geschwind and Levitt, 2007).

High-resolution structural imaging and postmortem anatomical analyses have been applied to assess morphological correlates of local hyper-connectivity and global hypo-connectivity in ASD. Morphological evidence of abnormal local circuitry in ASD has come almost exclusively from post mortem anatomical studies, which show minicolumns to be narrower and more numerous in several cortical areas within autistic

brains (Casanova et al., 2002) (**Fig. 1D,E**). This pathological feature is consistent with the local bias in neocortical activation in ASD as revealed by fMRI, and it also portends structural abnormalities at the single cell level, including reduced pyramidal dendritic arbor size, which lend themselves to further postmortem study (Amaral et al., 2008). Volumetric MRI and diffusion tensor imaging (DTI) of the corpus callosum indicate fewer and less organized interhemispheric connections in ASD. Studies employing MRI-based volumetry have revealed varying decreases in callosal volume along the rostro-caudal extent of the structure (Piven et al., 1997; Just et al., 2007; Frazier and Hardan, 2009; Hardan et al., 2009), consistent both with disruptions in long-range connectivity in ASD and the heterogeneity of the disorder (Geschwind and Levitt, 2007). In general, these callosal volumetric deficits are corroborated by DTI data, which show increased ratios of radial to longitudinal diffusion within this fiber tract in affected individuals (Alexander et al., 2007; Keller et al., 2007). Structural studies of the corpus callosum in ASD have thus far predominated, but fMRI data indicate that similar studies of intrahemispheric long-range projections also are warranted (Folstein and Rutter, 1977; Steffenburg et al., 1989; Just et al., 2007).

ASD-associated genes: understanding etiological mechanisms at the level of forebrain connectivity

Heritability and heterogeneity are two defining characteristics of ASD. Strong genetic heritability in ASD is evident from traditional twin studies, which have demonstrated concordance values between 50-91% for monozygotic twins and 0% for dizygotic twins (Folstein and Rutter, 1977; Steffenburg et al., 1989). However, in both general and extreme populations, bivariate concordance among individual traits of the

ASD triad (e.g., social impairment and communication impairment or social impairment and restrictive and repetitive behaviors and interests) has proven to be modest, indicating that distinct groups of genes may influence each trait (Ronald et al., 2006a; Ronald et al., 2006b). This is consistent with heterogeneity in both the severity of core deficits and the comorbidity of disorders such as mental retardation and seizures in ASD (Geschwind and Levitt, 2007). Understanding how different groups of ASD risk genes yield the developmental disruptions in forebrain connectivity that result in distinct subtypes of ASD is an outstanding challenge.

Two genetic models, which do not exclude each other, may be useful in conceptualizing etiological mechanisms of ASD that account for the heterogeneity of the disorder. First, risk genes may selectively confer vulnerability to developing circuitry that relates to a specific ASD core deficit. In this case, enhanced vulnerability to ASD would require the inheritance or *de novo* occurrence of risk genes related to each of the three core features of the disorder; vulnerability to a specific subtype of ASD would depend on the degree of risk incurred for one core deficit relative to the others as well as the co-occurrence of exacerbating genetic and/or environmental factors that might otherwise more broadly impact forebrain connectivity. A second model dictates that large groups of ASD-associated gene variants and mutations may, through epistatic relationships, converge on signaling pathways that generally impact the social and emotional circuits that are affected in autism. Phenotypic heterogeneity in this model results from the pleiotropic functions of the risk genes in various other pathways (Bill and Geschwind, 2009). Finally, both models allow for the introduction of even further heterogeneity related to the timing of the genetic insult. For example, in the context of

the first model, two risk genes may specifically impact circuits related to social interaction but do so during distinct developmental epochs. If the expression of one gene is related to neurogenesis and expression of the other is related to a later process such as synaptogenesis, the qualitative nature of their impact on that circuitry may be quite different.

Regardless of the genetic model that is favored, significant progress in understanding the etiology of ASD will surely come from directly relating the neurobiological functions of ASD risk alleles to the development of circuits that are disrupted in the disorder. Progress in this endeavor is only just beginning to be realized. Rare mutations found to be enriched in ASD compared to controls, such as NLGN3, NLGN4, NRXN1, NRXN3, and SHANK3, are particularly exciting because of their clearly established roles in synaptogenesis and the maintenance of synaptic connectivity (Varoqueaux et al., 2006; Tabuchi et al., 2007; Hung et al., 2008; Gibson et al., 2009). However, to date, expression studies of these genes (Lim et al., 1999; Varoqueaux et al., 2006) have not provided the resolution required to understand their potential relationships to the development of forebrain circuits affected in ASD. Moreover, because the mutations are rare, expressed by only a few individuals with ASD, it is unlikely that the mutations are associated with specific subtypes of ASD. Further confusing the issue is the fact that the rare mutations of these genes have been associated with both mental retardation and ASD in the same family (Laumonnier et al., 2004). Thus, although the findings provide clues to neurobiological etiology, the contribution of these specific genes broadly to ASD, which affects 1 in 150 children, is minimal.

An example of a strong link between an ASD risk allele and potential etiological mechanisms has come from studies of the PTEN locus. In 2005, Butler and colleagues found rare loss of function mutations in the PTEN gene to associate with a subset of individuals with ASD and comorbid macrocephaly (Butler et al., 2005). Remarkably, subsequent studies in a mouse model of postnatal, forebrain-specific PTEN loss of function revealed ethologically relevant deficits in social behavior as well as macrocephaly that was due to increased dendritic and axonal arborization (Kwon et al., 2006). Excitement concerning this finding, however, is tempered by the fact that germ-line PTEN mutations are rare (>1 in 10,000) and relevant to only a few ASD cases. Etiological mechanisms that are more broadly relevant to ideopathic cases of ASD will necessarily come from studies of common ASD risk alleles.

The emergence of the Met receptor tyrosine kinase as an ASD risk gene

Allelic variants of the gene encoding the MET receptor tyrosine kinase (*MET*) have recently been identified as ASD risk factors, in the truest sense of the term. Over the past three years, four independent studies, using 7 independent family cohorts, have demonstrated the association of two allelic variants of the *MET* gene with ASD (Campbell et al., 2006; Campbell et al., 2008; Jackson et al., 2009; Sousa et al., 2009). The rs1858830-C and rs38845-A ASD-associated *MET* alleles are remarkably common, with population frequencies ranging from approximately .35-.55. Also, each allele results from a single nucleotide variation in the 5' regulatory region of the gene, which suggests that they influence ASD risk at the level of gene expression. Thus far, *in vitro* assays have shown the rs1858830-C allele to recruit different transcriptional complexes to the *MET* promoter than its ASD-protective rs1858830-G allele counterpart; with the

result being reduced MET transcriptional efficiency (Campbell et al., 2006). This finding is consistent with the reported 2-fold decrease in neocortical MET expression in ASD postmortem cases (Campbell et al., 2007). Moreover, two other genes encoding genes in the Met signaling pathway carry common alleles associated with ASD (Campbell et al., 2008). Considering that ASD is a neurodevelopmental disorder, a very basic mechanistic hypothesis concerning the relationship of *MET* and ASD risk has emerged: decreased *MET* expression during development increases the chance that forebrain circuit miswiring events characteristic of ASD will occur. Because the process of wiring together forebrain connections during development is extremely complex, further refinement of this hypothesis will require a detailed understanding of the *MET* gene products (i.e., MET proteins) and their molecular functions. A current synopsis of MET protein function in the context of neurodevelopment is presented below. General experimental directives for elucidating mechanistic relationships between MET signaling and ASD etiology and risk are also presented.

The human *MET* gene encodes the transmembrane MET receptor tyrosine kinase. This signaling enzyme is initially translated as an inactive precursor of approximately 190 kD that, via furin-dependent proteolysis, is cleaved into an α– (45 kD) and β–chain (145 kD) within late endosomes en route to the cell membrane (Komada et al., 1993). Disulfide bridges subsequently form between the α- and β-chains to yield a mature, heavily glycosylated transmembrane protein capable of transducing extracellular signals into intracellular signaling events. Specifically, MET signaling commences upon the binding of its polypeptide ligand, hepatocyte growth factor (HGF), in the extracellular space. Although HGF is a soluble protein, its local concentration, and therefore, its

availability to bind Met can be influenced by extracellular matrix molecules such as heparin sulphate (Kemp et al., 2006). HGF binding induces MET receptor oligomerization and the autophosphorylation of intracellular tyrosine residues that serve as multi-substrate docking sites for signaling adaptor proteins (Ponzetto et al., 1994). These adaptor proteins in turn facilitate the activation of several major signaling cascades including the PI3K, Erk, and P38 systems (Stefan et al., 2001; Xiao et al., 2001). The nature of MET signaling is extremely context- and cell type-dependent and reflects the pleiotropic functions of this receptor in cellular development.

Although first discovered as a proto-oncogene (Cooper et al., 1984), MET was soon after found to be involved in a variety of normal cell developmental processes including cell proliferation, migration, differentiation, and survival. MET signaling also influences development at the tissue-level. For example, the formation of duct systems within the developing pancreas, kidney, and liver is dependent upon MET signaling (Rosario and Birchmeier, 2003; Zhang and Vande Woude, 2003). Duct formation is based on the process of epithelial tubulogenesis, which requires the organization of complex interactions among many polarized cells. The exquisite coordination of interactions among polarized cells is also a dominant theme in the development of forebrain connectivity, and *in vitro* studies have recently implicated MET signaling in this process as well.

MET signaling in cells grown in vitro has been shown to potentiate virtually every aspect of neurodevelopment that is required to establish connections between forebrain neurons. Nearly all of this work has been done on neurons and tissues harvested from rodent species where, by convention, the gene and mRNA molecules are

designated as "*Met*" and the protein is designated as "Met". HGF stimulation enhances the motility of olfactory and neocortical interneurons (Powell et al., 2001; Garzotto et al., 2008) as well as that of gonadotropin hormone releasing neurons of the hypothalamus (Giacobini et al., 2007), indicating that Met signaling may regulate the migration of forebrain neurons. Met signaling also has been shown to promote the axonal outgrowth of thalamic neurons (Powell et al., 2003) and the dendritic outgrowth of neocortical and hippocampal pyramidal neurons (Gutierrez et al., 2004; Lim and Walikonis, 2008) *in vitro*. Finally, evidence that Met may influence the actual formation (Tyndall and Walikonis, 2006; Tyndall et al., 2007) and function (Akimoto et al., 2004) of synaptic connections between forebrain neurons has recently been demonstrated in dissociated hippocampal neurons and acute hippocampal slices, respectively. As discussed above, deficits in any of these processes can yield pathological alterations in forebrain patterning and circuitry. However, incorporating such a wide range of potential deficits into a conceptualization of MET-associated ASD risk is a daunting task- especially when the neurodevelopmental capacity of MET signaling to influence forebrain connectivity *in vivo* is largely unknown.

Comprehensive spatiotemporal MET expression mapping in the developing forebrain will provide an essential foundation upon which to build an understanding of MET signaling in the context of typical forebrain development as well as ASD susceptibility. Because neurodevelopment occurs in a logical, stereotyped sequence (e.g., migration necessarily occurs before synaptogenesis), knowing when the receptor is expressed during rodent and primate forebrain development will help to identify the processes to which MET signaling is most relevant. Knowing the spatial patterns of

MET expression during forebrain development is also crucial. Although the *in vitro* literature seems to indicate that MET is expressed in every neuronal subtype in the forebrain, stressful environments, perhaps like those in tissue culture systems, are known to induce and/or enhance MET expression (Honda et al., 1995; Su et al., 2007). Thus, the distribution of the receptor *in vivo* may be much more restricted. In fact, an enriched association of the rs1858830-C allele with social and communication phenotypes of ASD was recently discovered (Campbell et al., 2009), suggesting that MET signaling may be especially important for the development of forebrain circuits governing social and emotional dimensions of behavior. If this is true, a further prediction would be that comparative studies of MET receptor distribution in the developing forebrain will reflect species-specific requirements for communication and social interaction.

MET expression mapping studies also will serve to focus functional studies aimed at elucidating the consequences of developmental MET signaling disruptions on forebrain circuit development *in vivo*. For example, MET is likely expressed in both axonal and dendritic compartments, so forebrain neurons which do not express the receptor, but receive MET-expressing axonal afferents, would constitute a useful population in which to study isolated circuit-level influences of MET signaling. Mouse models that allow for the genetic ablation of Met signaling from specific populations of forebrain neurons will of course be essential to these studies. Such models also will provide an *in vivo* platform for studying Met signaling mechanisms that are pertinent to forebrain circuit development, as the protein complexes that allow Met to engage specific downstream pathways should be intact.

Literature Cited

Acker CD, Antic SD. 2009. Quantitative assessment of the distributions of membrane conductances involved in action potential backpropagation along basal dendrites. J Neurophysiol 101(3):1524-1541.

Akimoto M, Baba A, Ikeda-Matsuo Y, Yamada MK, Itamura R, Nishiyama N, Ikegaya Y, Matsuki N. 2004. Hepatocyte growth factor as an enhancer of nmda currents and synaptic plasticity in the hippocampus. Neuroscience 128(1):155-162.

Alexander AL, Lee JE, Lazar M, Boudos R, DuBray MB, Oakes TR, Miller JN, Lu J, Jeong EK, McMahon WM, Bigler ED, Lainhart JE. 2007. Diffusion tensor imaging of the corpus callosum in Autism. Neuroimage 34(1):61-73.

Allendoerfer KL, Shatz CJ. 1994. The subplate, a transient neocortical structure: its role in the development of connections between thalamus and cortex. Annu Rev Neurosci 17:185-218.

Amaral DG, Schumann CM, Nordahl CW. 2008. Neuroanatomy of autism. Trends Neurosci 31(3):137-145.

American Psychiatric Association., American Psychiatric Association. Task Force on DSM-IV. 2000. Diagnostic and statistical manual of mental disorders: DSM-IV-TR. Washington, DC: American Psychiatric Association. xxxvii, 943 p. p.

Anderson SA, Eisenstat DD, Shi L, Rubenstein JL. 1997. Interneuron migration from basal forebrain to neocortex: dependence on Dlx genes. Science 278(5337):474-476.

Angevine JB, Jr., Sidman RL. 1961. Autoradiographic study of cell migration during histogenesis of cerebral cortex in the mouse. Nature 192:766-768.

Barbe MF, Levitt P. 1992. Attraction of specific thalamic input by cerebral grafts depends on the molecular identity of the implant. Proc Natl Acad Sci U S A 89(9):3706-3710.

Bill BR, Geschwind DH. 2009. Genetic advances in autism: heterogeneity and convergence on shared pathways. Curr Opin Genet Dev 19(3):271-278.

Bonnin A, Torii M, Wang L, Rakic P, Levitt P. 2007. Serotonin modulates the response of embryonic thalamocortical axons to netrin-1. Nat Neurosci 10(5):588-597.

Bradke F, Dotti CG. 1999. The role of local actin instability in axon formation. Science 283(5409):1931-1934.

Butler MG, Dasouki MJ, Zhou XP, Talebizadeh Z, Brown M, Takahashi TN, Miles JH, Wang CH, Stratton R, Pilarski R, Eng C. 2005. Subset of individuals with autism spectrum disorders and extreme macrocephaly associated with germline PTEN tumour suppressor gene mutations. J Med Genet 42(4):318-321.

Buxhoeveden DP, Casanova MF. 2002. The minicolumn hypothesis in neuroscience. Brain 125(Pt 5):935-951.

Campbell DB, D'Oronzio R, Garbett K, Ebert PJ, Mirnics K, Levitt P, Persico AM. 2007. Disruption of cerebral cortex MET signaling in autism spectrum disorder. Ann Neurol 62(3):243-250.

Campbell DB, Li C, Sutcliffe JS, Persico AM, Levitt P. 2008. Genetic evidence implicating multiple genes in the MET receptor tyrosine kinase pathway in autism spectrum disorder. Autism Res 1(3):159-168.

Campbell DB, Sutcliffe JS, Ebert PJ, Militerni R, Bravaccio C, Trillo S, Elia M, Schneider C, Melmed R, Sacco R, Persico AM, Levitt P. 2006. A genetic variant that disrupts MET transcription is associated with autism. Proc Natl Acad Sci U S A 103(45):16834-16839.

Campbell DB, Warren D, Sutcliffe JS, Lee EB, Levitt P. 2009. Association of MET with social and communication phenotypes in individuals with autism spectrum disorder. Am J Med Genet B Neuropsychiatr Genet.

Casanova MF, Buxhoeveden DP, Switala AE, Roy E. 2002. Minicolumnar pathology in autism. Neurology 58(3):428-432.

Chilton JK. 2006. Molecular mechanisms of axon guidance. Dev Biol 292(1):13-24.

Cooper CS, Park M, Blair DG, Tainsky MA, Huebner K, Croce CM, Vande Woude GF. 1984. Molecular cloning of a new transforming gene from a chemically transformed human cell line. Nature 311(5981):29-33.

de Carlos JA, Lopez-Mascaraque L, Valverde F. 1996. Dynamics of cell migration from the lateral ganglionic eminence in the rat. J Neurosci 16(19):6146-6156.

DeFelipe J, Hendry SH, Hashikawa T, Molinari M, Jones EG. 1990. A microcolumnar structure of monkey cerebral cortex revealed by immunocytochemical studies of double bouquet cell axons. Neuroscience 37(3):655-673.

Dotti CG, Sullivan CA, Banker GA. 1988. The establishment of polarity by hippocampal neurons in culture. J Neurosci 8(4):1454-1468.

Dufour A, Seibt J, Passante L, Depaepe V, Ciossek T, Frisen J, Kullander K, Flanagan JG, Polleux F, Vanderhaeghen P. 2003. Area specificity and topography of thalamocortical projections are controlled by ephrin/Eph genes. Neuron 39(3):453-465.

Fannon AM, Colman DR. 1996. A model for central synaptic junctional complex formation based on the differential adhesive specificities of the cadherins. Neuron 17(3):423-434.

Fishell G, Mason CA, Hatten ME. 1993. Dispersion of neural progenitors within the germinal zones of the forebrain. Nature 362(6421):636-638.

Folstein S, Rutter M. 1977. Infantile autism: a genetic study of 21 twin pairs. J Child Psychol Psychiatry 18(4):297-321.

Frazier TW, Hardan AY. 2009. A meta-analysis of the corpus callosum in autism. Biol Psychiatry 66(10):935-941.

Friauf E, McConnell SK, Shatz CJ. 1990. Functional synaptic circuits in the subplate during fetal and early postnatal development of cat visual cortex. J Neurosci 10(8):2601-2613.

Garzotto D, Giacobini P, Crepaldi T, Fasolo A, De Marchis S. 2008. Hepatocyte growth factor regulates migration of olfactory interneuron precursors in the rostral migratory stream through Met-Grb2 coupling. J Neurosci 28(23):5901-5909.

Gerrow K, Romorini S, Nabi SM, Colicos MA, Sala C, El-Husseini A. 2006. A preformed complex of postsynaptic proteins is involved in excitatory synapse development. Neuron 49(4):547-562.

Geschwind DH, Levitt P. 2007. Autism spectrum disorders: developmental disconnection syndromes. Curr Opin Neurobiol 17(1):103-111.

Ghosh A, Shatz CJ. 1992. Pathfinding and target selection by developing geniculocortical axons. J Neurosci 12(1):39-55.

Giacobini P, Messina A, Wray S, Giampietro C, Crepaldi T, Carmeliet P, Fasolo A. 2007. Hepatocyte growth factor acts as a motogen and guidance signal for gonadotropin hormone-releasing hormone-1 neuronal migration. J Neurosci 27(2):431-445.
Gibson JR, Huber KM, Sudhof TC. 2009. Neuroligin-2 deletion selectively decreases inhibitory synaptic transmission originating from fast-spiking but not from somatostatin-positive interneurons. J Neurosci 29(44):13883-13897.
Gonzalez-Billault C, Avila J, Caceres A. 2001. Evidence for the role of MAP1B in axon formation. Mol Biol Cell 12(7):2087-2098.
Graf ER, Zhang X, Jin SX, Linhoff MW, Craig AM. 2004. Neurexins induce differentiation of GABA and glutamate postsynaptic specializations via neuroligins. Cell 119(7):1013-1026.
Grueber WB, Jan LY, Jan YN. 2002. Tiling of the Drosophila epidermis by multidendritic sensory neurons. Development 129(12):2867-2878.
Grueber WB, Ye B, Moore AW, Jan LY, Jan YN. 2003. Dendrites of distinct classes of Drosophila sensory neurons show different capacities for homotypic repulsion. Curr Biol 13(8):618-626.
Gutierrez H, Dolcet X, Tolcos M, Davies A. 2004. HGF regulates the development of cortical pyramidal dendrites. Development 131(15):3717-3726.
Happe F, Frith U. 1996. The neuropsychology of autism. Brain 119 (Pt 4):1377-1400.
Hardan AY, Pabalan M, Gupta N, Bansal R, Melhem NM, Fedorov S, Keshavan MS, Minshew NJ. 2009. Corpus callosum volume in children with autism. Psychiatry Res 174(1):57-61.
Hausser M, Spruston N, Stuart GJ. 2000. Diversity and dynamics of dendritic signaling. Science 290(5492):739-744.
Hensch TK. 2003. Controlling the critical period. Neurosci Res 47(1):17-22.
Hofer SB, Mrsic-Flogel TD, Bonhoeffer T, Hubener M. 2006. Lifelong learning: ocular dominance plasticity in mouse visual cortex. Curr Opin Neurobiol 16(4):451-459.
Honda S, Kagoshima M, Wanaka A, Tohyama M, Matsumoto K, Nakamura T. 1995. Localization and functional coupling of HGF and c-Met/HGF receptor in rat brain: implication as neurotrophic factor. Brain Res Mol Brain Res 32(2):197-210.
Horton AC, Yi JJ, Ehlers MD. 2006. Cell type-specific dendritic polarity in the absence of spatially organized external cues. Brain Cell Biol 35(1):29-38.
Hubel DH, Wiesel TN. 1970. The period of susceptibility to the physiological effects of unilateral eye closure in kittens. J Physiol 206(2):419-436.
Huckfeldt RM, Schubert T, Morgan JL, Godinho L, Di Cristo G, Huang ZJ, Wong RO. 2009. Transient neurites of retinal horizontal cells exhibit columnar tiling via homotypic interactions. Nat Neurosci 12(1):35-43.
Hung AY, Futai K, Sala C, Valtschanoff JG, Ryu J, Woodworth MA, Kidd FL, Sung CC, Miyakawa T, Bear MF, Weinberg RJ, Sheng M. 2008. Smaller dendritic spines, weaker synaptic transmission, but enhanced spatial learning in mice lacking Shank1. J Neurosci 28(7):1697-1708.
Jackson PB, Boccuto L, Skinner C, Collins JS, Neri G, Gurrieri F, Schwartz CE. 2009. Further evidence that the rs1858830 C variant in the promoter region of the MET gene is associated with autistic disorder. Autism Res 2(4):232-236.
Jan YN, Jan LY. 2003. The control of dendrite development. Neuron 40(2):229-242.

Jones EG. 2002. Thalamic circuitry and thalamocortical synchrony. Philos Trans R Soc Lond B Biol Sci 357(1428):1659-1673.
Just MA, Cherkassky VL, Keller TA, Kana RK, Minshew NJ. 2007. Functional and anatomical cortical underconnectivity in autism: evidence from an FMRI study of an executive function task and corpus callosum morphometry. Cereb Cortex 17(4):951-961.
Just MA, Cherkassky VL, Keller TA, Minshew NJ. 2004. Cortical activation and synchronization during sentence comprehension in high-functioning autism: evidence of underconnectivity. Brain 127(Pt 8):1811-1821.
Kandel ER, Schwartz JH, Jessell TM. 2000. Principles of neural science. New York: McGraw-Hill, Health Professions Division. xli, 1414 p. p.
Kanner L, Eisenberg L. 1957. Early infantile autism, 1943-1955. Psychiatr Res Rep Am Psychiatr Assoc(7):55-65.
Katz LC, Crowley JC. 2002. Development of cortical circuits: lessons from ocular dominance columns. Nat Rev Neurosci 3(1):34-42.
Keller TA, Kana RK, Just MA. 2007. A developmental study of the structural integrity of white matter in autism. Neuroreport 18(1):23-27.
Kemp LE, Mulloy B, Gherardi E. 2006. Signalling by HGF/SF and Met: the role of heparan sulphate co-receptors. Biochem Soc Trans 34(Pt 3):414-417.
Knudsen EI. 2004. Sensitive periods in the development of the brain and behavior. J Cogn Neurosci 16(8):1412-1425.
Komada M, Hatsuzawa K, Shibamoto S, Ito F, Nakayama K, Kitamura N. 1993. Proteolytic processing of the hepatocyte growth factor/scatter factor receptor by furin. FEBS Lett 328(1-2):25-29.
Kornack DR, Rakic P. 1998. Changes in cell-cycle kinetics during the development and evolution of primate neocortex. Proc Natl Acad Sci U S A 95(3):1242-1246.
Koshino H, Kana RK, Keller TA, Cherkassky VL, Minshew NJ, Just MA. 2008. fMRI investigation of working memory for faces in autism: visual coding and underconnectivity with frontal areas. Cereb Cortex 18(2):289-300.
Krimer LS, Goldman-Rakic PS. 2001. Prefrontal microcircuits: membrane properties and excitatory input of local, medium, and wide arbor interneurons. J Neurosci 21(11):3788-3796.
Kwon CH, Luikart BW, Powell CM, Zhou J, Matheny SA, Zhang W, Li Y, Baker SJ, Parada LF. 2006. Pten regulates neuronal arborization and social interaction in mice. Neuron 50(3):377-388.
Laumonnier F, Bonnet-Brilhault F, Gomot M, Blanc R, David A, Moizard MP, Raynaud M, Ronce N, Lemonnier E, Calvas P, Laudier B, Chelly J, Fryns JP, Ropers HH, Hamel BC, Andres C, Barthelemy C, Moraine C, Briault S. 2004. X-linked mental retardation and autism are associated with a mutation in the NLGN4 gene, a member of the neuroligin family. Am J Hum Genet 74(3):552-557.
Letinic K, Zoncu R, Rakic P. 2002. Origin of GABAergic neurons in the human neocortex. Nature 417(6889):645-649.
Lim CS, Walikonis RS. 2008. Hepatocyte growth factor and c-Met promote dendritic maturation during hippocampal neuron differentiation via the Akt pathway. Cell Signal 20(5):825-835.

Lim S, Naisbitt S, Yoon J, Hwang JI, Suh PG, Sheng M, Kim E. 1999. Characterization of the Shank family of synaptic proteins. Multiple genes, alternative splicing, and differential expression in brain and development. J Biol Chem 274(41):29510-29518.

Lindwall C, Fothergill T, Richards LJ. 2007. Commissure formation in the mammalian forebrain. Curr Opin Neurobiol 17(1):3-14.

Losonczy A, Makara JK, Magee JC. 2008. Compartmentalized dendritic plasticity and input feature storage in neurons. Nature 452(7186):436-441.

Lund JS, Holbach SM, Chung WW. 1991. Postnatal development of thalamic recipient neurons in the monkey striate cortex: II. Influence of afferent driving on spine acquisition and dendritic growth of layer 4C spiny stellate neurons. J Comp Neurol 309(1):129-140.

Lund RD, Mustari MJ. 1977. Development of the geniculocortical pathway in rats. J Comp Neurol 173(2):289-306.

Markram H. 2008. Fixing the location and dimensions of functional neocortical columns. Hfsp J 2(3):132-135.

Markram H, Toledo-Rodriguez M, Wang Y, Gupta A, Silberberg G, Wu C. 2004. Interneurons of the neocortical inhibitory system. Nat Rev Neurosci 5(10):793-807.

McAllister AK. 2007. Dynamic aspects of CNS synapse formation. Annu Rev Neurosci 30:425-450.

McAllister AK, Katz LC, Lo DC. 1996. Neurotrophin regulation of cortical dendritic growth requires activity. Neuron 17(6):1057-1064.

McAllister AK, Katz LC, Lo DC. 1997. Opposing roles for endogenous BDNF and NT-3 in regulating cortical dendritic growth. Neuron 18(5):767-778.

McGee AW, Bredt DS. 2003. Assembly and plasticity of the glutamatergic postsynaptic specialization. Curr Opin Neurobiol 13(1):111-118.

Mountcastle VB. 1997. The columnar organization of the neocortex. Brain 120 (Pt 4):701-722.

Mountcastle VB. 2003. Introduction. Computation in cortical columns. Cereb Cortex 13(1):2-4.

Nevian T, Larkum ME, Polsky A, Schiller J. 2007. Properties of basal dendrites of layer 5 pyramidal neurons: a direct patch-clamp recording study. Nat Neurosci 10(2):206-214.

Neyt C, Welch M, Langston A, Kohtz J, Fishell G. 1997. A short-range signal restricts cell movement between telencephalic proliferative zones. J Neurosci 17(23):9194-9203.

Niell CM, Meyer MP, Smith SJ. 2004. In vivo imaging of synapse formation on a growing dendritic arbor. Nat Neurosci 7(3):254-260.

O'Donnell M, Chance RK, Bashaw GJ. 2009. Axon growth and guidance: receptor regulation and signal transduction. Annu Rev Neurosci 32:383-412.

O'Rourke NA, Dailey ME, Smith SJ, McConnell SK. 1992. Diverse migratory pathways in the developing cerebral cortex. Science 258(5080):299-302.

Okabe S. 2007. Molecular anatomy of the postsynaptic density. Mol Cell Neurosci 34(4):503-518.

Perez Velazquez JL, Barcelo F, Hung Y, Leshchenko Y, Nenadovic V, Belkas J, Raghavan V, Brian J, Garcia Dominguez L. 2009. Decreased brain coordinated activity in autism spectrum disorders during executive tasks: reduced long-range synchronization in the fronto-parietal networks. Int J Psychophysiol 73(3):341-349.

Petreanu L, Mao T, Sternson SM, Svoboda K. 2009. The subcellular organization of neocortical excitatory connections. Nature 457(7233):1142-1145.

Piven J, Bailey J, Ranson BJ, Arndt S. 1997. An MRI study of the corpus callosum in autism. Am J Psychiatry 154(8):1051-1056.

Polleux F, Morrow T, Ghosh A. 2000. Semaphorin 3A is a chemoattractant for cortical apical dendrites. Nature 404(6778):567-573.

Ponzetto C, Bardelli A, Zhen Z, Maina F, dalla Zonca P, Giordano S, Graziani A, Panayotou G, Comoglio PM. 1994. A multifunctional docking site mediates signaling and transformation by the hepatocyte growth factor/scatter factor receptor family. Cell 77(2):261-271.

Porter JT, Johnson CK, Agmon A. 2001. Diverse types of interneurons generate thalamus-evoked feedforward inhibition in the mouse barrel cortex. J Neurosci 21(8):2699-2710.

Powell EM, Mars WM, Levitt P. 2001. Hepatocyte growth factor/scatter factor is a motogen for interneurons migrating from the ventral to dorsal telencephalon. Neuron 30(1):79-89.

Powell EM, Muhlfriedel S, Bolz J, Levitt P. 2003. Differential regulation of thalamic and cortical axonal growth by hepatocyte growth factor/scatter factor. Dev Neurosci 25(2-4):197-206.

Quinn CC, Wadsworth WG. 2008. Axon guidance: asymmetric signaling orients polarized outgrowth. Trends Cell Biol 18(12):597-603.

Rakic P. 1977. Prenatal development of the visual system in rhesus monkey. Philos Trans R Soc Lond B Biol Sci 278(961):245-260.

Rakic P. 1988. Specification of cerebral cortical areas. Science 241(4862):170-176.

Rakic P. 2009. Evolution of the neocortex: a perspective from developmental biology. Nat Rev Neurosci 10(10):724-735.

Ronald A, Happe F, Bolton P, Butcher LM, Price TS, Wheelwright S, Baron-Cohen S, Plomin R. 2006a. Genetic heterogeneity between the three components of the autism spectrum: a twin study. J Am Acad Child Adolesc Psychiatry 45(6):691-699.

Ronald A, Happe F, Price TS, Baron-Cohen S, Plomin R. 2006b. Phenotypic and genetic overlap between autistic traits at the extremes of the general population. J Am Acad Child Adolesc Psychiatry 45(10):1206-1214.

Rosario M, Birchmeier W. 2003. How to make tubes: signaling by the Met receptor tyrosine kinase. Trends Cell Biol 13(6):328-335.

Rubio-Garrido P, Perez-de-Manzo F, Porrero C, Galazo MJ, Clasca F. 2009. Thalamic input to distal apical dendrites in neocortical layer 1 is massive and highly convergent. Cereb Cortex 19(10):2380-2395.

Sabo SL, Gomes RA, McAllister AK. 2006. Formation of presynaptic terminals at predefined sites along axons. J Neurosci 26(42):10813-10825.

Sawtell NB, Frenkel MY, Philpot BD, Nakazawa K, Tonegawa S, Bear MF. 2003. NMDA receptor-dependent ocular dominance plasticity in adult visual cortex. Neuron 38(6):977-985.

Serafini T, Colamarino SA, Leonardo ED, Wang H, Beddington R, Skarnes WC, Tessier-Lavigne M. 1996. Netrin-1 is required for commissural axon guidance in the developing vertebrate nervous system. Cell 87(6):1001-1014.

Shatz CJ, Luskin MB. 1986. The relationship between the geniculocortical afferents and their cortical target cells during development of the cat's primary visual cortex. J Neurosci 6(12):3655-3668.

Shatz CJ, Stryker MP. 1978. Ocular dominance in layer IV of the cat's visual cortex and the effects of monocular deprivation. J Physiol 281:267-283.

Shepherd GM, Stepanyants A, Bureau I, Chklovskii D, Svoboda K. 2005. Geometric and functional organization of cortical circuits. Nat Neurosci 8(6):782-790.

Shu T, Sundaresan V, McCarthy MM, Richards LJ. 2003. Slit2 guides both precrossing and postcrossing callosal axons at the midline in vivo. J Neurosci 23(22):8176-8184.

Sidman RL, Rakic P. 1973. Neuronal migration, with special reference to developing human brain: a review. Brain Res 62(1):1-35.

Siksou L, Triller A, Marty S. 2009. An emerging view of presynaptic structure from electron microscopic studies. J Neurochem 108(6):1336-1342.

Sousa I, Clark TG, Toma C, Kobayashi K, Choma M, Holt R, Sykes NH, Lamb JA, Bailey AJ, Battaglia A, Maestrini E, Monaco AP. 2009. MET and autism susceptibility: family and case-control studies. Eur J Hum Genet 17(6):749-758.

Stefan M, Koch A, Mancini A, Mohr A, Weidner KM, Niemann H, Tamura T. 2001. Src homology 2-containing inositol 5-phosphatase 1 binds to the multifunctional docking site of c-Met and potentiates hepatocyte growth factor-induced branching tubulogenesis. J Biol Chem 276(5):3017-3023.

Steffenburg S, Gillberg C, Hellgren L, Andersson L, Gillberg IC, Jakobsson G, Bohman M. 1989. A twin study of autism in Denmark, Finland, Iceland, Norway and Sweden. J Child Psychol Psychiatry 30(3):405-416.

Su W, Xing R, Guha A, Gutmann DH, Sherman LS. 2007. Mice with GFAP-targeted loss of neurofibromin demonstrate increased axonal MET expression with aging. Glia 55(7):723-733.

Tabuchi K, Blundell J, Etherton MR, Hammer RE, Liu X, Powell CM, Sudhof TC. 2007. A neuroligin-3 mutation implicated in autism increases inhibitory synaptic transmission in mice. Science 318(5847):71-76.

Tager-Flusberg H. 1996. Brief report: current theory and research on language and communication in autism. J Autism Dev Disord 26(2):169-172.

Takahashi T, Nowakowski RS, Caviness VS, Jr. 1996. The leaving or Q fraction of the murine cerebral proliferative epithelium: a general model of neocortical neuronogenesis. J Neurosci 16(19):6183-6196.

Takahashi T, Nowakowski RS, Caviness VS, Jr. 1997. The mathematics of neocortical neuronogenesis. Dev Neurosci 19(1):17-22.

Torii M, Levitt P. 2005. Dissociation of corticothalamic and thalamocortical axon targeting by an EphA7-mediated mechanism. Neuron 48(4):563-575.

Tripodi M, Evers JF, Mauss A, Bate M, Landgraf M. 2008. Structural homeostasis: compensatory adjustments of dendritic arbor geometry in response to variations of synaptic input. PLoS Biol 6(10):e260.

Tyndall SJ, Patel SJ, Walikonis RS. 2007. Hepatocyte growth factor-induced enhancement of dendritic branching is blocked by inhibitors of N-methyl-D-aspartate receptors and calcium/calmodulin-dependent kinases. J Neurosci Res 85(11):2343-2351.

Tyndall SJ, Walikonis RS. 2006. The receptor tyrosine kinase Met and its ligand hepatocyte growth factor are clustered at excitatory synapses and can enhance clustering of synaptic proteins. Cell Cycle 5(14):1560-1568.

Uziel D, Muhlfriedel S, Zarbalis K, Wurst W, Levitt P, Bolz J. 2002. Miswiring of limbic thalamocortical projections in the absence of ephrin-A5. J Neurosci 22(21):9352-9357.

Varoqueaux F, Aramuni G, Rawson RL, Mohrmann R, Missler M, Gottmann K, Zhang W, Sudhof TC, Brose N. 2006. Neuroligins determine synapse maturation and function. Neuron 51(6):741-754.

Wassle H, Peichl L, Boycott BB. 1981. Dendritic territories of cat retinal ganglion cells. Nature 292(5821):344-345.

Whitford KL, Marillat V, Stein E, Goodman CS, Tessier-Lavigne M, Chedotal A, Ghosh A. 2002. Regulation of cortical dendrite development by Slit-Robo interactions. Neuron 33(1):47-61.

Witte H, Neukirchen D, Bradke F. 2008. Microtubule stabilization specifies initial neuronal polarization. J Cell Biol 180(3):619-632.

Xiao GH, Jeffers M, Bellacosa A, Mitsuuchi Y, Vande Woude GF, Testa JR. 2001. Anti-apoptotic signaling by hepatocyte growth factor/Met via the phosphatidylinositol 3-kinase/Akt and mitogen-activated protein kinase pathways. Proc Natl Acad Sci U S A 98(1):247-252.

Yamamoto N. 2002. Cellular and molecular basis for the formation of lamina-specific thalamocortical projections. Neurosci Res 42(3):167-173.

Yanez IB, Munoz A, Contreras J, Gonzalez J, Rodriguez-Veiga E, DeFelipe J. 2005. Double bouquet cell in the human cerebral cortex and a comparison with other mammals. J Comp Neurol 486(4):344-360.

Yoshikawa S, McKinnon RD, Kokel M, Thomas JB. 2003. Wnt-mediated axon guidance via the Drosophila Derailed receptor. Nature 422(6932):583-588.

Zhang YW, Vande Woude GF. 2003. HGF/SF-met signaling in the control of branching morphogenesis and invasion. J Cell Biochem 88(2):408-417.

CHAPTER II

DYNAMIC GENE AND PROTEIN EXPRESSION PATTERNS OF THE AUTISM-ASSOCIATED MET RECEPTOR TYROSINE KINASE IN THE DEVELOPING MOUSE FOREBRAIN

Matthew C. Judson[3,*], Mica Y. Bergman[3,*], Daniel B. Campbell[1,2], Kathie L. Eagleson[1,2] and Pat Levitt[1,2]

[1]Vanderbilt Kennedy Center for Research on Human Development, [2]Department of Pharmacology and [3]Graduate Program in Neuroscience

Vanderbilt University Medical Center
Nashville, TN 37203

[*]These authors contributed equally to this work

Correspondence to:
Pat Levitt, Ph.D.
Vanderbilt Kennedy Center for Research on Human Development
PO Box 40 Peabody
Nashville, TN 37203
615-322-8242
615-322-5910 (fax)
pat.levitt@vanderbilt.edu

Grant sponsor: National Institutes of Health (NIH)/National Insitute of Mental Health (NIMH); Grant number MH67842 (PL); Grant Sponsor: NIH/National Institute of Child Health and Human Development; Grant number: P30 HD15052; Grant sponsor: NIH/NIMH; Grant number MH083474 (MYB); and Funds from the Annette Schaffer Eskind Endowed Chair (PL).

Abstract

The establishment of appropriate neural circuitry depends upon the coordination of multiple developmental events across space and time. These events include proliferation, migration, differentiation, and survival - all of which can be mediated by hepatocyte growth factor (HGF) signaling through the Met receptor tyrosine kinase. We previously found a functional promoter variant of the *MET* gene to be associated with autism spectrum disorder, suggesting that forebrain circuits governing social and emotional function may be especially vulnerable to developmental disruptions in HGF/Met signaling. However, little is known about the spatiotemporal distribution of Met expression in the forebrain during the development of such circuits. To advance our understanding of the neurodevelopmental influences of Met activation, we employed complementary Western blotting, *in situ* hybridization and immunohistochemistry to comprehensively map Met transcript and protein expression throughout perinatal and postnatal development of the mouse forebrain. Our studies reveal complex and dynamic spatiotemporal patterns of expression during this period. Spatially, *Met* transcript is localized primarily to specific populations of projection neurons within the neocortex and in structures of the limbic system, including the amygdala, hippocampus and septum. Met protein appears to be principally located in axon tracts. Temporally, peak expression of transcript and protein occurs during the second postnatal week. This period is characterized by extensive neurite outgrowth and synaptogenesis, supporting a role for the receptor in these processes. Collectively, these data suggest that Met signaling may be necessary for the appropriate wiring of forebrain circuits with particular relevance to social and emotional dimensions of behavior.

Introduction

The Met receptor tyrosine kinase is a pleiotropic, α,β-heterodimeric transmembrane protein that was first discovered as a proto-oncogene (Cooper et al., 1984), and soon after found to be involved in a number of normal physiological processes. The Met receptor and its endogenous ligand, hepatocyte growth factor (HGF), are expressed in the developing and adult nervous systems, and signal to mediate multiple neurodevelopmental and neurophysiological processes, including peripheral and central neuron survival (Hamanoue et al., 1996; Zhang et al., 2000), migration (Powell et al., 2001; Giacobini et al., 2007; Garzotto et al., 2008), axon guidance (Ebens et al., 1996; Caton et al., 2000; Powell et al., 2003), dendritic arborization (Gutierrez et al., 2004; Lim and Walikonis, 2008), and synapse maturation and activity (Akimoto et al., 2004; Tyndall and Walikonis, 2006; Tyndall et al., 2007). Deficits in any of these processes can yield pathological alterations in brain patterning and circuitry. It is of particular note, therefore, that the human orthologue, *MET*, is located on chromosome 7q31, a region implicated in autism spectrum disorder (ASD) (IMGSAC, 1998; Ashley-Koch et al., 1999; Barrett et al., 1999; Yonan et al., 2003), and a large family-based genetic analysis determined that an allelic variant in the 5' promoter region of *MET* is associated with ASD, increasing risk approximately 2.25 fold (Campbell et al., 2006). Furthermore, postmortem tissue analyses revealed an approximately two-fold reduction in MET protein expression in the temporal neocortex of ASD subjects compared to unaffected controls (Campbell et al., 2007).

Roles for Met in the development of the diencephalon and telencephalon have been demonstrated *in vitro*. In the diencephalon, Met signaling is required for migration

of gonadotropin hormone-releasing hormone-1 neurons from the nasal placode to the hypothalamus (Giacobini et al., 2007), and HGF has both growth-promoting and chemoattractive influences on axons from thalamic explants (Powell et al., 2003). In the telencephalon, Met disruption diminishes the elaboration of dendritic arbors in cortical organotypic cultures (Gutierrez et al., 2004), while HGF enhances dendritic outgrowth and excitatory synaptic development of dissociated hippocampal neurons (Tyndall and Walikonis, 2006; Nakano et al., 2007; Tyndall et al., 2007; Lim and Walikonis, 2008), and stimulates the motility of developing interneurons from basal forebrain explants (Powell et al., 2001).

These *in vitro* studies illustrate the developmental capacities of Met, but the extent to which they represent the neurodevelopmental roles of Met *in vivo* is unclear. To date, only two *in vivo* studies have attempted to examine the consequences of direct Met signaling manipulations in the context of mammalian forebrain development (Martins et al., 2007; Ohya et al., 2007). To place the human genetic studies in perspective and to advance our understanding of the putative neurodevelopmental influences of Met activation, we used complementary Western blotting, *in situ* hybridization and immunohistochemical approaches to comprehensively map Met transcript and protein expression throughout late embryonic and postnatal development of the mouse forebrain (E17.5– P35). We also examined protein expression patterns in mutant mice in which *Met* was conditionally deleted from structures originating from the dorsal pallium. We show here that *Met* is expressed by discrete subtypes of long-projecting neurons of the forebrain, particularly, though not exclusively, of dorsal pallial origin, and that Met protein is enriched in the developing axons of these cells. Moreover, we demonstrate that

the peak of Met expression in these cell populations coincides with principal periods of axon outgrowth and synaptogenesis, supporting a functional role for Met signaling in the development of forebrain connectivity.

Materials and Methods

Breeding and genotyping mice

C57BL/6^J mice were purchased from the Jackson Laboratory (Bar Harbor, ME, USA). Conditional Met mutant mice ($Emx1^{cre}/Met^{fx/fx}$) were generated by mating mice homozygous for a Met allele, in which exon 16 is flanked by loxP sites (Huh et al., 2004) ($Met^{fx/fx}$, courtesy of Dr. Snorri Thorgeirsson, NIH/Center for Cancer Research, Bethesda, MD) to Emx1-cre mice (Gorski et al., 2002) (courtesy of Dr. Kevin Jones, University of Colorado, Boulder, CO) that were also heterozygous for the floxed allele ($Emx1^{cre}/Met^{fx/+}$). Both $Met^{fx/fx}$ and $Emx1^{cre}/Met^{fx/+}$ breeding lines were back-crossed onto the C57BL/6^J background for greater than 10 generations, and their progeny (i.e., $Emx1^{cre}/Met^{fx/fx}$ and littermate control mice), were genotyped via polymerase chain reaction (PCR). The PCR primer sets were as follows: $Emx1^{cre}$ forward 5'-TTCGGCTATACGTAACAGGG-3' and reverse 5'-TGCATGCAACGAGTGATGAG-3'; Met^{fx} forward 5'-GCAACTGTCTTTTGATCCCTGC-3' and reverse 5'-TGTCCAGCAAAGTCCCATGATAG-3'. For the $Emx1^{cre}$ reaction, DNA samples are submitted to an initial denaturation step of 5 minutes at 94°C, then 35 amplification cycles [(denaturation: 94°C for 45 seconds), (annealing: 55°C for 30 seconds), (elongation: 72°C for 1 minute)], and then a final elongation step of 5 minutes at 72°C. The expected PCR product size is 350 bp. For the Met^{fx} reaction, DNA samples are

submitted to an initial denaturation step of 5 minutes at 94^{o}C, then 35 amplification cycles [(denaturation: 94^{o}C for 45 seconds), (annealing: 60^{o}C for 1 minute), (elongation: 72^{o}C for 2 minutes)], and then a final elongation step of 5 minutes at 72^{o}C. The expected PCR product size is 500 bp for the wild type *Met* allele and 580 bp for the *Met^{fx}* allele.

A cross-sectional approach was employed to assess patterns of *Met* transcript and total Met protein expression in the developing mouse forebrain. For each experimental methodology described, forebrains from at least 3 mice from at least two independent litters were analyzed at each developmental time point of interest. In the case of immunohistochemical studies requiring comparisons of Emx1^{cre}/Met$^{fx/fx}$ and littermates, at least 3 experimental pairs from independent litters were analyzed per time point.

All research procedures using mice were approved by the Institutional Animal Care and Use Committee at Vanderbilt University and conformed to NIH guide-lines. All efforts were made to minimize animal suffering and to reduce the number of animals used.

In situ hybridization

In situ hybridization was performed as previously described (Campbell and Levitt, 2003), with modification. Two cDNA probe templates specific to the mouse *Met* gene were generated by RT-PCR: a 1,387 bp fragment corresponding to nucleotides 2665-4051 of NM_008591 and a 1,404 bp fragment corresponding to nucleotides 37-1440 of NM_008591. Antisense and sense cRNA probes were transcribed from these templates with incorporation of ^{35}S-CTP.

Pregnant dams were deeply anesthetized with isofluorane, fetuses were harvested and the dissected brain rapidly removed, frozen in isopentane, and stored at -80^{o} C until

cryosectioning at 20 μm. Cryosections were thaw-mounted onto Superfrost Plus glass slides (Fisher) and stored at -80^{o}C.

Slide-mounted sections were postfixed in buffered 4% paraformaldehyde for 15 minutes, washed in 0.1 M phosphate-buffered saline (PBS) for 5 minutes, acetylated with 0.25% acetic anhydride in 0.1M triethanolamine-HCl/0.15 M NaCl with 0.16%HCl for 10 minutes, and washed in 2X standard saline citrate (SSC; 0.15 M NaCl, 0.015 M sodium citrate) for 1 minute. Tissue was then dehydrated in graded alcohols (50%, 70%, 95%, 100%; 1 minute incubation each), delipidated in chloroform (two 5 minute incubations), and incubated in 100% and 95% ethanol (1 minute each). Slides were dried at 37^{o}C for at least 2 hours.

Each slide was hybridized with 3 ng radiolabeled probe in 100 μl hybridization buffer (50% formamide, 0.75 M NaCl, 20 mM 1,4-piperazine diethane sulfonic acid, 10 mM EDTA, 10% dextran sulfate, 5X Denhardt's solution, 50 mM DTT, 0.2% sodium dodecyl sulfate, 100 μg/ml sonicated salmon sperm DNA, and 10 μg/ml yeast tRNA) per slide. Hybridization was performed at 55°C for 16 hours in a humid chamber.

Following hybridization, coverslips were removed in 4X SSC plus 390mM 2-mercaptoethanol and slides were incubated in this solution for 15 minutes at room temperature followed by 4X SSC without 2-mercaptoethanol for 15 minutes at room temperature. Sections were then treated with 1:1 formamide/buffer (0.6M NaCl, 40 mM Tris base, 2 mM EDTA, 0.06% HCl) at 60^{o}C for 30 minutes and washed in room temperature 2X SSC for 5 minutes. Sections were then treated with 20ug/ml RNase A in 0.5 M NaCl, 10 mM Tris, pH 8.0, and 1 mM EDTA at 37^{o}C for 30 minutes. The slides were then washed in graded salt solutions (2X, 1X, and 0.5X SSC each for 5 minutes at

room temperature, and 0.1X SSC at 65^{o}C for 30 minutes). Slides were cooled to room temperature in 0.1X SSC for 5 minutes and dipped in 60% ethanol with 0.33 M ammonium acetate. Slides were dried at 37^{o}C for 3-6 hours and exposed to X-ray film (Biomax MR; Eastman Kodak, Rochester, NY) for 3-15 days. A subset of sections were prepared for emulsion dipping, following the protocol noted in (Campbell and Levitt, 2003) and exposed for 3-6 days prior to development.

Immunohistochemistry

The primary antibody used for Met immunohistochemical study was mouse anti-Met (Met, B-2; sc-8057; lot No. C2807; Santa Cruz Biotechnology, Santa Cruz, CA; immunogen: peptide corresponding to amino acids 1330-1379 of mouse Met (NCBI# NP 032617)). Using immunoblotting methods, the antibody recognizes the recombinant Met protein (Santa Cruz), and a minor band at 170 kD and a major band at 140 kD in brain tissue homogenates (see below). These bands represent pre-processed and processed forms, respectively, of the Met receptor. Only the pre-processed band was detected in homogenates prepared from mouse neocortex in which the *Met* gene was deleted from the dorsal pallium (data not shown). A mouse monoclonal antibody, 1G9, generated in the laboratory against adult mouse hippocampal homogenates, cross-reacts specifically with phosphorylated neurofilament-H (NF-H) (Pennypacker et al., 1991), and was used to stain developing axons.

Postnatal mice were deeply anesthetized with sodium pentobarbital (60 mg/kg i.p.) prior to transcardial perfusion with room temperature phosphate-buffered 4% paraformaldehyde (pH 7.3) containing 1.3% L-lysine and 0.24% sodium periodate. After postfixation overnight at 4^{o}C, brains were cryoprotected via sequential 12-hour

incubations in 10%, 20%, and 30% sucrose in PBS, pH 7.5. Fetal brains were harvested and immersion-fixed overnight at 4^{o}C prior to cryoprotection.

Fetal and P0 fixed brains were frozen in embedding medium (Triangle Biomedical Sciences; Durham, NC) over liquid nitrogen vapors and stored at -80^{o}C until sectioned with a cryostat at 20 μM. Sections were collected on gelatin-subbed slides and stored at -80^{o}C until processed. Fixed brains from P7 through P35 were frozen, cut at 40 μM with a sliding microtome (Leica, Bannockburn, IL) and free-floating sections were stored in a cryopreservative solution at -20^{o}C until processed. One series of sections from selected brains were stained with Cresyl Violet as previously described (Hockfield, 1993).

For Met immunohistochemical processing, both cryostat and free-floating sections were rinsed in PBS and then incubated for 5 minutes in 0.5% H_20_2 in PBS to quench endogenous peroxidases. The sections were then rinsed in PBS before 25 min incubation in 0.1 M Tris-glycine (pH 7.4). Several more PBS rinses preceded a 1.5 hr incubation in unlabeled donkey anti-mouse IgG (Fab; Jackson Immunoresearch, West Grove, PA) to block endogenous mouse immunoglobulins. Sections were further blocked in several rinses of Blotto-T (4% Carnation dried milk in PBS containing 0.2% Triton-X-100). Blocked sections were incubated in primary mouse anti-Met antibody diluted 1:250 in Blotto-T. Cryosections were incubated for 2-4 hours at room temperature; free-floating sections were incubated for 48-72 hours at 4^{o}C. Following washes in Blotto-T, sections were incubated for 1 hour at room temperature in 1:1000 biotin-SP-conjugated donkey anti-mouse IgG (Jackson Immunoresearch) diluted in Blotto-T. Sections then were rinsed several times in PBS and processed by the ABC Elite histochemical method (Vector, Burlingame, CA). Met-specific antibody complexes were visualized by

incubating the sections for 2-4 minutes at room temperature in 0.05% 3'3'-diaminobenzidine (DAB) with 0.015% H_20_2. The stained sections were rinsed in PBS, and free-floating sections were mounted on gelatin coated slides. Finally, sections were dehydrated with ethanol, cleared with xylene, and coverslipped in DPX (Fisher, Pittsburgh, PA) for microscopic analysis. Phosphorylated NF-H staining was performed using a similar immunohistochemical protocol for free-floating sections, but with the following specific parameters: 1) The 1G9 primary antibody was diluted 1:200 in Blotto-T, 2) biotin –SP-conjugated donkey anti-mouse IgM secondary antibodies were diluted 1:1,000 in Blotto-T, and 3) antigen/antibody complexes were visualized using standard ABC reagents (Vector), followed by DAB histochemistry.

Western blotting

The following primary antibodies were used for Western blotting studies: rabbit anti-Met (Met; # 07-283; lot No. 27208; Millipore (Upstate), Billerica, MA; immunogen: peptide corresponding to amino acids 1361-1379 of mouse Met (NCBI# NP 032617)), mouse anti-Met (Santa Cruz, sc-8057), mouse anti-alpha-tubulin loading control (alpha-tubulin, Ab-1; # CP06; lot No. D16509-5; Oncogene Research Products, San Diego, CA; immunogen: native chick brain microtubules), mouse anti-GAPDH loading control (GAPDH; #AM4300; lot No. 08608176A; Ambion, Austin, TX; immunogen: purified rabbit muscle GAPDH).

Mice were deeply anesthetized with sodium pentobarbital (60 mg/kg i.p.) prior to decapitation and brain removal. Harvested brains were immediately immersed in room temperature Hanks' balanced salt solution (Sigma, Saint Louis, MO). With the aid of an MZ-6 stereozoom microscope (Leica), the cerebral cortex from each hemisphere was

divided evenly midway along the antero-posterior axis to generate two tissue samples. The underlying striatum also was rapidly dissected before all samples were snap-frozen on liquid nitrogen and stored at -80^{o}C.

P0 through >P90 cortical and striatal samples were prepared by homogenizing frozen tissue samples in a glass tissue homogenizer (Wheaton, Millville, NJ) with ice-cold homogenization buffer (50 mM Tris HCl, pH 8.0, 150 mM NaCl, 1% Nonidet P-40, 0.1% SDS, 0.5% deoxycholate, 0.5mM DTT , 2 mM EDTA, pH 8.0, 2 mM EGTA, 0.2mM PMSF) containing a protease inhibitor cocktail (Sigma), 50 mM activated Na_3VO_4, 100 nM microcystin, and 0.5 nM cypermethrin. E16 tissue was sonicated briefly in the same buffer. Tissue homogenates were cleared by a 16,000 x g centrifugation for 20 minutes at 4^{o}C, and protein concentrations of the supernatants were determined using the Dc protein assay (Bio-Rad, Hercules, CA).

Protein samples (35 μg protein per lane) were fractionated by SDS-PAGE and transferred to supported nitrocellulose membranes. The membranes were then blocked for 1 hr at room temperature in Blotto (3% Carnation dried milk in PBS) before being incubated with primary antibodies. Polyclonal rabbit anti-Met antibodies and alpha-tubulin antibodies were diluted 1:2500 and 1:100,000, respectively, in Blotto containing 0.05% Tween-20. Monoclonal mouse anti-Met antibodies were diluted 1:500 in Blotto alone, and GAPDH antibodies were diluted 1:200,000 in Blotto + 0.02% Tween-20. The membranes were then rinsed repeatedly in PBS and incubated for 1.5 hr at room temperature with anti-rabbit and anti-mouse horseradish peroxidase-conjugated secondary antibodies (Jackson Immunoresearch). Following several more rinses in PBS, the membranes were reacted with enhanced chemiluminescence reagents (GE/Amersham

ECL) and detected with autoradiography film (GE/Amersham hyperfilm). Autoradiographic films were imaged with a high resolution scanner and subjected to densitometric quantification using IMAGE-J.

Digital illustrations

Microscopy was performed with the aid of an Axioplan II microscope (Zeiss, Jena, Germany), and micrographs were acquired with a Zeiss AxioCam HRc camera (Zeiss) in Axiovision 4.1 software (Zeiss). No image alteration other than re-sizing was performed. Figures were prepared digitally in Microsoft Office Powerpoint 2003 (Microsoft Incorporated, Redmond, WA).

Abbreviations used in the figures

3V 3rd ventricle
AB accessory basal amygdaloid nucleus
aca anterior commissure, anterior
aci anterior commissure, intrabulbar
acp anterior commissure, posterior
AD anterodorsal thalamic nucleus
AV anteroventral thalamic nucleus
alv alveus
AOM anterior olfactory nucleus, medial
AOL anterior olfactory nucleus, lateral
B basal amygdaloid nucleus
BST bed nucleus of stria terminalis
CA1 cornu ammonis 1 of hippocampus
CA3 cornu ammonis 3 of hippocampus
cg cingulum
Cg cingulate cortex
COa anterior cortical amygdaloid nucleus
COp posterior cortical amygdaloid nucleus
cp cerebral peduncle
CP cortical plate
CPu caudate putamen (striatum)
DG dentate gyrus
dhc dorsal hippocampal commissure
DL dorsolateral thalamic nuclei
ec external capsule
En endopiriform nucleus

fi fimbria of hippocampus
GrDG granule layer of dentate gyrus
hbc habenular commissure
HDB nucleus of the diagonal band, horizontal limb
ic internal capsule
IP interpeduncular nucleus
L lateral amygdaloid nucleus
LEnt lateral entorhinal cortex
LGP lateral globus pallidus
LHb lateral habenula
LM lateral mammillary nucleus
LSD lateral septal nucleus, dorsal part
LSI lateral septal nucleus, intermediate
LSV lateral septal nucleus, ventral part
LV lateral ventricle
M medial amygdaloid nucleus
MHb medial habenula
MM medial mammillary nucleus
Mol molecular layer of hippocampus
MPO medial preoptic nucleus
MS medial septal nucleus
mt mammillothalamic tract
mtg mammillotegmental tract
NLOT nucleus of lateral olfactory tract
opt optic tract
Or oriens layer of hippocampus
Pir piriform cortex
Py pyramidal cell layer of hippocampus
Rad stratum radiatum of hippocampus
RSG retrosplenial granular cortex
S subiculum
SHy septohypothalamic nucleus
SI substantia innominata
sm stria medullaris
SP subplate
st stria terminalis
SuM supramammillary nucleus
SVZ subventricular zone, striatum
SVZC subventricular zone, cortex
vhc ventral hippocampal commissure
VL ventrolateral thalamic nuclei
VTM ventral tuberomammillary nucleu

Results

Temporal patterns of Met expression during forebrain development

Met signaling has been implicated *in vitro* in diverse neurodevelopmental processes in the forebrain, including cell migration (Powell et al., 2001; Giacobini et al., 2007; Garzotto et al., 2008), neurite outgrowth (Powell et al., 2003; Gutierrez et al., 2004; Lim and Walikonis, 2008), and synaptogenesis (Madhavan and Peng, 2006; Tyndall and Walikonis, 2006; Nakano et al., 2007), each of which occurs *in vivo* during well defined, though overlapping, temporal windows. As a first step in identifying the neurodevelopmental processes for which Met signaling may be most relevant *in vivo*, we utilized Western blotting to assess Met receptor protein expression levels in three forebrain regions across development. Anterior cortex, posterior cortex, and striatum exhibit strikingly similar temporal patterns of Met expression (**Fig. 1**). Total Met protein levels in these regions are relatively low from peak to late periods of neurogenesis (E16.5). There is a marked increase in expression levels during the perinatal period (P0), corresponding to a time when most cortical and striatal neurons have finished their migration and are actively extending both axonal and dendritic processes (Parnavelas and Uylings, 1980; Miller and Peters, 1981; Miller, 1986; Tepper and Trent, 1993; Tepper et al., 1998). Met protein expression increases dramatically between P0 and P7 (**Fig. 1**), peaking at a period coincident with extensive neurite outgrowth and the onset of synaptogenesis (Blue and Parnavelas, 1983; Micheva and Beaulieu, 1996; De Felipe et al., 1997). This is followed by a gradual decrease in Met expression during the peak period of synaptogenesis (Aghajanian and Bloom, 1967; Dyson and Jones, 1980; Blue and Parnavelas, 1983; Markus and Petit, 1987; Micheva and Beaulieu,

1996; De Felipe et al., 1997) (P14, P21). Met levels continue to decrease through the onset of puberty (P35) to reach a low baseline of expression in the adult (P90).

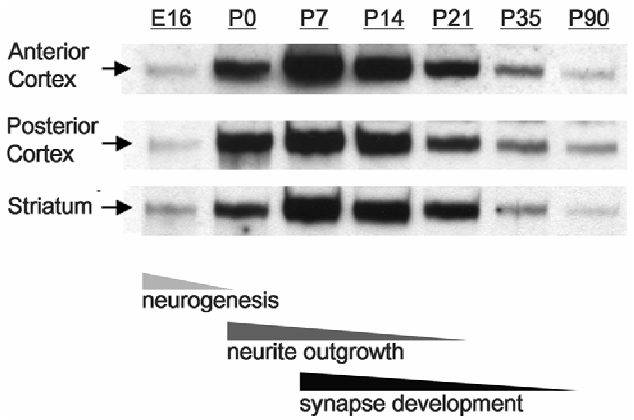

Figure 1. Western blotting analysis of Met protein expression during forebrain development in wild type mice. The temporal profile of Met expression is strikingly similar regardless of the forebrain region assayed: protein levels are relatively low embryonically (E16), but increase dramatically during perinatal development (P0) to reach a peak at P7. Levels remain high through the second postnatal week (P14), but decline dramatically thereafter (P21) to relatively low levels in the adolescent (P35) and adult (>P90). Note that peak periods of Met expression overlap with principal periods of neurite outgrowth and synaptogenesis in the mouse forebrain. Samples from each forebrain region were probed on separate blots and optimal film exposure times were independently determined.

The Western blotting data are consistent with a hypothesized role *in vivo* for Met signaling during multiple neurodevelopmental events, but especially neurite outgrowth and synaptogenesis. To gain complementary, spatially-resolved data regarding Met receptor expression, we undertook detailed *in situ* hybridization and immunohistochemistry studies. We also present immunohistochemical mapping data using tissue from *Emx1*^{cre}*/Met*$^{fx/fx}$ mice, in which the targeted deletion preferentially ablates the processed, membrane-bound form of the Met receptor from all cells arising from the dorsal pallium, including the projection neurons of the cerebral cortex, hippocampus, and select amygdaloid nuclei, by E10.5 (Gorski et al., 2002). Unlike

constitutive Met knockout mice, which exhibit early embryonic lethality (Bladt et al., 1995), *Emx1^{cre}/Met$^{fx/fx}$* mice are indistinguishable from wild type mice with regard to survival and reproductive capacity. Gross analyses also show *Emx1^{cre}/Met$^{fx/fx}$* mice to have normal cortical lamination and thickness, and normal fiber tract development (**Supplemental Fig. 1**). Thus, this targeted deletion provides an opportunity to 1) establish Met antibody specificity and 2) define more accurately the cellular origin of Met expression in axons and neuropil elements. The results of the *in situ* hybridization and immunohistochemical mapping studies are organized by neuroanatomical region in two epochs: 1) during (E17.5-P16) and 2) after (P21-P35) the rise and peak of Met expression in the forebrain. By convention, and to distinguish between mRNA and protein products, we italicize when referring to the transcript ("*Met*") and do not italicize when referring to the protein ("Met").

Expression of Met in developing projection neurons of the cerebral cortex (E17.5-P16)

We readily observed *Met* transcript to be present in the somites as well as the primordial heart, kidney, and liver as early as E11.5. However, using the specific hybridization conditions noted above, we did not reliably observe *Met* in the forebrain until E15, when low levels in the cerebral cortex were first detected. Therefore, detailed *Met* expression analyses prior to E15 are most relevant to the periphery and extra-forebrain regions of the central nervous system, and thus, are beyond the focus of the present study. At all postnatal ages examined, there was little, if any, *Met* detected in developing or mature fiber tracts. In contrast, Met protein localization revealed dense staining of developing axons in forebrain tracts (see below).

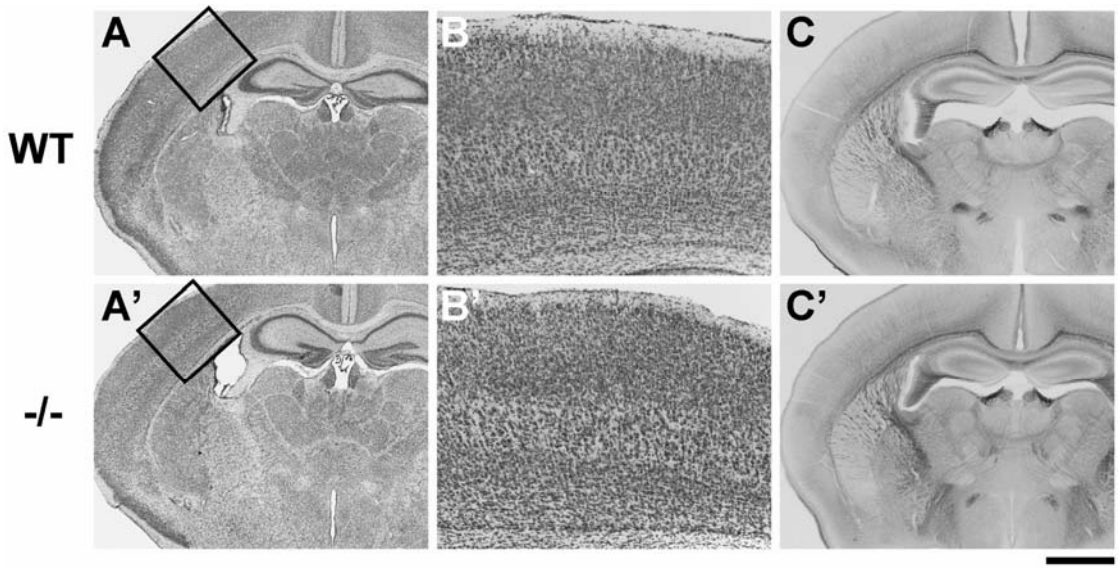

Supplemental Figure 1. Qualitative histological and cytoarchitectural analyses in the early postnatal forebrain of *Emx1*^{cre}/*Met*$^{fx/fx}$ mice. **A** and **A'**: Low-magnification photomicrographs of Cresyl Violet-stained coronal sections demonstrate grossly similar anatomical structure in wild type (**A**) and *Emx1*^{cre}/*Met*$^{fx/fx}$ (**A'**) forebrains at P8. **B** and **B'**: High-magnification photomicrographs of the boxed regions in A and A' show comparable cortical lamination and cytoarchitecture in wild type and *Emx1*^{cre}/*Met*$^{fx/fx}$ mice, respectively. **C** and **C'**: Low-magnification photomicrographs of phosphorylated neurofilament-H immunoreactivity in coronal sections illustrate the grossly normal development of major axon tracts in *Emx1*^{cre}/*Met*$^{fx/fx}$ (**C'**) mice as compared to wild type mice (**C**) at P7. Scale bar = 1.1 mm for **A**, **A'**, **C**, and **C'**; 275 μm for **B** and **B'**.

At birth, Western blot analysis reveals a more than three-fold increase in the total level of Met protein in the posterior cortex compared to the anterior cortex (**Fig. 2E**). This finding is corroborated by both i*n situ* hybridization and immunohistochemical staining (**Fig. 2A,C**). Thus, *Met* expression in the dorsal pallium exhibits a posterior (high) to anterior (low) gradient, which is most evident in the cortical plate. *Met* is also expressed in the subplate, but is relatively uniform throughout its posterior-anterior extent. Immunohistochemical staining reveals that Met expression in the cortex is localized to more posterior white matter tracts underlying the cortical plate (**Fig. 2C**). By P7, the posterior-anterior gradient of cortical Met expression abates (**Fig. 2B,D,E**). The radial distribution of Met expression in the cortex can be observed more clearly in the coronal plane. At birth, there is an emerging bi-laminar pattern of labeling (**Fig. 3A-**

C), which becomes more evident by P7 (**Fig. 3D-F**). At the transcript level, *Met* expression is most dense in layers II/III and in deeper layers V and VI, but essentially absent in layer IV (**Fig. 3D,E**). Met protein is also expressed in a bilaminar pattern, with maximal signal in the deepest portion of the cortex, where it appears to be localized to the coalescing fibers of subcortically and cortico-cortically projecting axons from throughout the cortex (**Fig. 3F**). The paucity of Met expression in layer IV is most evident in primary sensory cortices, particularly the somatosensory barrel fields; this is not surprising given the low levels of *Met* transcript in the dorsal thalamus (see below), and its absence in layer IV itself. Though the bilaminar pattern of *Met* transcript expression remains similar at P14 compared to P7, Met immunoreactivity at the later time point is substantially reduced (**Fig. 3G-I**).

Cortically Projecting Fiber Tracts (P0 – P16)

Immunohistochemical analysis during the first two weeks postnatal reveals Met protein expression in several fiber tracts, including the corpus callosum, cingulum, anterior commissure, internal capsule, and external capsule, which arise from cerebral cortical neurons expressing *Met* transcript. The level of Met expression in these tracts is dynamic over this period, as described below.

Corpus Callosum

During the perinatal period, the corpus callosum exhibits intense Met staining, though expression is limited in its rostro-caudal extent (**Fig. 4A,B)**. At the most anterior level, staining of callosal fibers is sparse, but increases in density posteriorly. At P7, the corpus callosum exhibits dense staining throughout its rostro-caudal extent (**Fig. 4C,D**).

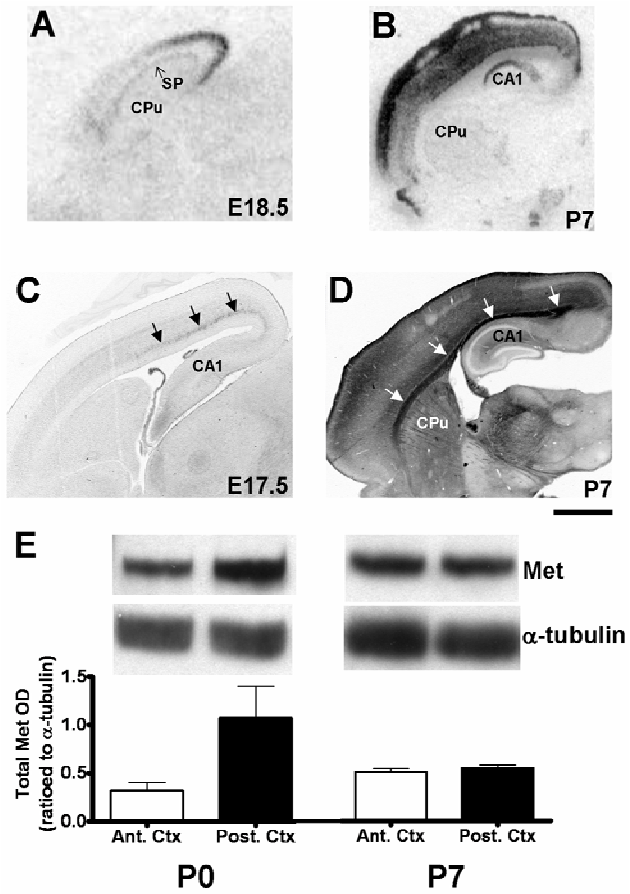

Figure 2. A transient tangential gradient of *Met* transcript and protein expression in the early postnatal neocortex. *In situ* hybridization analysis of *Met* in sagittal sections of wild type forebrain reveals a strong posterior (high) to anterior (low) gradient of signal in the neocortex, which is present at E18.5 (**A**), but normalizes by P7 (**B**). DIC photomicrographs of Met immunoreactivity in wild type sagittal sections show increased axonal labeling (arrows) in the posterior neocortex at E17.5 (**C**), but distributed axonal (arrows) and neuropil labeling throughout the anteroposterior extent by P7 (**D**). Semiquantitative Western blotting confirms the protein gradient revealed by immunohistochemistry; Met protein levels are found on average to be approximately three-fold greater in posterior versus anterior neocortex at P0 but not P7 (**E**). Error bars in **E** represent reflect standard error of the mean, N = 3 in each group. Scale bar = 925μm for **A**, 1.75mm for **B,** 550 μm for **C** and 1.1 mm for **D**.

By P14, and even more evident at P16, Met immunoreactivity in this tract becomes less **Fig. 4E-H**), and an additional pattern is observed; Met immunoreactivity is present in more dorsally situated axons at rostral levels (**Fig. 4E,G**), whereas stained fibers are localized ventrally at more caudal levels (**Fig. 4F,H**). These staining patterns may reflect

unique patterns of maturation of distinct subpopulations of cortico-cortical projection neurons during this time period.

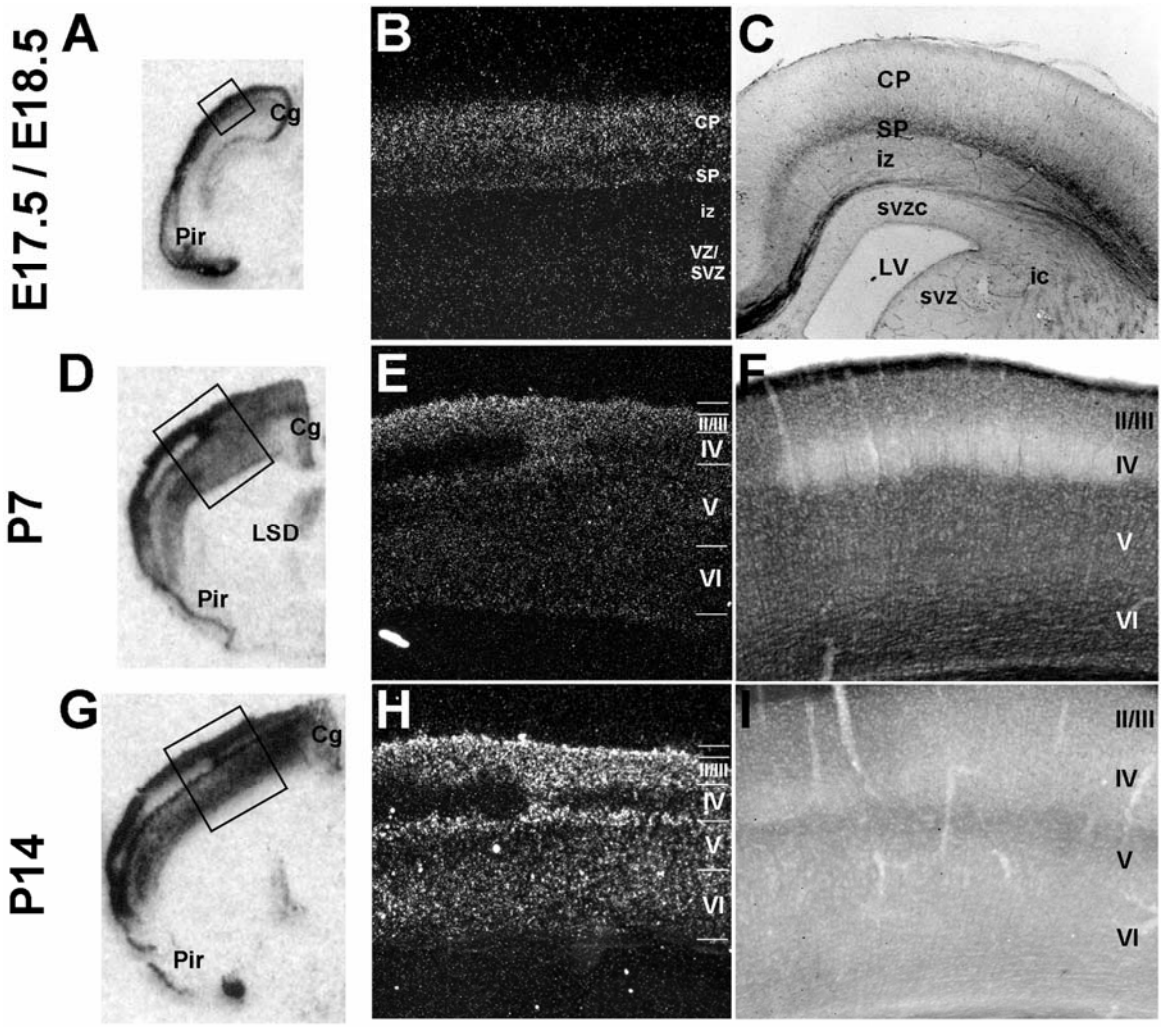

Figure 3. Laminar patterning of *Met* transcript and protein expression in the neocortex. **A, D, G**: Autoradiographic images of *Met* transcript in coronal sections from wild type mice, scanned from film. **B, E, H**: DIC photomicrographs of coronal sections from wild type mice after processing for autoradiography and emulsion-dipping. **C, F, I**: DIC photomicrographs of Met immunoreactivity in coronal sections from wild type mice. At birth, low levels of *Met* transcript (**A,B**) and protein (**C**) are present throughout the extent of the neocortex, but a bi-laminar pattern of expression is emerging. By P7 (**D,E,F**), laminar patterning is apparent, with a distinct absence of *Met* signal in layer IV. This pattern of transcript expression is maintained at P14 (**G,H**), but immunohistochemical signal is reduced at this age (**I**). Scale bar = 1.55mm for **A,D,G;** 275μm for **B,C,F,I**; 550μm for **E,H**.

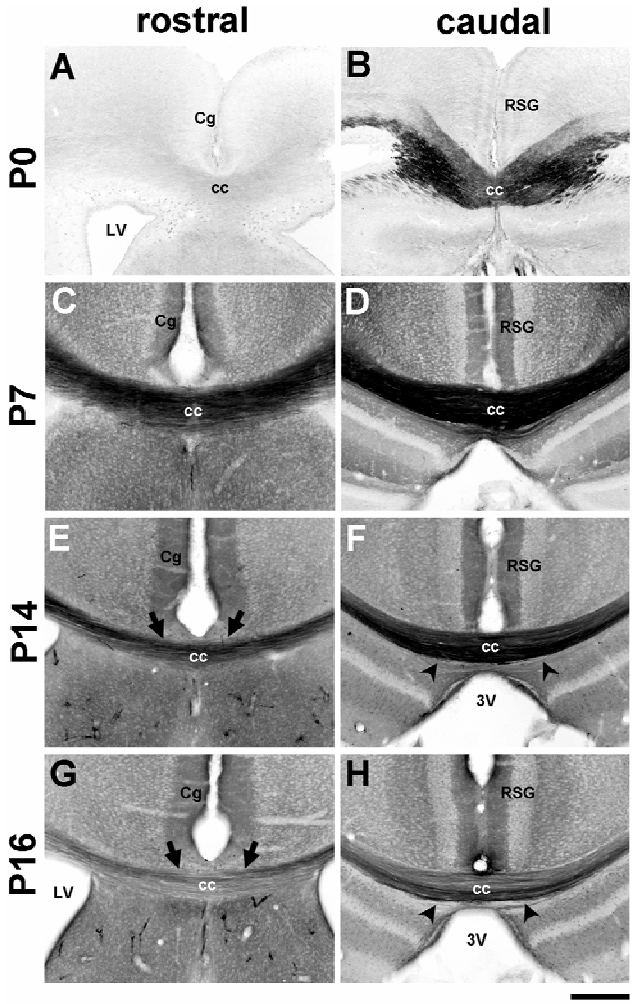

Figure 4. Met protein expression in the corpus callosum. DIC photomicrographs show Met immunoreactivity in coronal sections from wild type mice. At P0 (**A, B**), Met immunoreactivity is observed in the caudal portion of the corpus callosum, but not in the rostral region. By P7 (**C, D**), Met expression is intense throughout the rostro-caudal extent of the tract. Expression remains high, but gradually declines at P14 (**E,F**) and P16 (**G,H**). Note that at P14 and P16, Met immunoreactivity is enriched in dorsally situated axons at rostral levels (arrows) and ventrally situated axons at caudal levels (arrowheads). Scale bar = 275μm for all panels.

Cingulum

Met immunoreactivity is observed in the cingulum during postnatal development, particularly at P7 (**Supplemental Fig. 2D**). This tract contains corticothalamic and thalamocortical projections that originate and terminate, respectively, in the cingulate

cortex, is a major pathway connecting the cingulate cortices and anterior thalamic nuclei to parahippocampal structures, and carries interhemispherically projecting axons of

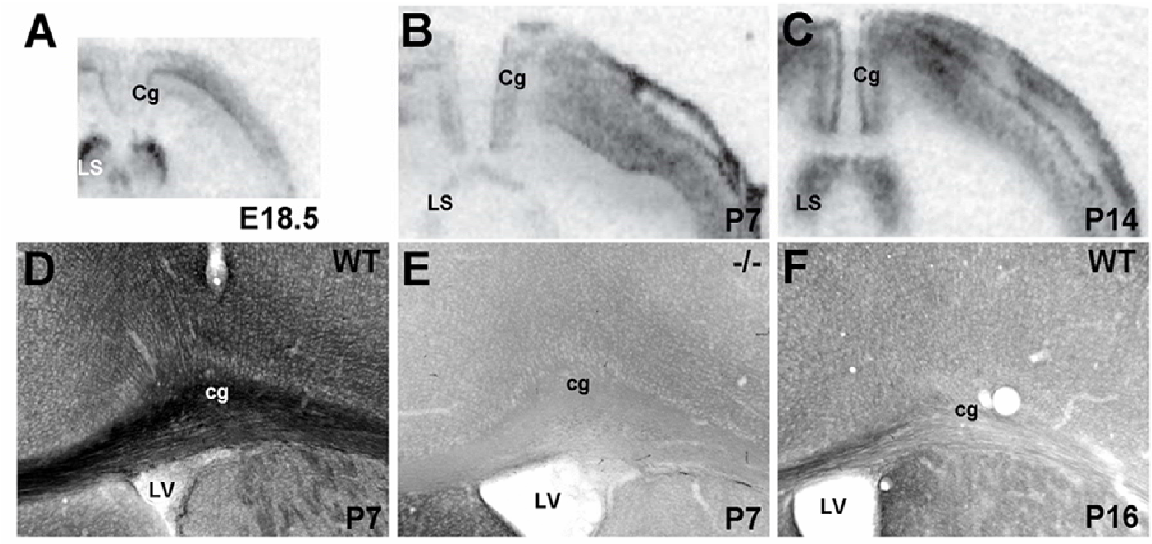

Supplemental Figure 2. *Met* transcript and protein expression in the cingulate cortex and cingulum. **A-C:** Autoradiographic images of cingulate cortex at E18.5, P7, and P14 show *Met* transcript expression. DIC photomicrographs of Met immunoreactivity demonstrate expression of the protein in the wild type (**D**), but not in the $Emx1^{cre}/Met^{fx/fx}$ (**E**) cingulum at P7. By P16 (**F**), expression is virtually absent in the wild type cingulum. Scale bar = 1.1mm for **A-C**; 275μm for **D-F**.

neurons in association cortices (White, 1959; Domesick, 1970; Mufson and Pandya, 1984; Shibata, 1993). Comparison of matched sections from wild type and $Emx1^{cre}/Met^{fx/fx}$ conditional null mice reveals an absence of cingulum staining in the mutant mice (**Supplemental Fig. 2E**), indicating that cortical efferents, not afferents, express Met in this tract. This is consistent with *Met* transcript expression in neurons of the cingulate cortex (**Supplemental Fig. 2A-C**), and its absence in primary dorsal thalamic nuclei, throughout the same developmental period. As observed in the corpus callosum, there is reduced Met immunostaining in the cingulum at later ages (P16, **Supplemental Fig. 2F**).

Anterior Commissure

The anterior commissure and the neurons that give rise to its axons exhibit substantial Met protein and transcript expression, respectively (**Fig. 5**). Met immunohistochemical labeling is apparent in both the anterior and posterior limbs of the anterior commissure, though staining is much more intense in the posterior limb, as demonstrated in coronal sections (**Fig. 5D-F**). The heavily Met-expressing axons of the posterior limb can be seen in horizontal sections coursing out of the posterior temporal cortices (**Supplemental Fig. 3A**). Staining is much lighter in fibers of the anterior limb, which emanate from the olfactory bulbs and anterior temporal cortices (**Supplemental Fig. 3B**) (Gurdjian, 1925; Brodal, 1948; Jouandet and Hartenstein, 1983). Comparison of anterior commissure staining between wild type and $Emx1^{cre}/Met^{fx/fx}$ mice confirms that the Met-expressing axons are mostly of dorsal pallial origin (**Fig. 5D'-F'**). We note, however, the presence of some residual Met-immunostained fibers in the P0 and P7 $Emx1^{cre}/Met^{fx/fx}$ posterior limb (**Fig. 5D'**). These fibers likely originate in the ventral endopiriform cortex, a region in which *Met* is not deleted due to low rates of Emx1-driven Cre recombination (Gorski et al., 2002). Met staining in the anterior commissure is reduced dramatically by P16 (**Fig. 5F**), despite continued transcript expression in the piriform cortex **(Fig 5C)**. Little, if any, protein is detected in the structure's anterior limb, whereas low levels of expression persist in the posterior limb. Comparison between staining patterns in the wild type and $Emx1^{cre}/Met^{fx/fx}$ tissue indicates that this residual expression in the posterior limb is authentic (**Fig. 5F'**).

Internal Capsule

From P0 through P7, Met protein expression is apparent in the fasciculated fibers of the internal capsule (**Fig. 6A,C**). The virtual absence of Met immunoreactivity in

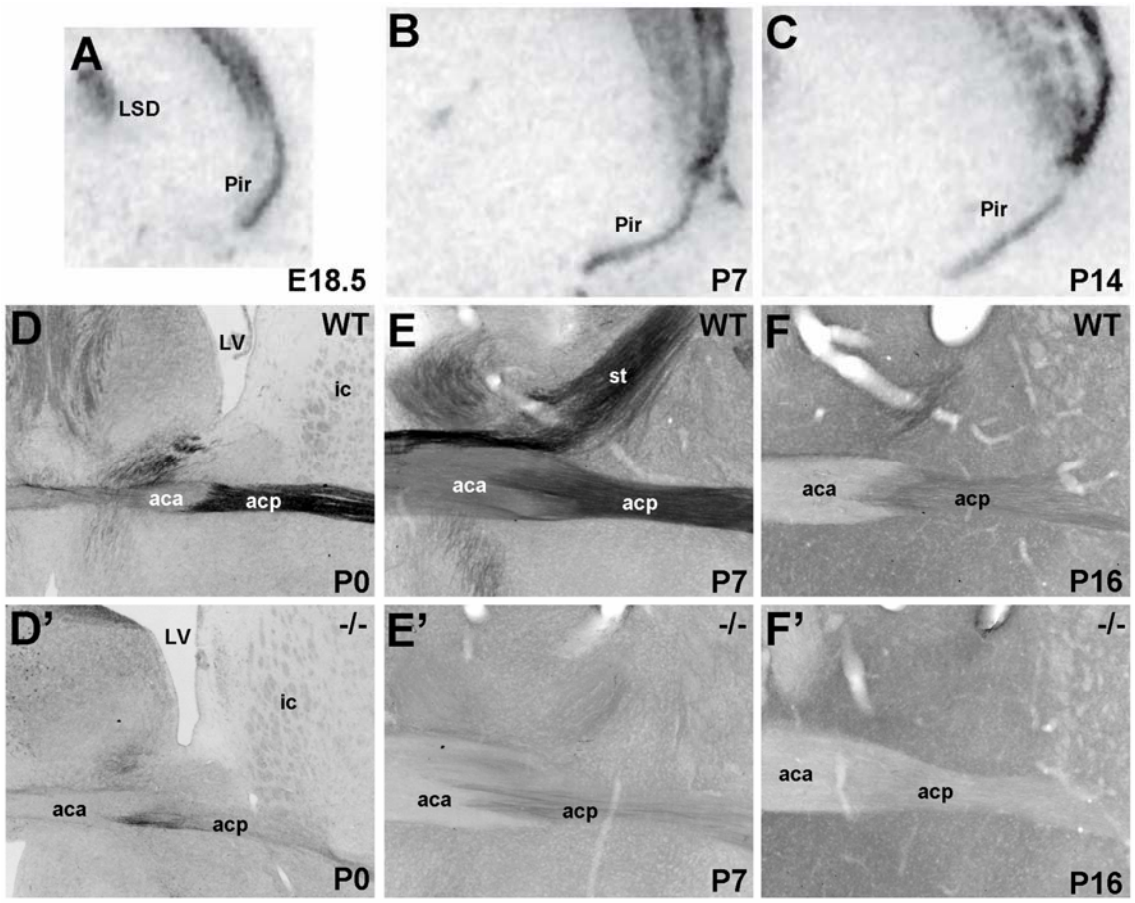

Figure 5. *Met* transcript and protein expression in the piriform cortex and anterior commissure. **A-C:** Autoradiographic images of piriform cortex at E18.5, P7, and P14 show *Met* transcript expression. DIC photomicrographs show Met immunoreactivity in coronal sections from wild type (**D,E,F**) and *Emx1*^{cre}*/Met*$^{fx/fx}$ (**D', E', F'**) mice. In the wild type sections, Met is expressed in both the anterior and posterior limbs of the commissure, though the staining is more intense in the posterior limb. Met immunoreactivity is largely depleted in both limbs in the *Emx1*^{cre}*/Met*$^{fx/fx}$ sections, owing to their dorsal pallial origin. We note residual staining in the P0 and P7 posterior limb (**D',E'**), likely due to a contribution from fibers originating in the ventral endopiriform cortex in which Emx1-mediated Cre recombination rates are low. Scale bar = 825μm for **A-C**; 275μm for **D-F** and **D'-F'**.

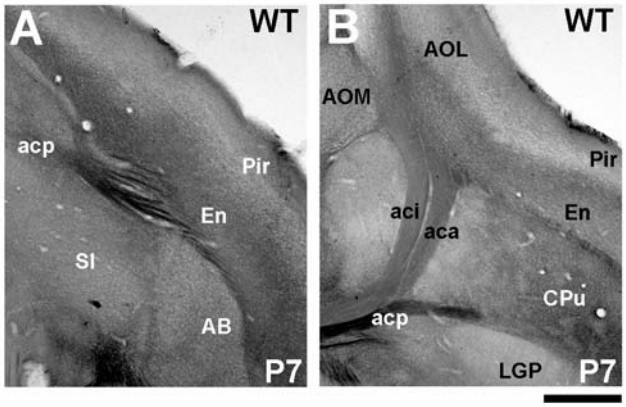

Supplemental Figure 3. Differential Met protein expression in the anterior commissure. DIC photomicrographs illustrate Met immunohistochemistry in the posterior and anterior limbs of the anterior commissure in horizontal sections from P7 wild type mice. Heavily stained axons within the posterior limb course between posterior piriform cortices (**A**). In a more dorsal section, lightly stained axons within the intrabulbar and anterior subdivisions of the anterior limb emanate from the olfactory bulbs and anterior piriform cortex (**B**). Scale bar = 550 μm for **A** and **B**.

these fibers in *Emx1*^{cre}*/Met*$^{fx/fx}$ mice at P0 and P7 (**Fig. 6A',C'**), together with very low *Met* expression in primary sensory and motor nuclei in the dorsal thalamus, indicates that cortical efferents, rather than thalamocortical fibers, are labeled. Futhermore, in wild type animals, Met staining in the cerebral peduncle is minimal (**Fig. 6B,D,G,H**), suggesting that cortico-tectal, -bulbar and -spinal fibers contribute little to the Met staining. Therefore, corticothalamic and corticostriatal projections seem to comprise the greatest proportion of Met-immunoreactive axons in the internal capsule.

By P7, additional, moderately intense Met immunnostaining appears throughout the striatal and dorsal thalamic neuropil (**Fig. 6C**), coinciding with active periods of axon branching and collateralization of cortico-striatal and cortico-thalamic axons (Frassoni et al., 1995; Nisenbaum et al., 1998; Sheth et al., 1998). This neuropil staining remains (albeit at lower intensity) through P14 and P16 (**Fig. 6E,F**), although by this time the internal capsule fibers are devoid of Met staining. At all ages, Met expression is absent

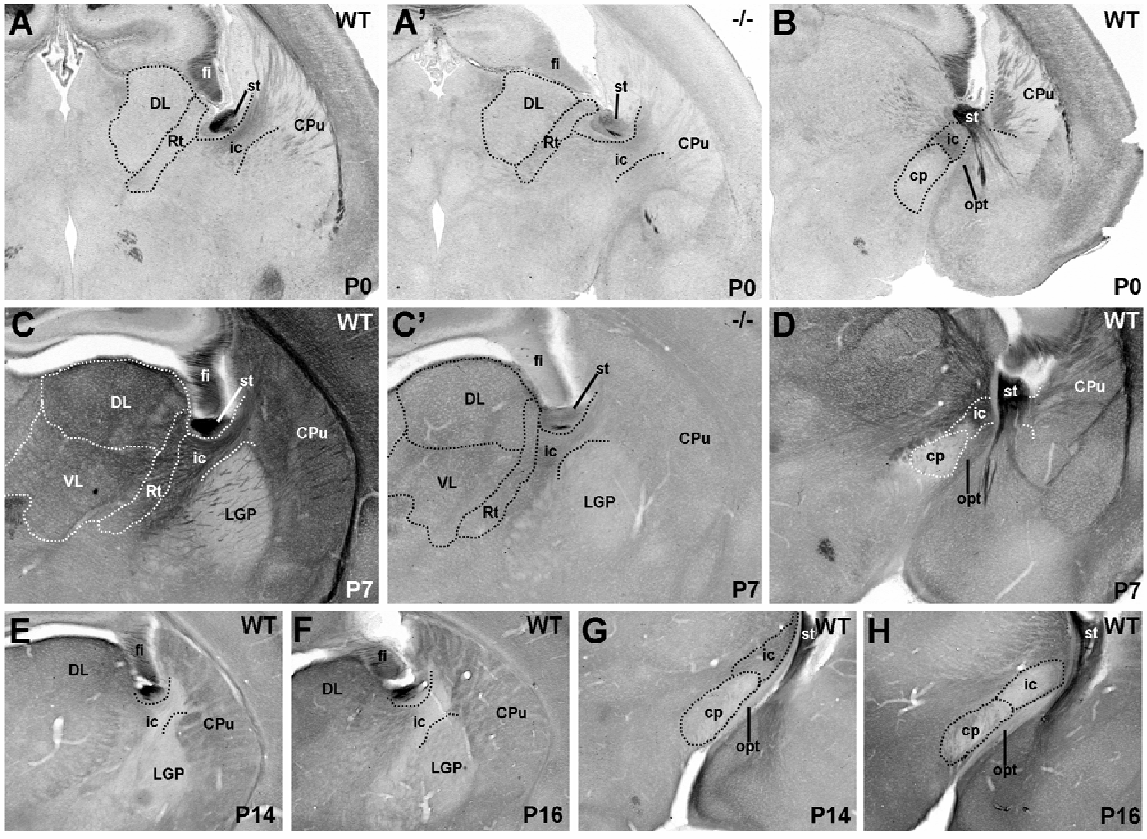

Figure 6. Met protein expression in the internal capsule and cerebral peduncle. DIC photomicrographs illustrate Met immunohistochemistry in the internal capsule and cerebral peduncle in coronal sections from wild type and *Emx1*^{cre}/*Met*$^{fx/fx}$ mice. Staining of internal capsule fibers is apparent in P0 and P7 wild type mice (**A,C**) but essentially absent in matched sections from *Emx1*^{cre}/*Met*$^{fx/fx}$ mice (**A',C'**). At P7, note the increase in Met immunoreactivity in the underlying striatal neuropil but the absence of such staining in the globus pallidus. By P14 (**E**) and P16 (**F**), the internal capsule fibers are nearly devoid of Met staining, but there is remaining immunoreactivity in the striatal neuropil. The paucity of Met labeling in the cerebral peduncle at all ages examined (P0, **B**; P7, **D**; P14, **G**; P16, **H**) suggests that cortico-tectal, -bulbar, and -spinal fibers contribute minimally to the Met immunoreactivity in the internal capsule. (Scale bar = 410μm for **A,A',B,C,C',D**; 550μm for **E-H**.

in the neuropil of the globus pallidus, consistent with the lack of *Met* transcript in the caudatoputamen, the primary contributor of afferents to this structure (Preston et al., 1980; Chang et al., 1981; Wilson and Phelan, 1982). Met-immunopositive fibers in the globus pallidus appear to be corticofugal fibers of passage.

External Capsule

The external capsule is a conduit for axons projecting between multiple cortical areas and the lateral, and other, subnuclei of the amygdaloid complex (Brothers and Finch, 1985; Faulkner and Brown, 1999; Weisskopf and LeDoux, 1999; Heinbockel and Pape, 2000; Szinyei et al., 2000). This tract contains fibers that are densely stained for Met during the first two postnatal weeks (**Supplemental Fig. 4**). As expected, there is a near-complete absence of Met expression in the external capsule in *Emx1^{cre}/Met$^{fx/fx}$* mice (**Supplemental Fig. 4A'**). By P16, consistent with a decrease in *Met* expression in both the cortex and amygdala, only low levels of Met staining are observed in the external capsule (**Supplemental Fig. 4B)**.

Expression of Met in developing projection neurons of the hippocampus (E18.5-P16)

In the hippocampus, *Met* transcript is expressed by pyramidal cells of the subiculum, CA1 and a subdomain of CA3 from birth through P14 (**Fig. 7A-C**). As in the cerebral cortex, Met protein expression in hippocampal neurons is localized to long projection neurons. At P0 and P7, immunohistochemical staining of Met reveals intense labeling of axons in the alveus and fimbria/fornix (**Fig. 7D,E**), which are comprised in part of the extrinsically projecting axons of the hippocampus. Specifically, Met immunostaining is dense in the precommissural and postcommissural divisions of the fornix (**Fig. 7J,K)**, which project to the septum and hypothalamus, respectively. The dorsal and ventral aspects of the hippocampal commissural division of the fornix also express Met protein (**Fig. 7I,J**). All fornix divisions in the *Emx1^{cre}/Met$^{fx/fx}$* mouse are devoid of Met protein (**Fig. 7M,N,O)**, demonstrating that Met-expressing axons in this

fiber tract originate from dorsally derived hippocampal pyramidal neurons, rather than from the various subcortical targets to which they are reciprocally connected.

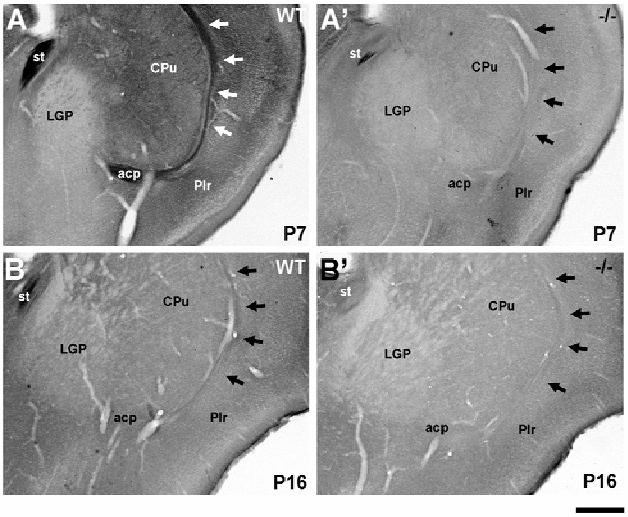

Supplemental Figure 4. DIC photomicrographs illustrate Met immunohistochemistry in the external capsule (arrows) in coronal sections. At P7, Met immunoreactivity is present in the external capsule in wild type (**A**), but not *Emx1*^{cre}/*Met*$^{fx/fx}$ (**A'**), mice. By P16, Met staining is not observed in the external capsule of wild type (**B**) or *Emx1*^{cre}/*Met*$^{fx/fx}$ (**B'**) mice. Scale bar = 400μm for all panels.

Throughout development, *Met* transcript is conspicuously absent in the dentate granule neurons of the hippocampus (**Fig. 7A-C)**. Consistent with this, axons projecting from these cells to CA3 via the mossy fiber pathway are not Met-immunoreactive. In contrast, Met immunolabeling is observed in the stratum moleculare of wild type (**Fig. 7H**), but not *Emx1*^{cre}/*Met*$^{fx/fx}$, mice (**Fig. 7L**), mostly likely representing perforant path fibers originating from layer II entorhinal cortex (Steward and Scoville, 1976; Dolorfo and Amaral, 1998; van Groen et al., 2002). The lighter immunostaining observed in the strata radiatum and oriens of CA1 and CA3 also is absent in *Emx1*^{cre}/*Met*$^{fx/fx}$ mice (**Fig. 7H,L**), consistent with Met-expression in the terminal fields of a subpopulation of bilaterally projecting CA3 neurons (Gottlieb and Cowan, 1973; Swanson et al., 1978).

We note, however, that this terminal axon Met staining cannot be differentiated from staining in the apical and distal dendrites of CA3, CA1, and subicular pyramidal neurons. Similar to the cerebral cortex, Met immunolabeling in the hippocampus and associated axon tracts is greatly reduced at P14 and P16 (**Fig. 7F,G**).

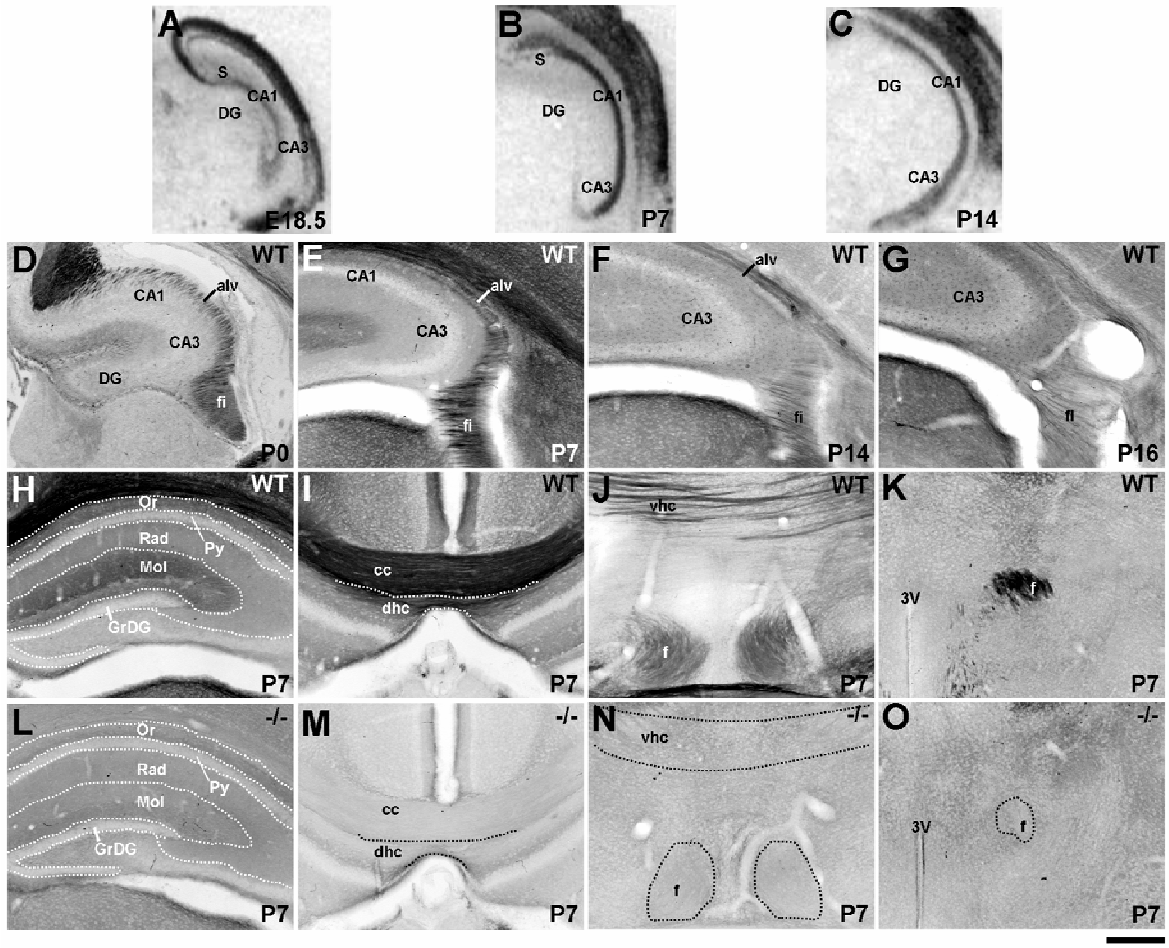

Figure 7. *Met* transcript and protein expression in the hippocampus. **A-C**: Autoradiographic images of *Met* transcript in coronal sections from wild type mice, scanned from film. At all ages, autoradiographic signal is observed in the stratum pyramidale of the subiculum, CA1, and a subregion of CA3. Signal is absent in the dentate gyrus (DG). **D-O**: DIC photomicrographs of Met immunoreactivity in coronal sections from wild type (**D-K)** and *Emx1*^{cre}/*Met*$^{fx/fx}$ (**L-O)** mice. **D and E:** DIC images of Met immunoreactivity from wild type mice show robust staining of the alveus and fimbria/fornix at P0 (**D**) and P7 (**E**), indicating that efferent axons of hippocampal pyramidal cells express Met. This staining decreases at later ages (P14, **F**; P16, **G**). Light staining in the strata oriens and radiatum and heavier staining in the stratum moleculare is observed in wild type (**H**), but not *Emx1*^{cre}/*Met*$^{fx/fx}$ (**L**), mice at P7. Heavy Met staining is present in the dorsal hippocampal commissure (**I**), ventral hippocampal commissure (**J**), precommissural fornix (**J**), and postcommissural fornix (**K**). This staining is completely absent in corresponding axon tracts in the *Emx1*^{cre}/*Met*$^{fx/fx}$ mouse (**M, N,** and **O**). Scale bar = 1mm for **A-C**; 275 μm for **D-O**.

Expression of Met in developing projection neurons of the septum (E18.5-P16)

Met transcript expression in the septum is robustly detected perinatally (**Fig. 8A**), with dense labeling restricted to dorsolateral neurons and lighter labeling in the medial nucleus. This pattern persists throughout the first two postnatal weeks (**Fig. 8B,C**). Met immunolabeling in the dorsolateral septum is considerable, and the pattern of staining is equivalent in wild type and $Emx1^{cre}/Met^{fx/fx}$ mice. This suggests localization to cell bodies or terminating afferent axons of a subpallial origin (**Fig. 8H,L**), but distinguishing between cell body and neuropil localization is difficult at the light microscopic level. In contrast, axonal Met immunoreactivity clearly predominates in the intermediate lateral and medial septal nuclei (**Fig. 8I**). This staining is greatly reduced in the $Emx1^{cre}/Met^{fx/fx}$ mouse (**Fig. 8M**), consistent with a loss of Met-expressing septal afferents of a dorsal pallial origin. Axons of dorsally derived hippocampal pyramidal neurons innervate both dorsal and intermediate lateral nuclei, and, to a lesser extent, the medial septal nucleus (Swanson and Cowan, 1979; Staiger and Nurnberger, 1991; Phelan et al., 1996), and a substantial proportion of these axons express Met (**Fig. 7**). Therefore, Met-expressing hippocampal neurons may selectively target specific septal nuclei.

Select septal efferents also express Met. For example, dorsolateral septum contributes a robust intra-septal projection to the nucleus of the horizontal diagonal band (Swanson and Cowan, 1979; Staiger and Nurnberger, 1991; Phelan et al., 1996), in which some terminal fibers appear to be Met-immunopositive in wild type mice. A lack of *Met* transcript labeling in the nucleus of the horizontal diagonal band, (see **Fig. 8A,B,C**) and a maintenance of Met-immunostained axons in the nucleus of the diagonal band in the $Emx1^{cre}/Met^{fx/fx}$ mouse (**Fig. 8M**) are consistent with this observation.

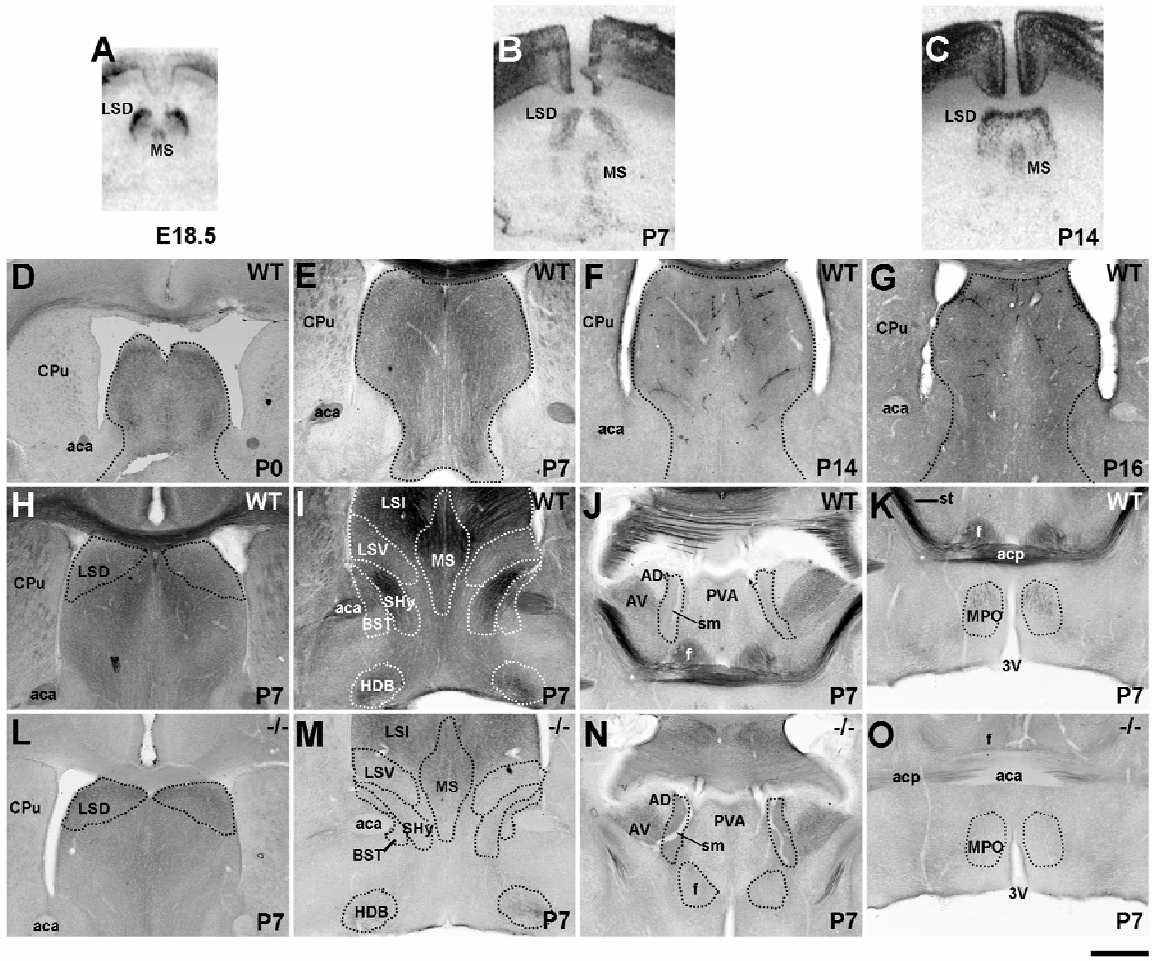

Figure 8. *Met* transcript and protein expression in the septum in coronal sections from wild type and *Emx1*^{cre}/*Met*$^{fx/fx}$ mice. **A-C:** *In situ* hybridization analysis of *Met* in wild type septum across perinatal (E18.5, **A**) and early postnatal development (P7, **B**; P14, **C**). At all ages, autoradiographic signal is observed specifically in dorsolateral and medial subnuclei. **D-G:** DIC photomicrographs of Met immunoreactivity from wild type mice show labeling throughout the septum (outlined regions) at P0 (**D**) and P7 (**E**), which is decreased by P14 (**F**) and hardly detectable above background levels at P16 (**G**). At P7, all Met staining of the dorsolateral septum (**H**) and partial staining of the nucleus of the diagonal band (**I**) of wild type mice is preserved in *Emx1*^{cre}/*Met*$^{fx/fx}$ mice (**L** and **M**). Stained afferents in the medial and intermediate septal nuclei (**I**) and the anteromedial hypothalamus (**K**) of wild type mice are absent in *Emx1*^{cre}/*Met*$^{fx/fx}$ mice (**M** and **O**) at P7, indicating a dorsal pallial rather than septal origin for Figure 8—cont. these fibers. Septo-habenular axons do not express Met as evidenced by a lack of staining in the stria medullaris in both wild type (**J**) and *Emx1*^{cre}/*Met*$^{fx/fx}$ (**N**) mice at P7. Scale bar = 1.35mm for **A-C**; 550 μm for **D-O**.

Neurons in the lateral and medial septal nuclei contribute descending projections to the medial preoptic area of the hypothalamus and ascending projections to the hippocampus, respectively (Swanson and Cowan, 1979; Chiba and Murata, 1985; Risold

and Swanson, 1997), but Met-expressing axons in these regions are undetectable in *Emx1^{cre}/Met$^{fx/fx}$* mice (**Figs. 8O and 7L**). This suggests that the fibers originate from projection neurons of the *Emx1*-expressing lineage, and not septal neurons. Additionally, though septal neurons are known to contribute efferents to the habenula via the stria medullaris, these cells predominantly reside in the septofimbrial and triangular nuclei (Herkenham and Nauta, 1977; Swanson and Cowan, 1979; Kawaja et al., 1990), where *Met* transcript is not detected (**data not shown**). Axons in the stria medullaris are also devoid of Met protein expression in both wild type and *Emx1^{cre}/Met$^{fx/fx}$* mice (**Fig. 8J,N**).

Though some Met immunohistochemical signal is evident on afferent axons within the medial and intermediate lateral nuclei of the septum at P14 and P16 (**Fig. 8F,G**), in contrast to earlier ages (**Fig. 8D,E**), staining is difficult to distinguish from background. There is also a concomitant reduction of Met staining on axons likely to be dorsolateral septal efferents to the nucleus of the diagonal band (**data not shown**). This downregulation of axonal Met expression mirrors that observed in both cerebral cortical and hippocampal projection neurons after the second postnatal week.

Expression of Met in developing projection neurons of the amygdala (E18.5-P16)

Of the 13 commonly recognized nuclei within the amygdaloid complex (Aggleton, 2000), 5 express Met during postnatal development. From caudal to rostral, these are the posterior cortical amygdala, basal amygdala, lateral amygdala, medial amygdala, and the nucleus of the lateral olfactory tract. *Met* transcript is detected within these nuclei perinatally (**Fig. 9A,B,C**), at P7 (**Fig. 9D,E,F**), and at P14 (**Fig. 9G,H,I**).

During this same period, Met protein expression is particularly dense in amygdalofugal axons of the stria terminalis.

At P7, there is intense Met immunostaining in the posterior cortical amygdaloid nucleus, from which Met-immunostained axons appear to project anteriorly via the stria terminalis (Canteras et al., 1992) (**Fig. 10A,B**). More rostrally, Met-expressing axons from the basal amygdaloid nucleus appear to join the stria terminalis (**Fig. 10C**) as it courses into the ventral forebrain to target the bed nucleus of the stria terminalis (**Fig. 10E,F**). Met-expressing axons in more medial aspects of the stria terminalis emanate from the medial amygdala (**Fig. 10C**), which contributes dense projections to the bed nucleus of the stria terminalis (Canteras et al., 1995). Intensely labeled axons are also present within the decussation of the stria terminalis, coursing beneath the precommissural fornix, directly superior to the anterior commissure (**Fig. 10F**). Therefore, in addition to ipsilateral projections, Met appears to be expressed on contralateral amygdalofugal projections to the bed nucleus of the stria terminalis, which most likely arise from the posterior cortical nucleus (Dong et al., 2001). The lateral amygdala, which contains *Met*-expressing neurons, projects to prefrontal cortex, other amygdaloid nuclei, and the nucleus accumbens (McDonald, 1991b; Aggleton, 2000). Of these, only the prefrontal cortex and posterior cortical amygdaloid nucleus exhibit robust Met immunostaining, which is lost in $Emx1^{cre}/Met^{fx/fx}$ mice (**Fig. 10A,A', data not shown**). However, because both of these regions receive numerous afferents of dorsal pallial origin, it is not possible to trace the origin of Met-expressing axons within these two regions to the lateral amygdala. Though likely, it is not absolutely certain that Met is expressed on efferents of the lateral amygdala.

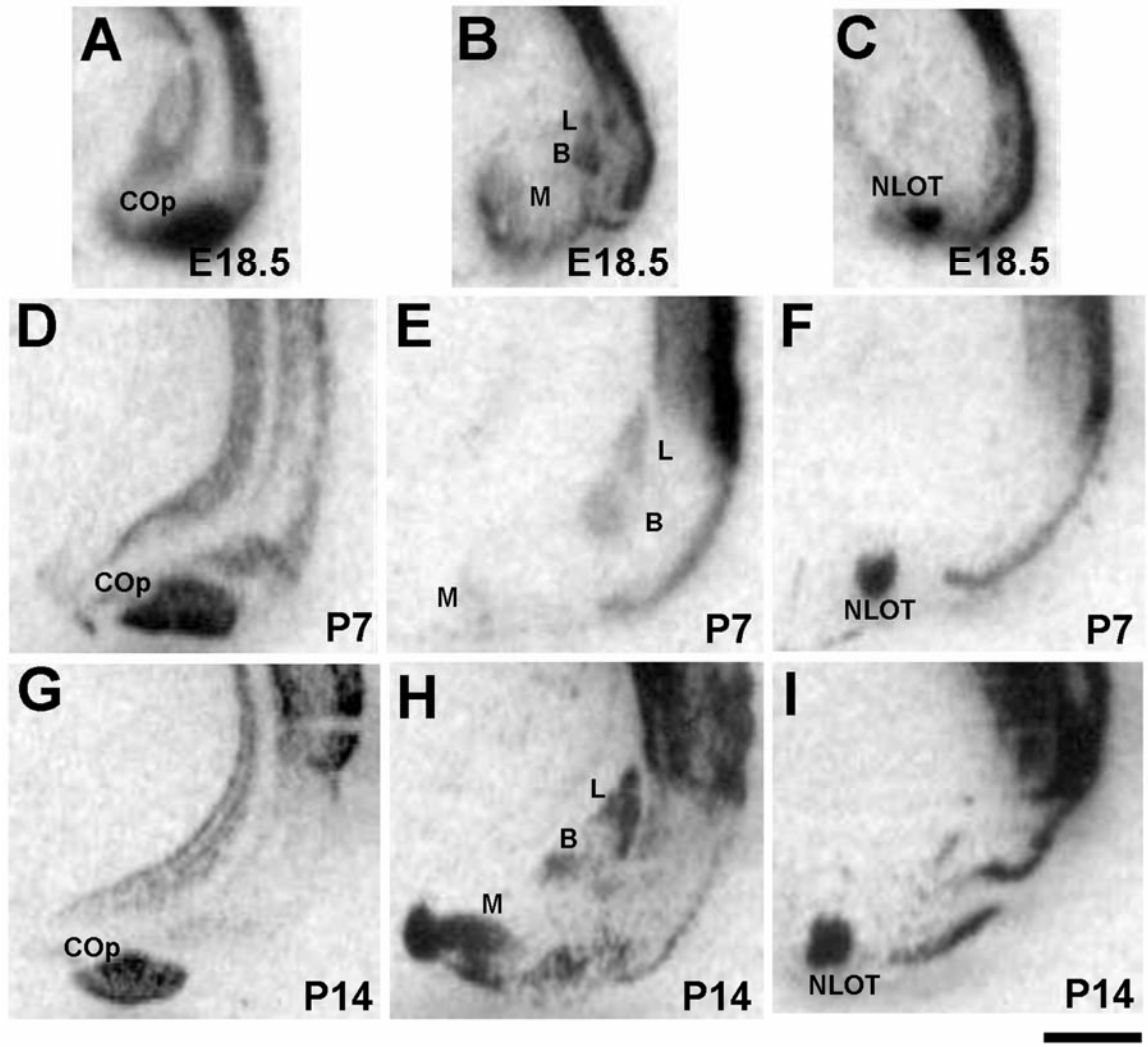

Figure 9. *In situ* hybridization analysis of *Met* in the rostro-caudal extent of the amygdala during development. Autoradiographic images of E18.5 coronal sections show signal in the posterior cortical amygdala (**A**), the lateral, basal, and medial amygdala (**B**), and the nucleus of the lateral olfactory tract at the most rostral extent of the structure (**C**). Signal is observed in these same amygdaloid nuclei at both P7 (**D, E,** and **F**) and P14 (**G, H,** and **I**). Scale bar = 925μm for all panels.

Based on recombination patterns in the *Emx1-cre* reporter mouse (Gorski et al., 2002), we expected only those Met-positive axons originating from medial amygdaloid neurons to remain immunoreactive in the stria terminalis of the $Emx1^{cre}/Met^{fx/fx}$ mouse. Indeed, this appears to be the case (**Fig. 10A'-F'**). Interestingly, immunohistochemical analysis in the null mouse indicates that only a subpopulation of medial amygdaloid

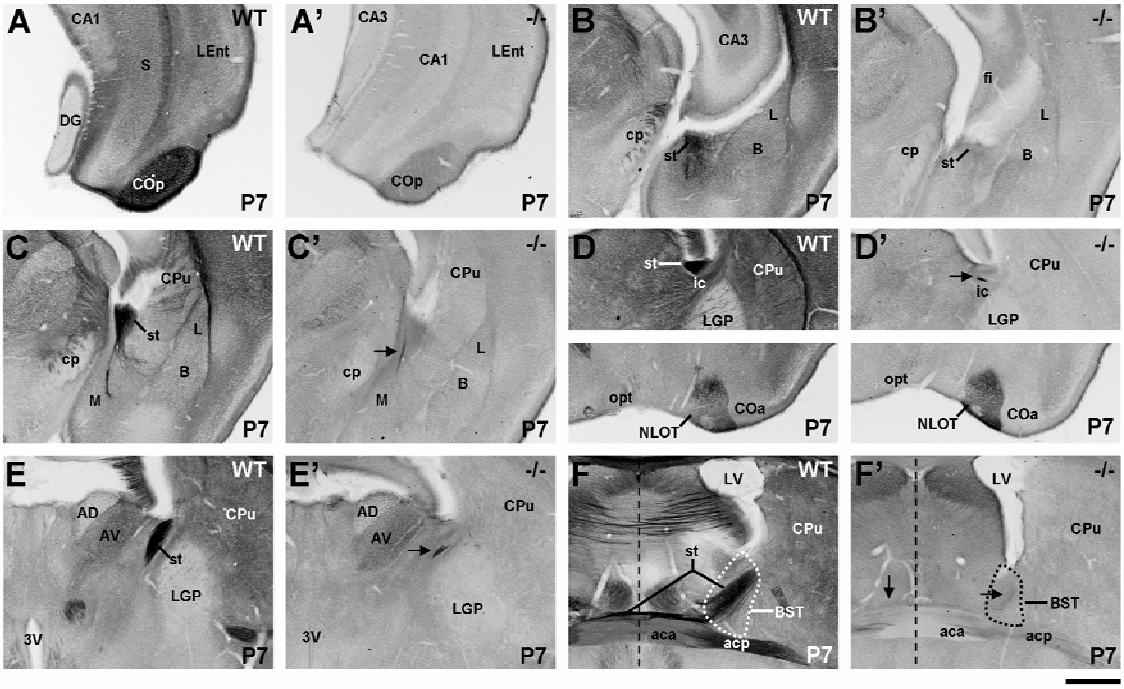

Figure 10. Met protein expression in the amygdala. DIC photomicrographs illustrate Met immunohistochemistry in coronal sections through the caudo-rostral extent of the amygdala and stria terminalis (st) in wild type (**A, B, C, D, E, F**) and *Emx1*^{cre}/*Met*$^{fx/fx}$ (**A', B', C', D', E', F'**) mice at P7. Met-expressing neurons in the posterior cortical amygdala (**A**) project labeled axons anteriorly in the st (**B**). More anteriorly, Met-expressing axons from the basal and medial amygdala (MeA) join the vertical limb of the st, course over the internal capsule (**C**, upper panel **D**, and **E**), and terminate in the ipsilateral bed nucleus of the stria terminalis (BST) and the contralateral BST via decussation at the midline (dashed line) (**F**). In *Emx1*^{cre}/*Met*$^{fx/fx}$ mice, Met staining persists in a subset of st axons that originate from the MeA (arrows in **C', D', E'**, and **F'**). Met staining is also present in the nucleus of the lateral olfactory tract in the rostral extent of the amygdala in both wild type and *Emx1*^{cre}/*Met*$^{fx/fx}$ mice (lower panel **D** and **D'**). Scale bar = 550 μm for all panels.

efferents express Met; although the medial amygdala projects to both the bed nucleus of the stria terminalis and the medial preoptic area of the hypothalamus (Canteras et al., 1995), only Met-stained axons in the latter are ablated in the *Emx1*^{cre}/*Met*$^{fx/fx}$ mouse, indicating that these axons arise from neurons derived from the dorsal pallium rather than the medial amygdala (**Fig. 8O**).

At the most anterior extent of the amygdala, dense Met immunostaining is evident in the nucleus of the lateral olfactory tract in both wild type (**Fig. 10D**) and *Emx1*^{cre}/*Met*$^{fx/fx}$ mice (**Fig. 10D'**). Thus, axonal staining in this nucleus likely arises from

a non-*Emx1-cre* expressing subcortical or intra-amygdaloid region. Considering the data from anterograde labeling studies (Santiago and Shammah-Lagnado, 2004), and reported minor potential for Emx1-cre-mediated recombination within the nucleus of the lateral olfactory tract (Gorski et al., 2002), the staining pattern is consistent with the nucleus of the lateral olfactory tract receiving Met-immunoreactive input primarily from its contralateral counterpart.

Consistent with other forebrain areas, there is a significant decrease in Met expression in the amygdaloid complex after P7. Specifically, Met immunostaining is reduced between P14-16 in the stria terminalis (**Supplemental Fig. 5E,F**) and various targets of amygdaloid projections, including the bed nucleus of the stria terminalis (**Supplemental Fig. 5G,H**), the nucleus of the lateral olfactory tract (**Supplemental Fig. 5C,D**), and the posterior cortical amydaloid nucleus (**Supplemental Fig. 5A,B**).

Expression of Met in developing projection neurons of the diencephalon (P0-P16)

Met mRNA expression is evident in the thalamic reticular nucleus, but no other dorsal thalamic nuclei, at P7 (**Fig. 11A**) and P14 (**Fig. 11B).** However, Met protein is expressed in the neuropil in several thalamic nuclei, including the reticular, dorsolateral, ventrolateral, and anterior thalamic nuclei. In most regions, this immunostaining is virtually absent in the $Emx1^{cre}/Met^{fx/fx}$ mouse (**Fig. 11D**), indicating corticofugal projections as the primary source of Met labeling. In contrast, Met immunostaining is equivalent in the anterior thalamic nucleus in wild type and $Emx1^{cre}/Met^{fx/fx}$ mice (**Fig. 11E,F**), particularly in its anteroventral division, and appears to be localized to axons. Continued expression of Met in these processes in the $Emx1^{cre}/Met^{fx/fx}$ mouse is somewhat

unexpected, considering that Met is dramatically downregulated in *Emx1^{cre}/Met$^{fx/fx}$* cingulate cortical neurons, which send projections to the anterior nucleus of the thalamus

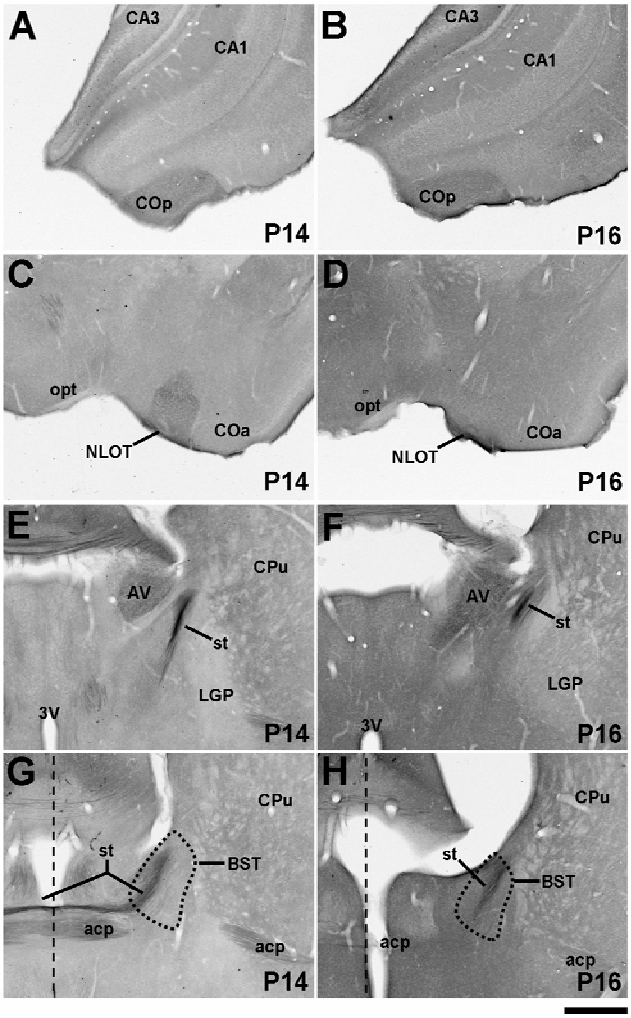

Supplemental Figure 5. Decreased postnatal Met expression in the amygdala. DIC photomicrographs illustrate Met immunoreactivity in coronal sections through the caudo-rostral extent of the amygdala and stria terminalis (st) in wild type mice at P14 and P16. Met staining in the posterior cortical amygdala (**A**), nucleus of the lateral olfactory tract (**C**), and st before (**E)** and after (**G**) decussation at the midline (dashed line), is light at P14 and is further reduced in intensity in these same structures just two days later, as shown at P16 (**B, D, F,** and **H**). Scale bar = 550 μm for all panels.

(**Supplemental Fig. 2D,E**). However, the mammillary nuclei of the posteromedial hypothalamus also contribute a major population of afferents to this structure via the

mamillothalamic tract, which, along with the mammillotegmental tract, heavily express Met protein (**Fig. 12A,B)**. Moreover, Met immunoreactivity is present in the anteroventral, but not the anterodorsal subnuclei of the anterior thalamus (**Fig. 11E,F**), consistent with the selective patterns of innervation within this nucleus by the medial mammillary nuclei (Guillery, 1957; Cruce, 1975; Watanabe and Kawana, 1980; Seki and Zyo, 1984). The medial mammillary nuclei themselves receive prominent input from

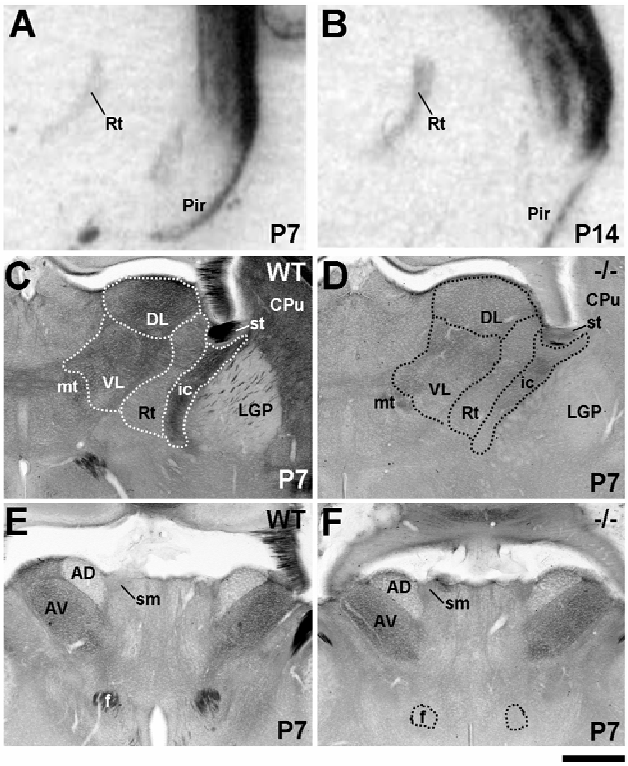

Figure 11. *Met* transcript and protein expression in the thalamus in coronal sections from wild type and *Emx1*^{cre}/*Met*$^{fx/fx}$ mice. **A** and **B:** *In situ* hybridization analysis of *Met* in wild type thalamus at P7 (**A**) and P14 (**B**). Autoradiographic signal is detected specifically in the thalamic reticular nucleus (Rt) at these ages. DIC images of Met immunoreactivity at P7 show that neuropil staining in the Rt and dorsolateral and ventrolateral thalamic nuclei in wild type mice (**C**) is greatly reduced in corresponding regions of *Emx1*^{cre}/*Met*$^{fx/fx}$ mice (**D**). Conversely, neuropil staining in specific anterior thalamic nuclei is equivalent in wild type (**E**) and *Emx1*^{cre}/*Met*$^{fx/fx}$ (**F**) mice. Scale bar = 900μm for **A,B**; 550 μm for **C, D, E,** and **F**.

subicular projection neurons at the septal pole of the hippocampus (Swanson and Cowan, 1977; Allen and Hopkins, 1989; Gonzalo-Ruiz et al., 1992). These fibers course via the postcommissural division of the fornix to terminate specifically within the medial mammillary nuclei, and are Met-immunopositive in wild type (**Fig. 12C**), but not *Emx1*^{cre}*/Met*$^{fx/fx}$, mice (**Fig. 12D**). The dense axonal staining observed in the ventral tuberomammillary nucleus (**Fig. 12C**) may be contributed by projection neurons in infralimbic cortex, ventral CA1 or the subiculum (Ericson et al., 1991; Canteras and Swanson, 1992; Cenquizca and Swanson, 2006).

In the anterior hypothalamus, there is no *Met* expression in the anterodorsal or medial preoptic nuclei at any stage of postnatal development, but Met immunoreactivity is observed in a sparse, but notable, population of axons in both regions (**Figs. 8K and 12E**). This staining is ablated in the *Emx1*^{cre}*/Met*$^{fx/fx}$ mouse (**Figs. 8O and 12F**). While the data do not definitively elucidate the sources of these Met-expressing fibers, likely candidates include CA1 and subicular pyramidal cells at the ventral pole of the hippocampus (Canteras and Swanson, 1992; Kishi et al., 2000; Cenquizca and Swanson, 2006). An intranuclear source for these stained axons is unlikely, as we do not detect *Met* mRNA in the anterodorsal nucleus or medial preoptic nucleus.

In the habenula, *Met* transcript and protein are expressed by projection neurons. *In situ* hybridization analysis from E18.5 to P14 reveals modest *Met* transcript expression of the medial, but not the lateral, nucleus (**Fig. 13A,B).** Over this period, the fasciculus retroflexus axons coursing between the habenula and interpeduncular nucleus (Akagi and Powell, 1968; Herkenham and Nauta, 1977) are also Met-immunoreactive (**Fig. 13C,E**). Light axonal staining in the habenular commissure is also observed (**Fig. 13C**).

Consistent with the subpallial origin of the medial habenula, comparable levels of Met protein are observed in the fasciculus retroflexus, habenular commissure, and interpeduncular nucleus of the wild type and *Emx1^{cre}/Met$^{fx/fx}$* mice throughout postnatal development (**Fig. 13D,F**). In general, decreased axonal Met staining is observed throughout the diencephalon soon after the end of the second postnatal week (**Supplemental Fig. 6**), mirroring the decline in other forebrain regions. A notable exception, however, is the relative preservation of Met staining in the fasciculus retroflexus and interpeduncular nucleus (**Supplemental Fig. 6C,D**).

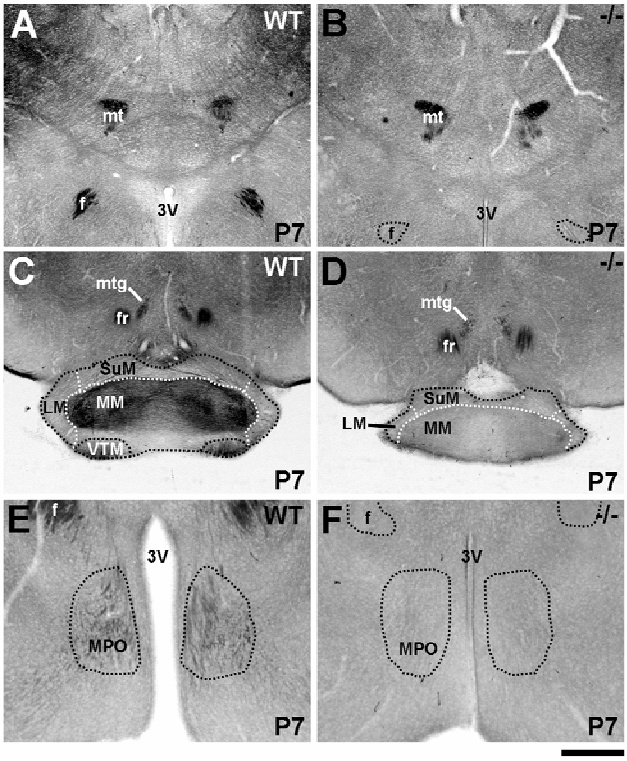

Figure 12. Met protein expression in the hypothalamus. DIC photomicrographs illustrate Met immunoreactivity in coronal sections of the hypothalamus and associated axon tracts in wild type (**A, C,** and **E**) and *Emx1^{cre}/Met$^{fx/fx}$* (**B, D,** and **F**) mice at P7. Intense Met staining in the mammillothalamic and mammillotegmental tracts of wild type mice (**A**) is maintained at equivalent levels in *Emx1^{cre}/Met$^{fx/fx}$* mice (**D**). Notable Met staining on afferents within specific mammillary nuclei (**C**) and the medial preoptic nucleus (**E**) in wild type mice is absent in *Emx1^{cre}/Met$^{fx/fx}$* mice (**D** and **F**), indicating a dorsal pallial origin for these fibers. Scale bar = 550 μm for **A, B, C,** and **D**; 275 μm for **E** and **F**.

Expression of Met (P21 – P35)

It is clear from *in situ* hybridization analysis that, after P21, *Met* transcript continues to be expressed in the forebrain, though at reduced intensity (**Fig. 14A**). Even more dramatic reductions in immunohistochemical staining are observed at these later postnatal ages, as demonstrated by a lack of differential staining in wild type and *Emx1*^{cre}*/Met*$^{fx/fx}$ mice (**Fig. 14B**). This contrasts with the observation that Met protein is detected by Western blot analysis in wild type but not *Emx1*^{cre}*/Met*$^{fx/fx}$ cortex (**Fig. 14C**), suggesting that the lack of detectable Met protein expression in tissue sections at P21 may be due to technical limitations. For example, subcellular redistribution of Met may reduce local protein concentration to levels beneath the threshold for immunohistochemical detection.

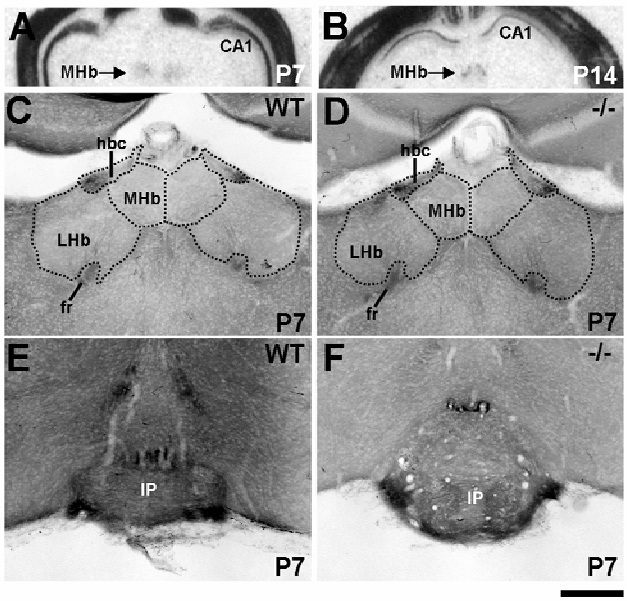

Figure 13. *Met* transcript and protein expression in the epithalamus in coronal sections from wild type and *Emx1*^{cre}*/Met*$^{fx/fx}$ mice. **A** and **B:** *In situ* hybridization analysis of *Met* in wild type habenula at P7 and P14. Autoradiographic signal at both ages is specific to the medial but not the lateral habenula. DIC photomicrographs of Met immunoreactivity show equivalent, dense staining of axons in the habenular commissure and fasciculus retroflexus (fr) in wild type (**C**) and *Emx1*^{cre}*/Met*$^{fx/fx}$ (**D**) mice at P7. Levels of axon staining also are equal within target areas of the fr, such as the interpeduncular nucleus, in wild type (**E**) and *Emx1*^{cre}*/Met*$^{fx/fx}$ (**F**) mice at this age. Scale bar = 1.9mm for **A,B**; 275 μm for **C, D, E** and **F**.

Discussion

The data in the present study provide a comprehensive map of Met receptor mRNA and proteinlabeling in the developing mouse forebrain, revealing a surprisingly restricted pattern of expression in functionally related circuits. The *in situ* hybridization data are consistent with, but significantly extend, findings from previous mapping studies (Jung et al., 1994; Thewke and Seeds, 1999). Previous studies reporting Met immunohistochemistry in the forebrain have had a limited neuroanatomical and developmental scope (Thewke and Seeds, 1999; Korhonen et al., 2000; Sun et al., 2002; Ohya et al., 2007), and the antibody reagents used yielded suboptimal and nonspecific labeling in our hands. We employed a novel immunohistochemical approach to localize Met receptor protein, providing compelling evidence that Met is expressed in specific developing axonal projections that reach select terminal regions in the forebrain. Furthermore, our Met immunohistochemical analyses in the $Emx1^{cre}/Met^{fx/fx}$ conditional knockout mouse provide an opportunity to attribute sources of Met labeling within a specific forebrain region as pallial or subpallial in origin.

Our complementary expression mapping tools allowed us to determine that Met receptor expression during forebrain development is restricted mainly to specific populations of projection neurons within the cortex and some classically defined limbic system components. Moreover, Met protein is localized primarily to the axons of these cells during peak periods of axon growth and synapse formation, consistent with a putative role for Met in regulating these functions. These data suggest that circuitry underlying socio-emotional processing may be selectively vulnerable to disrupted Met signaling or expression during development. This is consistent with data demonstrating

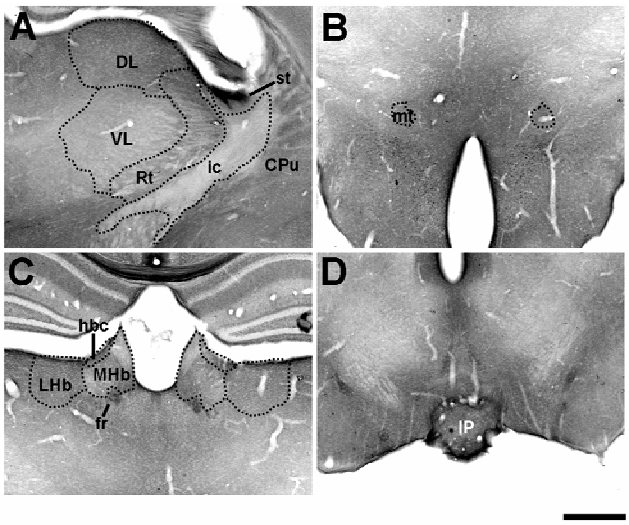

Supplemental Figure 6. Decreased postnatal Met expression in the diencephalon. DIC photomicrographs illustrate Met immunoreactivity in coronal sections through the diencephalon of wild type mice at P16. Previously robust Met staining in the thalamic reticular nucleus and dorsolateral and ventrolateral thalamus (**A**) and mammillothalamic tract (**B**) is scarcely detectable above background at P16. Axonal Met staining is comparatively preserved in the fasciculus retroflexus (**C**) and interpeduncular nucleus (**D**) at this same age. Scale bar = 550 μm for all panels.

that a *MET* allelic variant increases risk for ASD, a disorder with core disruptions in social behavior (Campbell et al., 2006).

Restricted cell types express Met in the developing forebrain

The present study identifies specific subsets of projection neurons expressing *Met* transcript and provides evidence that these developing neurons traffic Met protein predominantly to their axonal compartments. This is consistent with the reported growth-promoting and attractive nature of HGF/Met signaling on axons in the spinal cord and thalamus *in vitro* (Ebens et al., 1996; Powell et al., 2003). However, here we demonstrate *in vivo* that the peak of axonal Met expression occurs after the initial establishment of fiber pathways, suggesting that Met may play a preferential role in collateralization and terminal field growth, rather than axon guidance - a distinction that

was previously unappreciated. This hypothesis is further supported by the appearance of Met immunoreactivity in the striatal and thalamic neuropil during periods of robust corticostriatal and corticothalamic axon collateralization (Frassoni et al., 1995; Nisenbaum et al., 1998; Sheth et al., 1998).

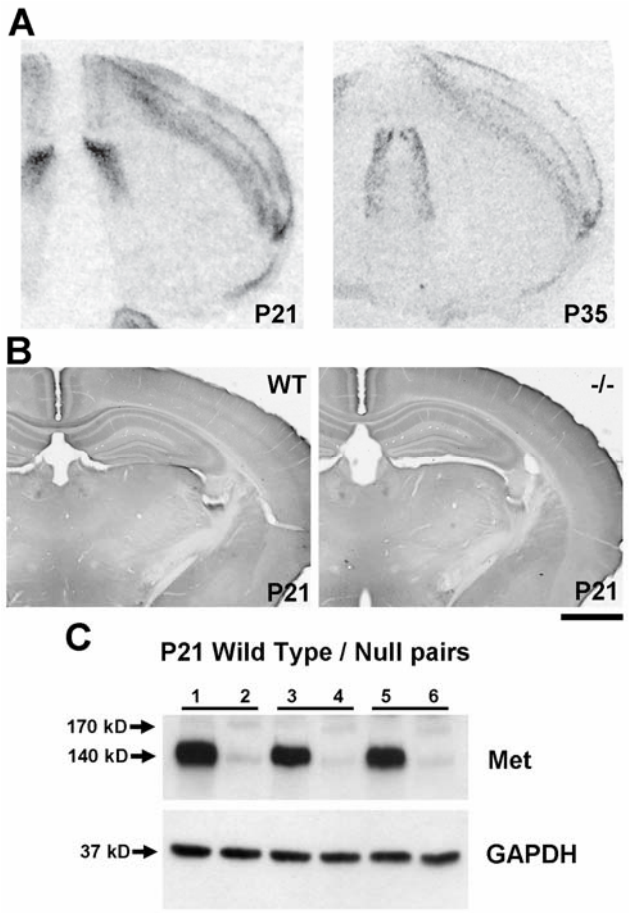

Figure 14. Analysis of *Met* transcript and protein expression in the developing mouse forebrain at P21 and P35. **A:** *In situ* hybridization analysis of *Met* in coronal sections from wild type mice at P21 and P35 shows equivalent patterns of expression to those observed in early postnatal development (P0 – P14). **B:** DIC photomicrographs of coronal sections from wild type (left) and $Emx1^{cre}/Met^{rx/fx}$ (right) mice demonstrate that at P21 (shown here) and later, no differences in Met immunoreactivity are observed. **C:** Western blot analysis of total Met protein in P21 wild type and $Emx1^{cre}/Met^{fx/fx}$ mice. Levels of Met in wild type mice (1,3,5) remain much higher than those in null mice (2,4,6) despite a lack of immunohistochemical staining as shown in **B**. Scale bar = 1.3 mm for both panels in **A**; 1.1 mm for both panels in **B**.

The general subsidence of Met protein expression in forebrain axons after the end of the second postnatal week coincides with a transition from axon outgrowth and elaboration to pruning and arbor refinement in most murine forebrain circuits (Stanfield et al., 1982; Stanfield et al., 1987; Gomez-Di Cesare et al., 1997; Portera-Cailliau et al., 2005). In the corpus callosum and stria terminalis, however, Met expression persists later and is detected through P21. This may reflect, relative to other axon tracts, more protracted periods of development, which, for the corpus callosum, have been determined by measurements of myelination (Jacobson, 1963; Tanaka et al., 2003; Vincze et al., 2008).

Though we found Met to be expressed predominantly by axons of projection neurons during forebrain development, our data do not preclude this receptor from being expressed at lower levels within dendrites and postsynaptic compartments, and even by other neuronal cell types. For example, though *Met* mRNA was not evident at any time in the ganglionic eminence and maturing striatum, Met protein labeling is seen on interneurons in explant cultures from the ganglionic eminence (Powell et al., 2001). Additionally, cultured dorsal thalamic neurons respond to HGF (Powell et al., 2003), indicating that either *in vitro* conditions may induce Met expression on neurons that normally do not express the transcript and protein during development, or the receptor is expressed below the limits of detection on certain cell types *in vivo*.

At the subcellular level, a shift to a predominantly synaptic localization after P14 may result in a more evenly distributed Met receptor population throughout the neuropil, which would be less readily detected by immunohistochemistry than axon fascicles and tracts, where protein levels are more concentrated. This may explain the discrepancy

between robust biochemical detection of Met protein at P21 and the lack of immunostaining in tissue sections. This interpretation is consistent with electrophysiological, biochemical and immuno-electron microscopy studies in the hippocampus that indicate Met to be present and functional at excitatory synapses in mature animals (Akimoto et al., 2004; Tyndall and Walikonis, 2006). Furthermore, there is emerging evidence that Met plays a developmental role in synaptic organization, as recent *in vitro* studies have demonstrated that HGF/Met signaling results in the enhanced expression and clustering of synaptic components (Madhavan and Peng, 2006; Tyndall and Walikonis, 2006; Nakano et al., 2007).

By adolescence and into adulthood, Met protein expression is low throughout the forebrain. Despite this dramatic down-regulation, however, patterns of transcript expression remain similar across early and late postnatal development, suggesting that the same populations of forebrain projection neurons express Met even during late developmental periods. This may reflect additional roles for Met in response to stress. For instance, Met is dramatically upregulated in cortical and hippocampal axons in adult animals with genetically compromised astrocytic populations (Su et al., 2007). HGF and Met are also upregulated in the cerebral cortex subsequent to a transient ischemic insult, though it is not known if Met protein levels specifically increase in cortical axons in this case (Honda et al., 1995).

In addition, there are reports of Met expression by non-neuronal cells of the CNS, including astrocytes, oligodendrocytes and microglia. Many of these studies report expression by these glial subtypes *in vitro* (Machide et al., 2000; Yan and Rivkees, 2002) or in injury or disease states (Lalive et al., 2005; Kitamura et al., 2007; Shimamura et al.,

2007), which may induce or enhance expression of the transcript and protein. In a developmental context, Ohya and colleagues report that striatal oligodendrocyte precursor cells (OPCs) express Met *in vivo* and respond to intrastriatal injections of HGF by remaining in a proliferative, immature state, delaying myelination (Ohya et al., 2007). However, we do not observe *Met* mRNA in cell bodies within either the gray matter or fiber tracts of the developing striatum, suggesting that the reported effects of HGF on OPC maturation may be axonally derived. While we cannot eliminate the possibility of Met expression by non-neuronal cells in the striatum and other forebrain regions, the patterns of labeling are not consistent with such expression during forebrain development.

Limbic system correlates of Met expression

While analysis of the spatio-temporal dynamics of Met expression provides insight into its cellular roles during development, analysis at the neural systems level lends insight into potential roles for Met signaling in the development of specific forebrain circuits. Patterns of Met expression overlap remarkably with classically defined limbic structures and their interconnecting fiber pathways (Broca, 1878; Papez, 1937; MacLean, 1955). It seems likely, therefore, that this receptor may be particularly important to the establishment of circuits that mediate social and emotional information processing. In the cortex, Met is expressed in multiple areas that have roles in processing limbic information, including the cingulate, prefrontal, orbitofrontal, temporal, and sensory association cortices. Additionally, Met is expressed in limbic structures involved in learning and memory, including the hippocampal formation and the mammillary

bodies of the hypothalamus. Finally, Met is expressed in amygdaloid subnuclei, which attach emotional valence to the processes of learning and memory (Davis and Whalen, 2001; Phelps and LeDoux, 2005), and the septum, which has roles in emotional regulation and the control of impulses (Gray and McNaughton, 1982; Menard and Treit, 1999).

Substantial Met expression is also present in axon pathways interconnecting principal limbic circuit nodes. For example, Met is expressed heavily in the cingulum, fornix, mammillothalamic tract, and internal capsule, all considered to be classic limbic pathways (Broca, 1878; Papez, 1937; MacLean, 1955). Additionally, Met expression is observed in the anterior commissure, which transmits information between temporal cortical areas, and tracts connecting the amygdala to other forebrain areas including the external capsule and the stria terminalis. Temporally, expression of Met in these fibers coincides with the period of maximal axonal outgrowth and collateralization, suggesting that Met is involved in these processes, and, therefore, in the development of limbic connections. As a corollary, aberrant Met signaling would likely result in deficient formation and subsequent function of these circuits. This is consistent with the first reported association of *MET* with a human, brain-based disorder, ASD (Campbell et al., 2006).

A role for Met in neurodevelopmental and neuropsychiatric disorders

Given the prevalence of Met in the forebrain structures discussed above, we hypothesize that this protein, or elements of its signaling pathway, may play a role in the etiology and/or pathophysiology of neurodevelopmental and psychiatric disorders with

socio-emotional valence. Three lines of evidence support this hypothesis. First, *MET*, the human homolog of *Met*, has been identified as an ASD susceptibility gene (Campbell et al., 2006). Second, MET protein expression is reduced in the superior temporal gyrus of individuals with autism (Campbell et al., 2007), whereas transcripts encoding other proteins in the MET signaling pathway are increased significantly. Third, an analysis of MET pathway genes reveals an association of an allelic variant of *PLAUR* with ASD (Campbell et al., 2008). *PLAUR* encodes the urokinase plasminogen activator receptor, which enhances HGF activation and signaling (Pepper et al., 1992; Mars et al., 1993).

At a cellular level, too, our findings suggest that disruption of MET may underlie or contribute to the pathophysiology of neuropsychiatric disorders. It has been suggested that many disorders, including ASD and schizophrenia, result from aberrant formation of neuronal connections during development (Rubenstein and Merzenich, 2003; Frith, 2004; Courchesne and Pierce, 2005; Geschwind and Levitt, 2007; Connors et al., 2008). The timing of expression, and the cellular compartmentalization of Met expression in the mouse suggests that the protein may have a larger than previously appreciated role in establishing and facilitating the maturation of appropriate connections. Consequently, errant Met signaling is likely to result in disruption of normal patterns of connectivity in the forebrain. Disrupted Met signaling could result from alterations in the regulation, timing, or levels of receptor expression. Ongoing analysis of the $Emx1^{cre}/Met^{fx/fx}$ mouse and other models of disrupted Met signaling will help to elucidate the roles of Met in developing forebrain connectivity.

Other Acknowledgements

We thank Deborah Gregory, Donte Smith, Kate Spencer and Paula Woods for excellent technical assistance. We also thank Drs. Elizabeth Hammock, Shenfeng Qiu, and Barbara Thompson for helpful comments on the manuscript.

Literature Cited

Aggleton JP. 2000. The amygdala : a functional analysis. Oxford, OX ; New York: Oxford University Press. xiv, 690 p.

Aghajanian GK, Bloom FE. 1967. The formation of synaptic junctions in developing rat brain: a quantitative electron microscopic study. Brain Res 6:716-727.

Akagi K, Powell EW. 1968. Differential projections of habenular nuclei. J Comp Neurol 132:263-274.

Akimoto M, Baba A, Ikeda-Matsuo Y, Yamada MK, Itamura R, Nishiyama N, Ikegaya Y, Matsuki N. 2004. Hepatocyte growth factor as an enhancer of nmda currents and synaptic plasticity in the hippocampus. Neuroscience 128:155-162.

Allen GV, Hopkins DA. 1989. Mamillary body in the rat: topography and synaptology of projections from the subicular complex, prefrontal cortex, and midbrain tegmentum. J Comp Neurol 286:311-336.

Ashley-Koch A, Wolpert CM, Menold MM, Zaeem L, Basu S, Donnelly SL, Ravan SA, Powell CM, Qumsiyeh MB, Aylsworth AS, Vance JM, Gilbert JR, Wright HH, Abramson RK, DeLong GR, Cuccaro ML, Pericak-Vance MA. 1999. Genetic studies of autistic disorder and chromosome 7. Genomics 61:227-236.

Barrett S, Beck JC, Bernier R, Bisson E, Braun TA, Casavant TL, Childress D, Folstein SE, Garcia M, Gardiner MB, Gilman S, Haines JL, Hopkins K, Landa R, Meyer NH, Mullane JA, Nishimura DY, Palmer P, Piven J, Purdy J, Santangelo SL, Searby C, Sheffield V, Singleton J, Slager S, et al. 1999. An autosomal genomic screen for autism. Collaborative linkage study of autism. American journal of medical genetics 88:609-615.

Bladt F, Riethmacher D, Isenmann S, Aguzzi A, Birchmeier C. 1995. Essential role for the c-Met receptor in the migration of myogenic precursor cells into the limb bud. Nature 376:768-771.

Blue ME, Parnavelas JG. 1983. The formation and maturation of synapses in the visual cortex of the rat. II. Quantitative analysis. J Neurocytol 12:697-712.

Broca P. 1878. Anatomie comparee des circonvolutions cerebrales: le grand lobe limbique. Rev Anthropol 1:385-498.

Brodal A. 1948. The origin of the fibers of the anterior commissure in the rat. Experimental studies. J Comp Neurol 88:157-205.

Brothers LA, Finch DM. 1985. Physiological evidence for an excitatory pathway from entorhinal cortex to amygdala in the rat. Brain Res 359:10-20.

Campbell DB, Levitt P. 2003. Regionally restricted expression of the transcription factor c-myc intron 1 binding protein during brain development. J Comp Neurol 467:581-592.
Campbell DB, Sutcliffe JS, Ebert PJ, Militerni R, Bravaccio C, Trillo S, Elia M, Schneider C, Melmed R, Sacco R, Persico AM, Levitt P. 2006. A genetic variant that disrupts MET transcription is associated with autism. Proc Natl Acad Sci U S A 103:16834-16839.
Campbell DB, D'Oronzio R, Garbett K, Ebert PJ, Mirnics K, Levitt P, Persico AM. 2007. Disruption of cerebral cortex MET signaling in autism spectrum disorder. Annals of neurology 62:243-250.
Campbell DB, Li C, Sutcliffe JS, Persico AM, Levitt P. 2008. Genetic evidence implicating multiple genes in the MET receptor tyrosine kinase pathway in autism spectrum disorder. Autism Research 1:159-168.
Canteras NS, Simerly RB, Swanson LW. 1992. Connections of the posterior nucleus of the amygdala. J Comp Neurol 324:143-179.
Canteras NS, Swanson LW. 1992. Projections of the ventral subiculum to the amygdala, septum, and hypothalamus: a PHAL anterograde tract-tracing study in the rat. J Comp Neurol 324:180-194.
Canteras NS, Simerly RB, Swanson LW. 1995. Organization of projections from the medial nucleus of the amygdala: a PHAL study in the rat. J Comp Neurol 360:213-245.
Caton A, Hacker A, Naeem A, Livet J, Maina F, Bladt F, Klein R, Birchmeier C, Guthrie S. 2000. The branchial arches and HGF are growth-promoting and chemoattractant for cranial motor axons. Development 127:1751-1766.
Cenquizca LA, Swanson LW. 2006. Analysis of direct hippocampal cortical field CA1 axonal projections to diencephalon in the rat. J Comp Neurol 497:101-114.
Chang HT, Wilson CJ, Kitai ST. 1981. Single neostriatal efferent axons in the globus pallidus: a light and electron microscopic study. Science 213:915-918.
Chiba T, Murata Y. 1985. Afferent and efferent connections of the medial preoptic area in the rat: a WGA-HRP study. Brain Res Bull 14:261-272.
Connors SL, Levitt P, Matthews SG, Slotkin TA, Johnston MV, Kinney HC, Johnson WG, Dailey RM, Zimmerman AW. 2008. Fetal mechanisms in neurodevelopmental disorders. Pediatric neurology 38:163-176.
Cooper CS, Park M, Blair DG, Tainsky MA, Huebner K, Croce CM, Vande Woude GF. 1984. Molecular cloning of a new transforming gene from a chemically transformed human cell line. Nature 311:29-33.
Courchesne E, Pierce K. 2005. Why the frontal cortex in autism might be talking only to itself: local over-connectivity but long-distance disconnection. Current opinion in neurobiology 15:225-230.
Cruce JA. 1975. An autoradiographic study of the projections of the mammillothalamic tract in the rat. Brain Res 85:211-219.
Davis M, Whalen PJ. 2001. The amygdala: vigilance and emotion. Molecular Psychiatry 6:13-34.
De Felipe J, Marco P, Fairen A, Jones EG. 1997. Inhibitory synaptogenesis in mouse somatosensory cortex. Cereb Cortex 7:619-634.

Dolorfo CL, Amaral DG. 1998. Entorhinal cortex of the rat: topographic organization of the cells of origin of the perforant path projection to the dentate gyrus. J Comp Neurol 398:25-48.
Domesick VB. 1970. The fasciculus cinguli in the rat. Brain Res 20:19-32.
Dong HW, Petrovich GD, Swanson LW. 2001. Topography of projections from amygdala to bed nuclei of the stria terminalis. Brain Res Brain Res Rev 38:192-246.
Dyson SE, Jones DG. 1980. Quantitation of terminal parameters and their inter-relationships in maturing central synapses: a perspective for experimental studies. Brain Res 183:43-59.
Ebens A, Brose K, Leonardo ED, Hanson MG, Jr., Bladt F, Birchmeier C, Barres BA, Tessier-Lavigne M. 1996. Hepatocyte growth factor/scatter factor is an axonal chemoattractant and a neurotrophic factor for spinal motor neurons. Neuron 17:1157-1172.
Ericson H, Blomqvist A, Kohler C. 1991. Origin of neuronal inputs to the region of the tuberomammillary nucleus of the rat brain. J Comp Neurol 311:45-64.
Faulkner B, Brown TH. 1999. Morphology and physiology of neurons in the rat perirhinal-lateral amygdala area. J Comp Neurol 411:613-642.
Frassoni C, Arcelli P, Regondi MC, Selvaggio M, De Biasi S, Spreafico R. 1995. Branching pattern of corticothalamic projections from the somatosensory cortex during postnatal development in the rat. Brain Res Dev Brain Res 90:111-121.
Frith C. 2004. Is autism a disconnection disorder? Lancet neurology 3:577.
Garzotto D, Giacobini P, Crepaldi T, Fasolo A, De Marchis S. 2008. Hepatocyte growth factor regulates migration of olfactory interneuron precursors in the rostral migratory stream through Met-Grb2 coupling. J Neurosci 28:5901-5909.
Geschwind DH, Levitt P. 2007. Autism spectrum disorders: developmental disconnection syndromes. Current opinion in neurobiology 17:103-111.
Giacobini P, Messina A, Wray S, Giampietro C, Crepaldi T, Carmeliet P, Fasolo A. 2007. Hepatocyte growth factor acts as a motogen and guidance signal for gonadotropin hormone-releasing hormone-1 neuronal migration. J Neurosci 27:431-445.
Gomez-Di Cesare CM, Smith KL, Rice FL, Swann JW. 1997. Axonal remodeling during postnatal maturation of CA3 hippocampal pyramidal neurons. J Comp Neurol 384:165-180.
Gonzalo-Ruiz A, Alonso A, Sanz JM, Llinas RR. 1992. Afferent projections to the mammillary complex of the rat, with special reference to those from surrounding hypothalamic regions. J Comp Neurol 321:277-299.
Gorski JA, Talley T, Qiu M, Puelles L, Rubenstein JL, Jones KR. 2002. Cortical excitatory neurons and glia, but not GABAergic neurons, are produced in the Emx1-expressing lineage. J Neurosci 22:6309-6314.
Gottlieb DI, Cowan WM. 1973. Autoradiographic studies of the commissural and ipsilateral association connection of the hippocampus and detentate gyrus of the rat. I. The commissural connections. J Comp Neurol 149:393-422.
Gray JA, McNaughton N. 1983. Comparison between the behavioural effects of septal and hippocampal lesions: a review. Neuroscience & Biobehavioral Reviews 7:119-188.

Guillery RW. 1957. Degeneration in the hypothalamic connexions of the albino rat. J Anat 91:91-115.
Gurdjian ES. 1925. Olfactory connections in the albino rat, with special reference to the stria medullaris and the anterior commissure. J Comp Neurol 38:127-163.
Gutierrez H, Dolcet X, Tolcos M, Davies A. 2004. HGF regulates the development of cortical pyramidal dendrites. Development 131:3717-3726.
Hamanoue M, Takemoto N, Matsumoto K, Nakamura T, Nakajima K, Kohsaka S. 1996. Neurotrophic effect of hepatocyte growth factor on central nervous system neurons in vitro. J Neurosci Res 43:554-564.
Heinbockel T, Pape HC. 2000. Input-specific long-term depression in the lateral amygdala evoked by theta frequency stimulation. J Neurosci 20:RC68.
Herkenham M, Nauta WJ. 1977. Afferent connections of the habenular nuclei in the rat. A horseradish peroxidase study, with a note on the fiber-of-passage problem. J Comp Neurol 173:123-146.
Hockfield S. 1993. Molecular probes of the nervous system; selected methods for antibody and nucleic acid probes. Plainview, NY: Cold Spring Harbor Laboratory Press. xxii, 679 p.
Honda S, Kagoshima M, Wanaka A, Tohyama M, Matsumoto K, Nakamura T. 1995. Localization and functional coupling of HGF and c-Met/HGF receptor in rat brain: implication as neurotrophic factor. Brain Res Mol Brain Res 32:197-210.
Huh CG, Factor VM, Sanchez A, Uchida K, Conner EA, Thorgeirsson SS. 2004. Hepatocyte growth factor/c-met signaling pathway is required for efficient liver regeneration and repair. Proc Natl Acad Sci U S A 101:4477-4482.
IMGSAC. 1998. A full genome screen for autism with evidence for linkage to a region on chromosome 7q. International Molecular Genetic Study of Autism Consortium Hum Mol Genet 7:571-578.
Jacobson S. 1963. Sequence Of Myelinization In The Brain Of The Albino Rat. A. Cerebral Cortex, Thalamus And Related Structures. J Comp Neurol 121:5-29.
Jouandet ML, Hartenstein V. 1983. Basal telencephalic origins of the anterior commissure of the rat. Experimental brain research Experimentelle Hirnforschung 50:183-192.
Jung W, Castren E, Odenthal M, Vande Woude GF, Ishii T, Dienes HP, Lindholm D, Schirmacher P. 1994. Expression and functional interaction of hepatocyte growth factor-scatter factor and its receptor c-met in mammalian brain. J Cell Biol 126:485-494.
Kawaja MD, Flumerfelt BA, Hrycyshyn AW. 1990. Synaptic organization of septal projections in the rat medial habenula: a wheat germ agglutinin-horseradish peroxidase and immunohistochemical study. Synapse 6:45-54.
Kishi T, Tsumori T, Ono K, Yokota S, Ishino H, Yasui Y. 2000. Topographical organization of projections from the subiculum to the hypothalamus in the rat. J Comp Neurol 419:205-222.
Kitamura K, Iwanami A, Nakamura M, Yamane J, Watanabe K, Suzuki Y, Miyazawa D, Shibata S, Funakoshi H, Miyatake S, Coffin RS, Nakamura T, Toyama Y, Okano H. 2007. Hepatocyte growth factor promotes endogenous repair and functional recovery after spinal cord injury. J Neurosci Res 85:2332-2342.

Korhonen L, Sjoholm U, Takei N, Kern MA, Schirmacher P, Castren E, Lindholm D. 2000. Expression of c-Met in developing rat hippocampus: evidence for HGF as a neurotrophic factor for calbindin D-expressing neurons. Eur J Neurosci 12:3453-3461.

Lalive PH, Paglinawan R, Biollaz G, Kappos EA, Leone DP, Malipiero U, Relvas JB, Moransard M, Suter T, Fontana A. 2005. TGF-beta-treated microglia induce oligodendrocyte precursor cell chemotaxis through the HGF-c-Met pathway. Eur J Immunol 35:727-737.

Lim CS, Walikonis RS. 2008. Hepatocyte growth factor and c-Met promote dendritic maturation during hippocampal neuron differentiation via the Akt pathway. Cell Signal 20:825-835.

Machide M, Kamitori K, Kohsaka S. 2000. Hepatocyte growth factor-induced differential activation of phospholipase cgamma 1 and phosphatidylinositol 3-kinase is regulated by tyrosine phosphatase SHP-1 in astrocytes. J Biol Chem 275:31392-31398.

MacLean PD. 1955. The limbic system ("visceral brain") and emotional behavior. Archives of Neurology and Psychiatry 73:130-134.

Madhavan R, Peng HB. 2006. HGF induction of postsynaptic specializations at the neuromuscular junction. J Neurobiol 66:134-147.

Markus EJ, Petit TL. 1987. Neocortical synaptogenesis, aging, and behavior: lifespan development in the motor-sensory system of the rat. Exp Neurol 96:262-278.

Mars WM, Zarnegar R, Michalopoulos GK. 1993. Activation of hepatocyte growth factor by the plasminogen activators uPA and tPA. Am J Pathol 143:949-958.

Martins GJ, Plachez C, Powell EM. 2007. Loss of embryonic MET signaling alters profiles of hippocampal interneurons. Dev Neurosci 29:143-158.

McDonald AJ. 1991a. Organization of amygdaloid projections to the prefrontal cortex and associated striatum in the rat. Neuroscience 44:1-14.

McDonald AJ. 1991b. Topographical organization of amygdaloid projections to the caudatoputamen, nucleus accumbens, and related striatal-like areas of the rat brain. Neuroscience 44:15-33.

Menard J, Treit D. 1999. Effects of centrally administered anxiolytic compounds in animal models of anxiety. Neuroscience & Biobehavioral Reviews 23:591-613.

Micheva KD, Beaulieu C. 1996. Quantitative aspects of synaptogenesis in the rat barrel field cortex with special reference to GABA circuitry. J Comp Neurol 373:340-354.

Miller M, Peters A. 1981. Maturation of rat visual cortex. II. A combined Golgi-electron microscope study of pyramidal neurons. J Comp Neurol 203:555-573.

Miller MW. 1986. Maturation of rat visual cortex. III. Postnatal morphogenesis and synaptogenesis of local circuit neurons. Brain Res 390:271-285.

Mufson EJ, Pandya DN. 1984. Some observations on the course and composition of the cingulum bundle in the rhesus monkey. J Comp Neurol 225:31-43.

Nakano M, Takagi N, Takagi K, Funakoshi H, Matsumoto K, Nakamura T, Takeo S. 2007. Hepatocyte growth factor promotes the number of PSD-95 clusters in young hippocampal neurons. Exp Neurol 207:195-202.

Nisenbaum LK, Webster SM, Chang SL, McQueeney KD, LoTurco JJ. 1998. Early patterning of prelimbic cortical axons to the striatal patch compartment in the neonatal mouse. Dev Neurosci 20:113-124.
Ohya W, Funakoshi H, Kurosawa T, Nakamura T. 2007. Hepatocyte growth factor (HGF) promotes oligodendrocyte progenitor cell proliferation and inhibits its differentiation during postnatal development in the rat. Brain Res 1147:51-65.
Papez JW. 1937. A proposed mechanism of emotion. Archives of Neurology and Psychiatry 38:725-743.
Parnavelas JG, Uylings HB. 1980. The growth of non-pyramidal neurons in the visual cortex of the rat: a morphometric study. Brain Res 193:373-382.
Pennypacker K, Fischer I, Levitt P. 1991. Early in vitro genesis and differentiation of axons and dendrites by hippocampal neurons analyzed quantitatively with neurofilament-H and microtubule-associated protein 2 antibodies. Exp Neurol 111:22-35.
Pepper MS, Matsumoto K, Nakamura T, Orci L, Montesano R. 1992. Hepatocyte growth factor increases urokinase-type plasminogen activator (u-PA) and u-PA receptor expression in Madin-Darby canine kidney epithelial cells. J Biol Chem 267:20493-20496.
Phelan KD, Sacaan A, Gallagher JP. 1996. Retrograde labeling of rat dorsolateral septal nucleus neurons following intraseptal injections of WGA-HRP. Synapse 22:261-268.
Phelps EA, LeDoux JE. 2005. Contributions of the amygdala to emotion processing: from animal models to human behavior. Neuron 48:175-187.
Portera-Cailliau C, Weimer RM, De Paola V, Caroni P, Svoboda K. 2005. Diverse modes of axon elaboration in the developing neocortex. PLoS Biol 3:e272.
Powell EM, Mars WM, Levitt P. 2001. Hepatocyte growth factor/scatter factor is a motogen for interneurons migrating from the ventral to dorsal telencephalon. Neuron 30:79-89.
Powell EM, Muhlfriedel S, Bolz J, Levitt P. 2003. Differential regulation of thalamic and cortical axonal growth by hepatocyte growth factor/scatter factor. Dev Neurosci 25:197-206.
Preston RJ, Bishop GA, Kitai ST. 1980. Medium spiny neuron projection from the rat striatum: an intracellular horseradish peroxidase study. Brain Res 183:253-263.
Risold PY, Swanson LW. 1997. Connections of the rat lateral septal complex. Brain Res Brain Res Rev 24:115-195.
Rubenstein JL, Merzenich MM. 2003. Model of autism: increased ratio of excitation/inhibition in key neural systems. Genes, brain, and behavior 2:255-267.
Santiago AC, Shammah-Lagnado SJ. 2004. Efferent connections of the nucleus of the lateral olfactory tract in the rat. J Comp Neurol 471:314-332.
Seki M, Zyo K. 1984. Anterior thalamic afferents from the mamillary body and the limbic cortex in the rat. J Comp Neurol 229:242-256.
Sheth AN, McKee ML, Bhide PG. 1998. The sequence of formation and development of corticostriate connections in mice. Dev Neurosci 20:98-112.
Shibata H. 1993. Efferent projections from the anterior thalamic nuclei to the cingulate cortex in the rat. J Comp Neurol 330:533-542.

Shimamura M, Sato N, Sata M, Wakayama K, Ogihara T, Morishita R. 2007. Expression of hepatocyte growth factor and c-Met after spinal cord injury in rats. Brain Res 1151:188-194.
Staiger JF, Nurnberger F. 1991. The efferent connections of the lateral septal nucleus in the guinea pig: intrinsic connectivity of the septum and projections to other telencephalic areas. Cell Tissue Res 264:415-426.
Stanfield BB, O'Leary DD, Fricks C. 1982. Selective collateral elimination in early postnatal development restricts cortical distribution of rat pyramidal tract neurones. Nature 298:371-373.
Stanfield BB, Nahin BR, O'Leary DD. 1987. A transient postmamillary component of the rat fornix during development: implications for interspecific differences in mature axonal projections. J Neurosci 7:3350-3361.
Steward O, Scoville SA. 1976. Cells of origin of entorhinal cortical afferents to the hippocampus and fascia dentata of the rat. J Comp Neurol 169:347-370.
Su W, Xing R, Guha A, Gutmann DH, Sherman LS. 2007. Mice with GFAP-targeted loss of neurofibromin demonstrate increased axonal MET expression with aging. Glia 55:723-733.
Sun W, Funakoshi H, Nakamura T. 2002. Localization and functional role of hepatocyte growth factor (HGF) and its receptor c-met in the rat developing cerebral cortex. Brain Res Mol Brain Res 103:36-48.
Swanson LW, Cowan WM. 1977. An autoradiographic study of the organization of the efferent connections of the hippocampal formation in the rat. J Comp Neurol 172:49-84.
Swanson LW, Wyss JM, Cowan WM. 1978. An autoradiographic study of the organization of intrahippocampal association pathways in the rat. J Comp Neurol 181:681-715.
Swanson LW, Cowan WM. 1979. The connections of the septal region in the rat. J Comp Neurol 186:621-655.
Szinyei C, Heinbockel T, Montagne J, Pape HC. 2000. Putative cortical and thalamic inputs elicit convergent excitation in a population of GABAergic interneurons of the lateral amygdala. J Neurosci 20:8909-8915.
Tanaka Y, Yamada K, Zhou CJ, Ban N, Shioda S, Inagaki N. 2003. Temporal and spatial profiles of ABCA2-expressing oligodendrocytes in the developing rat brain. J Comp Neurol 455:353-367.
Tepper JM, Trent F. 1993. In vivo studies of the postnatal development of rat neostriatal neurons. Prog Brain Res 99:35-50.
Tepper JM, Sharpe NA, Koos TZ, Trent F. 1998. Postnatal development of the rat neostriatum: electrophysiological, light- and electron-microscopic studies. Dev Neurosci 20:125-145.
Thewke DP, Seeds NW. 1999. The expression of mRNAs for hepatocyte growth factor/scatter factor, its receptor c-met, and one of its activators tissue-type plasminogen activator show a systematic relationship in the developing and adult cerebral cortex and hippocampus. Brain Res 821:356-367.
Tyndall SJ, Walikonis RS. 2006. The receptor tyrosine kinase Met and its ligand hepatocyte growth factor are clustered at excitatory synapses and can enhance clustering of synaptic proteins. Cell Cycle 5:1560-1568.

Tyndall SJ, Patel SJ, Walikonis RS. 2007. Hepatocyte growth factor-induced enhancement of dendritic branching is blocked by inhibitors of N-methyl-D-aspartate receptors and calcium/calmodulin-dependent kinases. J Neurosci Res 85:2343-2351.

van Groen T, Kadish I, Wyss JM. 2002. Species differences in the projections from the entorhinal cortex to the hippocampus. Brain Res Bull 57:553-556.

Vincze A, Mazlo M, Seress L, Komoly S, Abraham H. 2008. A correlative light and electron microscopic study of postnatal myelination in the murine corpus callosum. Int J Dev Neurosci.

Watanabe K, Kawana E. 1980. A horseradish peroxidase study on the mammillothalamic tract in the rat. Acta Anat (Basel) 108:394-401.

Weisskopf MG, LeDoux JE. 1999. Distinct populations of NMDA receptors at subcortical and cortical inputs to principal cells of the lateral amygdala. Journal of neurophysiology 81:930-934.

White LE, Jr. 1959. Ipsilateral afferents to the hippocampal formation in the albino rat. I. Cingulum projections. J Comp Neurol 113:1-41.

Wilson CJ, Phelan KD. 1982. Dual topographic representation of neostriatum in the globus pallidus of rats. Brain Res 243:354-359.

Yan H, Rivkees SA. 2002. Hepatocyte growth factor stimulates the proliferation and migration of oligodendrocyte precursor cells. J Neurosci Res 69:597-606.

Yonan AL, Alarcon M, Cheng R, Magnusson PK, Spence SJ, Palmer AA, Grunn A, Juo SH, Terwilliger JD, Liu J, Cantor RM, Geschwind DH, Gilliam TC. 2003. A genomewide screen of 345 families for autism-susceptibility loci. American journal of human genetics 73:886-897.

Zhang L, Himi T, Morita I, Murota S. 2000. Hepatocyte growth factor protects cultured rat cerebellar granule neurons from apoptosis via the phosphatidylinositol-3 kinase/Akt pathway. J Neurosci Res 59:489-496.

CHAPTER III

CONSERVED AND DIVERGENT EXPRESSION PATTERNS OF THE MET RECEPTOR REFLECT SPECIES-SPECIFIC FUNCTIONAL SPECIALIZATIONS RELEVANT TO AUTISM

Matthew C. Judson[3,*], David Amaral[5] and Pat Levitt[1,2,4]

[1]Vanderbilt Kennedy Center for Research on Human Development, [2]Department of Pharmacology and [3]Graduate Program in Neuroscience, Vanderbilt University Medical Center
Nashville, TN 37203

[4]Zilkha Neurogenetic Institute and the Department of Cell and Neurobiology, Keck School of Medicine, University of Southern California, Los Angeles, CA 90089.

[5]MIND Institute, University of California, Davis

Correspondence to:
Pat Levitt, Ph.D.
Director, Zilkha Neurogenetic Institute
Provost Professor of Neuroscience, Pediatrics, Psychiatry and Pharmacy
Chair, Dept. Cell and Neurobiology
Keck School of Medicine of USC
1501 San Pablo Street
Los Angeles, CA 90089-2821
323-442-1509
323-442-2145 (fax)
www.usc.edu/zni

Grant sponsor: National Institutes of Health (NIH)/National Institute of Mental Health (NIMH); Grant number MH067842 (PL); Grant Sponsor: NIH/National Institute of Child Health and Human Development; Grant number: P30 HD15052 (E. Dykens); Grant sponsor: NIH/National Institute on Drug Abuse (NIDA); Grant number DA022785 (PL); Simons Foundation (PL)

Abstract

Two lines of evidence support the hypothesis that MET receptor tyrosine kinase signaling regulates the wiring of socially and emotionally relevant forebrain circuits. First, a functional *MET* promoter variant is associated with the social and communication phenotypes of autism spectrum disorders (ASD). Second, the homologous murine receptor, Met, is expressed most heavily in long-projecting axons of the neocortex and limbic system during the developmental period when connections between these structures are being established. This study tests the hypothesis that MET forebrain expression reflects species-specific specialization of circuits that underlie social interaction, a core behavior that is disrupted in ASD. We compared patterns of Met/MET protein expression in the developing mouse and rhesus macaque forebrain. There was a strong temporal conservation of expression during the time of rapid axon pathway development and the onset of terminal growth and robust synapse formation. Moreover, expression patterns of Met/MET in limbic-related structures were almost identical in both species. These conserved patterns were in marked contrast to the highly divergent expression that was evident in the neocortex. In mouse, Met was broadly distributed throughout neocortex. In the macaque, only selective regions of anterior cingulate, inferior temporal, posterior parietal and visual cortices expressed MET, including face processing regions. Overall, the pattern is consistent with the importance of vision in the social repertoire of the primate. These data suggest an evolutionarily conserved, developmental function of the MET receptor in wiring together limbic and neocortical circuits that facilitate species-appropriate social behaviors.

Introduction

Current etiological theories of autism spectrum disorders (ASD), defined in part by deficits in social interaction and communication, are based on the concept of developmental disruptions in forebrain connectivity (Frith, 2004; Geschwind and Levitt, 2007; Levy, 2007). Evidence supporting these theories has largely come from genetic susceptibility, correlated clinical phenotypes, and functional imaging studies. The latter have revealed altered patterns of brain activity and synchronization in individuals with ASD during social information processing and communication tasks (Just et al., 2004; Koshino et al., 2008; Acker and Antic, 2009). However, a mechanistic understanding of the development of aberrant social circuitry is currently limited.

One approach to elucidating etiological mechanisms of ASD is to study the developmental functions of associated, variant genes. Independent genetic studies of ASD have revealed CNVs (Marshall et al., 2008), rare mutations (Campbell, et al, 2006) and the association of two common allelic variants (rs1858830-C and rs38845-A) of the *MET* receptor tyrosine kinase gene (Campbell et al., 2006; Campbell et al., 2008; Jackson et al., 2009; Sousa et al., 2009). Moreover, an enriched association of the rs1858830-C allele with social and communication phenotypes of ASD was recently demonstrated (Campbell et al., 2009). Because Met signaling *in vitro* potentiates axon outgrowth, dendritogenesis, and synaptogenesis (Ebens et al., 1996; Gutierrez et al., 2004; Madhavan and Peng, 2006; Tyndall and Walikonis, 2006; Nakano et al., 2007), a basic mechanistic hypothesis relating *MET* gene function and ASD risk has emerged: decreased MET protein expression during development increases the risk of ASD-relevant circuit miswiring. Met is expressed in selective patterns in the mouse forebrain that include

circuitry involved in social behavior (Judson et al., 2009), but how this translates to relevant at-risk primate circuitry is unknown.

Mammalian conspecifics, including primates, exchange information concerning fitness, mating status, and other factors influencing individual or group survival. Stereotyped forebrain circuitry has evolved to support the cognitive processing that underlies this conserved social behavior. For example, circuits involving the hippocampal formation and mammillary nuclei facilitate the encoding of socially relevant spatial cues and social recognition (Steckler et al., 1998; Sanchez-Andrade et al., 2005). The emotional quality of social stimuli is processed by the amygdala in all mammalian species (Phelps and LeDoux, 2005). The input pathways that route social information to these conserved cognitive circuits, however, are divergent across mammalian taxa, reflecting the various communication modes utilized within this class of animals (Hauser, 1996). Primates, for instance, communicate primarily by issuing physical gestures and vocalizations, the receipt of which requires visual and auditory system function, respectively. In contrast, rodents depend more heavily on somatosensation and olfaction to communicate. Appropriate species-specific social behavior, therefore, necessarily depends on the wiring together of relevant sensory and cognitive circuitry during development.

Here we test a prediction of the hypothesis that Met/MET receptor signaling regulates the development of socially relevant forebrain circuitry: Met/MET expression patterns will reflect species-specific requirements for social interaction. Specifically, we compare Met receptor expression in the mouse forebrain with that of its homologue,

MET, in the macaque forebrain across corresponding periods of development related to circuit formation.

Materials and Methods

Preparation of fixed brain sections

Wild type C57BL/6J mice were either purchased from the Jackson Laboratory (Bar Harbor, ME) or harvested from $Emx1^{cre}$/ $Met^{fx/+}$ X $Emx1^{+}$/ $Met^{fx/fx}$ matings using previously described mouse husbandry and genotyping strategies (Judson et al., 2009). In the latter case, mice with a $Met^{fx/fx}$ or $Met^{fx/+}$ genotype were considered wild type if they did not have cre recombinase knocked-in to the 3' untranslated region of either Emx1 allele. Mice aged between postnatal (P) day 0 and 21 were deeply anesthetized with sodium pentobarbital (60 mg/kg i.p.) prior to transcardial perfusion with room temperature phosphate-buffered 4% paraformaldehyde (pH 7.3) containing 1.3% L-lysine and 0.24% sodium periodate. After postfixation overnight at 4°C, brains were cryoprotected via sequential 12-hour incubations in 10%, 20%, and 30% sucrose in PBS, pH 7.5. Fixed brains were then sectioned as previously described (Judson et al., 2009). Briefly, P0 brains were sectioned at 20 μM with a cryostat and P7-P21 brains were sectioned at 40 μM with a sliding microtome (Leica, Bannockburn, IL). Prior to immunohistochemical processing, P0 sections were stored at -80°C on gelatin-coated slides and P7-P21 sections were stored at -20°C, free-floating in a cryopreservative solution.

Series of pre- and postnatal macaque (*Macaca mulatta*) brain sections (N = 2, each age) were from animals housed at the California National Primate Research Center (University of California, Davis, Davis, CA), and were prepared as previously described.

All research procedures using mice and macaques conformed to NIH guidelines and were approved by the Institutional Animal Care and Use Committees at Vanderbilt University and the University of California at Davis, respectively. All efforts were made to minimize animal suffering and to reduce the number of animals used.

Met/MET immunohistochemistry

Two different monoclonal antibodies were used for Met/MET immunohistochemical study: 1) mouse anti-Met (Met, B-2; sc-8057; Lot No. C2807; Santa Cruz Biotechnology, Santa Cruz, CA), and 2) mouse anti-Met (Met, 25H2; #3127; Lot No. 3; Cell Signaling Technology, Beverly, MA). Met immunohistochemistry was performed as previously described (Judson et al., 2009). Briefly, free-floating mouse or macaque brain sections were rinsed several times in PBS before the following blocking procedures were applied: 1) 5 minutes in 0.3% H_20_2 in methanol, 2) 25 minutes in 0.1 M Tris-glycine (pH 7.4), and 3) 25 minutes in Blotto-T (4% Carnation dried milk in PBS containing 0.2% Triton-X-100). PBS rinses preceded both the Tris-Glycine and Blotto-T blocking steps. For mouse tissue, an additional 1.5-hour incubation in unlabeled donkey anti-mouse IgG (Fab; Jackson Immunoresearch, West Grove, PA) was performed immediately before the Blotto-T step in order to block endogenous immunoglobulins. After blocking, brain sections were incubated in primary anti-Met antibodies for 48 hours at 4°C. Specifically, sections were incubated in either 1:250 anti-Met (Santa Cruz sc-8057, mouse sections only) or 1:400 anti-Met (Cell Signaling #3127, some mouse

sections and all macaque sections) diluted in Blotto-T. Following washes in Blotto-T, sections were then incubated for 1 hour at room temperature in 1:1,000 biotin-SP-conjugated donkey antimouse IgG (Jackson Immunoresearch) diluted in Blotto-T. Sections were then rinsed several times in PBS and processed by the ABC Elite histochemical method (Vector, Burlingame, CA). Met-specific antibody complexes were visualized by incubating the sections for 2–4 minutes at room temperature in 0.05% 3'3'-diaminobenzidine (DAB) with 0.015% H_20_2.

Cross-species use of antibodies

We examined the cross-species reactivity of the two commercially available mouse monoclonal antibodies used to immunohistochemically label mouse Met protein and homologous monkey MET protein in the present study. These antibodies were generated against synthetic peptides corresponding to evolutionarily conserved intracellular domains of the mouse (Santa Cruz #8057; immunogen: peptide corresponding to amino acids 1330–1379 of mouse Met [NCBI No. NP 032617) and human (Cell Signaling #3127; immunogen: peptide corresponding to C-terminal amino acids of human Met [NCBI No. AAA59591) receptors, and they exhibited remarkably high species cross-reactivity when substituted for each other in a previously described immunohistochemical staining protocol (see "Met/MET immunohistochemistry" subsection of Materials and Methods)(Judson et al., 2009). For example, these antibodies yielded indistinguishable staining patterns in comparable regions of the somatosensory cortex (**Supplemental Fig. 1A,B**) and hippocampus (**Supplemental Fig. 1C,D**) in postnatal day (P) 7 mice.

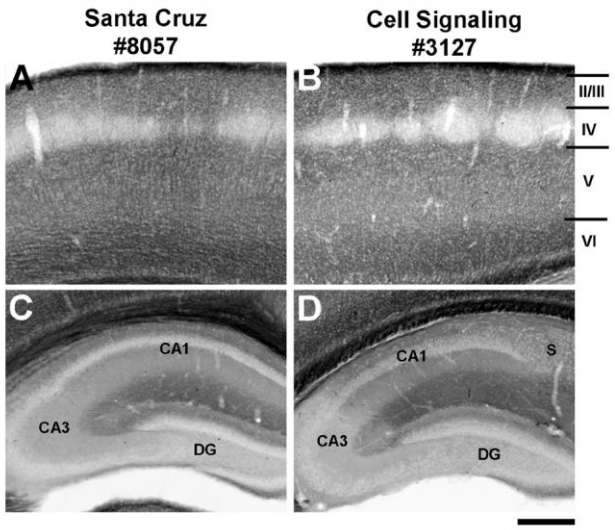

Supplemental Figure 1. Equivalent specificity of commercially available Met/MET antibodies. DIC photomicrographs illustrate Met immunohistochemistry in coronal sections (**A** and **C**, Santa Cruz mouse anti-mouse Met #8057) and sagittal sections (**B** and **D**, Cell Signaling mouse anti-human MET #3127) from P7 mice. Identical staining patterns are obtained with both antibodies as shown in the somatosensory cortex (**A** and **B**) and the hippocampus (**C** and **D**). II-VI, neocortical layers 2 through 6; CA1, cornu ammonis 1 of hippocampus; CA3, cornu ammonis 3 of hippocampus; DG, dentate gyrus; S, subiculum. Scale bar = 275 μM for all images.

Digital illustrations

Microscopy was performed with the aid of an Axioplan II microscope (Zeiss, Jena, Germany), and micrographs were acquired with a Zeiss AxioCam HRc camera (Zeiss) in Axiovision 4.1 software (Zeiss). Low-magnification, montage images of macaque brain sections were prepared and linearly adjusted for brightness and contrast using Adobe Photoshop (Version 7.0, Adobe, San Jose, CA**).** No other image alterations other than resizing were performed. All figures were prepared digitally in Microsoft Office Powerpoint 2003 (Redmond, WA).

Results

Conserved temporal patterns of Met/MET expression

Beginning in late neurogenesis and persisting through the first postnatal week in the mouse, neocortical Met expression increases dramatically, and the receptor is readily detected by immunohistochemical methods first in the efferent axons, and later in the neuropil, of the neocortex (Judson et al., 2009). By the end of the second postnatal week, corresponding with a winding down of axonal outgrowth and the beginning of the peak synaptogenic period, neocortical Met expression begins to decline. In fact, by P21, Met is only detected sparsely in the neocortical neuropil (Judson et al., 2009). Collectively, these data are consistent with a preferential role for the receptor in orchestrating aspects of forebrain development such as axon terminal arborization and the initiation of connectivity between circuit-related neurons.

To address the possibility of an evolutionary conserved role for the homologous MET receptor in the developing forebrain, we performed MET immunohistochemistry at corresponding developmental time-points in the macaque. These included gestational day (GD) 100 during late neocortical neurogenesis (Rakic, 1974) and GD150 and P21, which mark the rise and plateau, respectively, of the peak synaptogenic phase in the macaque (Bourgeois and Rakic, 1993; Bourgeois et al., 1994). MET immunohistochemical staining in the GD100 macaque was restricted to select regions of the neocortex. Here, receptor localization was evident in outgrowing axons of projection neurons and, though more broadly distributed across the radial dimension of the cortex, closely resembled the pattern of Met-labeling observed in the mouse at P0 (**Fig. 1A,D**),. At the cellular level by GD150, the pattern of MET labeling expanded to include the

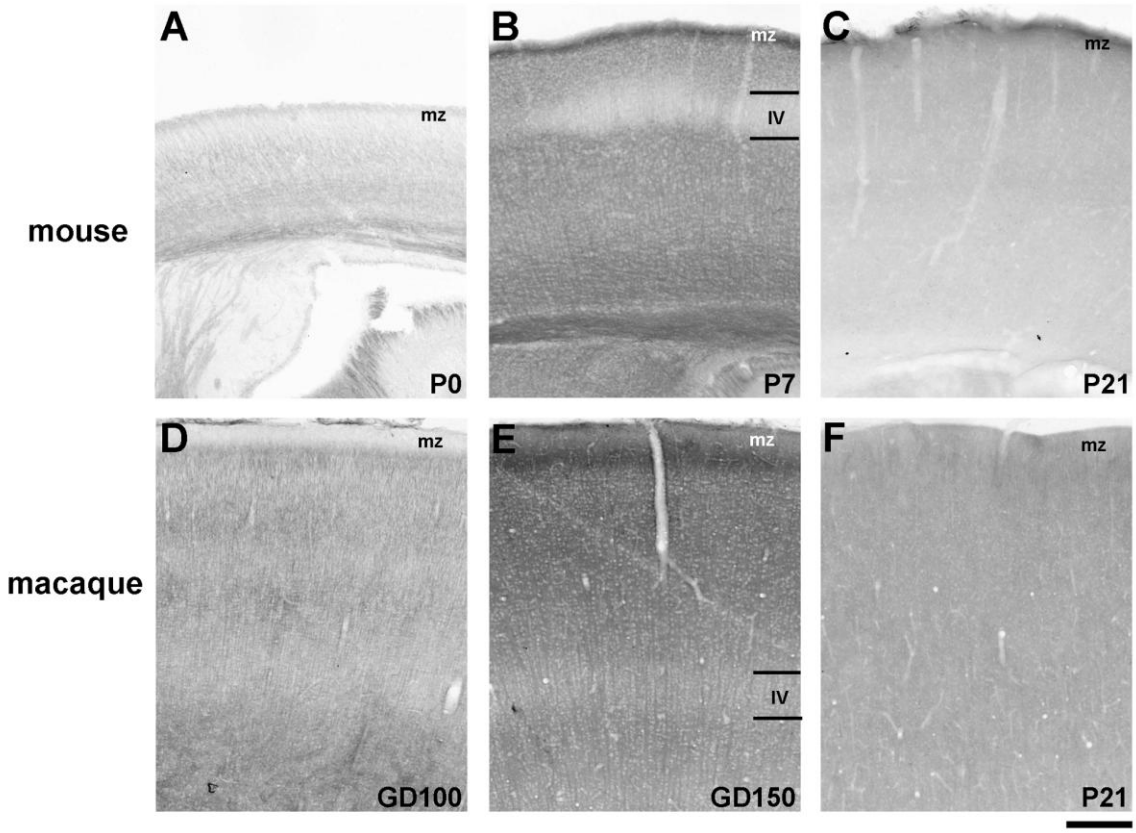

Figure 1. Conserved temporal patterns of Met/MET expression in mouse and macaque neocortex. DIC photomicrographs illustrate Met/MET immunohistochemistry in coronal brain sections during development. Labeling is predominantly seen in the outgrowing axons of cortical projection neurons in the cortex of the P0 mouse (**A**) and GD100 macaque (**D**). During axon collateralization and the onset of synaptogenesis, Met/MET labeling is readily observed in neuropil compartments in both species (**B,E**). Note especially the emergence of heavy expression in the marginal zone (mz) and the relative paucity of labeling in neocortical layer IV at this developmental stage. By three weeks of age (**C,F**), early periods of axon wiring have past in both mice and macaques, corresponding with drastically decreased immunohistochemical detection of Met/MET. Scale bar = 138 μM for all images.

neocortical neuropil in a manner similar to that observed in the mouse at P7. Membrane staining within the neuropil yielded salient patterns including images of cell bodies in negative relief, a noticeable increase in marginal zone labeling, and a relative paucity of layer IV labeling in both species during this developmental period (**Fig. 1B,E**). Whereas cortical neuropil labeling increased toward the onset of peak synaptogenesis, staining in forebrain axon tracts that carry corticocortically-projecting axons, such as the anterior commissure, concomitantly declined (**Fig. 2A,B** and **D,E**).

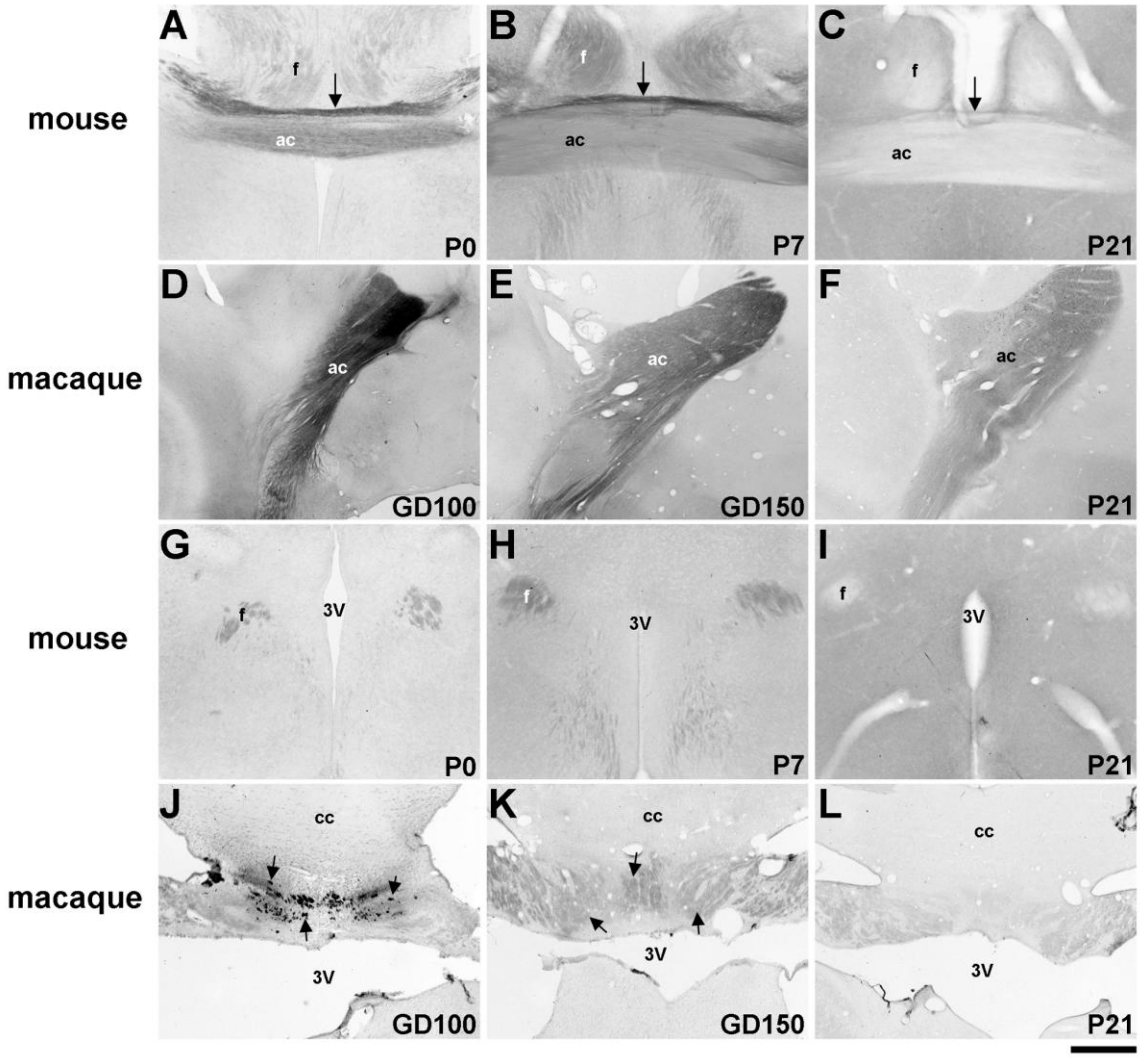

Figure 2. Conserved temporal patterns of Met/MET expression in major forebrain fiber tracts in the mouse and macaque. DIC photomicrographs illustrate Met/MET immunohistochemistry in coronal brain sections during development. In both the mouse (**A**) and macaque (**D**), intense Met/MET staining of corticofugal axons within the anterior commissure (ac) is observed at time-points just after the end of cortical neurogenesis. Axon staining within this structure gradually decreases in intensity throughout perinatal/early postnatal development in both species (mouse **B** and **C**; macaque **E** and **F**). The body of the ac, located just inferior to a commissural division of the stria terminalis (arrows), is depicted in mouse panels A-C, whereas the temporal limb of the ac is depicted in macaque panels D-F. Met/MET staining in efferent fibers of the hippocampus also decreases developmentally in the mouse (**G-I**) and macaque (**J-L**). Axons of the postcommissural fornix (f) are shown in cross-section in mouse panels G-I. The macaque f, inferior to the corpus callosum (cc), is depicted in J-L. Examples of select, intensely stained axon bundles are indicated by arrows (J and K). 3V, third ventricle. Scale bar = 275 μM for A-C and G-L; 1.1 mm for D-F.

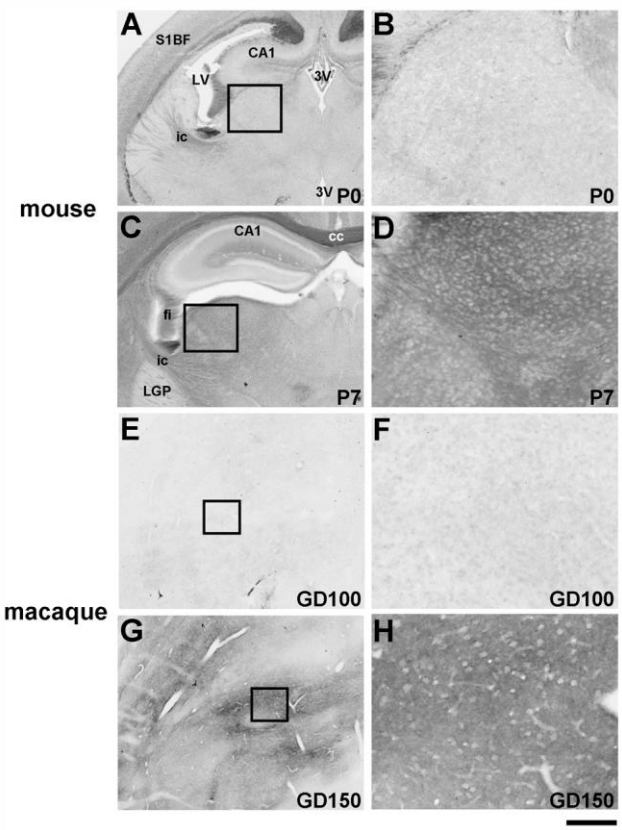

Figure 3. Conserved temporal patterns of Met/MET expression in the corticothalamic projection. DIC photomicrographs illustrate Met/MET immunohistochemistry in coronal brain sections during development. Axonal Met staining is evident in the internal capsule (ic, **A**) but not corticothalamic terminal fields (**B**, boxed region in **A**) in the dorsal thalamus in the P0 mouse. A similar pattern of expression is observed in low- (**E**) and high-magnification (**F**) images of the pulvinar in the GD100 macaque. Corresponding images in the P7 mouse (**C** and **D**) and GD150 macaque (**G** and **H**) show dramatically increased Met-labeling of the thalamic neuropil, concurrent with robust periods of corticothalamic terminal arborization in each species. 3V, third ventricle; CA1, cornu ammonis 1 of hippocampus; cc, corpus callosum; fi, fimbria of hippocampus; LGP, lateral globus pallidus; S1BF, barrel field of primary somatosensory cortex. Scale bar = 550 μM for A and C; 825 μM for E and G; 138 μM for B,D,F, and H.

There were comparable temporal dynamics of Met/MET expression within the terminal fields of subcortically-projecting neocortical axons. In the mouse at P0 and in the monkey at GD100, Met/MET was expressed in developing principle fiber tracts including the internal capsule (**Fig. 3A; Supplemental Fig. 2A,B**) and anterior commissure (**Fig. 2A,D**), which contain corticofugal projections to the thalamus and striatum. However, there was no apparent neuropil labeling in either the corticothalamic

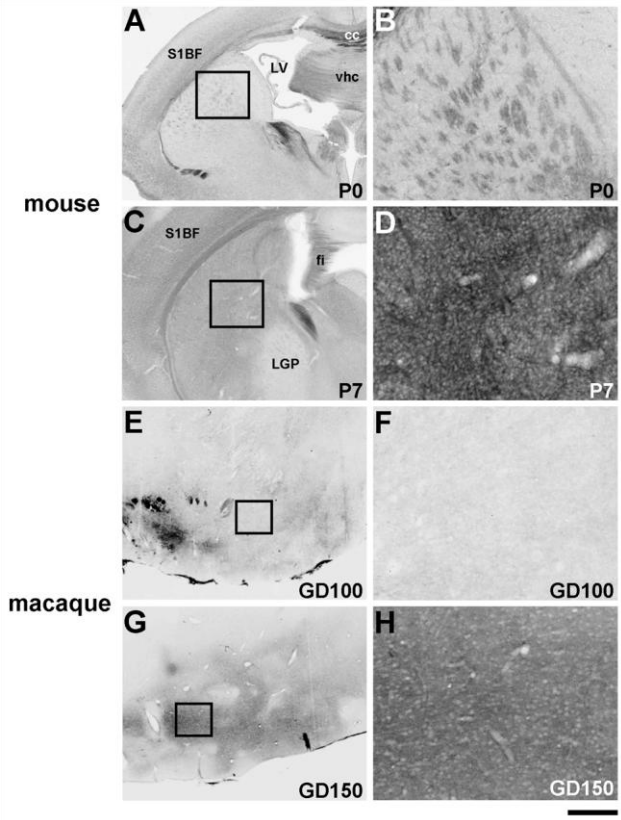

Supplemental Figure 2. Conserved temporal patterns of Met/MET expression in the corticostriatal projection. DIC photomicrographs illustrate Met/MET immunohistochemistry in coronal brain sections during development. Met- labeled axon fascicles pass through the striatum while the corticostriatal neuropil is unlabeled (**B**, boxed region in **A**). A similar pattern of expression is observed in low- (**E**) and high-magnification (**F**) images of the ventromedial striatum in the GD100 macaque. Corresponding images in the P7 mouse (**C** and **D**) and GD150 macaque (**G** and **H**) show a dramatic increase in Met-labeling of the striatal neuropil, concurrent with robust periods of corticostriatal terminal arborization in each species. cc, corpus callosum; fi, fimbria of hippocampus; LGP, lateral globus pallidus; S1BF, barrel field of primary somatosensory cortex; vhc, ventral hippocampal commissure. Scale bar = 550 μM for A and C; 825 μM for E and G; 138 μM for B,D,F, and H.

(**Fig. 3A,B,E,F**) or the corticostriatal terminal fields (**Supplemental Fig. 2A,B,E,F**) at this developmental stage. Robust Met/MET staining in the thalamic (**Fig. 3C,D,G,H**) and striatal (**Supplemental Fig. 2C,D,G,H**) neuropil became evident by P7 in the mouse and GD150 in the macaque, and, as shown in high-magnification images (**Fig. 1B,E; Fig. 3D,H; Supplemental Fig. 2D,H**), the pattern of labeling was reminiscent of that seen in the neocortex at this same stage of development. Finally, as in the mouse, immunohistochemical detection of MET was dramatically reduced in major forebrain

axon tracts as well as neocortical and subcortical axon terminal fields at P21, the plateau of the peak synaptogenic period (**Fig. 1C,F; Fig. 2C,F**).

Expression of Met/MET in the limbic system

In both the P7 mouse and GD150 macaque, Met/MET staining was evident throughout the anteroposterior extent of the amygdala, but the intensity of the staining varied within individual amygdaloid nuclei at each level. We observed robust neuropil staining in the P7 mouse amygdala in the nucleus of the lateral olfactory tract, anteriorly (**Fig. 4A**), and the posterior cortical nucleus, posteriorly (**Fig. 4C**). These two nuclei of the olfactory amygdala, as per (Swanson and Petrovich, 1998), were apparently devoid of labeling in the macaque (**data not shown**). More moderate staining in the lateral (LA), basolateral (BLA), and basomedial (BMA) nuclei at intermediate levels of the amygdala was generally conserved between the two species (**Fig. 4B,D-F**). Moreover, there was a conserved LA (high) to BMA (low) gradient of Met/MET staining across these contiguous deep amygdaloid nuclei, although the difference was more pronounced in the monkey. This pattern suggests that the majority of MET-expressing afferents within the basolateral complex of the amygdala have origins in the inferior temporal and perirhinal cortices of the macaque (Stefanacci et al., 1996; Stefanacci and Amaral, 2002).

The efferent projections of the immunolabeled neurons in select amygdala nuclei in both species expressed Met/MET. The stria terminalis (st), which is the principle fiber tract carrying amygdalofugal axons within the mammalian forebrain, was densely labeled in the mouse at P7 at the level of the anterior commissure (**Fig. 5A**). At a comparable anteroposterior level, we observed MET labeling of relatively modest intensity within

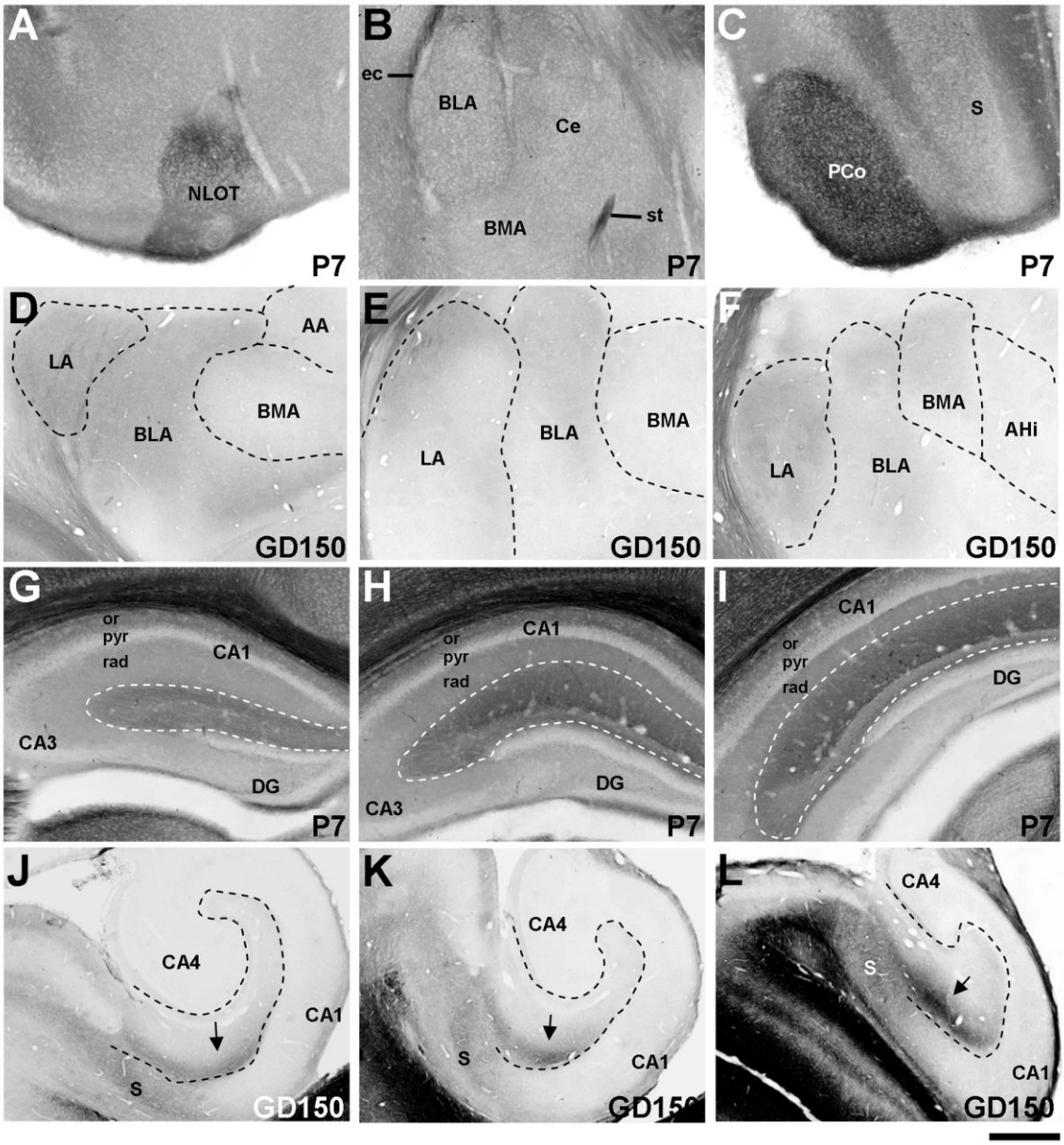

Figure 4. Conserved Met/Met expression in amydaloid and hippocampal afferents. DIC photomicrographs illustrate Met/MET immunohistochemistry at various anteroposterior levels of the amygdala and hippocampus in coronal brain sections from the P7 mouse and GD150 macaque. Though Met expression is widespread in the mouse amygdala during axon collateralization, subnuclei such as the nucleus of the lateral olfactory tract (NLOT, **A**) and the posterior cortical nucleus (PCo, **C**) exhibit exceptionally heavy Met-labeling as compared to basolateral (BLA), basomedial (BMA), and central (Ce) amygdaloid subnuclei (**B**). In the macaque, MET staining is enriched in the BLA and especially the lateral (LA) subnucleus (**D** and **E**) as compared to the BMA and amygdalohippocampal (AHi) subnuclei (**E** and **F**), indicating that, as in the mouse, MET is expressed by select amygdaloid afferents during development. In both the developing mouse (**G-I**) and macaque (**J-L**) forebrain, Met/MET staining is observed in entorhinal cortical efferents within the molecular layer (identified by perforated boundary). However, MET labeling in the macaque is focused in the molecular layer region overlaying the stratum radiatum at the subiculum/CA1 boundary (arrows in **J, K,** and **L**). Staining is enriched in posterior (mouse **H** and **I**; macaque **K** and **L**) as opposed to anterior (mouse **G**; macaque **J**) levels of the molecular layer in both species. AA, anterior amygdaloid nucleus; CA1, cornu ammonis 1 of hippocampus; CA3, cornu ammonis 3 of hippocampus; CA4, cornu ammonis 4 of hippocampus; DG, dendtate gyrus; ec, external capsule; or,

Figure 4—cont. stratum oriens of hippocampus; pyr, pyramidal cell layer of hippocampus; rad, stratum radiatum of hippocampus; S, subiculum; st, stria terminalis. Scale bar = 275 μM for A-C and G-I; 770 μM for D-F and J-L.

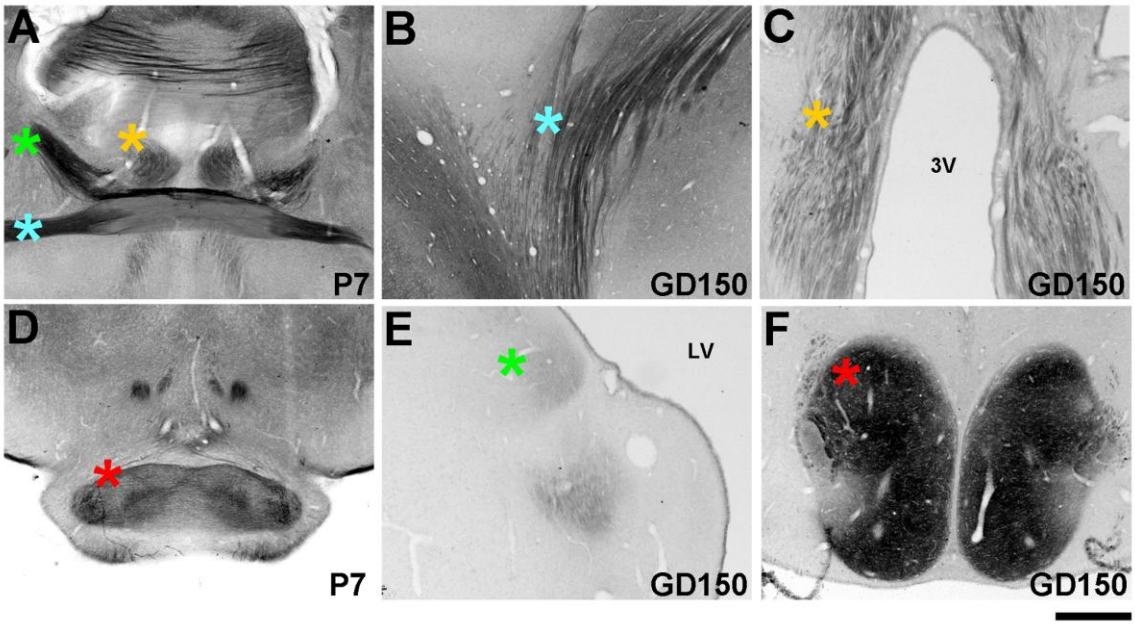

Figure 5. Conserved Met/MET expression in amygdaloid and hippocampal efferents. DIC photomicrographs illustrate Met/MET immunohistochemistry in fiber tracts and axon terminal fields in coronal forebrain sections from the P7 mouse and GD150 macaque. **A** and **D**: Examples of Met staining in the stria terminalis (green asterisk), posterior limb of the anterior commissure (blue asterisk), precommissural fornix (orange asterisk), and mammillary bodies (red asterisk) in the developing mouse forebrain. Asterisks of the same color mark corresponding MET-stained structures in the macaque during a similar developmental period (**B,C,E**, and **F**). 3V, third ventricle; LV, lateral ventricle. Scale bar = 550 μM for all images.

this fiber tract in the GD150 macaque (**Fig. 5E**). Despite this apparent quantitative difference in st staining, it was evident at more posterior levels of the tract that only select populations of amygdalofugal axons are stained in each species (**Supplemental Fig. 3B,E**). Moreover, decremental staining was observed within these axon subpopulations with increasing developmental age (**Supplemental Fig. 3A-C** and **D-F**), mirroring the conserved temporal pattern of expression for corticocortical and corticofugal axon tracts. Efferent amygdala fibers also course within the external capsule

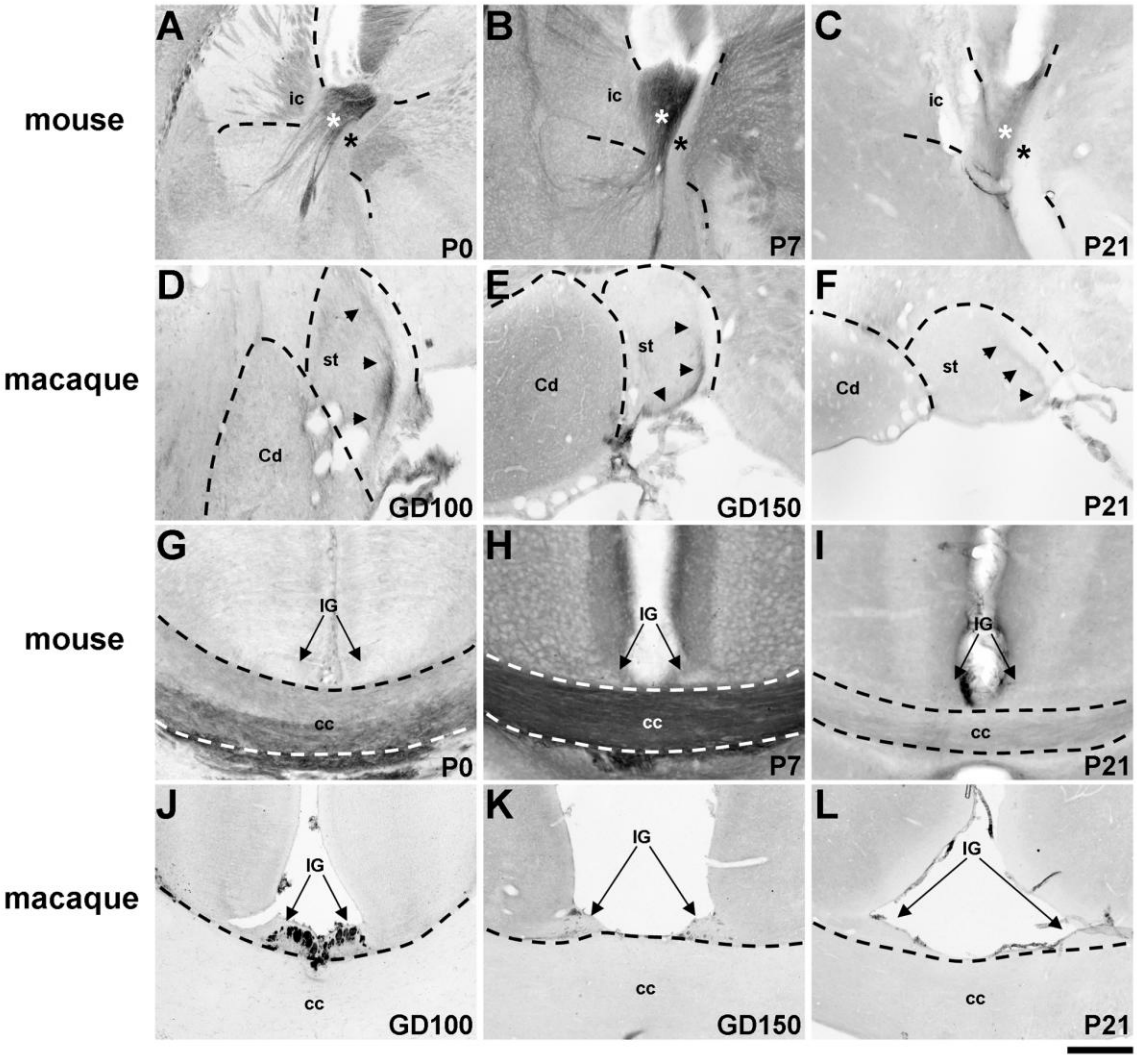

Supplemental Figure 3. Conserved temporal patterns of Met/MET expression in axons of the amygdala but not the indusium griseum in the mouse and macaque. DIC photomicrographs illustrate Met/MET immunohistochemistry in coronal brain sections during development. Select bundles of presumably amygdalofugal axons are heavily stained (white asterisks) within the stria terminalis (st) in the mouse at P0 (**A**) and P7 (**B**), but this labeling is greatly diminished by P21 (**C**). Black asterisks indicated unstained axons within this tract (A-C). A similar temporal pattern of staining is observed in medially coursing axons (black arrowheads, **D-F**) of the macaque st. Met-stained fibers are absent bilaterally in the mouse indusium griseum (arrows, IG) at P0 (**G**), P7 (**H**), or P21 (**I**) time-points. However, distinct, heavily labeled IG axon bundles are readily observed in the macaque at GD100 (**J**). This staining is dramatically reduced by GD150 (**K**) and undetectable by P21 (**L**). cc, corpus callosum; Cd, tail of the caudate; ic, internal capsule. Scale bar = 275 μM for all images.

and the anterior commissure, both of which are heavily stained in the mouse (**Fig. 5A; Fig. 8A,C, and E**) and macaque (**Fig. 5B; Fig. 8G,H**) forebrain at this developmental age.

Patterns of Met/MET expression within the mouse and macaque hippocampus were generally conserved. The molecular layer of the dendate gyrus and CA fields of the hippocampus, throughout the anteroposterior extent, contained Met/MET immunoreactivity in both the P7 mouse (**Fig. 4G-I**) and GD150 macaque (**Fig. 4J-L**), consistent with Met/MET expression in hippocampal afferents from entorhinal cortex in both species. However, there were two key differences in this expression feature between the mouse and the macaque: 1) the intensity of Met/MET staining in the molecular layer was relatively stronger in the mouse compared to the macaque, and 2) while staining appeared to be evenly distributed throughout the mouse molecular layer, it was concentrated in regions of the molecular layer apposed to the stratum radiatum near the subiculum/CA1 boundary in the macaque.

Met/MET labeling was intense at P7 in the mouse and GD150 in the monkey in the fiber tracts that contain, and the target regions that receive, hippocampal efferent projections. For example, immunnostaining was observed in the precommissural fornix (**Fig. 5A,C**) and the hippocampal commissure (**Supplemental Fig. 4I,L**). However, a subset of axon fascicles in the indusium griseum (IG), a structure considered an extension of the hippocampus (Wyss and Sripanidkulchai, 1983), was densely labeled in the macaque (**Supplemental Figs. 3J; 4D-F**) but not the mouse (**Supplemental Figs. 3G-I; 4A-C and G-I**). Moreover, the staining was much less intense at GD150 than GD100, and was undetectable by P21 **(Supplemental Fig. 3J-L**). As shown in coronal sections

that include the postcommissural fornix, a similar temporal dynamic of MET expression was observed in hippocampal efferents of the macaque (**Fig. 3J-L**), a pattern that also was evident in the mouse (**Fig. 3G-I**). One of the most robust projections of the hippocampus via the postcommissural fornix is that to the medial mammillary bodies. Met/MET labeling was extremely dense in the medial mammiallary bodies in both the P7 mouse (**Fig. 5D**) and GD150 macaque (**Fig. 5F**), consistent with high expression levels of the receptor in axons of this hippocampal efferent pathway. Collectively, these data demonstrate that Met/MET is expressed transiently at high levels in afferents and efferents of the amygdala and hippocampus during early periods of circuit wiring in the mouse and macaque forebrain, followed by a significant reduction later postnatally.

Comparative analysis of tangential patterns of neocortical Met/MET expression

Mice and primates depend differentially on specific sensory modalities for communicating with conspecifics. Thus, we extended our analysis to interspecies comparisons of Met/MET expression within sensory and associative neocortical areas during forebrain circuit development. As shown in low-magnification images representing the anteroposterior extent of the P0 mouse forebrain (**Fig. 6A-D**), Met immunohistochemical staining was broadly distributed across the tangential domain of the mouse neocortex, with particularly robust labeling throughout the extent of the major axon tracts carrying corticocoritical and corticofugal projections, including the corpus callosum, anterior commissure, and internal capsule. This broad tangential distribution of neocortical Met expression was more readily apparent in a similar anteroposterior array of Met-stained sections at P7 (**Fig. 7A-D**), when neuropil expression of the receptor

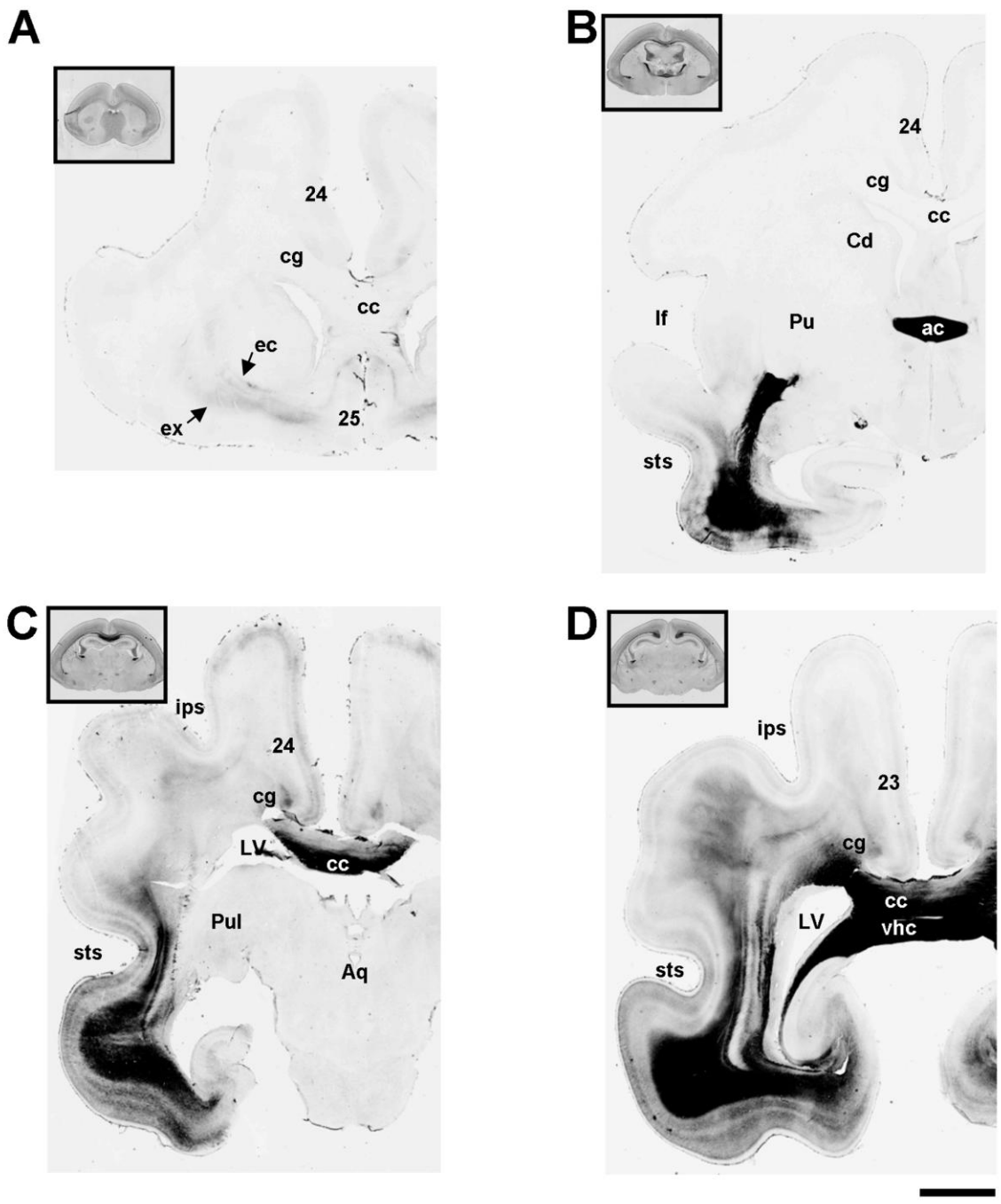

Figure 6. Divergent spatial patterns of neocortical Met/MET expression in the developing mouse and macaque forebrain. DIC photomicrographs illustrate the anterior (**A**) to posterior (**D**) progression of Met/MET immunohistochemistry in coronal forebrain sections from the P0 mouse and GD100 macaque. Notably, all major fiber tracts that carry corticofugal projections as well as the subplate exhibit intense Met staining in the mouse forebrain (inset images, **A**-**D**). Robust MET expression in the macaque is largely confined to the subplate underlying cortices inferior to the superior temporal sulcus (sts) and in select corticofugal fiber tracts of the incipient temporal lobe including, most notably, the anterior commissure (ac, **B**) as well as the external (ec) and extreme (ex) capusules anteriorly (**A**). Additional staining in the cingulum (cg, **A**-**D**) likely reflects MET expression in the efferent fibers of the posterior cingulate cortex, whereas labeled axons of the corpus callosum (cc, **A**-**D**) may originate in the posterior cingulate and/or cortices inferior to the intraparietal sulcus (ips). 24, cortical area 24; 25, cortical area 25; Aq, cerebral

Figure 6—cont. aquaduct; Cd, caudate; ips, intraparietal sulcus; lf, lateral fissure; LV, lateral ventricle; Pu, putamen; Pul, pulvinar; vhc, ventral hippocampal commissure. Scale bar = 3.15 mm for all macaque images; 3.6 mm for inset mouse images.

proved to be at its peak. Moreover, the patterns of staining within major subcortical, corticofugal terminal fields reflected the widespread Met expression in the neocortical neuropil and fiber tracts containing corticofugal efferents (e.g., the internal capsule). As shown at P7, Met-labeled neuropil was evident both throughout the striatum (**Fig. 8A,C,E**) and within many nuclei of the thalamus (**Fig. 8B,D,F**).

In contrast, there was a remarkably restricted pattern of MET expression in the macaque neocortex at GD100 and GD150. MET labeling was largely absent in the frontal lobes, except for low expression in medial areas that included the anterior cingulate and subgenual cortices (**Figs. 6A; 7A**). While still modest in staining intensity, there was a progressive increase in the intensity of MET labeling at increasingly posterior levels of the cinguate cortex (areas 24 and 23). This pattern was marked most saliently by staining in the cingulum at GD100 and in the cortical neuropil at GD150 (**Figs. 6A-D; 7A-D**). The most robust staining for MET at GD100 was evident in the subplate and neocortical white matter underlying extrastriate visual and auditory cortices of the temporal, inferior parietal, and occipital lobes across anteroposterior levels of the macaque forebrain (**Fig. 6B-D**). By GD150, expression had expanded to include the neuropil within these selective neocortical regions (**Fig. 7B-D**). Staining patterns at GD150 also were highly complex within these regions, especially in the temporal lobe. Labeling was most intense inferior to the superior temporal sulcus (sts) in high-order, unimodal visual areas, which contain neurons that are responsive to complex stimuli including scenes, objects, and primate faces (Baylis et al., 1987; Tsao et al., 2006)

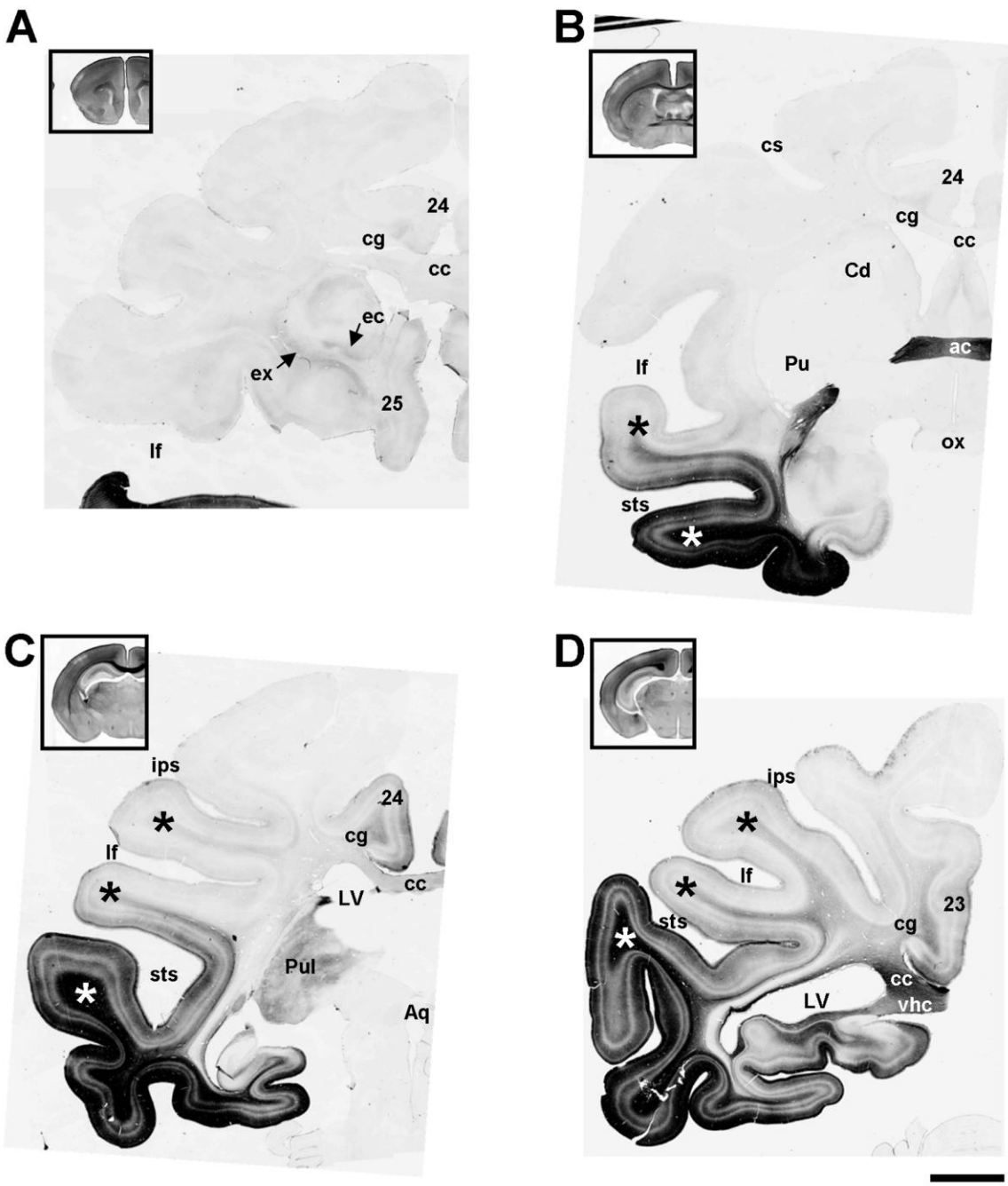

Figure 7. Divergent spatial patterns of neocortical Met/MET expression in the developing mouse and macaque forebrain. DIC photomicrographs illustrate the anterior (**A**) to posterior (**D**) progression of Met/MET immunohistochemistry in coronal forebrain sections from the P7 mouse and GD150 macaque. While Met expression in the mouse (inset images, **A-D**) is broadly distributed throughout the tangential domain of the neocortex, MET expression in the macaque is largely restricted to the temporal cortices (white and black asterisks, **B-D**) and midline cortices including the anterior cingulate cortex (cortical area 24, **A-C**; area 23, **D**) and subgenual cortex (area 25, **A**). MET is also differentially expressed within the macaque temporal lobe; staining is strong inferior to (white asterisks, **B-D**), and of modest intensity superior to (black asterisks, **B-D**), the superior temporal sulcus (sts). Axon staining within the cingulum (cg, **A-D**), anterior commissure (ac, **B**), and posterior regions of the corpus callosum (cc, **C** and **D**) reflect the restricted populations of neocorticocortical projection neurons that express MET. Aq, cerebral aquaduct; Cd, caudate; cs, central sulcus; ec, external capsule; ex, extreme capsule; lf, lateral fissure; LV,

Figure 7—cont. lateral ventricle; ox, optic chiasm; Pu, putamen; Pul, pulvinar; vhc, ventral hippocampal commissure. Scale bar = 4.6 mm for all macaque images; 4.2 mm for inset mouse images.

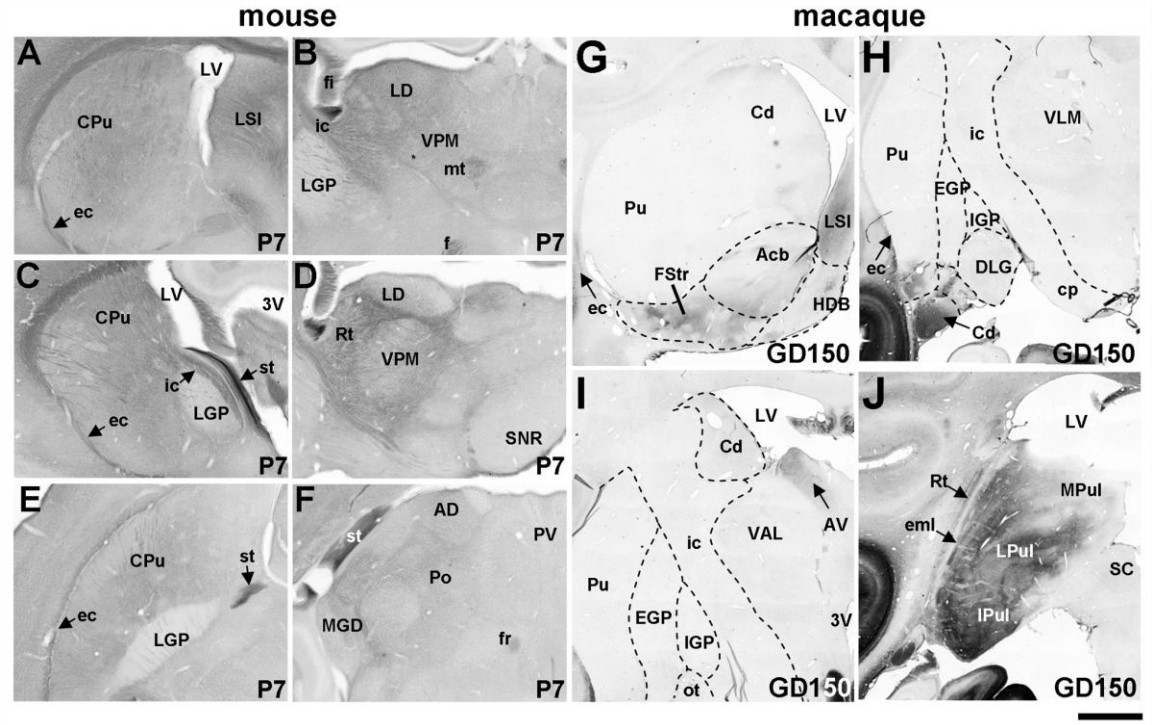

Figure 8. Met/MET expression in neocortical efferents in the developing mouse and macaque forebrain. DIC photomicrographs illustrate Met/MET immunohistochemistry in forebrain sections from the P7 mouse and GD150 macaque. Widespread Met labeling is observed in the neuropil of the caudatoputamen (CPu) (**A, C,** and **E**) and lateral thalamus (**B,D,** and **F**) in coronal (**A** and **B**), sagittal (**C** and **D**), and horizontal (**E** and **F**) brain sections of the develping mouse forebrain, consistent with widespread Met expression in long-projecting axons of the neocortex. The distribution of MET-labeled neocortical efferents in the developing macaque striatum is much more restricted, as robust staining is observed only in the nucleus accumbens (NAc) and fundus striari (Fstr) (**G**), and the ventral putamen (Pu) and caudate (Cd) (**H**). Restricted areas of lighter striatal MET staining are observed in the dorsal Cd (**I**). MET-labeled neocortical efferents to the macaque thalamus are predominantly restricted to the reticular nucleus (Rt) (**J**), lateral (LPul) and inferior (IPul) pulvinar nuclei (**J**) and limbic thalamic nuclei including the anteroventral nucleus (AV) (**I**). 3V, third ventricle; AD, ; cp, cerebral peduncle; DLG, dorsolateral geniculate nucleus; EGP, external globus palidus; ec, external capsule; eml, external medullary lamina; f, fornix; fi, fimbria of hippocampus; fr, fasciculus retroflexus; HDB, horizontal limb of the diagonal band; ic, internal capsule; IGP, internal globus palidus; LD, laterodorsal thalamic nucleus; LGP, lateral globus palidus; LV; lateral ventricle; LSI, intermediate lateral septal nucleus; MGD, medial geniculate nucleus, dorsal part; MPul, medial pulvinar nucleus; mt, mammillothalamic tract; ot, optic tract; Po, posterior thalamic nuclear group; PV, paraventricular thalamic nucleus; SC, superior colliculus; SNR, substantia nigra pars reticulata; st, stria terminalis; VAL, ventral anterior thalamic nucleus, lateral part; VLM, ventrolateral thalamic nucleus, medial part; VPM, ventral posteromedial thalamic nucleus. Scale bar = 550 μM for A-F; 2.48 mm for G-J.

(**Fig. 7B-D**). Less intense MET staining was present superior to the STS in polysensory and associative auditory cortices within the superior temporal gyri (**Fig. 7B-D**) and inferior parietal lobes (**Fig. 7C,D**).

The limited tangential extent of MET expression in the developing macaque neocortex was reflected in the restricted subsets of forebrain fiber tracts and cortical efferent target areas in the striatum and dorsal thalamus that contained MET-stained axons. Dense MET labeling in the anterior commissure was evident, consistent with receptor expression in cortico-cortically projecting neurons within the temporal lobes (**Figs. 6B; 7B**). MET staining also was present in the external and extreme capsules within the ventral forebrain, which presumably distribute MET-expressing axons ipsilaterally among interconnected temporal cortices and to highly specific regions of the striatum (**Figs. 6A; 7A; 8G,H**). Ventral striatal areas, including the nucleus accumbens, fundus striari, and the ventral putamen and tail of the caudate nucleus, constituted the most notable target areas of MET-labeled axons (**Fig. 8H,I**). There also was very light and spatially limited staining in the dorsal caudate nucleus (**Fig. 8G,I**), with all other striatal areas consistently devoid of MET staining (**Fig. 8G-I**). This pattern of staining is highly divergent from the mouse.

There also was MET expression in a small subgroup of presumed corticothalamic efferents, consistent again with the highly restricted staining in the neocortex. For example, moderate staining in the laterodorsal superficial **(data not shown**) and anteroventral (**Fig. 8I**) thalamic nuclei are consistent with the observation of MET expression in the cingulate cortices. The most robust MET staining in the dorsal thalamus was found in subnuclei of the pulvinar. Specifically, the staining was

concentrated in the inferior and lateral subdivisions of the pulvinar, with much reduced labeling in the medial subdivsion (**Fig. 8J**). This pattern reflects the foci of MET expression in the temporal and inferior parietal lobes. Finally, like in mouse, the posterior reticular nucleus has MET-labeled neuropil in the monkey (**Fig. 8J**). All other thalamic nuclei in the developing macaque were devoid of MET staining.

Interspecies conservation of anatomical expression gradients

Despite the general observation of widespread Met expression in the mouse neocortex and highly restricted neocortical MET expression in the macaque, there was a clearly conserved anterior (low) to posterior (high) expression gradient in cortically-associated structures in both species. This gradient was best appreciated in anteroposterior images of the corpus callosum from the P0 (**Supplemental Fig. 4A-C**) and P7 (**Supplemental Fig. 4G-I**) mouse and the GD100 (**Supplemental Fig. 4D-F**) and GD150 (**Supplemental Fig. 4J-L**) macaque. There also was a similar gradient in the hippocampus in both species (**Fig. 4G-H and J-L**). Finally, in the macaque, increased posterior staining was readily apparent in the cingulate cortex, as previously mentioned (**Figs. 6A-D; 7A-D**), as well as the thalamic reticular nucleus (**Fig. 8J**).

Discussion

Here we present comparative forebrain expression mapping data that are consistent with an evolutionarily conserved role for the Met/MET receptor tyrosine kinase in the wiring of circuits governing social and emotional dimensions of behavior. We propose a shared function for mouse Met and the macaque homologue, MET, in

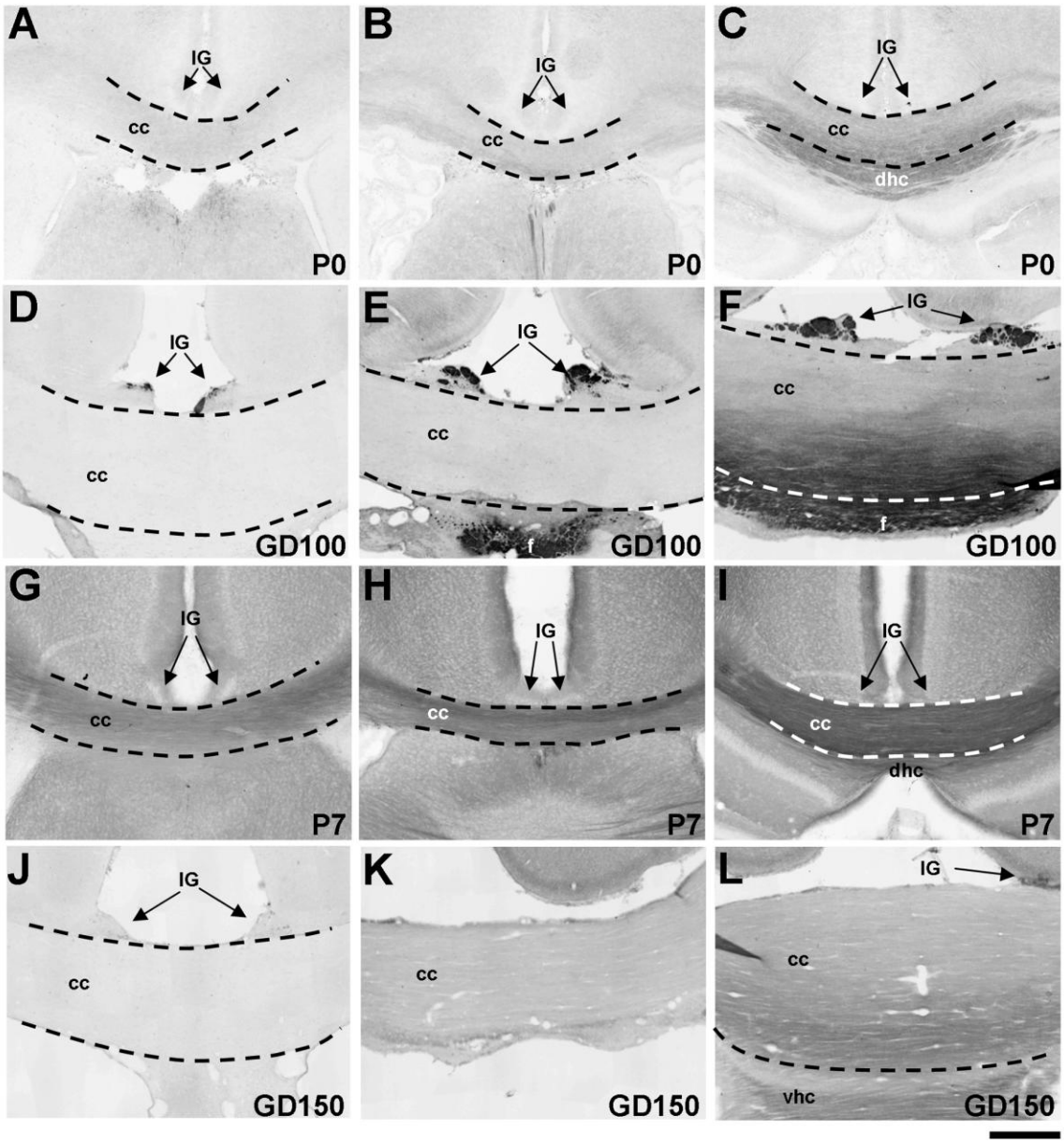

Supplemental Figure 4. Conserved anterior (low) to posterior (high) gradient of Met/MET expression in the tangential domain of neocortex. DIC photomicrographs illustrate Met/MET immunohistochemistry in coronal forebrain sections from the developing mouse and macaque. Met immunoreactivity is observed to gradually intensify in increasingly posterior regions of the mouse corpus callosum (cc) at both P0 (**A**-**C**) and P7 (**G**-**I**), consistent with increased Met expression within projection neurons of the posterior neocortex. An even sharper gradient in MET immunoreactivity is seen in this fiber tract at corresponding time-points in macaque development including GD100 (**D**-**F**) and GD150 (**J**-**L**). A similar anterior (low) to posterior (high) gradient of axonal MET expression is a unique feature of the developing macaque indusium griseum (IG) and is largely a phenomenon of the GD100 time-point (**D**-**F**). dhc, dorsal hippocampal commissure; f, fornix; vhc, ventral hippocampal commissure. Scale bar = 275 μM for A-C and G-I; 620 μM for D-F and J-L.

forebrain circuit wiring, which is supported by the striking temporal and subcellular similarities in expression that we observed in these species. In both the mouse and macaque, Met/MET was enriched in the axons of projection neurons within the neocortex, hippocampus, and amygdala as early as the end of neurogenesis. Prior to the plateau phase of peak synaptogenesis, receptor expression expanded within the cortical and subcortical neuropil, coinciding with the robust collateralization of these axons within their terminal fields. These data suggest a presynaptically-derived influence of Met/MET signaling in the initial establishment of forebrain circuits important for social and emotional behavior. Consistent with this, we have recently demonstrated that the ablation of Met signaling from corticostriatal axons results in cell-nonautonomous changes in the dendritic morphology of medium spiny neurons (M. Judson, K. Eagleson, P. Levitt, unpublished observations).

Despite the remarkable similarity in subcellular receptor distributions discussed above, it should be noted that our Met/MET immunohistochemical stain provides inadequate resolution to distinguish either the staining of axonal versus dendritic elements, or to differentiate between multiple sources of axonal afferents, within the neuropil. We previously circumvented this issue in the mouse by additionally analyzing wild type patterns of *Met* transcript expression as well as Met staining patterns in a dorsal pallium-specific conditional Met knockout mouse. This approach allowed us to determine that nearly all Met staining in the subcortical neuropil is localized to axonal afferents of a dorsal pallial origin. In order to determine the extent to which this finding applies to similar MET staining patterns in the macaque forebrain, we would ultimately need to analyze developmental *MET* transcript expression. There is, however,

considerable indirect evidence supporting the preferential localization of MET to dorsally-derived axonal compartments in the subcortical neuropil. For example, the ventral (high) to dorsal (low) gradient of MET staining in the temporal cortex is reflected with remarkable fidelity in the ventrolateral (high) to dorsomedial (low)) gradient of staining in the pulvinar, constistent with the topographical organization of temporal corticothalmic axon projections within this nucleus (Romanski et al., 1997; Yeterian and Pandya, 1997; Shipp, 2003).

Spatial patterns of Met/MET expression reflect species-specific modes of social communication

This study has revealed two themes concerning spatial patterns of Met/MET expression and its putative developmental role in the wiring of socially relevant forebrain circuitry: 1) receptor expression is highly conserved within limbic structures that are essential for social cognition and memory, including the hippocampus, amygdala, and cingulate cortices, and 2) receptor expression patterns diverge within sensory and associative neocortical areas according to species-specific requirements for the perception of socially relevant stimuli. Evidence supporting the first theme comes from the observation of shared Met/MET expression in the structures and fiber pathways that constitute core limbic circuitry (Papez, 1937; MacLean, 1955). Both the mouse and macaque exhibited significant developmental Met/MET expression in hippocampal efferent fibers projecting to the medial mammillary bodies, in axon terminals within the anteroventral thalamic nucleus, in cingulate cortex and axons within the cingulum, and in the hippocampal complex, effectively completing the classically defined circuit of Papez (Papez, 1937). Met/MET expression also was shared in the main efferent pathway of the

amygdala, the stria terminalis, indicating conserved receptor function in the development of more broadly defined limbic circuits (MacLean, 1955). This evolutionary conservation of Met/MET expression is not necessarily surprising; the limbic brain is phylogenetically old, and conserved expression of other molecules that participate in limbic circuit wiring has been reported (Horton and Levitt, 1988; Chesselet et al., 1991; Pimenta et al., 1996). Approximately 50 million years of evolution has, though, allowed for at least some redefinition of Met/MET receptor roles in the development of limbic circuitry in monkeys as compared to mice. For example, MET expression in the indusium griseum appeared to be a unique feature of the developing primate limbic system, whereas Met-labeled afferents of a presumed olfactory origin were uniquely detected in the nucleus of the lateral olfactory tract and posterior cortical nucleus of the mouse amygdala. Additionally, MET staining in the ventromedial striatum may be localized in part to afferents originating in the basolateral amygdala and/or hippocampal formation (Friedman et al., 2002), a pattern not detected in the mouse (Judson et al., 2009). However, as demonstrated in the present study, the greatest interspecies divergence in patterns of Met/MET expression during social circuit development is at the level of the neocortex.

In the context of social circuit integration, structures such as the basolateral amygdala, cingulate cortex, perirhinal cortex, and entorhinal cortex are critical, because they are broadly interconnected with the neocortex, and thus, serve as an interface between the circuits required for social perception and downstream limbic circuits that facilitate social cognitive processes such as social recognition, arousal, and awareness (Adolphs, 2001; Amaral, 2003; Phelps and LeDoux, 2005). We observed Met/MET

staining within the neuropil of each of these areas in the mouse and the macaque, strongly suggesting that this receptor is involved in establishing connections between neocortical and limbic circuits. Because the neocortical expression patterns overlap functional areas required for the receipt of social stimuli characteristic of each species, we reason that Met/MET signaling may have been evolutionarily co-opted to integrate circuits governing social perception and social cognition.

In primate species such as the macaque, sensory faculties such as vision and audition are critically important for the perception of socially relevant stimuli, and they are largely rooted in neocortical areas of the temporal, occipital, and inferior parietal lobes. Remarkably, during the period of social circuit wiring, we observed a nearly exclusive localization of MET to the axons of projection neurons within these select neocortical areas. MET expression was particularly dense in the inferior temporal gyrus, which houses cortical areas in the ventral visual stream that facilitate the processing of complex socially-relevant visual features including body parts and faces (Pinsk et al., 2005; Pinsk et al., 2009). Because we also observed MET staining of presumed inferotemporocortical efferent axons within the perirhinal and entorhinal cortices of the hippocampal complex, we suggest that the receptor may regulate the development of circuits required for social recognition (Malkova et al., 1995; Thornton et al., 1997) – an essential cognitive process supporting social interaction among primate conspecifics. Additionally, staining was observed in the ventral putamen and caudate nucleus of the striatum, indicating that the development of circuits governing the formation of socially adaptive visual habits also may depend on intact MET signaling (Fernandez-Ruiz et al., 2001). We hypothesize that genetic variation that impacts MET expression may disrupt

the formation of these circuits and contribute to social interaction phenotypes characteristic of ASD.

Whereas neocortical MET expression was spatially restricted in the tangential domain, Met expression in the mouse neocortex was broadly distributed, perhaps reflecting the relatively full employment by this species of its sensory faculties for social behavior. Excepting sexual behavior, olfaction and somatosensation are minor tools in the social repertoire of the primate, but mice and other rodent species depend on these senses in order to communicate with conspecifics. In fact, social recognition in mice is almost exclusively mediated by olfaction (Brennan and Kendrick, 2006; Spehr et al., 2006). Yet mice also rely on vision and audition in order to extract socially relevant information from their environment. Langford and colleagues recently demonstrated that the visual observation of pain-related behavior in a conspecific subject can modulate pain responses in an observer mouse through an empathy-like process (Langford et al., 2006). A more recent study employed a fear-conditioning paradigm to show that auditory cues can also facilitate empathy-like social behavior in mice (Chen et al., 2009). Tail-rattling, which has been shown to be an important behavioral trait associated with mouse aggression (St John, 1973), also is perceived by the auditory and/or visual senses.

Though the present study supports our hypothesis that Met/MET signaling regulates the development of species-specific social circuits in the developing forebrain, much can be gained by further Met/MET expression studies comparing other species. Two specific experimental approaches may prove useful: 1) patterns of developmental Met/MET forebrain staining could be compared in genetically distant mammalian species with convergent social ethologies, and/or 2) staining patterns could be compared in

genetically related species with divergent social ethologies. A comparison of developmental forebrain Met staining in solitary versus eusocial African naked mole rats (*Bathyergidae*) would constitute an extreme example of the second approach. Fortunately, such experiments are possible owing to the evolutionarily conserved epitopes recognized by immunohistochemistry-compatible Met/MET antibodies.

MET expression patterns and circuit vulnerability in autism

Recent studies have served to establish human *MET* gene promoter variants as causative risk alleles for ASD. The *MET* rs1858830-C allele in particular has been shown to promote less efficient MET transcription in *in vitro* assays (Campbell et al., 2006)), consistent with the observed 2-fold reduction in the temporal cortex of postmortem ASD brains (Campbell et al., 2007). We also recently demonstrated presynaptically-derived alterations in forebrain circuitry in a mouse model of developmentally abrogated Met signaling (M. Judson, K. Eagleson, P. Levitt, unpublished observations), indicating a possible causal link between reduced MET expression and circuit malformation in ASD. However, as indicated by the findings of the present study, alterations in the spatial distribution of MET expression may be as important to consider as absolute levels of expression in regard to the wiring of social circuitry and ASD risk.

MET protein expression mapping in the developing human forebrain is currently the best available approach to gain knowledge of the specific social circuits that may be vulnerable in *MET*-related cases of idiopathic ASD. Moreover, considering the population frequencies (.35-.55) of ASD-associated *MET* alleles (Campbell et al., 2006;

Campbell et al., 2008; Jackson et al., 2009; Sousa et al., 2009), mapping studies of brains with *MET* risk allele genotypes may help to elucidate broadly relevant etiological mechanisms of the disorder. However, these studies are necessarily hindered by the ethical and practical considerations that are associated with any approach requiring postmortem human tissue of embryonic origin. Comparative analysis of conserved and divergent regulatory elements within the murine and primate genes may thus constitute a useful alternative approach.

Considering the posterior (high) to anterior (low) neocortical gradient of Met/MET expression shared by the mouse and macaque, conserved *Met/MET* regulatory elements may contain binding sites for transcription factors known to exhibit anterior-posterior gradients of expression during cortical development (Kudo et al., 2007). Divergent regulatory elements, on the other hand, may contribute to the remarkable areal restriction of MET expression within the primate neocortex. Recombineered mice that carry the 5' regulatory region of the human *MET* gene in place of the homologous murine sequence could be generated to test this possibility. Furthermore, inclusion of the various single nucleotide variations that are associated with ASD risk could potentially yield animal models of ASD-relevant circuit vulnerability with high external validity. Studies of such "humanized" Met mice would, however, be limited by certain neuroanatomical constraints. For example, mice possess only an evolutionary rudiment of the pulvinar, which receives heavily MET-labeled projections from the temporal cortex in the developing macaque.

Other Acknowledgements

We thank Deborah Gregory, Donte Smith, and Kate Spencer in the Levitt laboratory for excellent assistance in maintaining the mouse colony. We also thank Jeff Bennett in the Amaral laboratory for preparing the macaque brain tissue, which made this study possible.

Literature Cited

Acker CD, Antic SD. 2009. Quantitative assessment of the distributions of membrane conductances involved in action potential backpropagation along basal dendrites. J Neurophysiol 101(3):1524-1541.

Adolphs R. 2001. The neurobiology of social cognition. Curr Opin Neurobiol 11(2):231-239.

Amaral DG. 2003. The amygdala, social behavior, and danger detection. Ann N Y Acad Sci 1000:337-347.

Baylis GC, Rolls ET, Leonard CM. 1987. Functional subdivisions of the temporal lobe neocortex. J Neurosci 7(2):330-342.

Bourgeois JP, Goldman-Rakic PS, Rakic P. 1994. Synaptogenesis in the prefrontal cortex of rhesus monkeys. Cereb Cortex 4(1):78-96.

Bourgeois JP, Rakic P. 1993. Changes of synaptic density in the primary visual cortex of the macaque monkey from fetal to adult stage. J Neurosci 13(7):2801-2820.

Brennan PA, Kendrick KM. 2006. Mammalian social odours: attraction and individual recognition. Philos Trans R Soc Lond B Biol Sci 361(1476):2061-2078.

Campbell DB, D'Oronzio R, Garbett K, Ebert PJ, Mirnics K, Levitt P, Persico AM. 2007. Disruption of cerebral cortex MET signaling in autism spectrum disorder. Ann Neurol 62(3):243-250.

Campbell DB, Li C, Sutcliffe JS, Persico AM, Levitt P. 2008. Genetic evidence implicating multiple genes in the MET receptor tyrosine kinase pathway in autism spectrum disorder. Autism Research 1:159-168.

Campbell DB, Sutcliffe JS, Ebert PJ, Militerni R, Bravaccio C, Trillo S, Elia M, Schneider C, Melmed R, Sacco R, Persico AM, Levitt P. 2006. A genetic variant that disrupts MET transcription is associated with autism. Proc Natl Acad Sci U S A 103(45):16834-16839.

Campbell DB, Warren D, Sutcliffe JS, Lee EB, Levitt P. 2009. Association of MET with social and communication phenotypes in individuals with autism spectrum disorder. Am J Med Genet B Neuropsychiatr Genet.

Chen Q, Panksepp JB, Lahvis GP. 2009. Empathy is moderated by genetic background in mice. PLoS One 4(2):e4387.

Chesselet MF, Gonzales C, Levitt P. 1991. Heterogeneous distribution of the limbic system-associated membrane protein in the caudate nucleus and substantia nigra of the cat. Neuroscience 40(3):725-733.
Ebens A, Brose K, Leonardo ED, Hanson MG, Jr., Bladt F, Birchmeier C, Barres BA, Tessier-Lavigne M. 1996. Hepatocyte growth factor/scatter factor is an axonal chemoattractant and a neurotrophic factor for spinal motor neurons. Neuron 17(6):1157-1172.
Fernandez-Ruiz J, Wang J, Aigner TG, Mishkin M. 2001. Visual habit formation in monkeys with neurotoxic lesions of the ventrocaudal neostriatum. Proc Natl Acad Sci U S A 98(7):4196-4201.
Friedman DP, Aggleton JP, Saunders RC. 2002. Comparison of hippocampal, amygdala, and perirhinal projections to the nucleus accumbens: combined anterograde and retrograde tracing study in the Macaque brain. J Comp Neurol 450(4):345-365.
Frith C. 2004. Is autism a disconnection disorder? Lancet Neurol 3(10):577.
Geschwind DH, Levitt P. 2007. Autism spectrum disorders: developmental disconnection syndromes. Curr Opin Neurobiol 17(1):103-111.
Gutierrez H, Dolcet X, Tolcos M, Davies A. 2004. HGF regulates the development of cortical pyramidal dendrites. Development 131(15):3717-3726.
Hauser MD. 1996. The evolution of communication. Cambridge, Mass.: MIT Press. xii, 760 p. p.
Horton HL, Levitt P. 1988. A unique membrane protein is expressed on early developing limbic system axons and cortical targets. J Neurosci 8(12):4653-4661.
Jackson PB, Boccuto L, Skinner C, Collins JS, Neri G, Gurrieri F, Schwartz CE. 2009. Further evidence that the rs1858830 C variant in the promoter region of the MET gene is associated with autistic disorder. Autism Res 2(4):232-236.
Judson MC, Bergman MY, Campbell DB, Eagleson KL, Levitt P. 2009. Dynamic gene and protein expression patterns of the autism-associated met receptor tyrosine kinase in the developing mouse forebrain. J Comp Neurol 513(5):511-531.
Just MA, Cherkassky VL, Keller TA, Minshew NJ. 2004. Cortical activation and synchronization during sentence comprehension in high-functioning autism: evidence of underconnectivity. Brain 127(Pt 8):1811-1821.
Koshino H, Kana RK, Keller TA, Cherkassky VL, Minshew NJ, Just MA. 2008. fMRI investigation of working memory for faces in autism: visual coding and underconnectivity with frontal areas. Cereb Cortex 18(2):289-300.
Kudo LC, Karsten SL, Chen J, Levitt P, Geschwind DH. 2007. Genetic analysis of anterior posterior expression gradients in the developing mammalian forebrain. Cereb Cortex 17(9):2108-2122.
Langford DJ, Crager SE, Shehzad Z, Smith SB, Sotocinal SG, Levenstadt JS, Chanda ML, Levitin DJ, Mogil JS. 2006. Social modulation of pain as evidence for empathy in mice. Science 312(5782):1967-1970.
Levy F. 2007. Theories of autism. Aust N Z J Psychiatry 41(11):859-868.
MacLean PD. 1955. The limbic system ("visceral brain") and emotional behavior. Archives of Neurology and Psychiatry 73:130-134.
Madhavan R, Peng HB. 2006. HGF induction of postsynaptic specializations at the neuromuscular junction. J Neurobiol 66(2):134-147.

Malkova L, Mishkin M, Bachevalier J. 1995. Long-term effects of selective neonatal temporal lobe lesions on learning and memory in monkeys. Behav Neurosci 109(2):212-226.

Marshall CR, Noor A, Vincent JB, Lionel AC, Feuk L, Skaug J, Shago M, Moessner R, Pinto D, Ren Y, Thiruvahindrapduram B, Fiebig A, Schreiber S, Friedman J, Ketelaars CE, Vos YJ, Ficicioglu C, Kirkpatrick S, Nicolson R, Sloman L, Summers A, Gibbons CA, Teebi A, Chitayat D, Weksberg R, Thompson A, Vardy C, Crosbie V, Luscombe S, Baatjes R, Zwaigenbaum L, Roberts W, Fernandez B, Szatmari P, Scherer SW. 2008. Structural variation of chromosomes in autism spectrum disorder. Am J Hum Genet 82(2):477-488.

Nakano M, Takagi N, Takagi K, Funakoshi H, Matsumoto K, Nakamura T, Takeo S. 2007. Hepatocyte growth factor promotes the number of PSD-95 clusters in young hippocampal neurons. Exp Neurol 207(2):195-202.

Papez JW. 1937. A proposed mechanism of emotion. Archives of Neurology and Psychiatry 38:725-743.

Phelps EA, LeDoux JE. 2005. Contributions of the amygdala to emotion processing: from animal models to human behavior. Neuron 48(2):175-187.

Pimenta AF, Reinoso BS, Levitt P. 1996. Expression of the mRNAs encoding the limbic system-associated membrane protein (LAMP): II. Fetal rat brain. J Comp Neurol 375(2):289-302.

Pinsk MA, Arcaro M, Weiner KS, Kalkus JF, Inati SJ, Gross CG, Kastner S. 2009. Neural representations of faces and body parts in macaque and human cortex: a comparative FMRI study. J Neurophysiol 101(5):2581-2600.

Pinsk MA, DeSimone K, Moore T, Gross CG, Kastner S. 2005. Representations of faces and body parts in macaque temporal cortex: a functional MRI study. Proc Natl Acad Sci U S A 102(19):6996-7001.

Rakic P. 1974. Neurons in rhesus monkey visual cortex: systematic relation between time of origin and eventual disposition. Science 183(123):425-427.

Romanski LM, Giguere M, Bates JF, Goldman-Rakic PS. 1997. Topographic organization of medial pulvinar connections with the prefrontal cortex in the rhesus monkey. J Comp Neurol 379(3):313-332.

Sanchez-Andrade G, James BM, Kendrick KM. 2005. Neural encoding of olfactory recognition memory. J Reprod Dev 51(5):547-558.

Shipp S. 2003. The functional logic of cortico-pulvinar connections. Philos Trans R Soc Lond B Biol Sci 358(1438):1605-1624.

Sousa I, Clark TG, Toma C, Kobayashi K, Choma M, Holt R, Sykes NH, Lamb JA, Bailey AJ, Battaglia A, Maestrini E, Monaco AP. 2009. MET and autism susceptibility: family and case-control studies. Eur J Hum Genet 17(6):749-758.

Spehr M, Kelliher KR, Li XH, Boehm T, Leinders-Zufall T, Zufall F. 2006. Essential role of the main olfactory system in social recognition of major histocompatibility complex peptide ligands. J Neurosci 26(7):1961-1970.

St John RD. 1973. Genetic analysis of tail rattling in the mouse. Nature 241(5391):549-551.

Steckler T, Drinkenburg WH, Sahgal A, Aggleton JP. 1998. Recognition memory in rats--II. Neuroanatomical substrates. Prog Neurobiol 54(3):313-332.

Stefanacci L, Amaral DG. 2002. Some observations on cortical inputs to the macaque monkey amygdala: an anterograde tracing study. J Comp Neurol 451(4):301-323.
Stefanacci L, Suzuki WA, Amaral DG. 1996. Organization of connections between the amygdaloid complex and the perirhinal and parahippocampal cortices in macaque monkeys. J Comp Neurol 375(4):552-582.
Swanson LW, Petrovich GD. 1998. What is the amygdala? Trends Neurosci 21(8):323-331.
Thornton JA, Rothblat LA, Murray EA. 1997. Rhinal cortex removal produces amnesia for preoperatively learned discrimination problems but fails to disrupt postoperative acquisition and retention in rhesus monkeys. J Neurosci 17(21):8536-8549.
Tsao DY, Freiwald WA, Tootell RB, Livingstone MS. 2006. A cortical region consisting entirely of face-selective cells. Science 311(5761):670-674.
Tyndall SJ, Walikonis RS. 2006. The receptor tyrosine kinase Met and its ligand hepatocyte growth factor are clustered at excitatory synapses and can enhance clustering of synaptic proteins. Cell Cycle 5(14):1560-1568.
Wyss JM, Sripanidkulchai K. 1983. The indusium griseum and anterior hippocampal continuation in the rat. J Comp Neurol 219(3):251-272.
Yeterian EH, Pandya DN. 1997. Corticothalamic connections of extrastriate visual areas in rhesus monkeys. J Comp Neurol 378(4):562-585.

CHAPTER IV

EVIDENCE OF CELL-NONAUTONOMOUS CHANGES IN DENDRITE AND DENDRITIC SPINE MORPHOLOGY IN THE MET-SIGNALING DEFICIENT MOUSE FOREBRAIN

Matthew C. Judson[3,*], Kathie L. Eagleson[5], Lily Wang[1,4] and Pat Levitt[1,2,5]

[1]Vanderbilt Kennedy Center for Research on Human Development, [2]Department of Pharmacology and [3]Graduate Program in Neuroscience, Department of Biostatistics[4], Vanderbilt University Medical Center, Nashville, TN 37203

[5]Zilkha Neurogenetic Institute and the Department of Cell and Neurobiology, Keck School of Medicine, University of Southern California, Los Angeles, CA 90089.

Correspondence to:
Pat Levitt, Ph.D.
Director, Zilkha Neurogenetic Institute
Chair, Dept. Cell and Neurobiology
Keck School of Medicine of USC
1501 San Pablo Street
Los Angeles, CA 90089-2821
323-442-1509
323-442-2145 (fax)
www.usc.edu/zni

Grant sponsor: National Institutes of Health (NIH)/National Institute of Mental Health (NIMH); Grant number MH067842 (PL); Grant Sponsor: NIH/National Institute of Child Health and Human Development; Grant number: P30 HD15052 (E. Dykens); Grant sponsor: NIH/National Institute on Drug Abuse (NIDA); Grant number DA022785 (PL); Simons Foundation (PL)

Abstract

Human genetic findings and murine neuroanatomical expression mapping have intersected to implicate Met receptor tyrosine kinase signaling in the development of forebrain circuits controlling social and emotional behaviors that are atypical in autism spectrum disorders (ASD). To clarify roles for Met signaling during forebrain circuit development *in vivo*, we generated mutant mice ($Emx1^{Cre}/Met^{fx/fx}$) with an Emx1-Cre-driven deletion of signaling-competent Met in dorsal pallially-derived forebrain neurons. Morphometric analyses of Lucifer Yellow-injected pyramidal neurons in postnatal day 40 anterior cingulate cortex (ACC) revealed no statistically significant changes in total dendritic length, but a selective reduction in apical arbor length distal to the soma in $Emx1^{Cre}/Met^{fx/fx}$ neurons relative to wild type, consistent with a decrease in the total tissue volume sampled by individual arbors in the cortex. The effects on dendritic structure appear to be circuit-selective, as basal arbor length was *increased* in $Emx1^{Cre}/Met^{fx/fx}$ layer 2/3 neurons. Spine number was not altered on $Emx1^{Cre}/Met^{fx/fx}$ pyramidal cell populations studied, but spine head diameter was increased modestly (4-8%). Cell-nonautonomous, circuit-level influences of Met signaling on dendritic development were confirmed by studies of medium spiny neurons (MSN), which do not express Met, but receive Met-expressing corticostriatal afferents during development. $Emx1^{Cre}/Met^{fx/fx}$ MSN exhibited robust increases in total arbor length (~20%). Like in the neocortex, average spine head diameter increased modestly (~5%). These data demonstrate that a developmental loss of presynaptic Met receptor signaling can affect postsynaptic morphogenesis and suggest a mechanism whereby attenuated Met signaling could disrupt both local and long-range connectivity within circuits relevant to ASD.

Introduction

The α,β-heterodimeric, transmembrane Met receptor tyrosine kinase binds its endogenous ligand, hepatocyte growth factor (HGF), and signals to promote a variety of developmental processes in epithelially-derived tissues. At the single-cell level these include cell proliferation, migration, differentiation, and survival (Ebens et al., 1996; Hamanoue et al., 1996; Caton et al., 2000; Ieraci et al., 2002; Gutierrez et al., 2004; Giacobini et al., 2007; Garzotto et al., 2008; Lim and Walikonis, 2008). HGF-Met signaling also plays a critical role in higher-order developmental processes such as epithelial tubulugenesis and duct formation, which requires the organization of complex interactions among many polarized cells (Rosario and Birchmeier, 2003; Zhang and Vande Woude, 2003).

Circuit wiring and synaptogenesis in the nervous system also require the exquisite control and coordination of interactions among polarized cells. Recent evidence indicates that HGF-Met signaling may help regulate these processes within specific circuits of the mammalian forebrain. Met expression mapping during the period of forebrain wiring and synaptogenesis reveals a striking enrichment of the receptor in the neuropil and long-projecting axons of the cerebral cortex, hippocampus and amygdala, suggesting that disrupted Met signaling could result in aberrant connectivity between these structures (Judson et al., 2009). Such a disruption would be predicted to impact the function of circuits governing social and emotional dimensions of behavior, consistent with recent genetic findings from ours and two other laboratories that two different alleles of the human *MET* gene are associated with autism spectrum disorders (ASD) (Campbell et al., 2006; Campbell et al., 2008; Jackson et al., 2009; Sousa et al., 2009). One variant

reduces transcriptional efficiency, consistent with the reported 2-fold decrease in neocortical MET protein expression in ASD postmortem cases (Campbell et al., 2007). Moreover, further family-based analyses have revealed an enriched association of this same promoter variant with social and communication phenotypes of ASD (Campbell et al., 2009).

There are a number of studies of neurons in vitro that demonstrate the importance of Met signaling for neuronal differentiation and synapse organization (Powell et al., 2003; Gutierrez et al., 2004; Madhavan and Peng, 2006; Tyndall and Walikonis, 2006; Nakano et al., 2007; David et al., 2008; Lim and Walikonis, 2008). However, despite these converging lines of evidence supporting a role for Met signaling in the proper wiring of circuits which in human may be vulnerable in ASD, precisely *how* disrupted Met signaling might affect *in vivo* circuit development has yet to be addressed experimentally. In the present study, we applied our neuroanatomically-based understanding of developmental forebrain Met expression to the study of dendritic morphology in neurons from wild type mice and conditional mutant mice in which Met receptors are functionally deleted in forebrain structures originating from the dorsal pallium. Specifically, we describe the dendritic morphometry of Lucifer Yellow-injected wild type and mutant projection neurons in both the anterior cingulate cortex (ACC) and the dorsolateral striatum. ACC pyramidal neurons are of interest due to their important roles in limbic circuit function and the shared expression of Met in these cells in mouse and primate cortex (M. Judson, D. Amaral, P. Levitt, unpublished observations). To address possible non-cell autonomous effects of deleting Met, we examined medium spiny neurons (MSN) of the dorsolateral striatum. These neurons do not express Met

transcript or protein, but receive abundant Met-expressing corticostriatal afferents during development (Judson et al., 2009).

Materials and Methods

Breeding and genotyping mice

Conditional Met mutant mice ($Emx1^{Cre}/Met^{fx/fx}$) were generated and genotyped using previously described strategies (Judson et al., 2009). Briefly, homozygous Met floxed ($Met^{fx/fx}$) mice were crossed to heterozygous Emx1-Cre knock-in mice that were also heterozygous for the floxed *Met* allele ($Emx1^{Cre}/ Met^{fx/+}$). All resultant progeny were genotyped by polymerase chain reaction (PCR) using the following PCR primer sets: *$Emx1^{Cre}$ forward 5_-TTCGGCTATACGTAACAGGG-3_ and reverse 5_-TCGATGCAACGAGTGATGAG-3_; Met^{fx} forward 5_-GCAACTGTCTTTTGATCCCTGC-3_ and reverse 5_TGTCCAGCAAAGTCCCATGATAG-3_*. Met^{fx} (Courtesy of Snorri Thorgeirsson, NIH/ Center for Cancer Research, Bethesda, MD) and $Emx1^{Cre}$ breeding lines (courtesy of Dr. Kevin Jones, University of Colorado, Boulder, CO) were backcrossed onto the C57BL/6J background for greater than 10 generations. All research procedures using mice were approved by the Institutional Animal Care and Use Committee at Vanderbilt University and conformed to NIH guidelines. All efforts were made to minimize animal suffering and to reduce the number of animals used.

Immunoprecipitation

The primary antibody used to immunoprecipitate (IP) the Met receptor was mouse anti-Met (Met, 25H2; #3127; Lot No. 3; Cell Signaling Technology, Beverly, MA;

immunogen: peptide corresponding to C-terminal amino acids of human Met [NCBI No. AAA59591]). Control immunoprecipitation experiments were conducted using anti-mouse IgG, whole molecule (Chroma Pure; #015000003; Lot No. 82958; Jackson Immunoresearch, West Grove, PA). Each IP antibody was covalently linked to magnetic M-280 Tosylactivated Dynabeads (Invitrogen, Carlsbad, CA) as per manufacturer's instructions.

Postnatal day 7 (P7) mice were deeply anesthetized with isofluorane prior to decapitation and brain removal. Each brain was immediately immersed in room temperature Hanks' balanced salt solution (Sigma, St. Louis, MO), and the cerebral cortex was rapidly dissected from each hemisphere with the aid of an MZ-6 stereozoom microscope (Leica, Bannockburn, IL). Harvested cerebral cortices were immediately snap-frozen in liquid nitrogen and stored at -80°C to await IP analysis.

Lysates for IP were prepared by homogenizing frozen P7 cerebral cortices in a glass tissue homogenizer (Wheaton, Millville, NJ) with ice-cold IP buffer (50 mM Tris HCl, pH 8.0, 150 mM NaCl, 1% Nonidet P-40) containing a protease inhibitor cocktail (Sigma), both serine/threonine and tyrosine phosphatase inhibitor cocktails (Sigma), 10 mM activated Na3VO4, 1mM EDTA, and 1mM EGTA. The lysates were cleared by a 16,000*g* centrifugation for 20 minutes at 4°C, and protein concentrations of the supernatants were determined using the Dc protein assay (Bio-Rad, Hercules, CA). Wild type and $Emx1^{Cre}/Met^{fx/fx}$ cortical lysates were diluted to a concentration of 2 mg/ml with IP buffer, and 1ml of 2 mg/ml lysate was incubated for 12 hours at 4°C with 75 μl of either anti-Met or anti mouse IgG IP antibodies linked to magnetic beads. Subsequently, the IP beads were pelleted with the application of a magnetic field, and washed 3 times

for 5 minutes each at 4°C in phosphate-buffered saline (PBS) containing protease and phosphatase inhibitors and 0.005% Nonidet P-40 detergent. The washed IP beads were then resuspended in 60 ul of Laemmli buffer containing 5% 2-Mercaptoethanol and incubated at 75°C for 5 minutes to elute the IP complexes. IP eluates were stored at -20C prior to SDS-PAGE and Western blotting.

HGF stimulation of cortical synaptosomes

Frozen cortices from P7 wild type and $Emx1^{Cre}/Met^{fx/fx}$ mice were thawed in ice-cold fractionation buffer (320 mM sucrose in 7mM Tris-HCL, pH 7.5, containing protease inhibitors (Sigma)) and then fractionated using a glass tissue homogenizer (Wheaton). One ml of fractionation buffer per whole cortex was used. The fractionated samples were then centrifuged at 4°C at 900*g* for 15 minutes to pellet nuclei and blood vessels. The nuclear pellets were discarded and the supernatants were further centrifuged at 14,500*g* for 15 minutes to yield pellets containing crude cell membranes and synaptosomes. Each crude synaptosomal pellet was then resuspended in ice-cold artificial cerebral spinal fluid (12.4 mM NaCl, 0.4 mM KCl, 0.1 mM KH_2PO_4, 0.25 mM $CaCl_2$, 0.1 mM $MgCl_2$, 1 mM dextrose, and 2.6 mM $NaHCO_3$), freshly bubbled with 95% O_2/5% CO_2. At this stage, human recombinant HGF (R&D Systems, Minneapolis, MN) was added to some of the resuspended synaptosomes at a final concentration of 50 ng/ml to stimulate Met receptor phosphorylation. After a 5 minute incubation on ice, both stimulated and unstimulated synaptosomes were centrifuged at 14,500*g* for 15 minutes at 4°C, and the resulting pellets were lysed with 100 μl of IP buffer and vigorous mixing. Synaptosomal lysates were cleared by a 16,000*g* centrifugation for 20 minutes at 4°C, and protein concentrations of the supernatants were determined using the Dc protein

assay (Bio-Rad). Samples were stored at -80°C prior to SDS-PAGE and Western blotting.

Western blotting

The following primary antibodies were used in Western blotting analyses**:** mouse anti-Met (Met, B-2; sc-8057; Lot No. C2807; Santa Cruz Biotechnology, Santa Cruz, CA; immunogen: peptide corresponding to amino acids 1330–1379 of mouse Met [NCBI No. NP 032617]), rabbit anti-phosphorylated Met ($pMet^{Y1234/1235}$, D26; #3077; Lot No. 2; Cell Signaling Technology; immunogen: synthetic, KLH-coupled phosphopeptide corresponding to C-terminal amino acids of human Met [NCBI No. AAA59591]), and mouse anti-phosphotyrosine (pY, 4G10; #05-321; Lot No. DAM1503375; Millipore, Billerica, MA; immunogen: KLH-coupled phosphotyramine).

Protein samples (15 μl of IP eluate per lane or 20 μg synaptosomal protein per lane) were fractionated by SDS-PAGE and transferred to supported nitrocellulose membranes. Western blotting was then performed as described previously (Judson et al., 2009), using the following primary antibody dilutions: rabbit anti-pMet and mouse anti-pY were diluted 1:1,000 in Blotto (3% Carnation dried milk in PBS) containing 0.1% Tween-20; mouse anti-Met was diluted 1:500 in Blotto alone. Anti-mouse and anti-rabbit horseradish peroxidase-conjugated secondary antibodies (Jackson Immunoresearch) were diluted to 1:5,000 with the same diluent as the primary antibody.

Intracellular injections, lucifer yellow immunohistochemistry, and morphometric reconstructions

A total of 11 P39-41 male mice (7 wild type and 4 $Emx1^{Cre}/Met^{fx/fx}$) were deeply anesthetized with sodium pentobarbital (60 mg/kg i.p.) prior to transcardial perfusion. To clear blood from the vasculature and facilitate more efficient tissue fixation, mice were

first perfused with ~10mls of 37°C PBS, which was immediately followed by ~100 mls of room-temperature phosphate-buffered 4% paraformaldehyde (pH 7.3). Each fixed brain was then removed from the skull and post-fixed for 2 hours at 4°C before being sectioned coronally at a thickness of 200 μM with a vibratome (Vibratome, Saint Louis, MO). Fixed vibratome sections were then post-fixed for an additional 2 hours at 4°C before being rinsed and stored in cold PBS. Sections were stored in PBS at 4°C for up to 5 days prior to intracellular injections of Lucifer Yellow dye. Equivalent intervals between post-fixation and intracellular injection were maintained across animals for each anatomical region of interest.

The cell bodies of layer 5 and layer 2/3 pyramidal neurons in anterior cingulate cortex (at the level of the genu of the corpus callosum) and medium spiny neurons in dorsolateral striatum (at the level of the body of the anterior commissure) were targeted for injection with the aid of an Axioskop2 microscope and 40x immersion objective (Zeiss, Jena, Germany). The injected cells were within 3 focal planes of the upper surface of the brain section and evenly spaced from previously injected cells. Then, a glass micropipette containing Lucifer Yellow dye (8% in 0.05 M Tris buffer, pH 7.4) was gently inserted into each targeted cell body using a micromanipulator, and a continuous current (5-15 nA) was applied until the tips of the most distal dendrites were brightly fluorescent.

Lucifer Yellow immunohistochemistry was used to yield a more photostable product within injected cells. Briefly, sections containing injected cells were placed in a stock solution (2% bovine serum albumin, 1% Triton X-100, and 5% sucrose in PBS) containing a 1:5,000 dilution of rabbit anti-Lucifer Yellow antibody (#L9163; Sigma).

Sections were incubated in the primary antibody solution at 4°C for 3-4 days before being rinsed several times in stock solution and incubated 2 hours at room-temperature in biotinylated anti-rabbit secondary antibody (RPN1004; GE/Amersham, Pittsburgh, PA). Several rinses in PBS followed, and sections were subjected to a final 2 hour room-temperature incubation in Alexa Fluor 488-conjugated streptavidin (Invitrogen) diluted 1:1,000 in PBS. After several more rinses in PBS, sections were mounted on uncoated glass slides and coverslipped with ProLong Gold mounting medium (Invitrogen).

An Olympus microscope with a motorized stage and Neurolucida software (Microbrightfield, Williston, VT) were used to three-dimensionally reconstruct the dendritic arbors of neurons whose dendrites were completely filled to the distal tips. Between 3 and 6 cells per anatomical region per animal were analyzed. Dendrites were frequently transected by the coronal plane of section, which severely limited the study of pyramidal apical dendritic arbors whenever the primary apical dendrite was cut off proximal to the cell body. Therefore, we chose to only analyze the arbors of layer 5 and layer 2/3 pyramidal cells with total apical dendritic lengths at least half that of their respective genotypic means. Seven wild type (3 layer 5 and 4 layer 2/3) and 6 $Emx1^{Cre}/Met^{fx/fx}$ (5 layer 2/3 and 1 layer 5) pyramidal cells were excluded from analysis based on this criterion. Investigators were blind to the genotypic identities of the samples from the time of animal perfusion through the morphometric analysis of dendritic arbor structure.

Confocal microscopy and semi-automated analysis of dendritic spines

Using an approach based on previously described methods (Shen et al., 2008), dendrites of the same neurons subjected to Neurolucida analyses were imaged by

confocal microscopy, and three-dimensional renderings of the images were used to facilitate semi-automated quantification of dendritic spine density and dendritic spine head diameter. Usually 2, but occasionally 1 or 3, dendritic segments located 60-120 μM (2^{nd}, 3^{rd}, or 4^{th} order) from the cell body were analyzed per cell. Briefly, a Zeiss LSM 510 confocal microscope (Zeiss, Jena, Germany) with 63x oil immersion objective, 4x digital cropping, and a frame size of 1024 x 1024 pixels was used to capture high-resolution images of dendritic segments with 0.035 μM x 0.035 μM pixel dimensions. Segments were scanned at 0.38 μM intervals along the Z axis.

Confocal images of dendritic segments were viewed using Imaris software (Version 6.3-64 bit, Bitplane, Saint Paul, MN) in the Surpass view. The Filament module (Autopath, no loops), was then used to generate a three-dimensional, segmented rendering of each dendritic segment that was between 30 μM and 35 μM in length on average. The minimum end-point diameter (smallest detected spine head) was set at 0.143 μM, and the fluorescence contrast threshold was set $\geq$ to 3. Renderings were subsequently edited for accuracy relative to the actual confocal image, and data concerning spine density and end-segment diameter were exported to Microsoft Excel 2003 (Microsoft Incorporated, Redmond, WA) for summary statistical analyses. Investigators were unaware of sample genotypes both during the imaging and three-dimensional rendering of dendritic segments.

Digital illustrations

Optical fluorescence microscopy was performed with the aid of an Axioplan II microscope (Zeiss), and low-power micrographs depicting fields of Lucifer Yellow-injected neurons were acquired with a Zeiss AxioCam HRc camera (Zeiss) in Axiovision

4.1 software (Zeiss). Alterations to contrast levels in these low-power images were performed using Adobe Photoshop (Version 7.0, Adobe, San Jose, CA). Figures were prepared digitally in Microsoft Office Powerpoint 2003 (Microsoft Incorporated).

Statistical analyses

All morphological data in the present study are summarized as means±SEM. Genotypic group differences in gross dendritic structure (e.g., total dendritic length and dendritic arbor volume) were assessed using the two-sample, two-tailed t-test within GraphPad Prism (Version 4.0, GraphPad Software, La Jolla, CA), the software program used for the production of all data graphs. P-values less than 0.05 were considered significant.

Sholl analysis data, which describe changes in dendritic structure that occur as a function of radial distance from a neuronal cell body (Sholl, 1953), were analyzed within SAS (version 9.1.3, SAS institute, Cary, NC) Procedure GLIMMIX. Specifically, genotypic group differences within each anatomical region of interest were analyzed using a linear mixed model with dendritic length as the outcome, fixed effects group, radius, group x radius interaction, and random effects animals. The random animal effects, along with an autoregressive covariance structure for each neuron within an animal account for correlations of repeated measurements from the same animal. Because both fixed and random effects are included, this model is a mixed effects model. To compare dendritic length at each radius for the two groups, parameters from the mixed model were estimated and compared. We used the Kenward-Roger's adjusted degrees of freedom solution (option DDFM=KR in Procedure GLIMMIX) for statistical inference (Kenward and Roger, 1997), an approach specifically proposed for small sample settings.

Normality of residuals from the mixed models was assessed using the Shapiro-Wilk test, and a Box-Cox transformed (Box and Cox, 1964) outcome variable for dendritic length was used when departure from normality was detected. Owing to the relatively small number of animals sampled, genotypic differences at each radius were considered statistically significant if the raw p-value was less than 0.05. All tests were two-tailed.

Results

Demonstration of Met signaling deficiency in the cortex of Emx1^{Cre}/Met$^{fx/fx}$ mice

A previous study reporting a Cre recombinase-driven deletion of the Met^{fx} allele from heaptocytes demonstrated successful removal of the ATP-binding site from the Met tyrosine kinase domain, and consequently, dramatic reductions in levels of signaling-competent Met protein, receptor activation and downstream signaling (Huh et al., 2004). We confirmed similar Met signaling deficiencies in forebrain tissues derived from the dorsal pallium in Emx1^{Cre}/Met$^{fx/fx}$ mice during the period of peak receptor expression in the postnatal mouse forebrain (Judson et al., 2009). First, a dramatically reduced ratio of processed (140 kD), presumably signaling-competent Met to unprocessed (170 kD) precursor protein was immunoprecipitated from lysates of Emx1^{Cre}/Met$^{fx/fx}$ postnatal day (P) 7 neocortex relative to wild type (**Fig. 1A**). Second, we observed a robust induction of Met receptor phosphorylation in HGF-stimulated synaptosomes prepared from P7 wild type but not Emx1^{Cre}/Met$^{fx/fx}$ synaptosomes (**Fig. 1B**). Collectively, these data demonstrate the utility of the Emx1^{Cre}/Met$^{fx/fx}$ mouse as a model in which to study the consequences of Met signaling deficiency during forebrain circuit development.

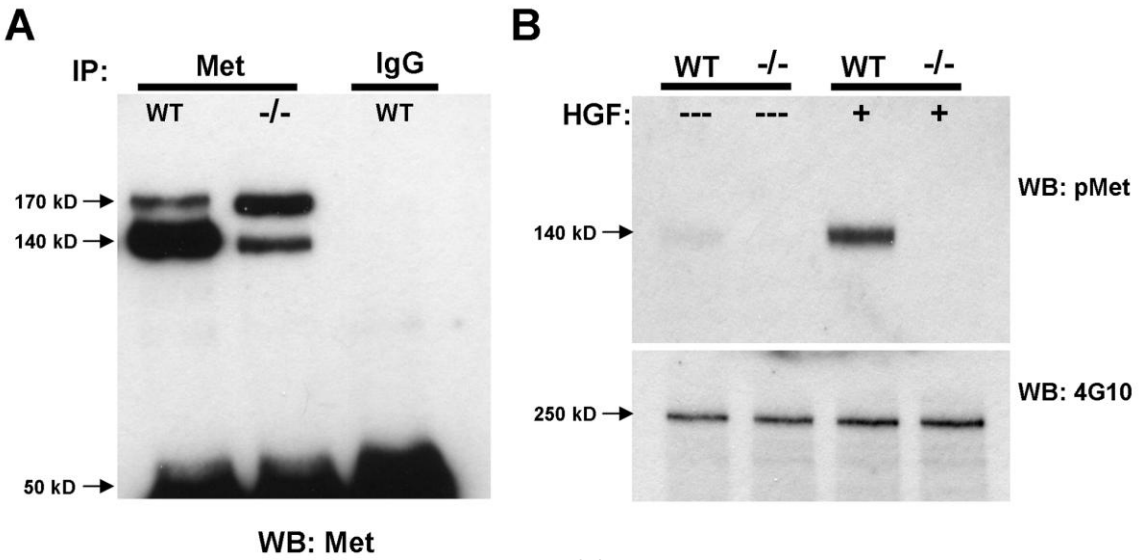

Figure 1. Met signaling deficiency in the Emx1^{cre}/Met$^{fx/fx}$ mouse. **A:** Total Met Western blotting of Met and control mouse IgG immunoprecipitates from P7 wild type (WT) and Emx1^{cre}/Met$^{fx/fx}$ (-/-) cortical lysates. Note the drastically reduced ratio of processed, signaling-competent Met receptor (140 kD band) to unprocessed receptor precursor (170 kD band) that is immunoprecipitated from the -/- lysate. No Met protein of either form was immunprecipitated with control mouse pre-immune IgG. **B:** Stimulation of P7 crude cortical synaptosomes with 50 ng/ml HGF. Western blotting for phosphorylated Met (pMet) demonstrates that HGF induces substantial Met receptor activation in WT but not -/- synaptosomes. Western blotting for total tyrosine phosphorylated protein (4G10) demonstrates equivalent protein loading across samples.

Met-dependent changes in layer- and compartment-specific dendritic arbors in pyramidal neurons of anterior cingulate cortex

To begin to understand the effects of attenuated Met signaling on forebrain circuit development, we focused on comparisons of dendritic morphology in wild type and Emx1^{Cre}/Met$^{fx/fx}$ pyramidal neurons of the anterior cingulate cortex (ACC) at a time-point (P40) just subsequent to the most robust periods of circuit connectivity and refinement. ACC pyramidal neurons presented as a compelling population for study for 3 reasons: 1) these neurons act as key integrators and processors of limbic circuit information, 2) these neurons constitute a Met-expressing population shared by mouse and non-human primate cortex (M. Judson, D. Amaral, P. Levitt, unpublished observations) and 3) corticocortical

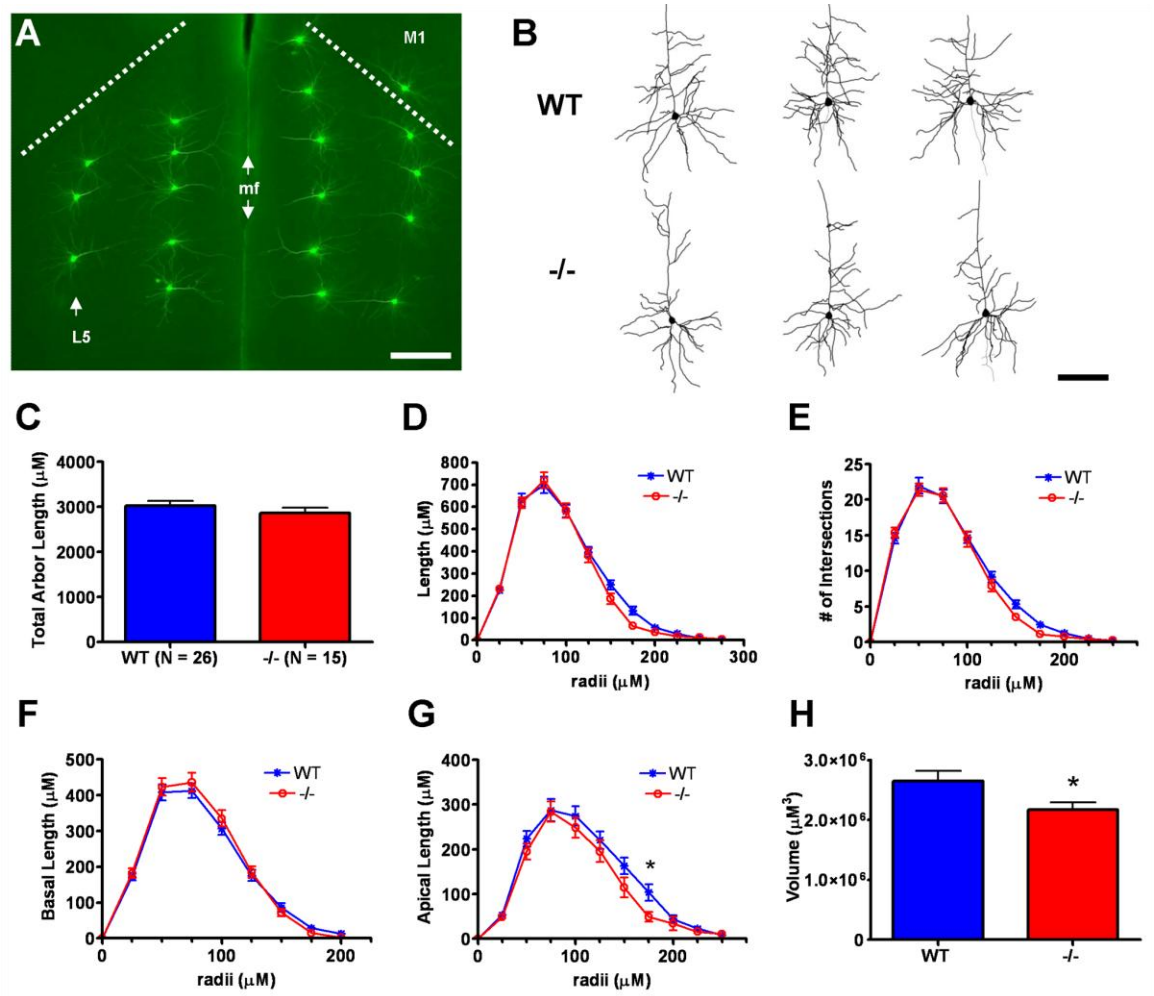

Figure 2. Analysis of layer 5 pyramidal cell morphometry in postnatal day 40 wild type (WT) versus $Emx1^{cre}/Met^{fx/fx}$ (-/-) anterior cingulate cortex (ACC). **A:** Representative fluorescence micrograph of lucifer yellow immunoreactivity in microinjected pyramidal cells in both left and right anterior cingulate cortex in a coronal brain section. Pyramidal cell injections could be precisely targeted within Layer 5 (arrow, left hemisphere). The dashed lines represent the anatomical boundary between ACC and primary motor cortex (M1) in each hemisphere. The median fissure (mf, double arrows) marks the boundary between hemispheres. **B:** Representative Neurolucida traces of layer 5 WT and -/- ACC pyramidal neurons. The neurons depicted have dendritic arbor morphometries approximate to the mean values of their genotypic group. **C-H:** Dendritic morphometry summary statistics. Though the average total dendritic arbor lengths are statistically equivalent (C), -/- arbors exhibit reduced dendritic length distal to the cell body (D). Sholl analysis indicates a corroborating reduction in -/- branching complexity in the same distal arbor regions (E). Subcomponent analyses for arbor length indicate that reductions in distal length in -/- layer 5 neurons are due to changes in the apical (G) but not the basilar (F) arbor. Three-dimensional convex hull analysis shows that reduced apical arbor length translates into reduced arbor volume in -/- layer 5 pyramidal neurons (H). Scale bar = 275 μM for A and 100 μM for B. *$p \leq 0.05$.

afferents to ACC pyramidal neurons express abundant levels of Met during limbic circuit formation, raising the possibility that dendritic morphologies of these neurons in $Emx1^{Cre}/Met^{fx/fx}$ mice would reflect both cell-autonomous and circuit-level effects of Met signaling disruption. To visualize and study ACC pyramidal dendrites, we employed the Lucifer Yellow microinjection technique, which allowed for the reliable sampling of both layer 5 and layer 2/3 pyramidals (**Figs. 2A and 3A**) as well as the faithful three-dimensional (3D) reconstruction of dendritic arbors and analysis of several morphometric parameters.

Contrary to the reported growth-promoting effects of HGF-signaling *in vitro*, but consistent with grossly normal ACC cytoarchitecture and histology (Judson et al., 2009), no statistically significant difference was found in either the number of primary dendrites (**Suppl. Fig. 1A,B**) or total dendritic arbor length (**Figs. 2C, 3C**) between wild type and $Emx1^{Cre}/Met^{fx/fx}$ ACC pyramidal neurons. However, both qualitative (**Figs. 2B, 3B**) and quantitative (**Figs. 2D, 3D**) comparisons revealed altered distributions of dendritic length within the arbors of layer 5 and layer 2/3 $Emx1^{Cre}/Met^{fx/fx}$ pyramidal neurons as compared to wild type. The reduction in distal arbor length was shared by layer 5 and layer 2/3 $Emx1^{Cre}/Met^{fx/fx}$ pyramidal neurons, and was corroborated by decreases in branching complexity in the same distal arbor regions (**Figs. 2E, 3E**). Moreover, these changes were specific to the apical dendritic compartment (**Figs. 2G, 3G**). Finally, as demonstrated by 3D convex hull analysis, which measures the volume contained within the arbor's most outward lying dendritic end-points (**Suppl. Fig. 2A-D**), the loss in distal apical length translated into an approximate 20% reduction in the average cortical volume sampled by $Emx1^{Cre}/Met^{fx/fx}$ ACC pyramidal neurons (**Figs. 2H, 3H**). Interestingly,

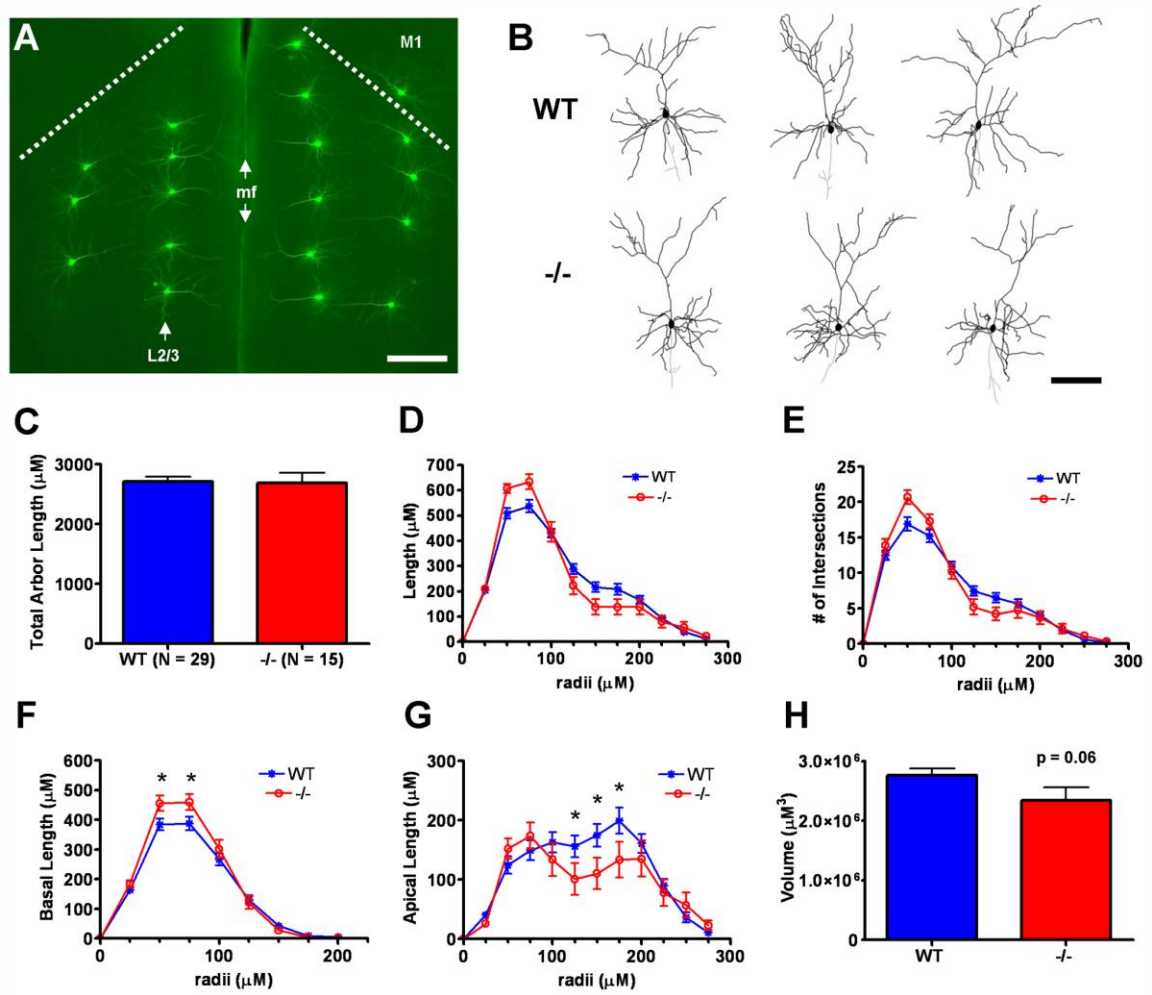

Figure 3. Analysis of layer 2/3 pyramidal cell morphometry in postnatal day 40 wild type (WT) versus $Emx1^{cre}/Met^{fx/fx}$ (-/-) anterior cingulate cortex (ACC). **A:** Representative fluorescence micrograph of lucifer yellow immunoreactivity in microinjected pyramidal cells in both left and right anterior cingulate cortex in a coronal brain section. Injections of Layer 2/3 pyramidal cells (arrow, left hemisphere) were highly reproducible across animals in terms of radial distance from the pial surface/median fissure (mf). The dashed lines represent the anatomical boundary between ACC and primary motor cortex (M1) in each hemisphere. **B:** Representative Neurolucida traces of layer 2/3 WT and -/- ACC pyramidal neurons. The neurons depicted have dendritic arbor morphometries approximate to the mean values of their genotypic group. **C-H:** Dendritic morphometry summary statistics. Though the average total dendritic arbor lengths are statistically equivalent (C), -/- arbors exhibit *increased* dendritic length proximal to, but *decreased* dendritic length distal to, the cell body (D). Sholl analysis shows that changes in branching complexity in -/- arbors mirror changes in dendritic length as a function of distance from the cell body (E). Subcomponent analyses for arbor length indicate that proximal increases in -/- arbor length reflect changes in the basilar arbor (F), while the apical arbor (G) accounts for decreases in distal arbor length. Three-dimensional convex hull analysis reveals a strong trend toward reduced arbor volume in -/- layer 2/3 pyramidal neurons (H), consistent with reduced apical arbor length distal to the cell body. Scale bar = 275 μM for A and 100 μM for B. *$p \leq 0.05$.

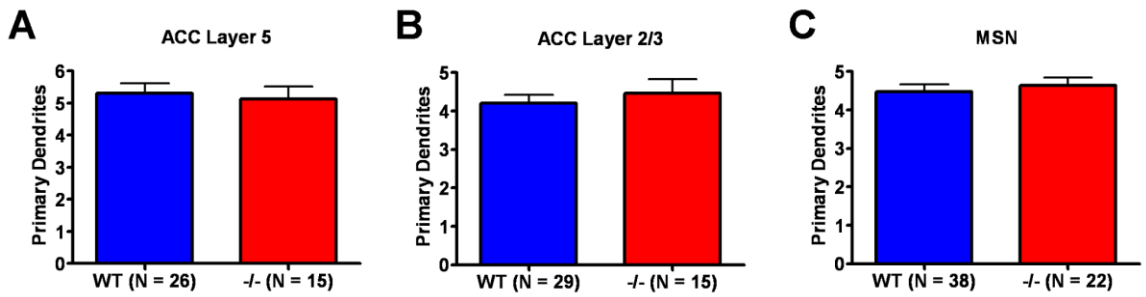

Supplementary Figure 1. Comparison of average primary dendrite number between postnatal day 40 wild type (WT) and $Emx1^{cre}/Met^{fx/fx}$ (-/-) neurons. No genotypic difference in primary dendrite number was detected within the basilar dendritic arbors of either layer 5 (**A**) or layer 2/3 (**B**) pyramidal neurons in anterior cingulate cortex. The number of primary dendrites within the arbors of medium spiny neurons was also equivalent between the WT and -/- groups (**C**).

despite these broad phenotypic similarities, there were different causes underlying the apical arbor deficits in these two groups of $Emx1^{Cre}/Met^{fx/fx}$ ACC pyramidal neurons. Specifically, the reduction in apical arbor length in layer 5 mutant pyramidal neurons were primarily a function of reduced dendritic segment length (**Suppl. Fig. 3A,C**), wheseas those in layer 2/3 pyramidal neurons were caused by reduced branching in select regions of the apical arbor (**Suppl. Fig. 4A,C**).

$Emx1^{Cre}/Met^{fx/fx}$ layer 5 and layer 2/3 ACC pyramidal neurons differed with regard to dendritic length proximal to the cell body (**Figs. 2D, 3D**). Proximal dendritic length and branching complexity (**Fig. 3D,E**) was significantly increased in $Emx1^{Cre}/Met^{fx/fx}$ layer 2/3 pyramidal neurons due to robust increases in branching. This occurred despite a trend toward modestly reduced dendritic segment length in the basal arbors of these cells (**Fig. 3F; Suppl. Fig. 4A,B**). The distribution of dendritic length both proximal to the cell body and within the basal arbors of $Emx1^{Cre}/Met^{fx/fx}$ layer 5 pyramidal neurons was statistically indistinguishable from that in wild type neurons (**Fig. 2D,F**). There was, however, a trend toward reduced basal dendritic segment length in

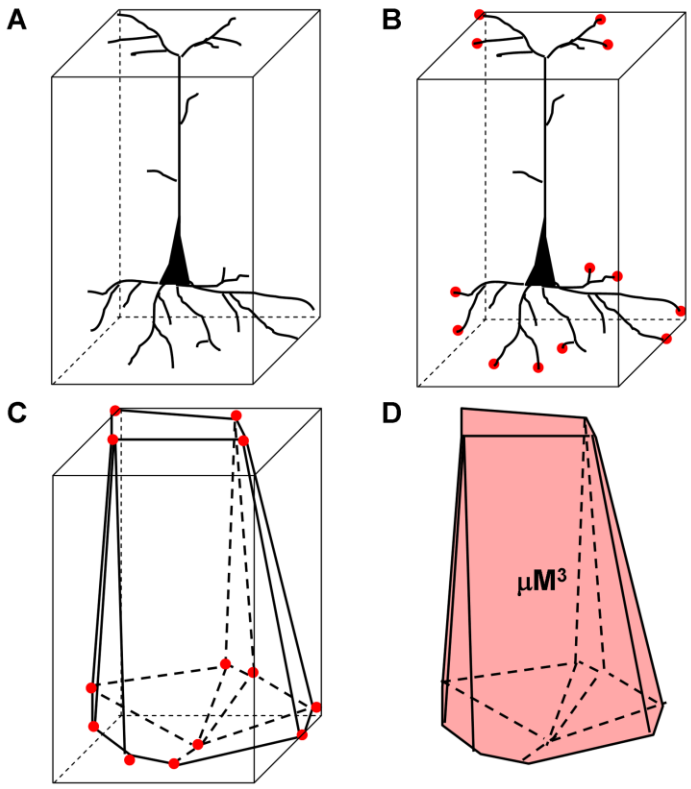

Supplementary Figure 2. Explanation of 3-dimensional (3D) convex hull analysis of dendritic arbor structures. First, the distal most dendritic end-points of a 3D reconstructed dendritic arbor (**A**) are identified (**B**, red circles). These distal end-points are then connected with line segments (**C**) to form a 3D polyhedron, or "convex hull", which bounds the extremities of the dendritic arbor. The volume contained within the convex hull (**D**) is the morphometric parameter of interest. This analysis is automatically performed within Neurolucida (Microbrightfield).

these cells (**Suppl. Fig. 3B**). These data suggest that in the absence of Met signaling, there are different adaptive changes in distinct neuronal compartments that may reflect circuit-specific influences.

Met-dependent changes in spine head size on ACC pyramidal neurons

Changes in the dendritic morphology of $Emx1^{Cre}/Met^{fx/fx}$ ACC pyramidal neurons were layer-specific in nature, prompting us to determine whether or not dendritic spine morphology across layers might also be differentially susceptible to Met signaling deficiency. Using high resolution 3D-renderings of confocal image stacks, we quantified

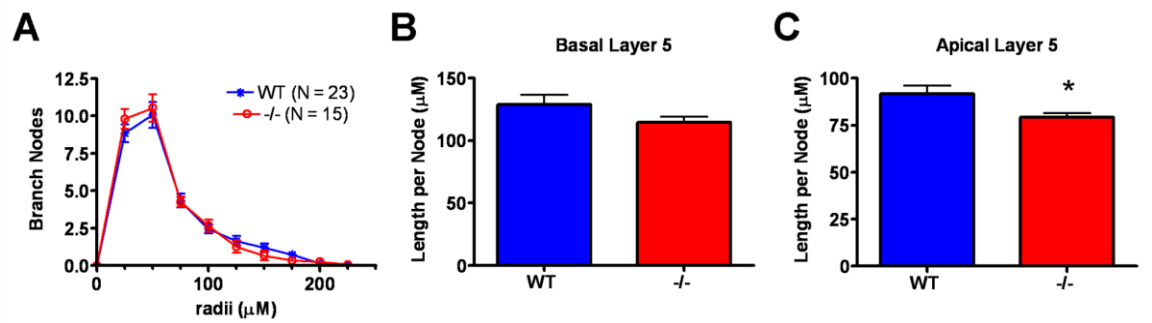

Supplementary Figure 3. Branching details of postnatal day 40 wild type (WT) and Emx1^{cre}/Met$^{fx/fx}$ (-/-) layer 5 pyramidal neurons in anterior cingulate cortex. Analysis of branch number as a function of distance from the cell body reveals equivalent branching between genotypic groups proximal to the cell body and a modest decrease in branching in distal regions of -/- dendritic arbors (**A**). Measures of dendritic length per branch node in layer 5 basilar arbors are not statistically different between WT and -/- groups (**B**). However, similar analyses in layer 5 apical arbors reveal an ~20% decrease in dendritic segment length in -/- neurons (**C**). *$p \leq 0.05$.

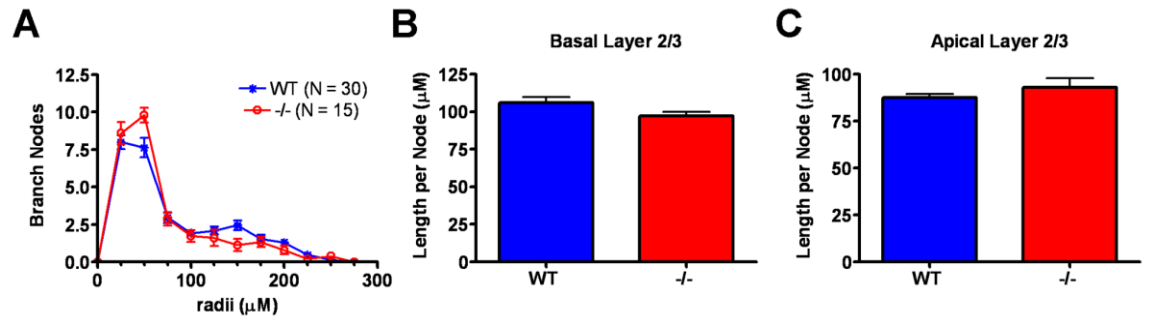

Supplementary Figure 4. Branching details of postnatal day 40 wild type (WT) and Emx1^{cre}/Met$^{fx/fx}$ (-/-) layer 2/3 pyramidal neurons in anterior cingulate cortex. Analysis of branch number as a function of distance from the cell body reveals increased branching in -/- neurons proximal to the cell body but a decrease in branching in more distal dendritic regions in these same cells (**A**). Measures of dendritic length per branch node show a trend toward modestly reduced dendritic length in the basilar dendritic segments of -/- layer 2/3 neurons (**B**), but there is no statistically significant difference between genotypic groups in regard to the length of apical dendritic segments (**C**).

dendritic spine density and spine head diameter within dendritic segments from the basal arbors of layer 5 and layer 2/3 ACC pyramidal neurons. Neither layer 5 (**Fig. 4A**) nor layer 2/3 (**Fig. 5A**) neurons exhibited changes in basal dendritic spine density in the

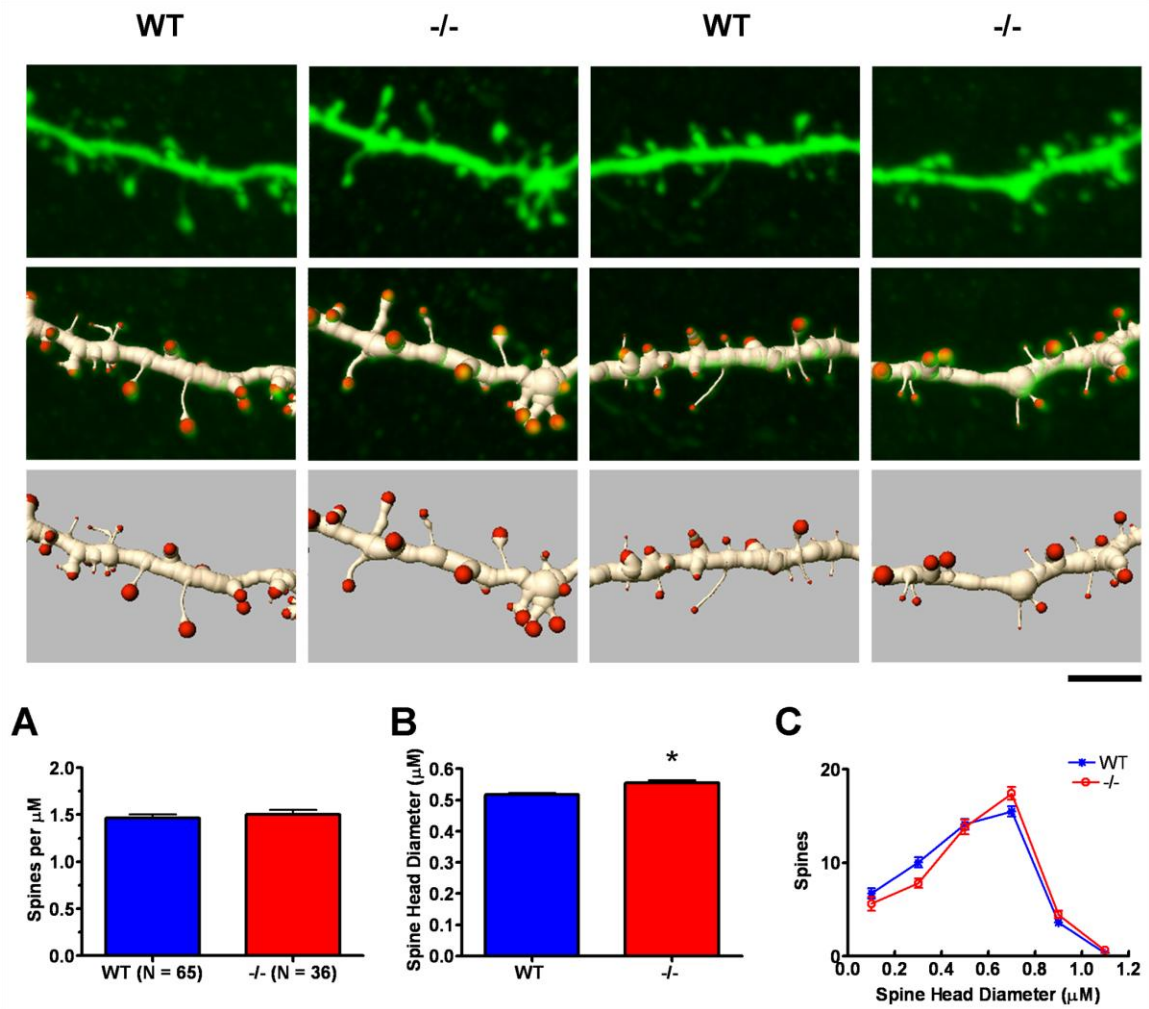

Figure 4. Analysis of basilar dendritic spines in P40 wild type (WT) versus Emx1^{cre}/Met$^{fx/fx}$ (-/-) layer 5 pyramidal cells. Confocal projection images of WT and -/- layer 5 pyramidal basilar dendritic segments (top row) and associated three-dimensional (3-D) segmented renderings shown in overlay (middle row) and apart (bottom row). The images depict portions of analyzed full-length segments with spine density and spine head diameter values similar to the mean values of their genotypic group. **A-C:** Quantification of spine density and spine head diameter based on 3-D renderings. No difference in spine density was observed between genotypic groups (A), but an ~8% increase in average spine head diameter was found for -/- layer 5 basilar dendritic segments as compared with WT (B). The frequency distribution of spine head diameters reveals greater numbers of larger spines and fewer thinner spines in -/- layer 5 basilar dendritic segments (C). Scale bar = 4 µM for all images. *$p \leq 0.05$.

Emx1^{Cre}/Met$^{fx/fx}$ as compared to wild type ACC. However, modest, but statistically significant, increases in basal dendritic spine head diameter were detected in both populations of Emx1^{Cre}/Met$^{fx/fx}$ cells (**Figs. 4B, 5B**). The data also revealed a leftward shift in the frequency distribution of Emx1^{Cre}/Met$^{fx/fx}$ versus wild type layer 5 basal

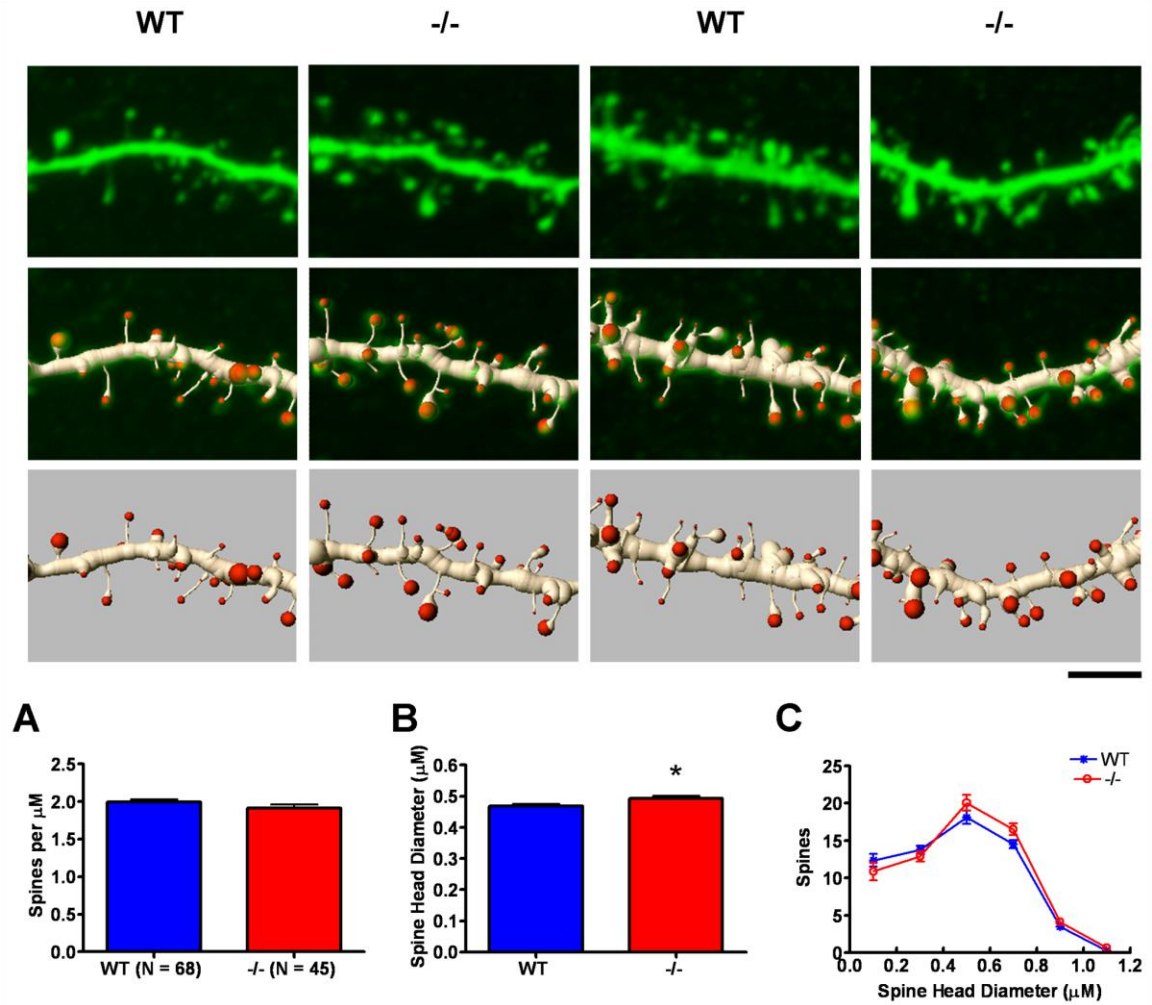

Figure 5. Analysis of basilar dendritic spines in P40 wild type (WT) versus $Emx1^{cre}/Met^{fx/fx}$ (-/-) layer 2/3 pyramidal cells. Confocal projection images of WT and -/- layer 2/3 pyramidal basilar dendritic segments (top row) and associated three-dimensional (3-D) segmented renderings shown in overlay (middle row) and apart (bottom row). The images depict portions of analyzed full-length segments with spine density and spine head diameter values similar to the mean values of their genotypic group. **A-C:** Quantification of spine density and spine head diameter based on 3-D renderings. No difference in spine density was observed between genotypic groups (A), but an ~5% increase in average spine head diameter was found for -/- layer 2/3 basilar dendritic segments as compared with WT (B). The frequency distribution of spine head diameters reveals a rightward shift toward larger spines in -/- layer 2/3 basilar dendritic segments (C). Scale bar = 4 μM for all images. *$p \leq 0.05$.

dendritic spine head diameters (**Fig. 4C**). Whereas an analysis of layer 2/3 pyramidal neurons revealed a similar increase in the frequency of larger basal dendritic spine head diameters, there was no obvious reduction in the frequency of thinner spines (**Fig. 5C**). Collectively, these data demonstrate similar alterations in dendritic spine morphology on

arbors whose branching morphologies are differentially affected by disrupted Met signaling.

Met-dependent changes in dendritic arbors and spine morphology in striatal medium spiny neurons

We analyzed the dendritic morphology of Lucifer Yellow-injected dorsolateral MSNs from the same wild type and $Emx1^{Cre}/Met^{fx/fx}$ mice used to study the morphology of ACC pyramidal neurons. Measures of total dendritic length revealed an approximate 20% increase in the dendritic arbors of MSNs in $Emx1^{Cre}/Met^{fx/fx}$ mice compared to wild type (**Fig. 6C**). This difference in dendritic growth is robust and readily appreciated qualitatively in two-dimensional projections of Neurolucida tracings (**Fig. 6B**). Sholl analysis of the distribution of dendritic length (**Fig. 6D**) revealed increases in the $Emx1^{Cre}/Met^{fx/fx}$ arbors beginning approximately 50 μM from the cell body and spanning the extent of the arbor. This finding is consistent with there being equivalent numbers of primary dendrites (**Suppl. Fig. 1C**), but increased branching (**Fig. 6F**) and branching complexity (**Fig 6E**) of higher order dendrites, in the $Emx1^{Cre}/Met^{fx/fx}$ arbors relative to wild type. Furthermore, we found that the approximate 20% increase in $Emx1^{Cre}/Met^{fx/fx}$ MSN dendritic arbor volume (**Fig. 6H**) was related to increased branching, and not from an increase in average length of dendritic segments (**Fig. 6G**).

At the level of the dendritic spine, we detected morphological differences in the $Emx1^{Cre}/Met^{fx/fx}$ MSN arbors that were more modest in nature. Relative to wild type MSN dendrites, MSN dendritic spine density was normal (**Fig. 7A**). Average spine head diameter was increased by approximately 5% (**Fig. 7B**). The frequency distribution of spine head size revealed reductions in thinner spines and extremely large spines in the

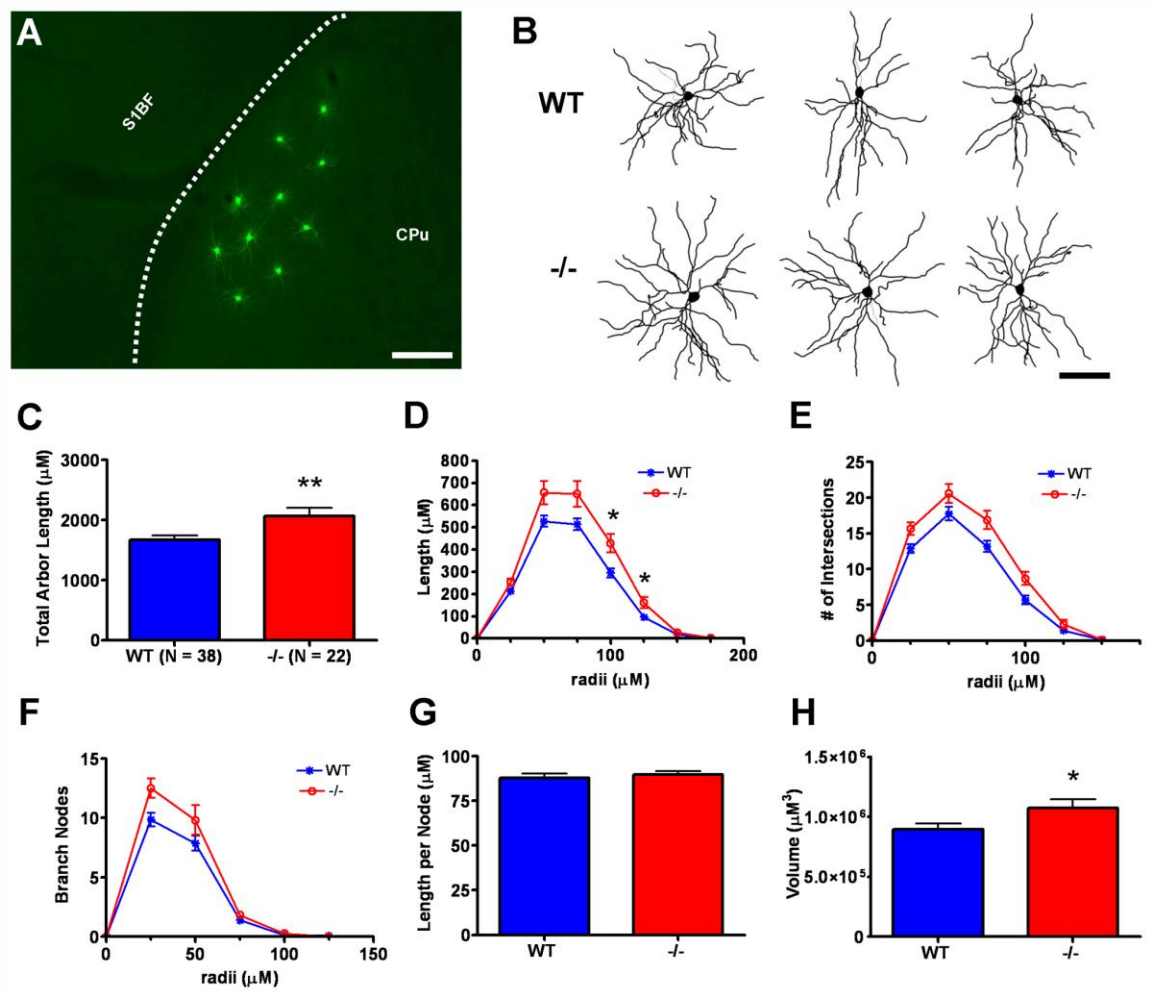

Figure 6. Analysis of medium spiny neuron (MSN) morphometry in the dorsolateral caudate putamen (CPu) of postnatal day 40 wild type (WT) versus $Emx1^{cre}/Met^{fx/fx}$ (-/-) mice. **A:** Representative fluorescence micrograph of lucifer yellow immunoreactivity in microinjected medium spiny neurons in dorsolateral CPu in a coronal section. The dashed line represents the white matter boundary between striatum and overlying somatosensory barrel cortex (S1BF). **B:** Representative Neurolucida traces of MSNs. The neurons depicted have dendritic arbor morphometries approximate to the mean values of their genotypic group. **C-H:** Dendritic morphometry summary statistics. -/- MSNs exhibit an ~25% increase in total dendritic arbor length relative to their WT counterparts (C). Further analyses shows that increases in -/- dendritic length (D) and branching complexity (E) are distributed throughout the arbor and are due to increases in the number of dendritic branches (F) rather than an increase in the length of each branch segment (G). Three-dimensional convex hull analysis indicates an ~20% increase in -/- MSN arbor volume (H). Scale bar = 275 μM for A and 167 μM for B. $^{**}p \leq 0.01$, $^{*}p \leq 0.05$.

$Emx1^{Cre}/Met^{fx/fx}$ arbors, whereas the frequency of intermediately sized spines was increased (**Fig. 7C).** Consequently, the overall dendritic phenotype of $Emx1^{Cre}/Met^{fx/fx}$ MSNs, which do not express Met, is reminiscent of the basal dendrites of layer 2/3 ACC

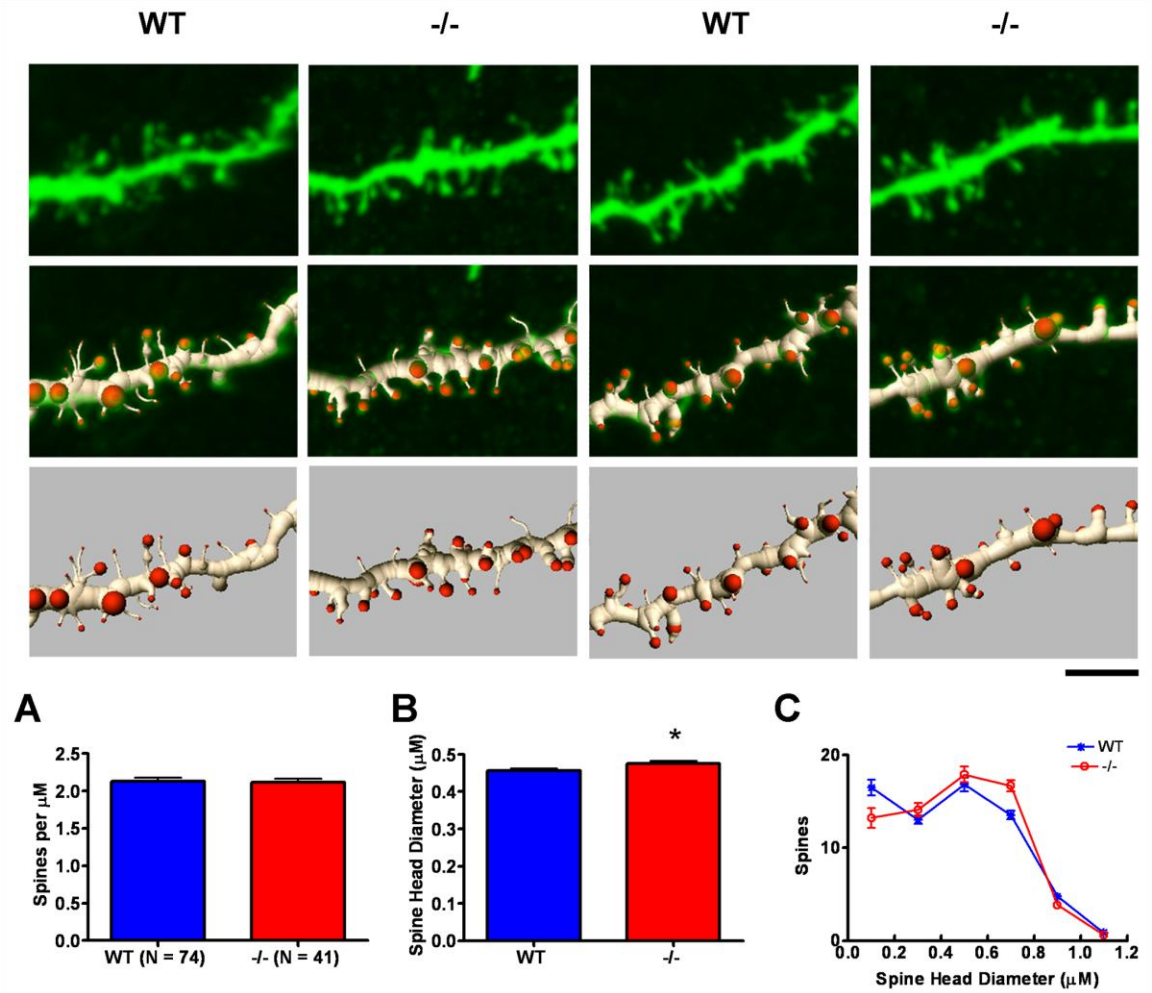

Figure 7. Analysis of dendritic spines in P40 wild type (WT) versus $Emx1^{cre}/Met^{fx/fx}$ (-/-) dorsolateral medium spiny neurons (MSNs). Confocal projection images of WT and -/- MSN dendritic segments (top row) and associated three-dimensional (3-D) segmented renderings shown in overlay (middle row) and apart (bottom row). The images depict portions of analyzed full-length segments with spine density and spine head diameter values similar to the mean values of their genotypic group. **A-C:** Quantification of spine density and spine head diameter based on 3-D renderings. No difference in spine density was observed between genotypic groups (A), but an ~4% increase in average spine head diameter was found for -/- MSN dendritic segments as compared with WT (B). The frequency distribution of spine head diameters reveals an increase in larger spines and a decrease in thinner spines in -/- MSN dendritic segments (C). Scale bar = 4 μM for all images. *$p \leq 0.05$.

pyramidal neurons. The collective data from neocortex and striatum suggest that disruption of Met signaling influences developing forebrain neurons in a circuit-dependent fashion.

Discussion

The major finding of this study is that the constitutive elimination of Met receptor tyrosine kinase signaling during development *in vivo* results in modest cell-nonautonomous changes in dendrite and dendritic spine morphology in forebrain neurons. Two critical features of our experimental approach allowed us to dissociate these changes from cell-autonomous effects on dendritic structure- a considerable challenge considering the well-documented roles for Met signaling in dendritic (Gutierrez et al., 2004; Tyndall et al., 2007; Lim and Walikonis, 2008) and axonal outgrowth *in vitro* (Ebens et al., 1996; David et al., 2008) as well as the localization of Met to both dendritic and axonal compartments *in vivo* (Tyndall and Walikonis, 2006; Judson et al., 2009). First, based on transcript and protein expression, Met expression is absent or expressed at very low levels in medium spiny neurons (MSN) in the developing pre- and postnatal striatum (Judson et al., 2009), suggesting that any alterations in their dendritic morphology subsequent to an ablation of Met signaling is not cell-autonomous in nature. Second, in the $Emx1^{Cre}/Met^{fx/fx}$ mouse, Met signaling is ablated from nearly all Met-expressing MSN afferents during development (Judson et al., 2009), rendering these cells vulnerable to cell-nonautonomous, presynaptically-derived changes in dendritic morphology. We documented such changes in $Emx1^{Cre}/Met^{fx/fx}$ MSN dendritic morphology using the Lucifer Yellow microinjection technique to visualize and assess dendritic morphology. Specifically, we detected a marked increase in dendritic branching and total dendritic length and a small, statistically significant increase in dendritic spine head diameter in $Emx1^{Cre}/Met^{fx/fx}$ MSN neurons relative to their wild type counterparts. Because similar changes in dendritic morphology were detected in the

basal arbors of Emx1^{Cre}/Met$^{fx/fx}$ ACC pyramidal neurons, it is possible that these circuit-level influences affect all dendritic compartments that receive Met-expressing axonal afferents.

Mechanisms of altered dendrite and dendritic spine morphology in the Emx1^{Cre}/Met$^{fx/fx}$ forebrain

This study provides, to our knowledge, the first evidence that Met signaling can influence the development of dendrites on select forebrain neurons in a circuit-related fashion. However, the mechanistic nature of the influences is unclear. One possibility is that Met signals directly within the developing preterminal axon to impact postsynaptic neuronal development. Though this signaling capacity has yet to be directly demonstrated, its potential is supported by observations of upregulated Met expression in the terminal fields of forebrain axons during, but not prior to, robust periods of axon collateralization and the beginning of synaptogenesis (Judson et al., 2009). Recently, an absence of presynaptically localized Met receptor was reported in the rat via immuno-electron microscopy (Tyndall and Walikonis, 2006), but this finding was limited to circumscribed regions of the hippocampus in adult animals. Assuming that Met signals within presynaptic compartments, elucidating its role in regulating presynaptic function will require additional morphological and electrophysiological analyses.

There are examples in the literature that would be consistent with the resultant MSN adaptive changes due to either increased or reduced presynaptic signaling. For example, both broad (Dierssen et al., 2003; Gelfo et al., 2009) and focal (Russell and Moore, 1999; Sorensen and Rubel, 2006) manipulations of afferent activity have been shown to positively correlate with changes in dendritic structure, suggesting that the

enhanced branching in Emx1^{Cre}/Met$^{fx/fx}$ MSN dendritic arbors could result from increased corticostriatal afferent activity. This would imply that Met signaling normally serves to limit corticostriatal activity and neurotransmitter release. Alternatively, reduced afferent activity or a mistargeting of presynaptic elements can sometimes evoke paradoxical increases in dendritic growth (Lund et al., 1991; McAllister et al., 1996; Tripodi et al., 2008). Such a scenario would require Met signaling to potentiate corticostriatal activity, perhaps during earlier developmental periods when pre- and postsynaptic elements are establishing initial contact (McAllister, 2000). Presynaptic roles for Met signaling are similarly difficult to predict from changes in Emx1^{Cre}/Met$^{fx/fx}$ MSN dendritic spine morphology. Larger spine heads predict stronger synapses (Schikorski and Stevens, 1997; Murthy et al., 2001), which could have been sculpted by modest increases in corticostriatal afferent activity and trophic support in Emx1^{Cre}/Met$^{fx/fx}$ mice. Alternatively, increased spine size may reflect a homeostatic scaling up of Emx1^{Cre}/Met$^{fx/fx}$ MSN excitability in response to decreased excitatory drive from corticostriatal afferents. Complimentary morphometric and electrophysiological studies of corticostriatal connectivity in the Emx1^{Cre}/Met$^{fx/fx}$ mouse are ongoing, and will clarify Met signaling roles in axonal and presynaptic development.

The distinct laminar- and compartment-specific changes expressed by ACC pyramidal neurons following disruption of Met signaling suggest circuit-level influences on dendritic growth. Because cortical afferents, efferents and intrinsic neurons express Met, however, distinguishing between cell-autonomous and presynaptically-driven effects of Met signaling will be challenging. There is additional complexity concerning these mechanisms in cortical neurons. For instance, it is known that other growth factor

receptors (McAllister et al., 1997) and distinct intracellular signaling pathways (Chow et al., 2009) can either promote or inhibit pyramidal dendritic growth in a layer- and/or compartment-specific manner. In addition, Met-expressing, corticocortically projecting afferents likely target different dendritic compartments within each ACC pyramidal neuron, depending on the radial position of its cell body within the cortex (Petreanu et al., 2009). That stated, reductions in tissue volume occupied by $Emx1^{Cre}/Met^{fx/fx}$ ACC apical arbors are most consistent with cell-autonomous effects of attenuated Met signaling on pyramidal dendritic growth as defined *in vitro* (Gutierrez et al., 2004). In contrast, the phenotypes of ACC basal pyramidal and MSN dendrites are similar to each other in $Emx1^{Cre}/Met^{fx/fx}$ mice, consistent with cell-nonautonomous influences.

Implications of $Emx1^{Cre}/Met^{fx/fx}$ dendrite and dendritic spine phenotypes for cellular and circuit function

The dendritic phenotypes of the $Emx1^{Cre}/Met^{fx/fx}$ neurons offer insight regarding the effects of Met signaling disruptions at the single cell- and circuit-levels. Rightward shifted frequency distributions of dendritic spine head diameter were observed for both ACC pyramidal and striatal MSN dendrites, indicating a gain of large, stable spines at the expense of thinner, more labile varieties. This is consistent with a possible impact on neuronal plasticity. Increases in dendritic spine size accompany the induction of long-term potentiation (LTP) (Engert and Bonhoeffer, 1999; Park et al., 2006; Roberts et al., 2009). In $Emx1^{Cre}/Met^{fx/fx}$ neurons, in which spine size is already shifted toward maximal levels, there may be a reduced potential to induce, or further increase, LTP. In fact, this is consistent with preliminary findings in hippocampal slices from

$Emx1^{Cre}/Met^{fx/fx}$ mice in which the induction and sustainability of LTP is reduced (S. Qiu and P. Levitt, unpublished observations).

Developmentally, Met expression begins to decline during the second postnatal week (Judson et al., 2009), coinciding with changes in presynaptic release probability (Bolshakov and Siegelbaum, 1995; Chavis and Westbrook, 2001) and postsynaptic excitability (Sheng et al., 1994; Petralia et al., 1999; Elias et al., 2008). This raises the possibility that Met signals to maintain developing synapses in an immature, labile state and that the ablation of Met signaling in $Emx1^{Cre}/Met^{fx/fx}$ mice might result in a precocious maturation of synaptic connections- a postulate tentatively supported by our observation of modestly increased spine head diameters in the dendrites of P40 $Emx1^{Cre}/Met^{fx/fx}$ neurons. An early onset of robust LTP induction (Harris and Teyler, 1984; Muller et al., 1989), premature gains in postsynaptic density size and thickness (Welch et al., 2007; Hung et al., 2008; Roberts et al., 2009), and shifts in NMDAR subunit composition (Sheng et al., 1994; Flint et al., 1997; Roberts et al., 2009) constitute logical phenotypic predictions for these mice if they indeed mature precociously. Of course, considering the potential for Met to signal in both postsynaptic and presynaptic compartments, these hypotheses will be addressed best by electrophysiological and biochemical studies of corticocortical as well as corticostriatal synapses.

The approximate 20% reduction in $Emx1^{Cre}/Met^{fx/fx}$ ACC pyramidal dendritic arbor volume indicates potentially significant alterations in information processing at the circuit-level. This reduction was due to decreases in dendritic length at approximately 150-175 μM in radial distance from the cell body, changes that were restricted to the apical arbor. Importantly, in layer 5 $Emx1^{Cre}/Met^{fx/fx}$ ACC pyramidal neurons, this

phenotype is explained entirely by shorter oblique apical branches, because the apical dendrite of these neurons was always transected before the bifurcation node and apical tuft. This change could be functionally significant for several reasons. For example, topographical mapping of inputs to layer 5 neurons in somatosensory cortex suggests that oblique branches of the apical arbor are an important convergence point of ascending thalamic and descending cortical information (Petreanu et al., 2009). In addition, in general terms, a loss of distal relative to proximal dendritic length should restrict the cortical territory sampled by a pyramidal neuron, which could limit the integration of information across the tangential domain. This functional consequence would be most relevant to the apical dendritic tuft, which receives highly convergent inputs from both the cortex (Kuhn et al., 2008; Petreanu et al., 2009) and the thalamus (Jones, 2002; Rubio-Garrido et al., 2009) that facilitate attention and associative processing.

Contrary to ACC pyramidal neurons, striatal MSNs exhibited an approximate 25% increase in dendrite arbor volume in $Emx1^{Cre}/Met^{fx/fx}$ mice, implying that they are capable of receiving more broadly distributed striatal afferents. Considering the patch-matrix compartmental organization of the striatum, this change could affect the quality of discrete information processing. MSN dendritic arbors are largely confined to the compartment of their cell body of origin (Gerfen, 1992), so without concomitant decreases in striatal cell density, the larger arbors of $Emx1^{Cre}/Met^{fx/fx}$ MSNs would be expected to extend beyond their compartmental boundaries. This might result in an atypical mixing of afferent sensorimotor and limbic information that usually is routed through the matrix and patch compartments, respectively (Gerfen, 1992).

Relevance of Met signaling disruptions to circuit vulnerability in ASD

Neurobiological hypotheses of ASD pathophysiology propose that forebrain connectivity is altered fundamentally, impacting the quality of simple and complex information processing (Frith, 2004; Geschwind and Levitt, 2007; Levy, 2007). These concepts have emerged primarily from anatomical and functional studies demonstrating the potential for, or examples of, local hyper-connectivity and global hypo-connectivity in forebrain circuits. For example, functional magnetic resonance imaging during either face processing or sentence comprehension tasks revealed reduced prefrontal activation relative to other cortical areas in the brains of individuals with autism (Just et al., 2004; Koshino et al., 2008). More recent magnetoencephalographic analyses of high-functioning children with ASD showed enhanced parietal lobe synchrony and decreased prefrontal lobe synchrony relative to typically developing children during the performance of tasks probing executive function (Perez Velazquez et al., 2009). Collectively, these and other studies indicate that long-range circuits between the neocortex and other brain regions are functionally disconnected. Evidence for local circuit abnormalities in ASD has come from post mortem anatomical studies, which show minicolumns to be narrower and more numerous in several cortical areas from subjects with ASD (Casanova et al., 2002). Interestingly, a bias toward an increased spread in local activation has been predicted from this pathological feature (Casanova, 2006).

Here, we present evidence that the mouse homologue of the ASD-associated *MET* gene can impact the development of both local and long-range forebrain circuits, consistent with connectivity-based theories of the disorder. Importantly, we wish to emphasize that the constitutive deletion in mice does not phenocopy the human clinical

findings of altered transcriptional regulation of *MET* due to the ASD-associated allele (Campbell et al., 2006). Thus, the moderate circuit-level phenotypes in the $Emx1^{Cre}/Met^{fx/fx}$ forebrain may be even less pronounced in the heterozygous condition, which is probably more relevant to ASD etiology. We suggest that even mild disruptions in Met signaling may render select forebrain circuits vulnerable to further genetic and environmental insults that would otherwise more broadly impact connectivity (Campbell et al., 2008; Bill and Geschwind, 2009; Judson et al., 2009). Behavioral analyses of $Emx1^{Cre}/Met^{fx/+}$ mice in compound genetic and/or environmental models of forebrain circuit disruption will constitute a useful, further test of this hypothesis. Additionally, mapping the expression of MET during the development of the human and nonhuman primate forebrain may promote a further understanding of the specific circuits that are vulnerable in ASD.

Other Acknowledgements

We thank Deborah Gregory, Donte Smith, and Kate Spencer for excellent assistance in maintaining the mouse colony and genotyping. We also thank Drs. Inmaculada Ballesteros-Yanez and Ariel Deutch for the generous introduction to the Lucifer Yellow injection technique and use of the Imaris software, respectively.

Literature Cited

Bill BR, Geschwind DH. 2009. Genetic advances in autism: heterogeneity and convergence on shared pathways. Curr Opin Genet Dev 19(3):271-278.

Bolshakov VY, Siegelbaum SA. 1995. Regulation of hippocampal transmitter release during development and long-term potentiation. Science 269(5231):1730-1734.

Campbell DB, D'Oronzio R, Garbett K, Ebert PJ, Mirnics K, Levitt P, Persico AM. 2007. Disruption of cerebral cortex MET signaling in autism spectrum disorder. Ann Neurol 62(3):243-250.

Campbell DB, Li C, Sutcliffe JS, Persico AM, Levitt P. 2008. Genetic evidence implicating multiple genes in the MET receptor tyrosine kinase pathway in autism spectrum disorder. Autism Research 1:159-168.

Campbell DB, Sutcliffe JS, Ebert PJ, Militerni R, Bravaccio C, Trillo S, Elia M, Schneider C, Melmed R, Sacco R, Persico AM, Levitt P. 2006. A genetic variant that disrupts MET transcription is associated with autism. Proc Natl Acad Sci U S A 103(45):16834-16839.

Campbell DB, Warren D, Sutcliffe JS, Lee EB, Levitt P. 2009. Association of MET with social and communication phenotypes in individuals with autism spectrum disorder. Am J Med Genet B Neuropsychiatr Genet.

Casanova MF. 2006. Neuropathological and genetic findings in autism: the significance of a putative minicolumnopathy. Neuroscientist 12(5):435-441.

Casanova MF, Buxhoeveden DP, Switala AE, Roy E. 2002. Minicolumnar pathology in autism. Neurology 58(3):428-432.

Caton A, Hacker A, Naeem A, Livet J, Maina F, Bladt F, Klein R, Birchmeier C, Guthrie S. 2000. The branchial arches and HGF are growth-promoting and chemoattractant for cranial motor axons. Development (Cambridge, England) 127(8):1751-1766.

Chavis P, Westbrook G. 2001. Integrins mediate functional pre- and postsynaptic maturation at a hippocampal synapse. Nature 411(6835):317-321.

Chow DK, Groszer M, Pribadi M, Machniki M, Carmichael ST, Liu X, Trachtenberg JT. 2009. Laminar and compartmental regulation of dendritic growth in mature cortex. Nat Neurosci 12(2):116-118.

David MD, Yeramian A, Dunach M, Llovera M, Canti C, de Herreros AG, Comella JX, Herreros J. 2008. Signalling by neurotrophins and hepatocyte growth factor regulates axon morphogenesis by differential beta-catenin phosphorylation. J Cell Sci 121(Pt 16):2718-2730.

Dierssen M, Benavides-Piccione R, Martinez-Cue C, Estivill X, Florez J, Elston GN, DeFelipe J. 2003. Alterations of neocortical pyramidal cell phenotype in the Ts65Dn mouse model of Down syndrome: effects of environmental enrichment. Cereb Cortex 13(7):758-764.

Ebens A, Brose K, Leonardo ED, Hanson MG, Jr., Bladt F, Birchmeier C, Barres BA, Tessier-Lavigne M. 1996. Hepatocyte growth factor/scatter factor is an axonal chemoattractant and a neurotrophic factor for spinal motor neurons. Neuron 17(6):1157-1172.

Elias GM, Elias LA, Apostolides PF, Kriegstein AR, Nicoll RA. 2008. Differential trafficking of AMPA and NMDA receptors by SAP102 and PSD-95 underlies synapse development. Proc Natl Acad Sci U S A 105(52):20953-20958.

Engert F, Bonhoeffer T. 1999. Dendritic spine changes associated with hippocampal long-term synaptic plasticity. Nature 399(6731):66-70.

Flint AC, Maisch US, Weishaupt JH, Kriegstein AR, Monyer H. 1997. NR2A subunit expression shortens NMDA receptor synaptic currents in developing neocortex. J Neurosci 17(7):2469-2476.

Frith C. 2004. Is autism a disconnection disorder? Lancet Neurol 3(10):577.
Garzotto D, Giacobini P, Crepaldi T, Fasolo A, De Marchis S. 2008. Hepatocyte growth factor regulates migration of olfactory interneuron precursors in the rostral migratory stream through Met-Grb2 coupling. J Neurosci 28(23):5901-5909.
Gelfo F, De Bartolo P, Giovine A, Petrosini L, Leggio MG. 2009. Layer and regional effects of environmental enrichment on the pyramidal neuron morphology of the rat. Neurobiol Learn Mem 91(4):353-365.
Gerfen CR. 1992. The neostriatal mosaic: multiple levels of compartmental organization. Trends Neurosci 15(4):133-139.
Geschwind DH, Levitt P. 2007. Autism spectrum disorders: developmental disconnection syndromes. Curr Opin Neurobiol 17(1):103-111.
Giacobini P, Messina A, Wray S, Giampietro C, Crepaldi T, Carmeliet P, Fasolo A. 2007. Hepatocyte growth factor acts as a motogen and guidance signal for gonadotropin hormone-releasing hormone-1 neuronal migration. J Neurosci 27(2):431-445.
Gutierrez H, Dolcet X, Tolcos M, Davies A. 2004. HGF regulates the development of cortical pyramidal dendrites. Development (Cambridge, England) 131(15):3717-3726.
Hamanoue M, Takemoto N, Matsumoto K, Nakamura T, Nakajima K, Kohsaka S. 1996. Neurotrophic effect of hepatocyte growth factor on central nervous system neurons in vitro. Journal of neuroscience research 43(5):554-564.
Harris KM, Teyler TJ. 1984. Developmental onset of long-term potentiation in area CA1 of the rat hippocampus. J Physiol 346:27-48.
Huh CG, Factor VM, Sanchez A, Uchida K, Conner EA, Thorgeirsson SS. 2004. Hepatocyte growth factor/c-met signaling pathway is required for efficient liver regeneration and repair. Proc Natl Acad Sci U S A 101(13):4477-4482.
Hung AY, Futai K, Sala C, Valtschanoff JG, Ryu J, Woodworth MA, Kidd FL, Sung CC, Miyakawa T, Bear MF, Weinberg RJ, Sheng M. 2008. Smaller dendritic spines, weaker synaptic transmission, but enhanced spatial learning in mice lacking Shank1. J Neurosci 28(7):1697-1708.
Ieraci A, Forni PE, Ponzetto C. 2002. Viable hypomorphic signaling mutant of the Met receptor reveals a role for hepatocyte growth factor in postnatal cerebellar development. Proc Natl Acad Sci U S A 99(23):15200-15205.
Jackson PB, Boccuto L, Skinner C, Collins JS, Neri G, Gurrieri F, Schwartz CE. 2009. Further evidence that the rs1858830 C variant in the promoter region of the MET gene is associated with autistic disorder. Autism Res 2(4):232-236.
Jones EG. 2002. Thalamic circuitry and thalamocortical synchrony. Philos Trans R Soc Lond B Biol Sci 357(1428):1659-1673.
Judson MC, Bergman MY, Campbell DB, Eagleson KL, Levitt P. 2009. Dynamic gene and protein expression patterns of the autism-associated met receptor tyrosine kinase in the developing mouse forebrain. J Comp Neurol 513(5):511-531.
Just MA, Cherkassky VL, Keller TA, Minshew NJ. 2004. Cortical activation and synchronization during sentence comprehension in high-functioning autism: evidence of underconnectivity. Brain 127(Pt 8):1811-1821.
Kenward MG, Roger JH. 1997. Small sample inference for fixed effects from restricted maximum likelihood. Biometrics 53(3):983-997.

Koshino H, Kana RK, Keller TA, Cherkassky VL, Minshew NJ, Just MA. 2008. fMRI investigation of working memory for faces in autism: visual coding and underconnectivity with frontal areas. Cereb Cortex 18(2):289-300.
Kuhn B, Denk W, Bruno RM. 2008. In vivo two-photon voltage-sensitive dye imaging reveals top-down control of cortical layers 1 and 2 during wakefulness. Proc Natl Acad Sci U S A 105(21):7588-7593.
Levy F. 2007. Theories of autism. Aust N Z J Psychiatry 41(11):859-868.
Lim CS, Walikonis RS. 2008. Hepatocyte growth factor and c-Met promote dendritic maturation during hippocampal neuron differentiation via the Akt pathway. Cell Signal 20(5):825-835.
Lund JS, Holbach SM, Chung WW. 1991. Postnatal development of thalamic recipient neurons in the monkey striate cortex: II. Influence of afferent driving on spine acquisition and dendritic growth of layer 4C spiny stellate neurons. J Comp Neurol 309(1):129-140.
Madhavan R, Peng HB. 2006. HGF induction of postsynaptic specializations at the neuromuscular junction. J Neurobiol 66(2):134-147.
McAllister AK. 2000. Cellular and molecular mechanisms of dendrite growth. Cereb Cortex 10(10):963-973.
McAllister AK, Katz LC, Lo DC. 1996. Neurotrophin regulation of cortical dendritic growth requires activity. Neuron 17(6):1057-1064.
McAllister AK, Katz LC, Lo DC. 1997. Opposing roles for endogenous BDNF and NT-3 in regulating cortical dendritic growth. Neuron 18(5):767-778.
Muller D, Oliver M, Lynch G. 1989. Developmental changes in synaptic properties in hippocampus of neonatal rats. Brain Res Dev Brain Res 49(1):105-114.
Murthy VN, Schikorski T, Stevens CF, Zhu Y. 2001. Inactivity produces increases in neurotransmitter release and synapse size. Neuron 32(4):673-682.
Nakano M, Takagi N, Takagi K, Funakoshi H, Matsumoto K, Nakamura T, Takeo S. 2007. Hepatocyte growth factor promotes the number of PSD-95 clusters in young hippocampal neurons. Exp Neurol 207(2):195-202.
Park M, Salgado JM, Ostroff L, Helton TD, Robinson CG, Harris KM, Ehlers MD. 2006. Plasticity-induced growth of dendritic spines by exocytic trafficking from recycling endosomes. Neuron 52(5):817-830.
Perez Velazquez JL, Barcelo F, Hung Y, Leshchenko Y, Nenadovic V, Belkas J, Raghavan V, Brian J, Garcia Dominguez L. 2009. Decreased brain coordinated activity in autism spectrum disorders during executive tasks: reduced long-range synchronization in the fronto-parietal networks. Int J Psychophysiol 73(3):341-349.
Petralia RS, Esteban JA, Wang YX, Partridge JG, Zhao HM, Wenthold RJ, Malinow R. 1999. Selective acquisition of AMPA receptors over postnatal development suggests a molecular basis for silent synapses. Nat Neurosci 2(1):31-36.
Petreanu L, Mao T, Sternson SM, Svoboda K. 2009. The subcellular organization of neocortical excitatory connections. Nature 457(7233):1142-1145.
Powell EM, Muhlfriedel S, Bolz J, Levitt P. 2003. Differential regulation of thalamic and cortical axonal growth by hepatocyte growth factor/scatter factor. Dev Neurosci 25(2-4):197-206.

Roberts AC, Diez-Garcia J, Rodriguiz RM, Lopez IP, Lujan R, Martinez-Turrillas R, Pico E, Henson MA, Bernardo DR, Jarrett TM, Clendeninn DJ, Lopez-Mascaraque L, Feng G, Lo DC, Wesseling JF, Wetsel WC, Philpot BD, Perez-Otano I. 2009. Downregulation of NR3A-containing NMDARs is required for synapse maturation and memory consolidation. Neuron 63(3):342-356.

Rosario M, Birchmeier W. 2003. How to make tubes: signaling by the Met receptor tyrosine kinase. Trends Cell Biol 13(6):328-335.

Rubio-Garrido P, Perez-de-Manzo F, Porrero C, Galazo MJ, Clasca F. 2009. Thalamic input to distal apical dendrites in neocortical layer 1 is massive and highly convergent. Cereb Cortex 19(10):2380-2395.

Russell FA, Moore DR. 1999. Effects of unilateral cochlear removal on dendrites in the gerbil medial superior olivary nucleus. Eur J Neurosci 11(4):1379-1390.

Schikorski T, Stevens CF. 1997. Quantitative ultrastructural analysis of hippocampal excitatory synapses. J Neurosci 17(15):5858-5867.

Shen H, Sesack SR, Toda S, Kalivas PW. 2008. Automated quantification of dendritic spine density and spine head diameter in medium spiny neurons of the nucleus accumbens. Brain Struct Funct 213(1-2):149-157.

Sheng M, Cummings J, Roldan LA, Jan YN, Jan LY. 1994. Changing subunit composition of heteromeric NMDA receptors during development of rat cortex. Nature 368(6467):144-147.

Sholl DA. 1953. Dendritic organization in the neurons of the visual and motor cortices of the cat. J Anat 87(4):387-406.

Sorensen SA, Rubel EW. 2006. The level and integrity of synaptic input regulates dendrite structure. J Neurosci 26(5):1539-1550.

Sousa I, Clark TG, Toma C, Kobayashi K, Choma M, Holt R, Sykes NH, Lamb JA, Bailey AJ, Battaglia A, Maestrini E, Monaco AP. 2009. MET and autism susceptibility: family and case-control studies. Eur J Hum Genet 17(6):749-758.

Tripodi M, Evers JF, Mauss A, Bate M, Landgraf M. 2008. Structural homeostasis: compensatory adjustments of dendritic arbor geometry in response to variations of synaptic input. PLoS Biol 6(10):e260.

Tyndall SJ, Patel SJ, Walikonis RS. 2007. Hepatocyte growth factor-induced enhancement of dendritic branching is blocked by inhibitors of N-methyl-D-aspartate receptors and calcium/calmodulin-dependent kinases. Journal of neuroscience research 85(11):2343-2351.

Tyndall SJ, Walikonis RS. 2006. The receptor tyrosine kinase Met and its ligand hepatocyte growth factor are clustered at excitatory synapses and can enhance clustering of synaptic proteins. Cell Cycle 5(14):1560-1568.

Welch JM, Lu J, Rodriguiz RM, Trotta NC, Peca J, Ding JD, Feliciano C, Chen M, Adams JP, Luo J, Dudek SM, Weinberg RJ, Calakos N, Wetsel WC, Feng G. 2007. Cortico-striatal synaptic defects and OCD-like behaviours in Sapap3-mutant mice. Nature 448(7156):894-900.

Zhang YW, Vande Woude GF. 2003. HGF/SF-met signaling in the control of branching morphogenesis and invasion. J Cell Biochem 88(2):408-417.

CHAPTER V

FUTURE DIRECTIONS

Following strong leads provided by human genetic studies of autism spectrum disorders (ASD), the overarching goal of this research project was to clarify the relationship of MET receptor tyrosine kinase function to the development of forebrain circuits which govern socioemotional dimensions of behavior. On two distinct fronts, our developmental Met/MET expression mapping studies in the mouse and nonhuman primate macaque forebrain (Judson et al., 2009; M. Judson, K. Eagleson, D. Amaral, P. Levitt, unpublished observations) provided the first real progress toward this end: 1) in both species, the temporal and subcellular profiles of expression were highly consistent with a preferential role for this pleiotropic receptor in axon outgrowth, collateralization and otherwise presynaptically-derived elements of circuit wiring, and 2) spatial patterns of Met/MET expression during forebrain development overlapped circuits involved in species-appropriate social behavior. Together, these findings support the idea that this receptor plays an evolutionarily conserved role in wiring socioemotionally-relevant forebrain circuits. They are also consistent with the recent human genetic finding that the rs1858830-C allele variant of the *MET* promoter exhibits an enriched association with social and communication phenotypes of ASD (Campbell et al., 2009).

Functional *in vitro* studies indicate that the rs1858830-C allele, as opposed to the ASD-protective rs1858830-G allele, reduces transcriptional efficiency from the *MET*

promoter (Campbell et al., 2006), which is consistent with the finding of 2-fold reductions in neocortical MET protein expression in postmortem ASD cases. Therefore, our studies of dendritic morphology in mice with forebrain-specific Met signaling deficiency may provide insight into the etiology of MET-associated cases of ASD. For example, through these studies, we revealed firm evidence that Met signaling influences both local and long-range circuit development through axonal, presynaptically-derived mechanisms (M. Judson, K. Eagleson, P. Levitt, unpublished observations). This finding relates to the local and global information processing deficits that characterize ASD (Frith, 2004; Levy, 2007; Levitt and Geschwind, 2007).

These considerable gains in relating the neurodevelopmental function of Met/MET signaling to the wiring of socially-relevant circuits have led to two immediate questions of further interest at the cellular and molecular levels: 1) Considering that this receptor may be expressed in both the axonal and dendritic compartments of forebrain projection neurons, are there cell-nonautonomous (i.e., axonal) as well as cell autonomous (i.e., dendritic) consequences of Met/MET signaling disruption for the development of forebrain circuit architecture?, and 2) how does the Met/MET receptor signal to regulate aspects of forebrain circuit wiring?

Strategies to distinguish cell-autonomous versus cell-nonautonomous influences of Met signaling during forebrain circuit development

A multitude of in vitro studies have implicated murine Met signaling in both axonal (Ebens et al., 1996; Powell et al., 2003; David et al., 2008) and dendritic (Gutierrez et al., 2004; Tyndall et al., 2007; Lim and Walikonis, 2008) development or growth, and evidence that this receptor is localized to both axonal and dendritic

compartments *in vivo* has recently emerged (Tyndall and Walikonis, 2006; Judson et al., 2009). Therefore, attributing cellular phenotypes to the influence of Met signaling in one neuronal compartment or the other is an unavoidable challenge- especially within an intact circuit where presynaptic and postsynaptic elements influence each other throughout development. We recently encountered this obstacle in our studies of dendritic morphology in the $Emx1^{cre}/Met^{fx/fx}$ mouse, a model of developmental, forebrain-specific Met signaling disruption.

In $Emx1^{cre}/Met^{fx/fx}$ mouse, we could reliably determine if alterations in dendritic structure were of a presynaptically-derived, cell-nonautonomous origin if they occurred in cell populations such as striatal medium spiny neurons, which do not express Met but receive Met-expressing axonal afferents during development (M. Judson, K. Eagleson, P. Levitt, unpublished observations). Conversely, pyramidal neurons of the anterior cingulate cortex (ACC) express Met and are contacted extensively by Met-expressing corticocortically projecting axons throughout the early postnatal period. Thus, it was impossible to determine if the dendritic phenotypes that we observed in $Emx1^{cre}/Met^{fx/fx}$ ACC pyramidal neurons were due to cell autonomous and/or cell-nonautonomous effects of disrupted Met signaling. Further confusing the issue is the fact that we observed both layer- and compartment-specific changes in the dendritic morphology of this pyramidal cell population in $Emx1^{cre}/Met^{fx/fx}$ mice (M. Judson, K. Eagleson, P. Levitt, unpublished observations).

Neurobiological precedent dictates that both cell-autonomous and cell-nonautonomous effects of developmental Met signaling disruption could contribute to the layer- and compartment-specific changes in dendritic morphology that we observe in

Emx1^{cre}/Met$^{fx/fx}$ ACC pyramidal neurons. First, cell-autonomous dendritic growth in layer 5 and layer 2/3 ACC pyramidal neurons may be differentially regulated by Met signaling, perhaps due to unique subcellular distributions of the receptor and its signaling partners. Consistent with this, McAllister and colleagues previously demonstrated that neurotrophin receptor signaling influences the dendritic growth of pyramidal neurons differentially in layers 4 and 6 of the developing visual cortex (McAllister et al., 1997). Also, forebrain-specific deletion of the gene encoding the signaling phosphatase PTEN results in a dramatic induction of dendritic growth that is restricted to the apical compartment of layer 2/3, but not layer 5, pyramidal neurons (Chow et al., 2009). Second, attenuated Met signaling within axonal compartments may compromise presynaptic integrity and induce compensatory changes in dendritic development that, within the ACC, reflect layer- and compartment-specific projection topographies of Met-expressing cortico-cortical afferents (Petreanu et al., 2009).

Advances in technology that allow for subcellular, compartment-specific manipulations of Met signaling will prove invaluable in dissecting these complex phenotypes within intact circuits. In the meantime, cell autonomous effects could be specifically dissected with the use of genetic approaches such as SLICK (Single-neuron Labeling with Inducible Cre-mediated Knockout) (Young et al., 2008) and MADM (Mosaic Analysis with Double Markers) (Zong et al., 2005) to disrupt Met signaling in just a few neurons within a typically developing cortical milieu. Conversely, a lentiviral-mediated mosaic rescue of Met signaling within select pyramidal cells of the Emx1^{cre}/Met$^{fx/fx}$ cortex could further our understanding of circuit-level, cell-nonautonomous influences of Met signaling on the development of pyramidal cell

dendritic morphology. Finally, it will be essential to directly determine the nature of aberrant axonal development in $Emx1^{cre}/Met^{fx/fx}$ forebrain. Considering the layer- and compartment-specific dendritic phenotypes of $Emx1^{cre}/Met^{fx/fx}$ ACC pyramidal neurons, determining whether the corticocortical afferents therein conform to typical compartmental and topographical input patterns is of the utmost importance. Subcellular channelrhodopsin-2 (ChR2)-assisted circuit mapping (Petreanu et al., 2007; Petreanu et al., 2009) is a cutting-edge technique that is suited to compare the topographies of local circuit connections made by long-projecting corticocortical axons in wild type and $Emx1^{cre}/Met^{fx/fx}$ mice.

Elucidating molecular mechanisms of Met signaling during forebrain circuit development

From the simple observation that Met is an extremely pleiotropic signaling molecule it can be inferred that this receptor is capable of engaging a variety downstream signaling pathways upon binding its constitutive endogenous ligand, hepatocyte growth factor (HGF). The specific pathways that are engaged as well as the amplitude and kinetics of the downstream signaling are likely to dictate the specific developmental response that HGF/Met signaling will mediate in a given context. For example, HGF/Met-mediated enhancement of nasopharyngeal cancer cell invasiveness has been shown to depend on downstream activation of the PI3K and JNK pathways but not the erk 1/2 or p38 MAPK pathways (Zhou et al., 2008), whereas the migration of rat mammary fibroblasts in response to HGF stimulation is dependent on the mutual activation of both the erk 1/2 and PI3K pathways (Delehedde et al., 2001). How an activated Met receptor engages one downstream signaling cascade versus another is an

important mechanistic question concerning any developmental process in which Met signaling plays a part.

What signaling pathways are engaged downstream of HGF/Met signaling in the context of forebrain circuit development? To our knowledge, this question had yet to be

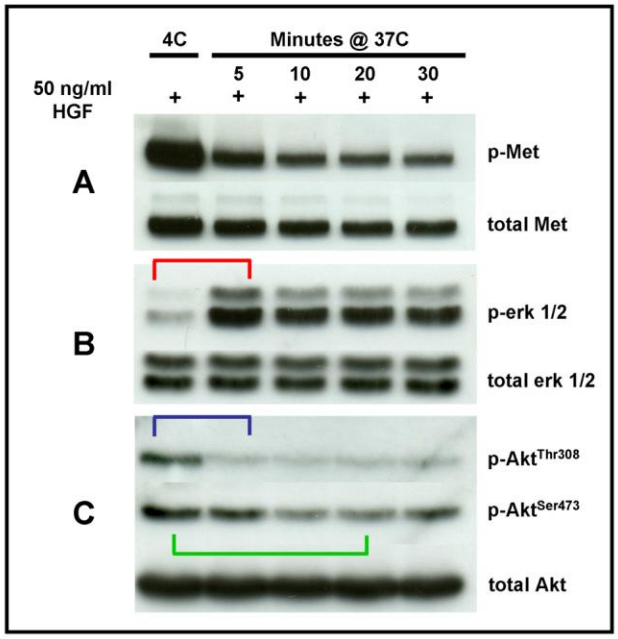

Figure 1. HGF stimulation of Met signaling *ex vivo*. Immunoblotting for Met and relevant Met signaling pathway proteins in lysates prepared from P7 wild type mouse cortical synaptosomes that were treated with 50 ng/ml HGF at sub-physiologic (4C) or physiologic temperature (37C) for periods of variable duration. **A:** Immunoblotting for phosphorylated (p-Met) and total Met receptor indicates that robust receptor phosphorylation occurs even at sub-physiologic temperature. Progressively decreased levels of total Met and especially p-Met are observed as the duration of HGF stimulation at physiologic temperature increases, consistent with energy-dependent mechanisms of receptor desensitization. **B:** Immunoblotting for phosphorylated erk 1/2 (p-erk 1/2) demonstrates that HGF stimulation of Met for as little as 5 minutes at 37C results in a dramatic increase in MAPK pathway signaling as compared to sub-physiologic baseline (see red bracket). MAPK signaling is only slightly attenuated over time as shown out to 30 minutes at 37C. C: Immunoblotting for phosphorylated Akt (p-Akt^{Thr308} and p-Akt^{Ser473}) demonstrates a surprising decrease in PI3K pathway stimulation downstream of HGF-stimulated Met receptor activation. Note that the levels of p-Akt^{Thr308} seem to decrease much more rapidly (blue bracket) than the levels of p-Akt^{Ser473} (green bracket).

addressed by any study employing native forebrain tissues. Therefore, we recently developed an *ex vivo* system to evaluate Met signaling in suspensions of crude synaptosomes prepared from postnatal day (P) 7 mouse neocortex subsequent to stimulation with physiologic concentrations of HGF (i.e., 50 ng/ml) (**see Chapter IV Materials and Methods for protocol details**). Using this system, we discovered two surprising features of HGF-stimulated Met signaling, which may be relevant to forebrain circuit wiring *in vivo*: 1) though downstream signaling is only engaged at physiologic temperature, Met receptor phosphorylation occurs robustly in the presence of HGF, even at sub-physiologic temperature (**Fig. 1A**), and 2) Met signals downstream to robustly potentiate the MAPK pathway but inhibit the PI3K pathway subsequent to HGF stimulation as evidenced by immunoblotting for phosphorylated erk 1/2 (**Fig. 1B**) and Akt proteins (**Fig. 1C**), respectively. We hypothesize that this opposing influence of Met signaling on downstream MAPK and PI3K pathway activation, which, to our knowledge, is a phenomenon unique to the Met receptor in this specific context, results from interactions with specific co-receptors and signaling adaptor proteins. Below, briefly outline and discuss a tandem immunoprecipitation/mass spectrometry approach designed to determine the identity of interacting proteins that facilitate the role of Met in forebrain circuit wiring.

Though conceptually straightforward, tandem immunoprecipitation/mass spectrometry experiments are technically challenging, and whether or not they are successful largely depends on the development of an optimized immunoprecipitation protocol and the availability of appropriate negative controls. Using a paramagnetic bead-based approach (**see Chapter IV Materials and Methods for protocol details**),

which is schematized in **Figure 2**, we have optimized an immunoprecipitation protocol that is suitable for purifying Met and associated proteins from native forebrain lysates. Moreover, the monoclonal Met antibody used in this protocol is capable of purifying HGF-stimulated, tyrosine-phosphoryalated forms of the Met receptor as well (**Fig. 3**), which will serve our ultimate goal of identifying the protein partners that facilitate Met signaling during forebrain circuit development.

However, the capacity to immunoprecipitate phosphorylated Met receptors alone will not ensure our success in purifying signaling partners of Met. Protein-protein interactions can be fleeting and of low affinity, especially when they pertain to signaling mechanisms with rapid on/off kinetics. Furthermore, even when immunoprecipitation conditions permit the co-purification of transient or weakly interacting proteins, at later steps in the process, such as washing (**Fig. 2, step 4**), the loss of these interactions may equate to the price of eliminating background. We plan to employ two general, non-mutually exclusive experimental strategies to maximize the chance of trapping weak or transient Met interactions with protein signaling partners. The first strategy requires that Met and phosphorylated Met be immunoprecipitated at multiple time-points subsequent to HGF-stimulation; increased experimental sampling should increase the chance of catching transient protein-protein interactions. The second strategy would incorporate the use of a chemical such as dithiobis-succinimidylpropionate to covalently cross-link Met to its directly and indirectly interacting signaling partners at pre-determined intervals following HGF-stimulation. This method succeeds in effectively cementing weak protein-protein interactions into place, and it has been used to identify weakly interacting TrkB signaling partners subsequent to stimulation with BDNF (Arevalo et al., 2004).

However, a potential pitfall of this approach is that cross-linking can change epitope structures and thus reduce or eliminate the affinity of the immunoprecipitation antibody for the target protein.

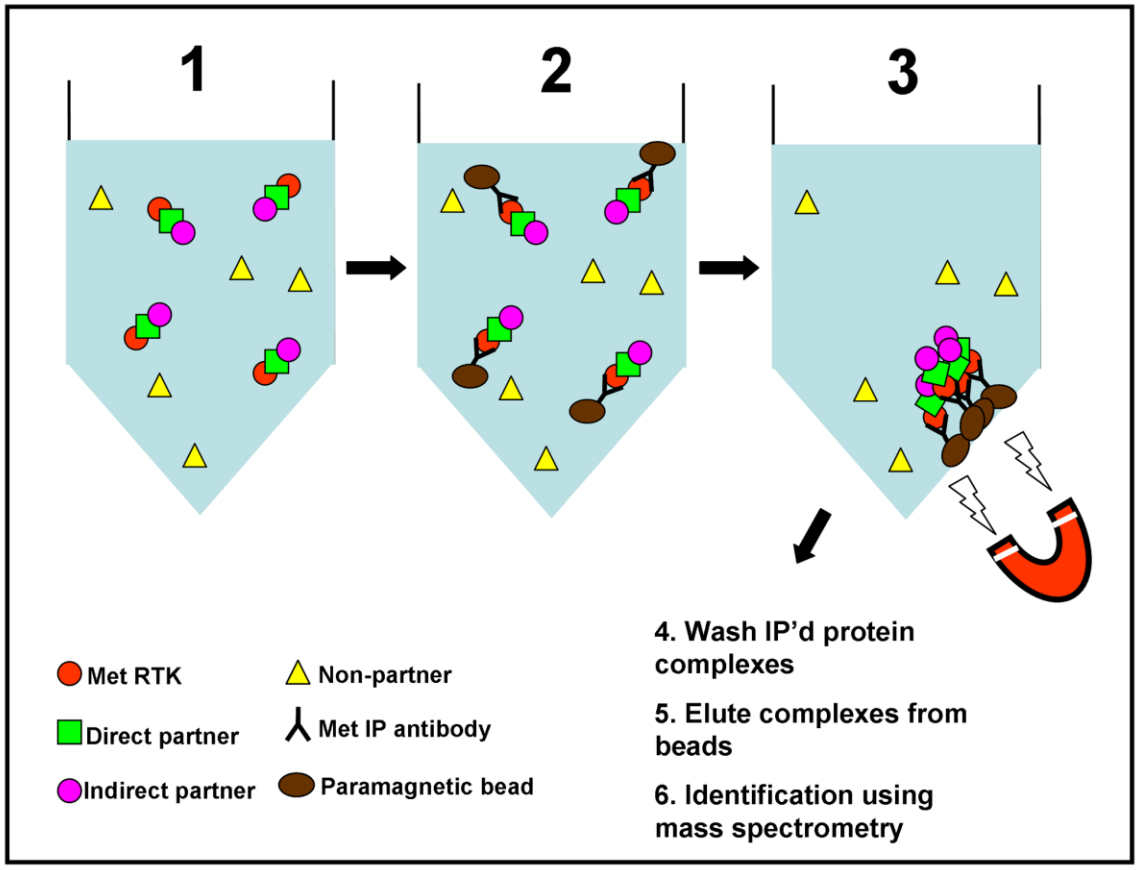

Figure 2. General Met immunoprecipitation approach. **Step1:** solubilized protein lysates are prepared from native forebrain tissues of interest. These include Met receptors (red circles), direct Met binding partner proteins (green squares), and indirect Met binding partner proteins (purple circles). All non-partner proteins are represented by yellow triangles. **Step 2:** Soluble Met protein complexes are made insoluble by the addition of high-affinity Met antibodies that have been covalently linked to insoluble paramagnetic beads. **Step 3:** The now insoluble Met protein complexes are precipitated out of solution by the application of a magnetic field. **Step 4:** The immunoprecipitated (IP'd) Met protein complexes are washed repeatedly to remove background, non-partner proteins. **Step 5:** Met protein complexes are removed from the beads, and thus resolubilized, in a reducing elution buffer. **Step 6:** Met partner proteins within the IP'd complexes can be identified via mass spectrometric analysis.

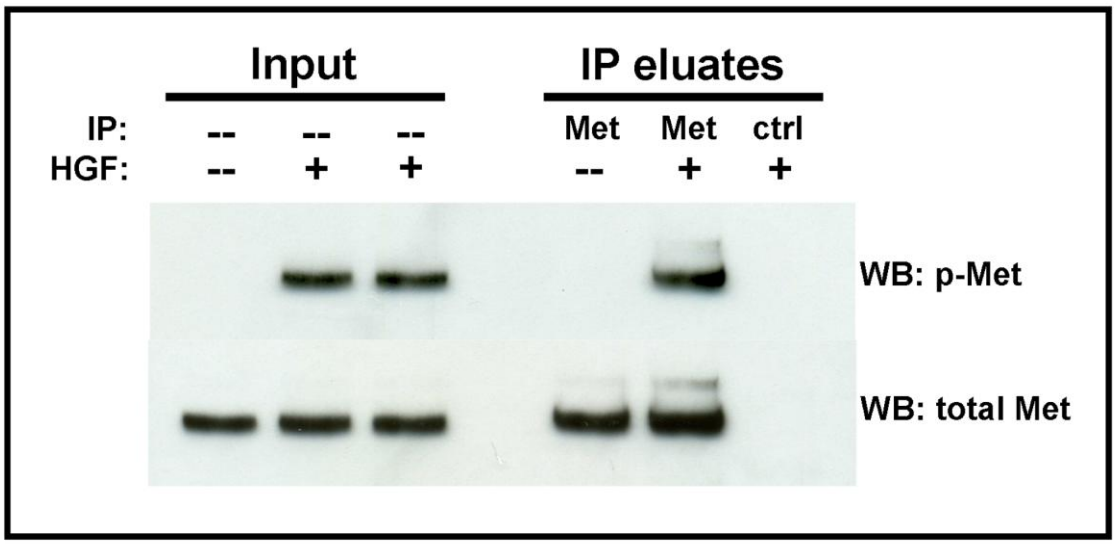

Figure 3. Immunoprecipitation of phosphorylated (p-Met) and total Met protein. Input lysates (left 3 lanes) were prepared from P7 wild type mouse cortical synaptosomes that were unstimulated (--, far left lane) or stimulated (+, right two lanes) with 50 ng/ml HGF for 5 minutes at 37C. As per immunoblotting, p-Met bands were only detected in the input lysates prepared from HGF-stimulated synaptosomes. Immunoprecipitation (IP) was performed using each of the 3 input lysate samples (right 3 lanes). As per immunoblotting, total Met protein was clearly detected in both Met IP (Met, left two lanes) samples, but p-Met was only detected in the Met IP sample prepared using HGF-stimulated input lysate (middle lane). No p-Met or Met was detected in the control (ctrl) IP sample prepared using HGF-stimulated input lysate (far right lane).

No amount of optimization will ever result in an immunoprecipitation protocol that allows for the perfect co-purification of a target protein and its interacting partners. Some amount of background protein will always co-elute with the protein complexes of interest, and, unfortunately, a mass spectrometer cannot tell the difference between them. Therefore, the implementation of appropriate negative controls is an important safeguard against excessive false-positive identifications of candidate partner proteins in any tandem immunoprecipitation/mass spectrometry approach. Succinctly, if the experimental and negative control immunoprecipitates are analyzed in the same mass spectrometer run, any identified proteins that they share in common can be eliminated from consideration as candidate partner proteins.

To reliably identify protein partners of the Met receptor in both signaling and non-signaling states, we plan to perform Met and control IgG antibody precipitations of lysates prepared from P7 wild type mouse cortical synaptosomes that have either been untreated or stimulated with HGF. Parallel mass spectrometric analyses comparing the control immunoprecipitates with either Met immunoprecipitation sample should allow for a broad identification of Met-specific protein partner candidates. Further comparisons between the unstimulated and HGF-stimulated Met immunoprecipitates may reveal protein interactions that are gained and/or lost subsequent to Met receptor activation. An even more sophisticated level of analysis would involve the mass spectrometric comparison of Met immunoprecipitates prepared from synaptosomes that have been HGF-treated at sub-physiologic versus physiologic temperatures. In the former condition, Met receptors are phosphorylated but apparently not engaging downstream signaling pathways (**Fig. 1A**), which could reflect an intermediate or incomplete recruitment of signaling adaptor proteins at this stage. A basic outline of our immunoprecipitation strategy to identify signaling Met signaling partners that are relevant to forebrain circuit development can be viewed in **Figure 4**. We have chosen to experiment initially with synaptosomes prepared from wild type P7 mouse cortex, primarily because Met is robustly expressed in cortical neuropil compartments during this early period of forebrain circuit wiring (Judson et al., 2009). Additionally, because the cortex is the largest forebrain structure, fewer animals will be required to satisfy these preliminary experimental aims. Pending the satisfactory identification of Met signaling partners within the P7 cortical neuropil, subsequent experiments will seek to determine if Met signaling complexes are differentially composed in forebrain structures such as the

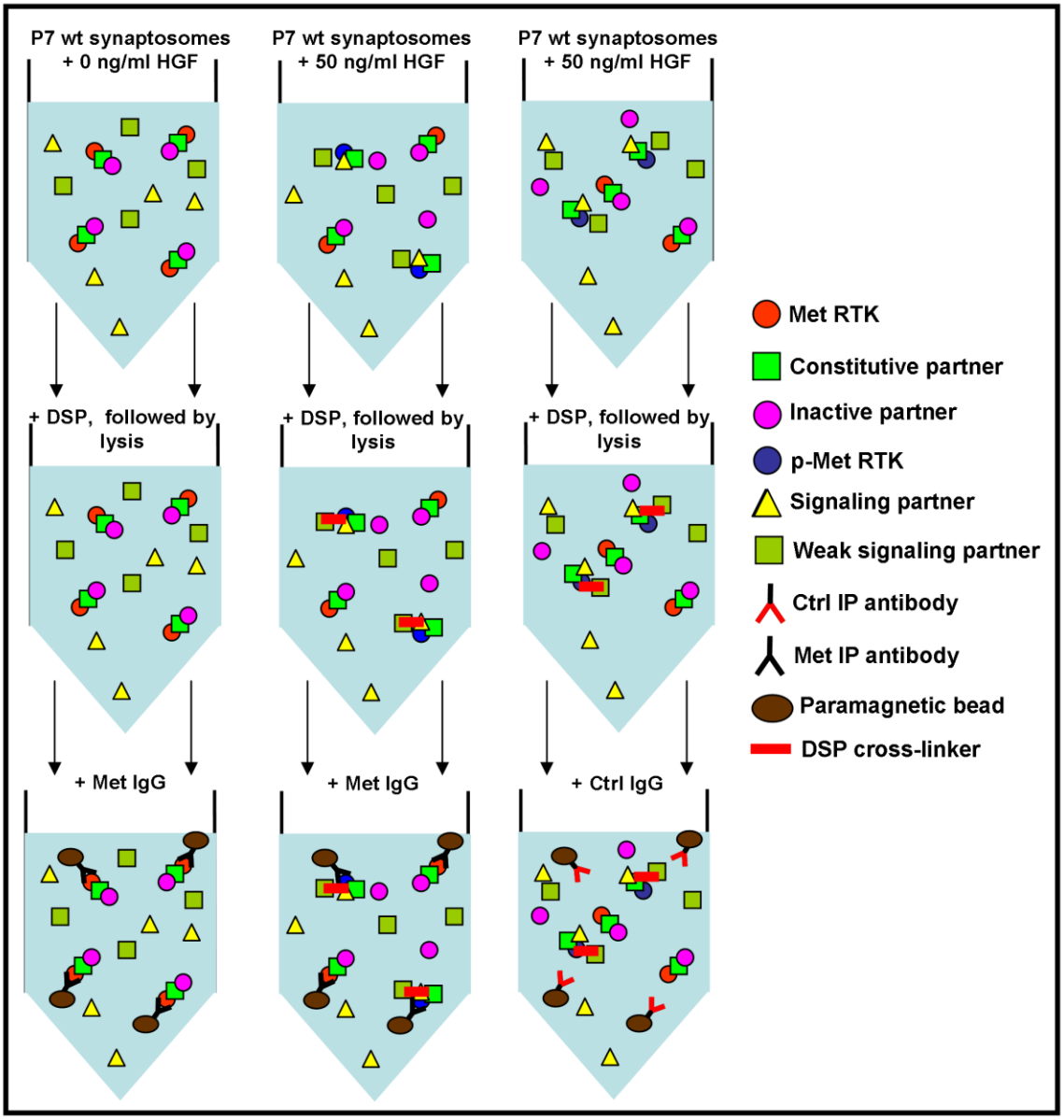

Figure 4. Immunoprecipitation strategy to identify Met signaling partners during forebrain circuit development. **Top row:** P7 wild type mouse cortical synaptosomes are treated with 0 (left column) or 50 (middle and right columns) ng/ml HGF. Colored shapes represent cortical synaptosomal proteins. **All columns:** inactive Met (red circle) interacts with a constitutive partner (green square) and its inactive state partner (purple circle). **Middle and right columns:** active, phosphorylated Met (p-Met, blue circle) still interacts with the green square but ceases interacting with the purple circle. p-Met also gains interactions with two new partners (yellow triangle, strong interaction; olive square, weak interaction). **Middle row:** DSP cross-linker (red bar) is added to all synaptosomal samples in order to trap weakly associated Met signaling partners (red bar now connects olive square to p-Met complexes). Lysis follows to solubilize all Figure 4—cont. synaptosomal proteins. **Bottow row:** lysed synaptosomal proteins are incubated with either specific Met immunoprecipitation antibodies (left and middle columns, black Fab region) or control antibodies (right column, red Fab region). Met-associated proteins are immunoprecipitated only by Met antibodies (left and middle columns), and p-Met-associated proteins are immunoprecipitated only by Met antibodies incubated lysates prepared from HGF-stimulated synaptosomes (middle column).

P7 striatum where the subcellular localization of Met is exclusively axonal (Judson et al., 2009). Temporal comparisons of immunoprecipitates prepared from corresponding forebrain structures at P7 and P21 will also be informative considering the evidence for a subcellular shift in Met localization that occurs between these ages (Judson et al., 2009).

Literature Cited

Arevalo JC, Yano H, Teng KK, Chao MV. 2004. A unique pathway for sustained neurotrophin signaling through an ankyrin-rich membrane-spanning protein. Embo J 23(12):2358-2368.

Campbell DB, Sutcliffe JS, Ebert PJ, Militerni R, Bravaccio C, Trillo S, Elia M, Schneider C, Melmed R, Sacco R, Persico AM, Levitt P. 2006. A genetic variant that disrupts MET transcription is associated with autism. Proc Natl Acad Sci U S A 103(45):16834-16839.

Campbell DB, Warren D, Sutcliffe JS, Lee EB, Levitt P. 2009. Association of MET with social and communication phenotypes in individuals with autism spectrum disorder. Am J Med Genet B Neuropsychiatr Genet.

Chow DK, Groszer M, Pribadi M, Machniki M, Carmichael ST, Liu X, Trachtenberg JT. 2009. Laminar and compartmental regulation of dendritic growth in mature cortex. Nat Neurosci 12(2):116-118.

David MD, Yeramian A, Dunach M, Llovera M, Canti C, de Herreros AG, Comella JX, Herreros J. 2008. Signalling by neurotrophins and hepatocyte growth factor regulates axon morphogenesis by differential beta-catenin phosphorylation. J Cell Sci 121(Pt 16):2718-2730.

Delehedde M, Sergeant N, Lyon M, Rudland PS, Fernig DG. 2001. Hepatocyte growth factor/scatter factor stimulates migration of rat mammary fibroblasts through both mitogen-activated protein kinase and phosphatidylinositol 3-kinase/Akt pathways. Eur J Biochem 268(16):4423-4429.

Ebens A, Brose K, Leonardo ED, Hanson MG, Jr., Bladt F, Birchmeier C, Barres BA, Tessier-Lavigne M. 1996. Hepatocyte growth factor/scatter factor is an axonal chemoattractant and a neurotrophic factor for spinal motor neurons. Neuron 17(6):1157-1172.

Gutierrez H, Dolcet X, Tolcos M, Davies A. 2004. HGF regulates the development of cortical pyramidal dendrites. Development (Cambridge, England) 131(15):3717-3726.

Judson MC, Bergman MY, Campbell DB, Eagleson KL, Levitt P. 2009. Dynamic gene and protein expression patterns of the autism-associated met receptor tyrosine kinase in the developing mouse forebrain. J Comp Neurol 513(5):511-531.

Lim CS, Walikonis RS. 2008. Hepatocyte growth factor and c-Met promote dendritic maturation during hippocampal neuron differentiation via the Akt pathway. Cell Signal 20(5):825-835.

McAllister AK, Katz LC, Lo DC. 1997. Opposing roles for endogenous BDNF and NT-3 in regulating cortical dendritic growth. Neuron 18(5):767-778.

Petreanu L, Huber D, Sobczyk A, Svoboda K. 2007. Channelrhodopsin-2-assisted circuit mapping of long-range callosal projections. Nat Neurosci 10(5):663-668.

Petreanu L, Mao T, Sternson SM, Svoboda K. 2009. The subcellular organization of neocortical excitatory connections. Nature 457(7233):1142-1145.

Powell EM, Muhlfriedel S, Bolz J, Levitt P. 2003. Differential regulation of thalamic and cortical axonal growth by hepatocyte growth factor/scatter factor. Dev Neurosci 25(2-4):197-206.

Tyndall SJ, Patel SJ, Walikonis RS. 2007. Hepatocyte growth factor-induced enhancement of dendritic branching is blocked by inhibitors of N-methyl-D-aspartate receptors and calcium/calmodulin-dependent kinases. Journal of neuroscience research 85(11):2343-2351.

Tyndall SJ, Walikonis RS. 2006. The receptor tyrosine kinase Met and its ligand hepatocyte growth factor are clustered at excitatory synapses and can enhance clustering of synaptic proteins. Cell Cycle 5(14):1560-1568.

Young P, Qiu L, Wang D, Zhao S, Gross J, Feng G. 2008. Single-neuron labeling with inducible Cre-mediated knockout in transgenic mice. Nat Neurosci 11(6):721-728.

Zhou HY, Wan KF, Ip CK, Wong CK, Mak NK, Lo KW, Wong AS. 2008. Hepatocyte growth factor enhances proteolysis and invasiveness of human nasopharyngeal cancer cells through activation of PI3K and JNK. FEBS Lett 582(23-24):3415-3422.

Zong H, Espinosa JS, Su HH, Muzumdar MD, Luo L. 2005. Mosaic analysis with double markers in mice. Cell 121(3):479-492.